Universidad de Málaga

Escuela Técnica Superior de Ingeniería de Telecomunicación

TESIS DOCTORAL

Analysis and Design of Enhanced Planar Devices Using Multiconductor Transmission Lines With Interconnected Alternate Lines

Autor:

JUAN JOSÉ SÁNCHEZ MARTÍNEZ

Director:

ENRIQUE MÁRQUEZ SEGURA

MÁLAGA 2014

UNIVERSIDAD DE MÁLAGA

Publicaciones y Divulgación Científica

AUTOR: Juan José Sánchez Martínez

EDITA: Publicaciones y Divulgación Científica. Universidad de Málaga

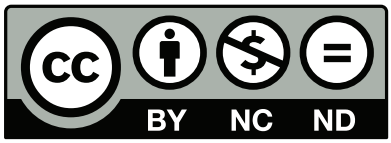

Dedicated to my parents

Contents

Abstract

Novel capabilities and applications of multiconductor transmission lines with interconnected alternate lines have been analyzed in this work. The interconnections among alternate strips broaden the operating frequency band by eliminating undesired resonances and allow the use of simplified analytical models. Phase shifters, baluns, reconfigurable systems for the characterization of balanced circuits, ultra-wideband differential bandpass filters and quasi-elliptic bandpass filters have been proposed and demonstrated. For all these circuits a systematic design procedure have been derived and validated by means of experimental work. The excellent agreement between the measurements and the predicted results validates the proposed procedures as reliable and quick design techniques.

Acknowledgments

First of all, I would like to express my gratitude to my supervisor Enrique Márquez Segura for giving me the opportunity to work during these last four years on different interesting topics. Thanks to him for his encouragement and discussions during the research process.

I would also like to thank Carlos Camacho Peñalosa and Teresa Martín Guerrero for their help and support. To my fellow lab-mates Yak and Elena for the good moments that we have spent together. Thanks to all of them for their company along the way.

I also want to thank Prof. Stepan Lucyszyn for allowing me to be part of the Optical and Semiconductor Devices group at Imperial College London during three months. I am gratefully with his warm welcome and advices during my stay.

In addition, I would like to thank Luis Díez, José Antonio Cortés and Francisco Javier Cañete. They are outstanding researchers in power line communications (PLC) and it was a pleasure to work with them before starting this PhD.

Last but not least, I would like to thank my family. Really, they deserve all my gratefulness because without their love and patient, this thesis would have not been possible.

This research has been supported by the Junta de Andalucía (Proyecto de Excelencia P09-TIC-5116).

Acronyms

ADM Amplitude Difference Measure.

BMC Broadband Multilayer Capacitor.

CMRR Common-Mode-Rejection Ratio.

CRLH Composite Right/Left Handed.

DMRR Differential-Mode-Rejection Ratio.

DUT Device Under Test.

FDM Frequency Difference Measure.

FSV Feature Selective Validation.

GDM Global Difference Measure.

LH Left-Handed.

MEMS Micro-Electro-Mechanical Systems.

MMR Multiple-Mode Resonators.

MoM Method of Moments.

MTL Multiconductor Transmission Line.

RF Radio Frequency.

RH Right-Handed.

SPDT Single-Pole Double-Throw.

TEM Transverse Electro-Magnetic.

TL Transmission Line.

TRL Thru-Reflect-Line.

UWB Ultra-Wide-Band.

VNA Vector Network Analyzer.

Chapter 1

Introduction

The present chapter will attempt to summarize the content of this dissertation. Section 1.1 begins with a description of the contextual framework upon which this work is built. Thereby, Section 1.2 presents the motivations and goals of this project. The aims and organization of this thesis with a brief outline of the main contents of each chapter are presented in Section 1.3. Finally, the publications that have been derived from this work are summarized in 1.4.

1.1. Contextual Framework

Coupled-line structures play an important role in many distributed RF and microwave circuits [1–7]. As circuit elements, coupled lines have been widely employed in baluns, directional couplers, phase shifters, impedance transformers, dc blocks, interdigital capacitors, filters, and spiral inductors. Planar edge-coupled lines with lines in the same plane are usually employed in microstrip technology. Nevertheless, they are not suitable for tight coupling values because they require a very small spacing between lines. Thus, edge-coupled structures are intended for coupling factors to about 10 or 8 dB, while for tighter couplings of the order of 2 to 3 dB, broadside-coupled lines are used [2]. This aspect is very important because in many practical circuits tight couplings of around 3 dB are required. Therefore, other alternatives that include multilayer configurations, Lange couplers or tandem couplers are employed [2].

The use of coupled lines to design directional couplers and filters is one of the most popular applications [8, 9]. The first directional coupler using a quarter-wavelength two-wire structure was reported en 1922 [8], and a significant progress was made during the 1940s and 1950s [10, 11]. Numerous works published in the 1960s and 1970s [12–18] described the theory and

applications of the parallel coupled transmission lines. In addition, there are different types of coupled filters, but the most common are paralled-coupled-line [11], interdigital [12, 15], combline [19] and hairpin line [20, 21] filters.

Parallel coupled lines configuration is attractive for realizing microstrip bandpass filters for broadband applications where the selectivity is not severe. Approximate design and synthesis formulas have been well documented for determining the dimensions of each stage for an all-pole bandpass filter [1]. The design of parallel-coupled line filters was introduced in [11], which have been refined or modified for specific conditions or applications [2]. To derive these formulas, each coupled stage is modeled as a two-port network of two quarter-wave transmission line sections with an impedance inverter in between. However, this approximation has only a good accuracy when the filter has a relatively small bandwidth around the center frequency. Therefore, filters designed using immittance inverter theory are best applied to narrow or moderate bandwidth filters.

In recent years, since conventional filter theory is based on the narrow-band assumption, several techniques in the design of ultra-wideband (UWB) filters have been proposed [22]. One of the proposed topologies is based on multiple-mode resonators (MMR) with stepped-impedance or stub-loaded configuration [23]. Most of these MMR-based filters combine input/output parallel coupled lines with different types of MMR structures. The formation of the desired ultra-wide passband is dependent on the coupling strength of the two input/output structures.

Reflection type phase shifters based on coupled structures consist of a 3-dB directional coupler and two identical reflection terminations. When equal power split and phase quadrature are maintained between the coupled and direct ports, perfect input and output matching with zero insertion loss is achieved. The relative phase shift is controlled by the reflection coefficient of the reflection terminations, and the bandwidth of operation is determined by both the coupler and the reactive loads [5]. Consequently, for this application it is necessary to use tight couplers.

Coupled-line structures are also used to synthesize baluns. A balun is a transformer used to convert an unbalanced input signal into a balanced differential output one. Different baluns configurations have been reported by using sections of single or coupled transmission lines. Planar baluns based on coupled lines can be divided into two groups, quarter-wave coupled line baluns and Marchand coupled-line baluns [2]. Marchand baluns are probably the most popular [24]. Marchand balun consists of two sections of quarter-wavelength coupled lines and in order to broaden the bandwidth a strong coupling level for the two coupled-line sections is required. However, the main limitation is its poor balanced output ports matching and isolation [25].

In general, all the commented circuits require of tight couplings in order to enhance the bandwidth of operation. Tight coupling values between edge-coupled lines can be achieved

by connecting several lines in an interdigital manner. One implementation of this idea is the Lange coupler [26], an interdigitated microstrip coupler that consists of three or more lines with alternate lines tied together. Other alternatives to increase the coupling are the use of multi-layer broadside coupled-structures, which is difficult to build on ceramic or monolithic substrates, as well as tandem sections or branch-line couplers, which have a narrower bandwidth.

The Lange coupler is a multiconductor directional coupler in which the mutual capacitance between the lines can be increased without the need for a very small space between them. By increasing the mutual capacitance the coupling between lines increases [2]. The design equations of a k-line interdigital coupler in terms of the even- and odd-mode impedances of a pair of coupled lines are given in [27, 28].

More recently, multiconductor coupled lines with interconnected alternate lines have been used to synthesize enhanced interdigital capacitors. The resulting device is the so-called wire-bonded interdigital capacitor, which exhibits a greater bandwidth since undesired resonances at higher frequencies are eliminated [29]. In an interdigitated directional coupler the electrical length of the transmission lines is 90^o at the center frequency of operation. On the contrary, the lines in the interdigital capacitor are always shorter than a quarter of wavelength in order to show a capacitive behaviour. An analytical model (valid for an even number of conductors) of this new circuit was published in [30] while an exact analysis (valid for any number of lines) was derived in [31]. Therefore, it can be noted that multiconductor coupled-line structures can be very attractive in order to design new devices or improving the performance of existing circuits. These structures provide greater coupling factors and can be analytically dealt with.

1.2. Motivation and Objectives

As described in previous section, coupled-line structures consisting of two single lines have been extensively used. Nevertheless, given that there is a direct relation between the achievable operational bandwidth and the coupling factor, the use of multiconductor transmission lines (MTL) appear ideal for wideband devices. Besides, thanks to the modeling and characterization of multiple coupled lines, it will be possible to obtain analytical design equations [27, 30, 31].

In this context, the purpose of this work is to study the advantages of using MTLs in order to enhance the performance of some existing applications, as well as to design novel structures and configurations. In addition, the main objective of this research work is to provide a design methodology for any of the studied devices. Besides, the theory proposed will be validated with experimental work.

1.3. Thesis Outline

This work, divided into six chapters, deals with the analysis and design of specific enhanced components such as phase shifters, baluns and filters.

In **Chapter 2**, multiconductor transmission lines are investigated to synthesize miniaturized and broadband reflection-type phase shifters. The analysis of wire-bonded MTLs is accomplished and generalized in order to extend the traditional theory where 3-dB quarter-wavelength directional couplers are usually employed. In this chapter some basic circuit parameters are established and two general equivalent circuits are obtained for two particular arrangements, when both coupled and direct ports are open or short-circuited. These simple equivalent circuits and the theory developed in this chapter will be used through the rest of the work.

In **Chapter 3**, a novel generalized design procedure of broadband planar baluns with two MTLs to convert single-ended input signals into differential signals is presented. Closed-form design equations to have perfect amplitude and phase balance are obtained. By using this balun, a new reconfigurable test set for the characterization of differential devices is designed and fabricated.

In **Chapter 4**, the analysis of MTL components when used as shunt stubs is presented. A general study is accomplished and some physical insights into the frequency behaviour of the different one-port MTL structures are provided. To validate the design equations, two artificial transmission lines with left-handed bandpass response and improved out-of-band rejection are synthesized.

Once the MTL elements have been thoroughly analyzed as two-port and one-port circuits in Chapters 2, 3, and 4, the next two Chapters use this theory to design bandpass filters. A systematic design procedure of ultra-wideband differential bandpass filters is presented in **Chapter 5**. Single- and double-section filters are considered to have a Butterworth or Chebyshev frequency response and some prototypes are manufactured to assess the developed theory.

Chapter 6 focuses on the study of high-selectivity filters with a quasi-elliptic frequency response. Two asymmetric and symmetric configurations are proposed and analyzed. These new topologies are suitable for implementing three- and/or five-pole bandpass filters. The experimental results demonstrate that both structures are suitable to synthesize bandpass filter with sharp cut-off slopes.

Finally, **Chapter 7** summarizes the main results and highlights the original contributions derived from this thesis.

1.4. Publications

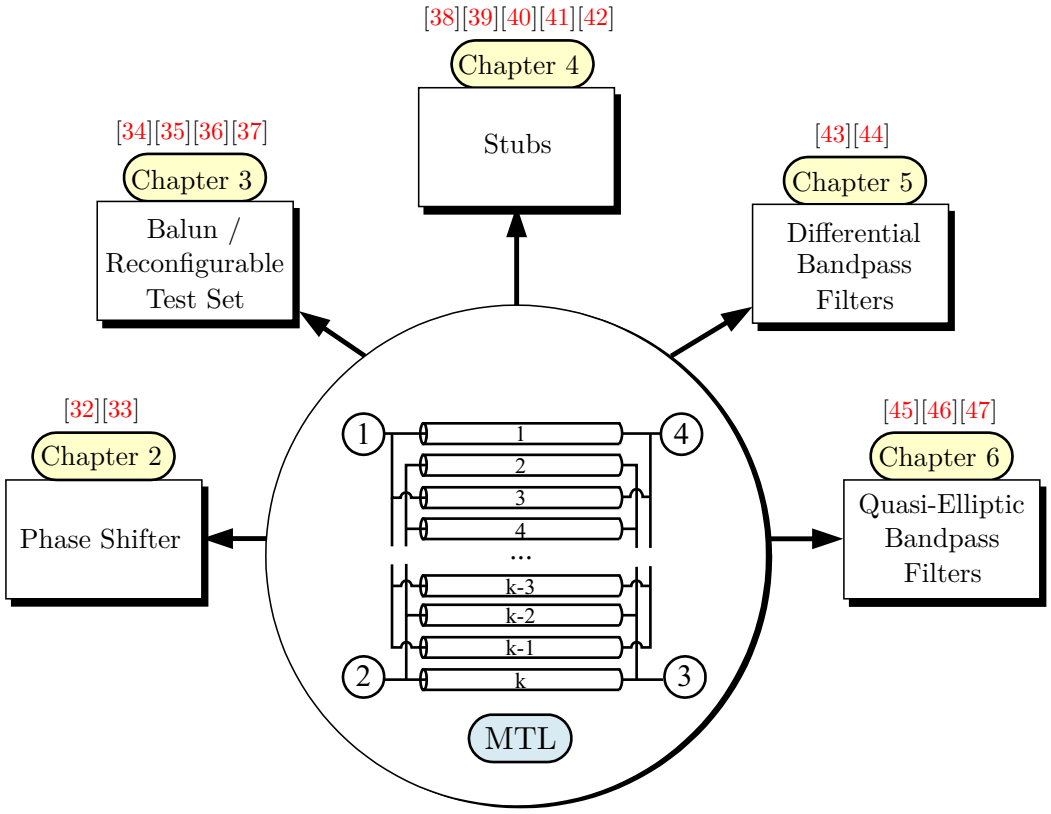

Figure 1.1.: Thesis structure and contributions.

The following publications have been derived from the work developed in this thesis (see Fig. 1.1).

Journals

- [38] J. J. Sánchez-Martínez, E. Márquez-Segura, P. Otero, and C. Camacho-Peñalosa "Artificial Transmission Line with Left/Right-Handed Behavior Based on Wire Bonded Interdigital Capacitors," *Progr. Electromagn. Res. B*, vol. 11, pp. 245-264, 2009.
- [32] J. J. Sánchez-Martínez and E. Márquez-Segura, "Analytical Study of Wide-band Bandpass Filters Based on Wire-Bonded Multiconductor Transmission Lines With LH Behaviour,"*Progr. Electromagn. Res. Lett.*, vol. 31, pp. 1-13, 2012.
- [39] J. J. Sánchez-Martínez and E. Márquez-Segura, "Comments on 'Wideband Coupled-Line Microstrip Filters With High-Impedance Short-Circuited Stubs'," *IEEE Microw. Wireless Compon. Lett.*, vol. 22, no. 9, p. 492, Sep. 2012.
- [34] J. J. Sánchez-Martínez and E. Márquez-Segura, "Generalized analytical design of broadband planar baluns based on wire-bonded multiconductor transmission lines,"

Progr. Electromagn. Res., vol. 134, pp. 169-187, 2013.

- [40] J. J. Sánchez-Martínez, E. Márquez-Segura, and C. Camacho-Peñalosa, "Analysis of wire-bonded multiconductor transmission-line-based stubs," *IEEE Trans. Microw. Theory Tech.*, vol. 61, no. 4, pp. 1467-1476, Apr. 2013.
- [33] J. J. Sánchez-Martínez and E. Márquez-Segura, "Analysis of wire-bonded multiconductor transmission line-based phase-shifting sections," *J. Electromagn. Waves Appl.*, vol. 27, no. 16, pp. 1997-2009, Sep. 2013.
- [45] J. J. Sánchez-Martínez, E. Márquez-Segura and S. Lucyszyn, "Design of Compact Wideband Bandpass Filters Based on Multiconductor Transmission Lines With Interconnected Alternate Lines," *IEEE Microw. Wireless Compon. Lett.*, vol. 24, no. 7, pp. 454-456, Jul. 2014.
- [43] J. J. Sánchez-Martínez and E. Márquez-Segura, "Analytical Design of Wire-Bonded Multiconductor Transmission Line-Based Ultra-Wideband Differential Bandpass Filters," Accepted to be published in *IEEE Trans. Microw. Theory Tech.*, Jun. 2014.
- [46] J. J. Sánchez-Martínez, E. Márquez-Segura and S. Lucyszyn, "Synthesis and Design of High-Selectivity Wideband Quasi-elliptic Bandpass Filters Using Multiconductor Transmission Lines," Submitted to *IEEE Trans. Microw. Theory Tech.*, Apr. 2014.

International Conferences

- [41] J. J. Sánchez-Martínez, E. Márquez-Segura, and C. Camacho-Peñalosa, "Analysis of Composite Left/Right-Handed Transmission Line Using Shunt Wire Bonded Interdigital Capacitors," in *4th Young Scientist Meeting on Metamaterials (YSMM)*, Feb. 2011, ISBN: 978-84-693-9971-2.
- [42] J. J. Sánchez-Martínez, E. Márquez-Segura, and C. Camacho-Peñalosa,"Synthesis of CRLH-TLs Based on a Shunt Coupled-line Section," in *42nd European Microwave Conference (EuMC)*, Oct. 2012, pp. 675-678.
- [35] S. Cobos-Bandera, J. J. Sánchez-Martínez, and E. Márquez-Segura, "Mems-based reconfigurable test-set for differential and common mode measurement using a two-port network analyzer," in *42nd European Microwave Conference (EuMC)*, Oct. 2012.

Spanish National Conferences

- [36] S. Cobos-Bandera, J. J. Sánchez-Martínez, and E. Márquez-Segura, "Sistema de Medida Reconfigurable para la Caracterización de Dispositivos Diferenciales de Microondas," in *XXVII Simposium Nacional de la Unión Científica Internacional de Radio (URSI)*, Sep. 2012, ISBN: 978-84-695-4326-9.

- [37] J. J. Sánchez-Martínez and E. Márquez-Segura, "Análisis de un Balun Basado en Líneas de Transmisión Multiconductoras," in *XXVII Simposium Nacional de la Unión Científica Internacional de Radio (URSI)*, Sep. 2012, ISBN: 978-84-695-4326-9.
- [47] J. J. Sánchez-Martínez and E. Márquez-Segura, "Análisis y Diseño de Filtros Paso Banda con Alta Selectividad Espectral Basados en Líneas de Transmisión Multiconductoras," in *XXVIII Simposium Nacional de la Unión Científica Internacional de Radio (URSI)*, Sep. 2013, ISBN: 978-84-941537-1-6.
- [44] J. J. Sánchez-Martínez and E. Márquez-Segura, "Análisis y Diseño de Filtros Diferenciales Basados en Líneas Acopladas," Accepted in *XXIX Simposium Nacional de la Unión Científica Internacional de Radio (URSI)*, Sep. 2014.

References

[1] G. L. Mattahei, L. Young, and E. M. T. Jones, *Microwave Filters, Impedance-Matching Networks, and Coupling Structures*, M. A. House, Ed. Norwood, 1985.

[2] R. Mongia, I. Bahl, and P. Bhartia, *RF and Microwave Coupled-Line Circuits*. Norwood, MA: Artech House, 1999.

[3] J. A. B. Faria, *Multiconductor Transmission-line Structures: Modal Analysis Techniques*. New York: Wiley, 1993.

[4] I. C. Hunter, *Theory and Design of Microwave Filters*, Stevenage, Ed. U.K.: IEE Press, 2001.

[5] I. D. Robertson and S. Lucyszyn, *RFIC and MMIC Design and Technology*. London, UK: IEE Press, 2001.

[6] J.-S. Hong and M. J. Lancaster, *Microstrip Filters for RF/Microwave Applications*, K. Chang, Ed. Wiley-Interscience, 2001.

[7] C. Caloz and I. Itoh, *Electromagnetic Metamaterials: Transmission Line Theory and Microwave Applications*. Wiley-Interscience, 2006.

[8] S. Cohn and R. Levy, "History of Microwave Passive Components with Particular Attention to Directional Couplers," *IEEE Trans. Microw. Theory Tech.*, vol. 32, no. 9, pp. 1046–1054, Sep. 1984.

[9] R. Levy and S. Cohn, "A History of Microwave Filter Research, Design, and Development," *IEEE Trans. Microw. Theory Tech.*, vol. 32, no. 9, pp. 1055–1067, Sep. 1984.

[10] E. M. T. Jones and J. T. Bolljahn, "Coupled-Strip-Transmission-Line Filters and Directional Couplers," *IRE Trans. Microw. Theory Tech.*, vol. 4, no. 2, pp. 75–81, Apr. 1956.

[11] S. B. Cohn, "Parallel-Coupled Transmission-Line-Resonator Filters," *IRE Trans. Microw. Theory Tech.*, vol. 6, no. 2, pp. 223–231, Apr. 1958.

[12] G. Matthaei, "Interdigital Band-Pass Filters," *IRE Trans. Microw. Theory Tech.*, vol. 10, no. 6, pp. 479–491, Nov. 1962.

[13] R. Levy, "General Synthesis of Asymmetric Multi-Element Coupled-Transmission-Line Directional Couplers," *IEEE Trans. Microw. Theory Tech.*, vol. 11, no. 4, pp. 226–237, Jul. 1963.

[14] H. Carlin and W. Kohler, "Direct Synthesis of Band-Pass Transmission Line Structures," *IEEE Trans. Microw. Theory Tech.*, vol. 13, no. 3, pp. 283–297, May 1965.

[15] R. Wenzel, "Exact Theory of Interdigital Band-Pass Filters and Related Coupled Band-Pass Structures," *IEEE Trans. Microw. Theory Tech.*, vol. 13, no. 5, pp. 559–575, Sep. 1965.

[16] E. Cristal, "Coupled-Transmission-Line Directional Couplers with Coupled Lines of Unequal Characteristic Impedances," *IEEE Trans. Microw. Theory Tech.*, vol. 14, no. 7, pp. 337–346, Jul. 1966.

[17] G. Zysman and A. Johnson, "Coupled transmission line networks in an inhomogeneous dielectric medium," *IEEE Trans. Microw. Theory Tech.*, vol. 17, no. 10, pp. 753–759, Oct. 1969.

[18] V. Tripathi, "Asymmetric Coupled Transmission Lines in an Inhomogeneous Medium," *IEEE Trans. Microw. Theory Tech.*, vol. 23, no. 9, pp. 734–739, Sep. 1975.

[19] R. Wenzel, "Synthesis of Combline and Capacitively Loaded Interdigital Bandpass Filters of Arbitrary Bandwidth," *IEEE Transactions on Microwave Theory and Techniques*, vol. 19, no. 8, pp. 678–686, Aug. 1971.

[20] E. Cristal and S. Frankel, "Hairpin-Line and Hybrid Hairpin-Line/Half-Wave Parallel-Coupled-Line Filters," *IEEE Trans. Microw. Theory Tech.*, vol. 20, no. 11, pp. 719–728, Nov. 1972.

[21] U. H. Gysel, "New Theory and Design for Hairpin-Line Filters," *IEEE Trans. Microw. Theory Tech.*, vol. 22, no. 5, pp. 523–531, May 1974.

[22] Z.-C. Hao and J.-S. Hong, "Ultrawideband Filter Technologies," *IEEE Microw. Mag.*, vol. 11, no. 4, pp. 56–68, Jun. 2010.

[23] S. Sun and L. Zhu, "Multiple-resonator-based bandpass filters," *IEEE Microw. Mag.*, vol. 10, no. 2, pp. 88–98, Apr. 2009.

[24] M. Tsai, "A new compact wideband balun," in *IEEE Microwave and Millimeter-Wave Monolithic Circuits Symposium*, 1993, pp. 123–125.

[25] M. Chongcheawchamnan, C. Y. Ng, K. Bandudej, A. Worapishet, and I. Robertson, "On miniaturization isolation network of an all-ports matched impedance-transforming marchand balun," *IEEE Microw. Wireless Compon. Lett.*, vol. 13, no. 7, pp. 281–283, Jul. 2003.

[26] J. Lange, "Interdigitated Strip-Line Quadrature Hybrid," in *Microwave Symposium, 1969 G-MTT International*, May 1969, pp. 10–13.

[27] W. Ou, "Design Equations for an Interdigitated Directional Coupler," *IEEE Trans. Microw. Theory Tech.*, vol. 23, no. 2, pp. 253–255, Feb. 1975.

[28] A. Presser, "Interdigitated microstrip coupler design," *IEEE Trans. Microw. Theory Tech.*, vol. 26, no. 10, pp. 801–805, Oct. 1978.

[29] F. Casares-Miranda, P. Otero, E. Márquez-Segura, and C. Camacho-Peñalosa, "Wire Bonded Interdigital Capacitor," *IEEE Microw. Wireless Compon. Lett.*, vol. 15, no. 10, pp. 700–702, Oct. 2005.

[30] E. Márquez-Segura, F. Casares-Miranda, P. Otero, C. Camacho-Peñalosa, and J. Page, "Analytical Model of the Wire-Bonded Interdigital Capacitor," *IEEE Trans. Microw. Theory Tech.*, vol. 54, no. 2, pp. 748–754, Feb. 2006.

[31] J. Page, E. Márquez-Segura, F. Casares-Miranda, J. Esteban, P. Otero, and C. Camacho-Peñalosa, "Exact Analysis of the Wire-Bonded Multiconductor Transmission Line," *IEEE Trans. Microw. Theory Tech.*, vol. 55, no. 8, pp. 1585–1592, Aug. 2007.

[32] J. J. Sánchez-Martínez and E. Márquez-Segura, "Analytical Study of Wide-band Bandpass Filters Based on Wire-Bonded Multiconductor Transmission Lines With LH Behaviour," *Progr. Electromagn. Res. Lett.*, vol. 31, pp. 1–13, 2012.

[33] ——, "Analysis of wire-bonded multiconductor transmission line-based phase-shifting sections," *J. Electromagn. Waves Appl.*, vol. 27, no. 16, pp. 1997–2009, Sep. 2013.

REFERENCES

[34] ——, "Generalized analytical design of broadband planar baluns based on wire-bonded multiconductor transmission lines," *Progr. Electromagn. Res.*, vol. 134, pp. 169–187, 2013.

[35] S. Cobos-Bandera, J. J. Sánchez-Martínez, and E. Márquez-Segura, "Mems-based reconfigurable test-set for differential and common mode measurement using a two-port network analyzer," in *42nd European Microwave Conference (EuMC)*, Oct. 2012, pp. 601–604.

[36] ——, "Sistema de Medida Reconfigurable para la Caracterización de Dispositivos Diferenciales de Microondas," in *XXVII Simposium Nacional de la Unión Científica Internacional de Radio (URSI)*, Sep. 2012, ISBN: 978-84-695-4326-9.

[37] J. J. Sánchez-Martínez and E. Márquez-Segura, "Análisis de un Balun Basado en Líneas de Transmisión Multiconductoras," in *XXVII Simposium Nacional de la Unión Científica Internacional de Radio (URSI)*, Sep. 2012, ISBN: 978-84-695-4326-9.

[38] J. J. Sánchez-Martínez, E. Márquez-Segura, P. Otero, and C. Camacho-Peñalosa, "Artificial Transmission Line with Left/Right-Handed Behavior Based on Wire Bonded Interdigital Capacitors," *Progr. Electromagn. Res. B*, vol. 11, pp. 245–264, 2009.

[39] J. J. Sánchez-Martínez and E. Márquez-Segura, "Comments on 'Wideband Coupled-Line Microstrip Filters With High-Impedance Short-Circuited Stubs'," *IEEE Microw. Wireless Compon. Lett.*, vol. 22, no. 9, p. 492, Sep. 2012.

[40] J. J. Sánchez-Martínez, E. Márquez-Segura, and C. Camacho-Peñalosa, "Analysis of wire-bonded multiconductor transmission-line-based stubs," *IEEE Trans. Microw. Theory Tech.*, vol. 61, no. 4, pp. 1467–1476, Apr. 2013.

[41] ——, "Analysis of Composite Left/Right-Handed Transmission Line Using Shunt Wire Bonded Interdigital Capacitors," in *4th Young Scientist Meeting on Metamaterials (YSMM)*, Feb. 2011, ISBN: 978-84-693-9971-2.

[42] ——, "Synthesis of CRLH-TLs Based on a Shunt Coupled-line Section," in *42nd European Microwave Conference (EuMC)*, Oct. 2012, pp. 675–678.

[43] J. J. Sánchez-Martínez and Márquez-Segura, "Analytical Design of Wire-Bonded Multiconductor Transmission Line-Based Ultra-Wideband Differential Bandpass Filters," *Submitted to IEEE Trans. Microw. Theory Tech.*, Mar. 2014.

[44] J. J. Sánchez-Martínez and E. Márquez-Segura, "Análisis y Diseño de Filtros Diferenciales Basados en Líneas Acopladas," in *enviado a XXIX Simposium Nacional de la Unión Científica Internacional de Radio (URSI)*, Sep. 2014.

[45] J. J. Sánchez-Martínez, E. Márquez-Segura, and S. Lucyszyn, "Design of Compact Wideband Bandpass Filters Based on Multiconductor Transmission Lines With Interconnected Alternate Lines," *IEEE Microw. Wireless Compon. Lett.*, vol. 24, no. 7, pp. 454–456, Jul. 2014.

[46] J. J. Sánchez-Martínez, Márquez-Segura, and S. Lucyszyn, "Synthesis and Design of High-Selectivity Wideband Quasi-elliptic Bandpass Filters Using Multiconductor Transmission Lines," *Submitted to Trans. Microw. Theory Tech.*, Apr. 2014.

[47] J. J. Sánchez-Martínez and E. Márquez-Segura, "Análisis y Diseño de Filtros Paso Banda con Alta Selectividad Espectral Basados en Líneas de Transmisión Multiconductoras," in *XXVIII Simposium Nacional de la Unión Científica Internacional de Radio (URSI)*, Sep. 2013, ISBN: 978-84-941537-1-6.

Chapter 2

Phase Shifters

THE use of coupled lines to realize reflection-type phase shifters is well known. Nevertheless, in this chapter the analysis of wire-bonded multiconductor transmission lines is accomplished and generalized in order to extend the traditional theory where 3-dB quarter-wavelength directional couplers are usually employed. Therefore, it will be demonstrated that this kind of reflection phase shifters, where the coupled and direct ports are terminated with reactive loads, can be designed for any coupling level. Analytical design equations are derived to compute both the insertion and return losses as well as the operating frequency band as a function of the coupling factor of the MTL. Furthermore, two general equivalent circuits as a function of the number of strips are derived for two particular arrangements, when both coupled and direct ports are open or short-circuited. These simple equivalent circuits provide some insight into the physical behaviour of the MTL and are expedient to the design of filtering structures and 90^o and -90^o phase shifters. These equations and models will be used through the rest of chapters.

2.1. Introduction

Phase shifting sections are key components in many microwave devices as phased arrays, modulators, frequency converters, baluns, radar and measurement systems. From the different phase shifter topologies, the reflection-type [1, 2] is perhaps the most common, where a quarter-wavelength 3-dB coupler with its coupled and direct ports terminated by reactive loads is employed. Furthermore, phase shifters play also an important role in designing baluns to convert an unbalanced input signal into a balanced differential output one. Advantages by using differential signal circuits have been widely exploited in audio, data transmission,

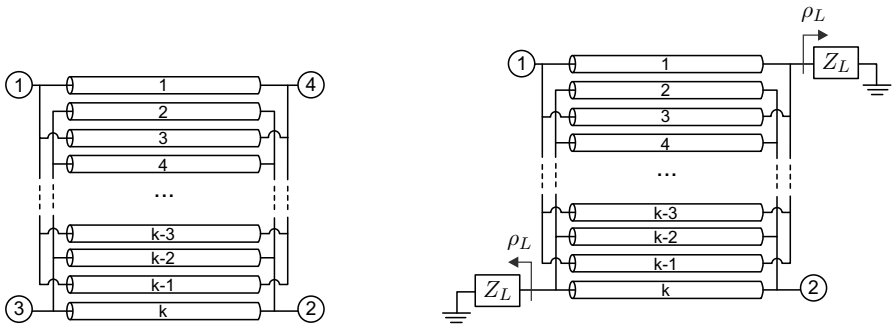

(a) (b)

Figure 2.1.: Transmission line equivalent of (a) a four-port wire-bonded MTL and of (b) a two-port wire-bonded MTL with reactive loads at the coupled and direct ports.

and telephone because of its inherent resistance to external noise sources. Other advantages of differential signalling are reduced even-order harmonics and increased dynamic range. Consequently, baluns are important and pre-eminent devices in balanced microwave front-end circuit such as balanced mixers, push-pull amplifiers, phase shifters, balanced modulators, two-wire antennas, and other applications.

In this chapter, a thorough and comprehensive study of reflection-type phase shifters by using wire-bonded multiconductor transmission lines (MTL) is carried out. The focus of this analysis is on finding the number of conductors and the even- and odd-mode impedances of the wire-bonded MTL (Fig. 2.1(a)) to achieve a required performance according to insertion losses, return losses and operating bandwidth. Notwithstanding, given that the use of open- and short-circuited coupled lines has been fostered for realizing bandpass or bandstop filters [3, 4], wideband baluns [5, 6] and composite right/left handed transmission lines (CRLH) [7–10], two general equivalent circuits as a function of the number of conductors and the coupling factor are presented. These two new circuits extend the known models for the classic two-strip coupled lines [3, 5] and thus, they can be easily used to derive the design equations of filters based on cascaded wire-bonded MTL sections.

Furthermore, the presented theoretical analysis emphasizes the worth of employing open- and short-circuited wire-bonded MTLs to design wideband baluns with good input match, amplitude and phase balance, and excellent output isolation. Many different balun topologies have been proposed in the literature [11–14], but most of them have either a narrow-band performance or poor balanced output ports matching and isolation (e.g. Marchand baluns). Therefore, based on the theory and new equivalent circuits developed in next chapter it will proved that wire-bonded MTL-based baluns overcome most of the awkward limitations of recently published baluns.

The comprehensive study of wire-bonded MTL-based phase shifting sections and the usefulness of the new equivalent circuits in the design of applications is assessed by means of measurements. The simplified closed-form design equations and equivalent circuits are used to

design and manufacture two critical- and over-coupling open- and short-circuited wire-bonded MTLs (-90^o and +90^o).

2.2. Analysis and Design Procedure

The wire-bonded MTL is a four-port device where the ends of alternate strips are connected by bonding wires (see Fig. 2.1(a)). Therefore, a wire-bonded MTL is a particular configuration of multiconductor transmission lines [5, 15, 16]. The interconnections among alternate strips broaden the operating frequency band of the MTL by eliminating undesired resonances and allow the use of simplified analytical models. Assuming ideal short circuits across alternate conductors the equivalent model of a wire-bonded MTL can be simplified as a pair of coupled lines [4, 5].

The input admittance matrix of a wire-bonded MTL was derived in [17] and design equations for an interdigital directional coupler were obtained. However, a new approach is accomplished in this work to obtain general design equations of reflection-type phase shifters based on wire-bonded MTLs. When losses are neglected and the coupling between non-adjacent strips is negligible, the admittance matrix of the wire-bonded MTL can be expressed as [17]

$$[Y_L] = j\begin{bmatrix} -M\cot\theta & -N\cot\theta & N\csc\theta & M\csc\theta \\ -N\cot\theta & -M\cot\theta & M\csc\theta & N\csc\theta \\ N\csc\theta & M\csc\theta & -M\cot\theta & -N\cot\theta \\ M\csc\theta & N\csc\theta & -N\cot\theta & -M\cot\theta \end{bmatrix} \tag{2.1}$$

where θ is the electrical length of the fingers, and M and N are defined by

$$M = \frac{k}{2}Y_{11} + \left(\frac{k}{2} - 1\right)\frac{Y_{12}^2}{Y_{11}} \tag{2.2a}$$

$$N = (k-1)Y_{12}. \tag{2.2b}$$

Admittances Y_{11} and Y_{12} are calculated as

$$Y_{11} = \frac{1}{2}\left(Y_{oo} + Y_{oe}\right), \quad Y_{12} = -\frac{1}{2}\left(Y_{oo} - Y_{oe}\right), \tag{2.3}$$

where Y_{oo} and Y_{oe} represent the odd and even mode admittances, respectively, of a pair of adjacent lines and k, which is even, stands for the number of conductors or strips in the case of planar technology (excluding the ground plane). When no losses are considered Y_{oo} and Y_{oe} are real numbers and it happens that

$$M > 0, \quad N < 0, \quad M^2 > N^2. \tag{2.4}$$

It is important to note that in previous equations pure TEM and lossless propagation are

assumed, and that the electrical length of the fingers θ is the average value of the even- and odd-mode electrical lengths θ_e and θ_o, given by

$$\theta = \frac{\theta_e + \theta_o}{2}. \tag{2.5}$$

Therefore, the presented model is conditioned by several assumptions. First, pure TEM and lossless propagation are assumed, where the effective relative permittivity is computed from the values of the even- and odd- modes of a pair of adjacent conductors as

$$\sqrt{\epsilon_{reff}} = \frac{\sqrt{\epsilon_{reffe}} + \sqrt{\epsilon_{reffo}}}{2}. \tag{2.6}$$

Second, the coupling between non-adjacent strips is neglected. Third, the bonding wires across alternate strips are considered ideal short circuits (bonding wires very short compared to the wavelength) and thus, the connections can be neglected and the equivalent model of a wire-bonded MTL can be simplified as a pair of coupled lines [4, 5, 18] (see Appendix A). Finally, the model was developed for a wire-bonded MTL with an even number of conductors [17]. The validity and accuracy of these approximations have been investigated and validated in [5–7, 9, 18–22], where it was demonstrated an excellent agreement between experimental and analytical results.

If all the four ports are loaded with the characteristic impedance Z_0 [17, 23]

$$Z_0 = \frac{1}{\sqrt{M^2 - N^2}}, \tag{2.7}$$

the S-parameters of the wire-bonded MTL (Fig. 2.1(a)) can be expressed as

$$[S] = \begin{bmatrix} 0 & 0 & \alpha & \beta \\ 0 & 0 & \beta & \alpha \\ \alpha & \beta & 0 & 0 \\ \beta & \alpha & 0 & 0 \end{bmatrix}, \tag{2.8}$$

where α and β are computed as

$$\alpha = \frac{c \sin\theta}{\sqrt{1 - c^2 \cos^2\theta}} e^{j(\pi/2+\phi)}, \quad \beta = \frac{\sqrt{1-c^2}}{\sqrt{1 - c^2 \cos^2\theta}} e^{j\phi}, \tag{2.9}$$

ϕ being

$$\phi = \arctan\left(\frac{-\sin\theta}{\sqrt{1-c^2}\cos\theta}\right). \tag{2.10}$$

c is the coupling coefficient of a quarter-wavelength k-line coupler given by

$$c = -\frac{N}{M} = \frac{(k-1)(Z_{oe}^2 - Z_{oo}^2)}{2Z_{oe}Z_{oo} + (k-1)(Z_{oe}^2 + Z_{oo}^2)}. \tag{2.11}$$

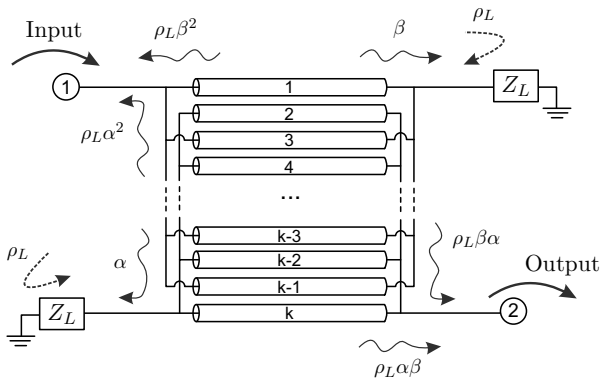

Figure 2.2.: Transmitted and reflected signals inside a two-port wire-bonded MTL, designed by means of (2.7), with reactive loads at the coupled and direct ports.

From (2.8) it is easy to note that if (2.7) is met, the wire-bonded MTL behaves as a backward-wave directional coupler [5] with its four input ports perfectly matched, with perfect isolation between port 1-3 and 2-4, and α and β stand for the quantity of transmitted signal to the coupled and direct ports, respectively. Therefore, when a signal is incident at port 1, the power is divided between ports 3 (α) and 4 (β) and no power reaches port 2 (see Fig. 2.1(a)). Furthermore, from (2.9) follows that the maximum value of coupling is c, that happens at θ=90^o.

One of the main applications of wire-bonded MTLs is the design of reflection type phase shifters by connecting reactive loads to the direct and coupled ports as shown in Fig. 2.1(b). Traditionally a coupling factor of c=-3 dB has been employed to design the phase shifter [24, 25], but in this work it is studied and verified that this is one particular solution. Hence, it is demonstrated that if the wire-bonded MTL is properly designed, any coupling level c can be used and that the higher the coupling factor the broader the operating frequency band. Assuming that both loads Z_L are equal, the reflection coefficient ρ_L is defined by

$$\rho_L = \frac{Z_L - Z_0}{Z_L + Z_0} = |\rho_L| e^{j\angle\rho_L}, \tag{2.12}$$

and the S-parameters of the resultant two-port structure can be easily computed as

$$S_{11} = \rho_L \left(\alpha^2 + \beta^2\right), \quad S_{21} = 2\rho_L\alpha\beta. \tag{2.13}$$

The physical meaning of (2.13) is graphically illustrated in Fig. 2.2. It can be seen that the input signal is split according to α and β to the coupled and direct ports. Then, the signals are reflected (ρ_L) and pass back through the wire-bonded MTL, being superimposed at the input and output ports. Thus, from (2.8), (2.9) and (2.13) and after some algebraic

manipulations, the S_{11} and S_{21} parameters can be expressed as

$$S_{11} = |\rho_L| \frac{1 - c^2(1 + \sin^2\theta)}{1 - c^2\cos^2\theta} e^{j(\angle\rho_L + 2\phi)} \tag{2.14a}$$

$$S_{21} = |\rho_L| \frac{2c\sqrt{1 - c^2}\sin\theta}{1 - c^2\cos^2\theta} e^{j(\angle\rho_L + 2\phi + \pi/2)}. \tag{2.14b}$$

From (2.14) and (2.10) it is straightforward to determine that the coupling factor c conditions both the input match (2.14a) and insertion loss (2.14b), but also the slope of the phase response (2.10). However, from these relationships it follows that if (2.7) is satisfied and two identical variable reactive loads are employed with $|\rho_L|$=1, any coupling factor c could be used to design a tunable phase shifter. The coupling level c determines the insertion and return losses, but clearly the use of c=-3 dB is one out of the possible solutions. The relative phase difference between the output and the input signals can be controlled and adjusted by the phase of the reactive loads. Besides, from (2.14a) the following relation is obtained

$$\theta_d = \arcsin\left(\sqrt{\frac{1}{c^2} - 1}\right), \tag{2.15}$$

that establishes the electrical lengths θ_d where the input match is perfect (S_{11}=0) as a function of c. Figure 2.3(a) draws the magnitude of S_{11} and S_{21} for several coupling values, and as can be deduced from (2.15), only for values of c greater than $1/\sqrt{2}$ the wire-bonded MTL is perfectly matched, at one, $c = 1/\sqrt{2}$ (c=-3 dB), or two frequencies $c > 1/\sqrt{2}$ (c <-3 dB). As a result, the wire-bonded MTL can be designed to have either a flat (θ_d=90^o) or a ripple response ($\theta_d \neq$90^o). This behaviour in frequency can be easily explained and understood if we think that the input port is only matched when equal power split between the coupled and direct ports is maintained ($|\alpha| = |\beta| = 1/\sqrt{2}$) and the superimposed signals at the input port are anti-phase and thus cancel (2.9)(2.14). Therefore, at the frequencies where the loaded wire-bonded MTL is matched, the coupling level α is always -3 dB, but only when θ_d=90^o happens that α=c=-3 dB. Consequently, it is clear that if we refer to c, an over-coupled wire-bonded MTL is required to have perfect match at a value of $\theta_d \neq \pi/2$ (α=-3 dB, c <-3 dB). If we analyze the wire-bonded MTL for $\theta = \theta_d$ (2.15), the following relations are obtained

$$\alpha_{\theta_d} = \frac{1}{\sqrt{2}} e^{j(\phi_{\theta_d} + \pi/2)}, \quad \beta_{\theta_d} = \frac{1}{\sqrt{2}} e^{j\phi_{\theta_d}}, \quad \phi_{\theta_d} = -\arctan\left(\sqrt{1 + 2\tan\theta_d^2}\right), \tag{2.16}$$

and consequently $|S_{11}|$=0 and $|S_{21}|$=1 (2.13). Finally, Fig. 2.3(b) represents the phase of S_{21} when $Z_L = \infty$ (ρ_L=1) and $Z_L = 0$ (ρ_L=-1) for several c values. It is noticeable that for a particular Z_L, all curves take the same value at θ=$\pi/2$, but their slope depend on c. Besides, it is seen that by controlling the reactive loads it is possible to adjust the phase of S_{21} regardless of the c value.

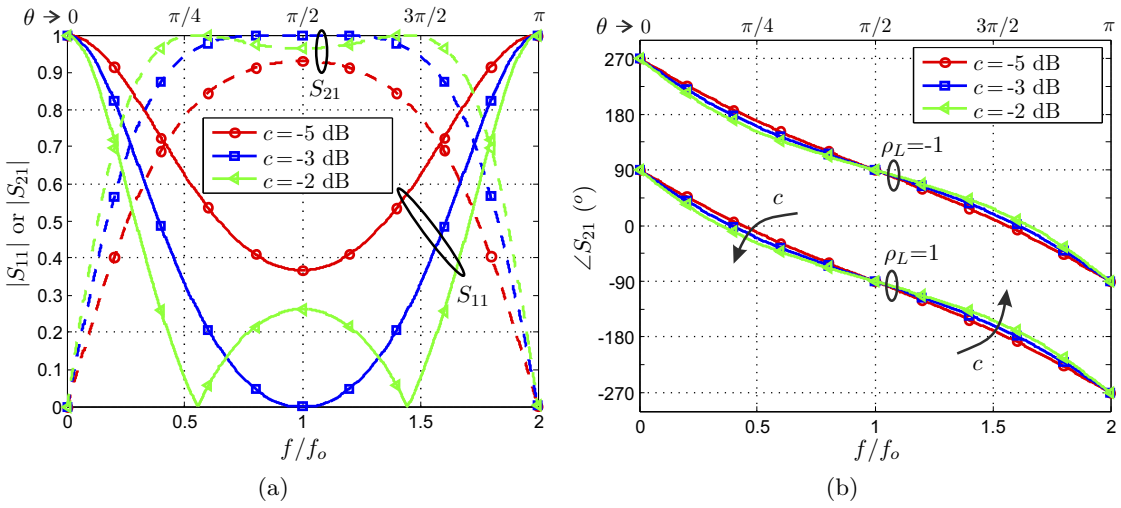

Figure 2.3.: (a) Magnitude of S_{11} and S_{21}, and (b) phase of S_{21} of a wire-bonded MTL designed by means of (2.7) with two identical reflection loads Z_L ($|\rho_L| = 1$) at its coupled and direct ports (Figure 2.1(b)) for several coupling values. For the phase of S_{21}, Z_L=∞ (ρ_L=1) and Z_L=0 (ρ_L=-1) have been used.

The preceding analysis is specially useful and provides some insight into the design of compact wire-bonded MTLs. As known, the operating bandwidth is maximum when the electrical length of the wire-bonded MTL is $\pi/2$ at the center design frequency, but a shorter MTL with perfect input match at the design frequency can be also achieved by means of (2.15). For example, if we want to use a wire-bonded MTL of length $\lambda/8$, the structure can be easily designed by solving (2.15) for θ_d=$\pi/4$. In that case, the necessary coupling factor c should be -1.76 dB and θ_d corresponds to the center frequency f_o. However, it is important to remark that this design solution has only relevance for narrow operating bandwidths because the symmetric bandwidth respect to the center design frequency will be reduced. This behaviour can be observed in Fig. 2.4(a), where the input and return loss of two wire-bonded MTLs designed for two coupling levels, -1 dB and -2 dB, and their associated bandwidths of operation are represented. The length of both MTLs is 0.085λ (θ=30.6^o) and 0.25λ (θ=90^o) at the design frequency f_o, for c=-1 dB and c=-2 dB, respectively. Therefore, the size of the -1 dB wire-bonded MTL is reduced by 66% compared to that of the -2 dB MTL, but its operating bandwidth is extremely narrowed. This design approach could be also used to obtain compact dual-band phase shifting sections, being θ_d and $\pi - \theta_d$ the electrical lengths at the dual design center frequencies.

However, it is worth to mention that these coupling factors imply some practical limitations in order to achieve the required high even- and odd-modes impedances values. Therefore, the use of wire-bonded MTLs is advisable to achieve such tight coupling factors that would be unapproachable with only two strips without any backside aperture. If k=2, by using the design equations (2.7), (2.11) and (2.15) for the wire-bonded MTL of length 0.085λ, it is obtained Z_{oe}=12 Ω and Z_{oo}=209 Ω as mode impedances. These values agree with the

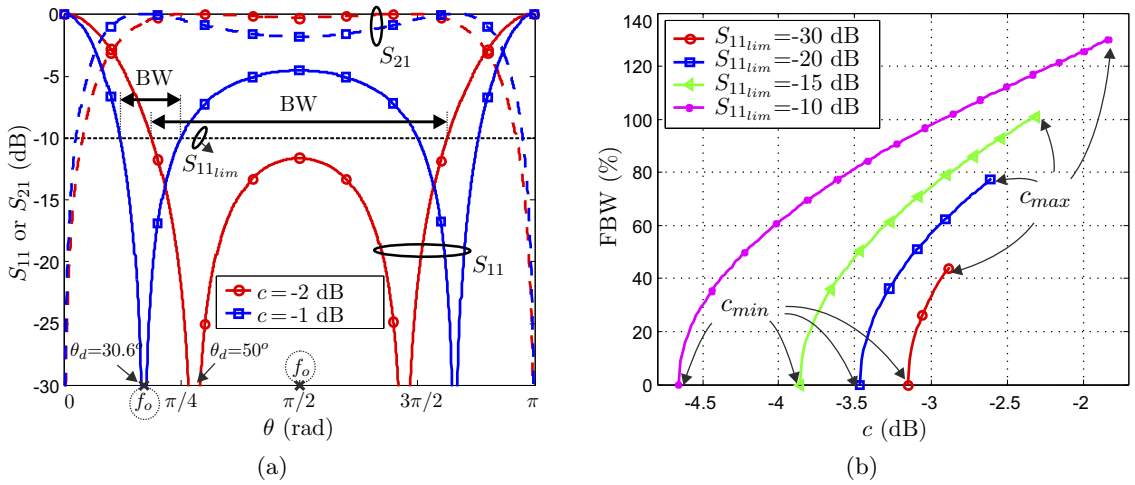

Figure 2.4.: (a) Magnitude of S-parameters and associated bandwidths (BW for S_{11} <-10 dB) for two wire-bonded MTLs with length 0.085λ and 0.25λ at the design frequency f_o. (b) Operating bandwidth of a quarter-wavelength wire-bonded MTL as a function of the coupling level that guarantees that the minimum insertion loss is under a threshold limit value $S_{11_{lim}}$(dB)=[-30, -20, -15, -10].

presented in [26], where a coupled structure of length 0.083 λ is employed. However, in [26] authors carry out a parametric study to obtain the values of such even- and odd-mode impedances for two lines, while in this work we provide general closed-form design equations that can be easily employed to obtain the mode impedances for any length and irrespective of the number of conductors.

From Fig. 2.3(a) and Fig. 2.4(a), we can also observe that if a quarter-wavelength wire-bonded MTL is considered at the design center frequency (θ=$\pi/2$), there are two limit coupling factors, minimum and maximum factors, in order to guarantee that return losses at mid-band frequency are under a threshold value. Being $S_{11_{lim}}$ the threshold limit value, the minimum and maximum allowed coupling factors can be computed as

$$c^2 = \frac{1 \mp S_{11_{lim}}}{2} \tag{2.17}$$

Thus from (2.17), if a typical limit value of $S_{11} = 10^{-1/2}$ (-10 dB) is used, we obtain c=-4.66 dB and c=-1.82 dB, approximately, as the limit coupling values that could be used to design the quarter-wave wire-bonded MTL. Furthermore, the associated bandwidths can be easily computed as

$$FBW(\%) = 200\left(1 - \frac{2}{\pi}\arccos\sqrt{\frac{2c^2 - 1 + S_{11_{lim}}}{c^2(1 + S_{11_{lim}})}}\right). \tag{2.18}$$

The result of evaluating (2.18) for several threshold limit values $S_{11_{lim}}$ is depicted in Fig. 2.4(b), where it is clear that the range of allowed coupling factors and the bandwidth

of operation are reduced as $S_{11_{lim}}$ decreases. Therefore, taking into account the presented study, it can be concluded that any coupling factor c within the limit values determined by (2.17) can be used for designing phase-shifting sections, but that there is a trade-off between the selected coupling factor and both, the bandwidth and the insertion loss.

2.3. Open- and Short-Circuited Wire-Bonded MTL

In previous section, a wire-bonded MTL loaded with reactive loads at the coupled and direct ports has been analyzed and some design rules have been deduced as a function of the coupling factor. However, in this point the study is extended for two particular arrangements, when two open or short circuits are used as loads. These two configurations are widely employed in designing filters, baluns, impedance transformers, DC blocks, interdigital capacitors, and spiral inductors [3–10]. Therefore, two general equivalent circuits for the open- and short-circuited wire-bonded MTL that provide some physical insight into their frequency behaviours and that can be easily used by designers, are obtained in this section.

By using the admittance matrix of a four-port wire-bonded MTL [17], and after some algebraic manipulations, it is straightforward to obtain the following equations for the two-port loaded wire-bonded MTLs,

$$[Z]_{oc} = j\frac{1}{N}\frac{c}{c+1}\cot\theta\begin{bmatrix}1 & 0\\ 0 & 1\end{bmatrix} - j\frac{1}{N}\frac{c^2}{c^2-1}\begin{bmatrix}\cot\theta & \csc\theta\\ \csc\theta & \cot\theta\end{bmatrix} \tag{2.19}$$

$$[Y]_{sc} = jN\frac{1-c}{c}\cot\theta\begin{bmatrix}1 & 0\\ 0 & 1\end{bmatrix} + jN\begin{bmatrix}\cot\theta & \csc\theta\\ \csc\theta & \cot\theta\end{bmatrix} \tag{2.20}$$

where Z and Y are the impedance and admittance matrices, and subscripts oc and sc stand for the open-circuited and short-circuited MTL, respectively. Now, from (2.19) and (2.20), it is worth to notice that both devices are equivalent to a circuit consisting of a transmission-line section with two stubs, series open stubs for the open-circuited MTL, and shunt short stubs for the short-circuited MTL. These equivalent circuits are shown in Fig. 2.5, where it is remarkable that, while the electrical length of the main line for the open-circuited MTL is θ, the equivalent transmission line for the short-circuited MTL is $\theta + \pi$. Therefore, there is an additional 180-degrees phase shift because of the short-circuited ends of the wire-bonded MTL [5].

The characteristic impedances of the main lines (Z_0) and stubs (Z_S) of the equivalent

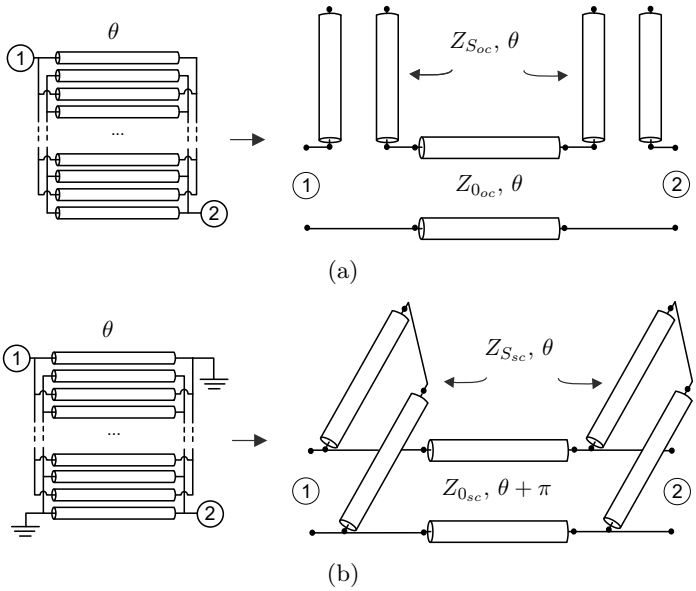

Figure 2.5.: Equivalent circuits for (a) open-circuited and (b) short-circuited wire-bonded MTLs.

circuits (see Fig. 2.5) for the open- and short-circuited wire-bonded MTLs are given by

$$Z_{0_{oc}} = \frac{-1}{N}\frac{c^2}{1-c^2} = \frac{(k-1)\,(Z_{oe}-Z_{oo})\,(Z_{oe}+Z_{oo})^2}{2\,[(k-1)Z_{oe}+Z_{oo}]\,[(k-1)Z_{oo}+Z_{oe}]} \tag{2.21a}$$

$$Z_{S_{oc}} = \frac{-1}{N}\frac{c}{1+c} = \frac{Z_{oo}\,(Z_{oe}+Z_{oo})}{(k-1)Z_{oe}+Z_{oo}} \tag{2.21b}$$

$$Z_{0_{sc}} = \frac{-1}{N} = \frac{2Z_{oe}Z_{oo}}{(k-1)\,(Z_{oe}-Z_{oo})} \tag{2.22a}$$

$$Z_{S_{sc}} = \frac{-1}{N}\frac{c}{1-c} = \frac{Z_{oe}\,(Z_{oe}+Z_{oo})}{(k-1)Z_{oo}+Z_{oe}}. \tag{2.22b}$$

When k=2, these equations simplify to

$$Z_{0_{oc}} = \frac{Z_{oe}-Z_{oo}}{2}, \quad Z_{S_{oc}} = Z_{oo}, \quad Z_{0_{sc}} = \frac{2Z_{oe}Z_{oe}}{Z_{oe}-Z_{oe}}, \quad Z_{S_{sc}} = Z_{oe}, \tag{2.23}$$

that are equal to the given in [3, 5] for a two-line coupled-line section. Furthermore, as can be seen in Fig. 2.5, when θ=90 degrees the stubs in both equivalent circuits appear as open circuit across the main transmission line [5]. Therefore, from (2.21a) and (2.22a), it is easy to deduce that a quarter-wavelength open- or short-circuited wire-bonded MTL is advisable to synthesize low- or high-impedance transmission line sections, respectively, with characteristic impedances $Z_{0_{oc}}$ and $Z_{0_{sc}}$.

In addition, it is important to remark another important property of both open- and

short-circuited wire-bonded MTLs: their duality. Both MTLs, when properly designed, are dual circuits and thus, are suited for implementing planar broadband baluns. In that sense, the equivalent circuits shown in Fig. 2.5, are useful to design both MTLs.

2.4. Experimental Results

To validate the theory and analysis carried out in Sections 2.2 and 2.3, two quarter-wavelength open-circuited and short-circuited wire-bonded MTLs with coupling factors of -3 dB and -2.6 dB, are designed, manufactured and measured at a design frequency of f_o=3.5 GHz with a characteristic impedance Z_0=50 Ω (2.7)(2.2)(2.11). These coupling factors, critical- and over-coupling levels, are computed according to (2.15) to have one or two frequencies of maximum input match within the operating frequency band at approximately θ_d=90^o and θ_d=65^o, respectively.

The employed substrate is Rogers 4350B with a relative permittivity of 3.66 and thickness of 30 mil. Two six-line (k=6) wire-bonded MTLs with a length of 13.6 mm are designed, the first one with a line-width (W) of 121 μm and spacing (S) of 131 μm for c=-3 dB, and the second one with W=114 μm and S=106 μm for c=-2.6 dB. The number of strips k is chosen taking into account the required tight coupling values and it is conditioned by our fabrication capability, which limits the minimum width W and spacing S between conductors to 100 μm.

Figure 2.6 represents the measured S-parameters for both open- and short-circuited MTLs. The magnitude of S_{11} and S_{21} parameters are depicted in Fig. 2.6(a) and Fig. 2.6(b), while the phase of S_{21} is shown in Fig. 2.6(c). From these curves, it is possible to observe the very good agreement between the theory presented in Section 2.2 and the measurements. The theoretical operating bandwidths, computed by means of (2.18) and considering S_{11}=-10 dB as the threshold limit value, are 97 % and 109 % for c=-3 dB and c=-2.6 dB, respectively. The measured bandwidths, by using the same threshold limit value, are 92 % and 106 %, that are very close to the maximum theoretical bandwidths. The small differences between the theoretical and measured results, that are mainly derived from fabrication tolerances, allow the accuracy of the analytical design equations to be validated. Therefore, by changing the loads at the direct and coupled ports the phase shift is adjusted and the larger the coupling factor, the broader the operating bandwidth. There is a slight shift towards low frequencies in the S-parameters of the open-circuited MTL because the open-end effect (small extra length) has not been compensated.

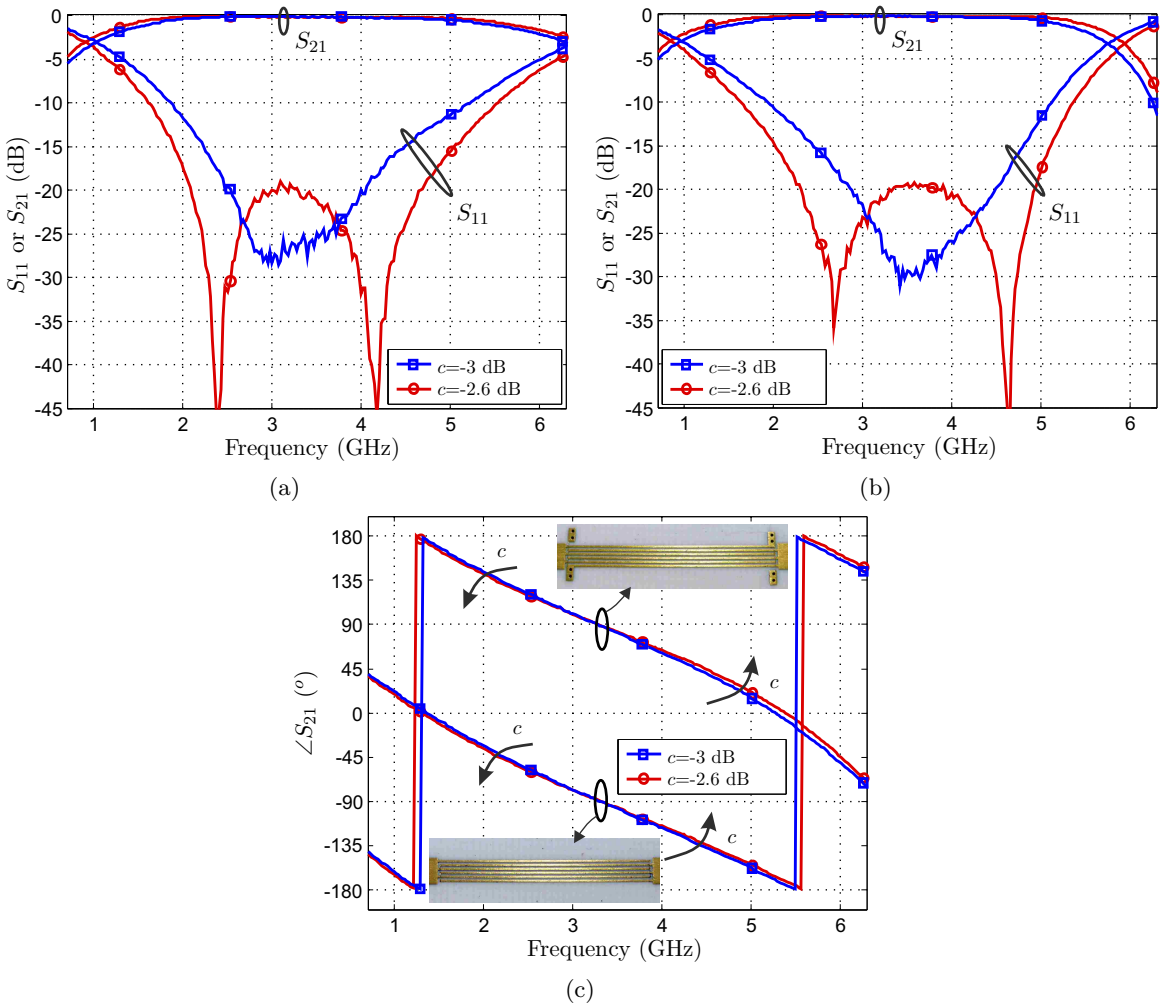

Figure 2.6.: Measured magnitude of S_{11} and S_{21} of the manufactured six-line (a) open-circuited and (b) short-circuited wire-bonded MTLs. (c) Phase of S_{21} for the fabricated open- and short-circuited MTLs (c=[-2.6,-3] dB).

2.5. Conclusion

In this chapter a comprehensive analysis of wire-bonded MTL-based phase-shifting sections has been presented. Analytical design equations as a function of the coupling factor has been given in order to obtain time-saving design procedures and wide frequency band of operation. It has been proved that by connecting two equal reactive loads to the coupled and direct ports of a wire-bonded MTL it is possible to control the phase shift. In that sense, the advantage of using more than two conductors is noticeable in order to achieve higher values of coupling and broader bandwidths because to obtain tight coupling values using only two strips, the spacing between the lines becomes too small to be implemented. Besides, two new equivalent circuits for the widely used open- and short-circuited wire-bonded MTL have been proposed. These equivalent circuits are useful and advisable for designing filters,

baluns, impedance transformers, and other microwave circuits. The analytical study carried out has been assessed by designing and manufacturing two critical- and over-coupling open- and short-circuited wire-bonded MTLs.

References

[1] R. Garver, "Broad-band diode phase shifters," *IEEE Trans. Microw. Theory Tech.*, vol. 20, no. 5, pp. 314 – 323, May 1972.

[2] I. D. Robertson and S. Lucyszyn, *RFIC and MMIC Design and Technology.* London, UK: IEE Press, 2001.

[3] G. L. Mattahei, L. Young, and E. M. T. Jones, *Microwave Filters, Impedance-Matching Networks, and Coupling Structures*, M. A. House, Ed. Norwood, 1985.

[4] D. Pozar, *Microwave Engineering*, 2nd ed. New York: Wiley, 1998.

[5] R. Mongia, I. Bahl, and P. Bhartia, *RF and Microwave Coupled-Line Circuits.* Norwood, MA: Artech House, 1999.

[6] J. J. Sánchez-Martínez and E. Márquez-Segura, "Generalized analytical design of broadband planar baluns based on wire-bonded multiconductor transmission lines," *Progr. Electromagn. Res.*, vol. 134, pp. 169–187, 2013.

[7] J. J. Sánchez-Martínez, E. Márquez-Segura, P. Otero, and C. Camacho-Peñalosa, "Artificial Transmission Line with Left/Right-Handed Behavior Based on Wire Bonded Interdigital Capacitors," *Progr. Electromagn. Res. B*, vol. 11, pp. 245–264, 2009.

[8] A. Safwat and T. M. Abuelfadl, "Coupled lines from filter to composite right/left handed-cells," *Progr. Electromagn. Res. B*, vol. 26, pp. 451–469, 2010.

[9] J. J. Sánchez-Martínez and E. Márquez-Segura, "Analytical Study of Wide-band Bandpass Filters Based on Wire-Bonded Multiconductor Transmission Lines With LH Behaviour," *Progr. Electromagn. Res. Lett.*, vol. 31, pp. 1–13, 2012.

[10] J. J. Sánchez-Martínez, E. Márquez-Segura, and C. Camacho-Peñalosa, "Synthesis of CRLH-TLs Based on a Shunt Coupled-line Section," in *42nd European Microwave Conference (EuMC)*, Oct. 2012, pp. 675–678.

[11] Z.-Y. Zhang, Y.-X. Guo, L. C. Ong, and M. Chia, "A new wide-band planar balun on a single-layer pcb," *IEEE Microw. Wireless Compon. Lett.*, vol. 15, no. 6, pp. 416–418, Jun. 2005.

[12] C.-H. Tseng and C.-L. Chang, "Wide-band balun using composite right/left-handed transmission line," *Electron. Lett.*, vol. 43, no. 21, pp. 1154–1155, Nov. 2007.

[13] R. Phromloungsri, M. Chongcheawchamnan, and I. Robertson, "Inductively compensated parallel coupled microstrip lines and their applications," *IEEE Trans. Microw. Theory Tech.*, vol. 54, no. 9, pp. 3571–3582, Sep. 2006.

[14] J.-L. Li and S.-W. Qu, "Miniaturised branch-line balun with bandwidth enhancement," *Electron. Lett.*, vol. 43, no. 17, pp. 931–932, Aug. 2007.

[15] J. A. B. Faria, *Multiconductor Transmission-line Structures: Modal Analysis Techniques.* New York: Wiley, 1993.

[16] C. R. Paul, *Analysis of Multiconductor Transmission Line.* New York: Wiley, 1994.

[17] W. Ou, "Design Equations for an Interdigitated Directional Coupler," *IEEE Trans. Microw. Theory Tech.*, vol. 23, no. 2, pp. 253–255, Feb. 1975.

[18] C.-S. Lin, P.-S. Wu, M.-C. Yeh, J.-S. Fu, H.-Y. Chang, K.-Y. Lin, and H. Wang, "Analysis of multiconductor coupled-line marchand baluns for miniature mmic design," *IEEE Trans. Microw. Theory Tech.*, vol. 55, no. 6, pp. 1190–1199, Jun. 2007.

[19] D. Kajfez and B. Vidula, "Design equations for symmetric microstrip dc blocks," *IEEE Trans. Microw. Theory Tech.*, vol. 28, no. 9, pp. 974–981, Sep. 1980.

[20] F. Casares-Miranda, P. Otero, E. Márquez-Segura, and C. Camacho-Peñalosa, "Wire Bonded Interdigital Capacitor," *IEEE Microw. Wireless Compon. Lett.*, vol. 15, no. 10, pp. 700–702, Oct. 2005.

[21] E. Márquez-Segura, F. Casares-Miranda, P. Otero, C. Camacho-Peñalosa, and J. Page, "Analytical Model of the Wire-Bonded Interdigital Capacitor," *IEEE Trans. Microw. Theory Tech.*, vol. 54, no. 2, pp. 748–754, Feb. 2006.

[22] J. Page, E. Márquez-Segura, F. Casares-Miranda, J. Esteban, P. Otero, and C. Camacho-Peñalosa, "Exact Analysis of the Wire-Bonded Multiconductor Transmission Line," *IEEE Trans. Microw. Theory Tech.*, vol. 55, no. 8, pp. 1585–1592, Aug. 2007.

[23] A. Presser, "Interdigitated microstrip coupler design," *IEEE Trans. Microw. Theory Tech.*, vol. 26, no. 10, pp. 801–805, Oct. 1978.

[24] S. Lucyszyn and I. Robertson, "Synthesis techniques for high performance octave bandwidth 180 deg; analog phase shifters," *IEEE Trans. Microw. Theory Tech.*, vol. 40, no. 4, pp. 731 –740, Apr. 1992.

[25] ——, "Analog reflection topology building blocks for adaptive microwave signal processing applications," *IEEE Trans. Microw. Theory Tech.*, vol. 43, no. 3, pp. 601 –611, Mar. 1995.

[26] A. Abbosh, "Compact tunable reflection phase shifters using short section of coupled lines," *IEEE Trans. Microw. Theory Tech.*, vol. 60, no. 8, pp. 2465–2472, Aug. 2012.

Chapter 3

Baluns

THE theoretical analysis presented in Chapter 2 emphasizes the worth of employing open- and short-circuited wire-bonded MTLs to design wideband baluns with good input match, amplitude and phase balance. Thus, in Section 3.2 a novel generalized design procedure of broadband planar baluns based on wire-bonded multiconductor transmission lines (MTL) is presented. The proposed balun consists of two parts. The first one is an in-phase power divider, which equally splits the input power through its two outputs. The later are two MTLs with wire bonding between alternate conductors configured to introduce +90 and -90 degrees phase shift respectively, so that the balanced output signal has a 180 degree phase difference. In Section 3.2.2 design equations in order to calculate the design parameters of both multiconductor elements are obtained. These equations allow the proper dimensions of both MTLs to be computed irrespective of the number of conductors and the coupling factor. Thus, in Section 3.2.4, a prototype of such balun is fabricated to validate the theory.

Finally, a reconfigurable test set for the characterization of differential devices by using a commercial two-port vector network analyzer is presented in Section 3.3. The MTL balun is used to convert single-ended input signals to differential signals, providing the required good port matching and high reverse isolation.

3.1. Introduction

Baluns are important 3-port devices necessary for feeding differential devices such as two-wire antennas, balanced mixers, push-pull amplifiers, balanced modulators, and many other applications. The primary function of a balun is to convert an unbalanced input signal into a balanced differential output one. Many different balun topologies have been proposed in

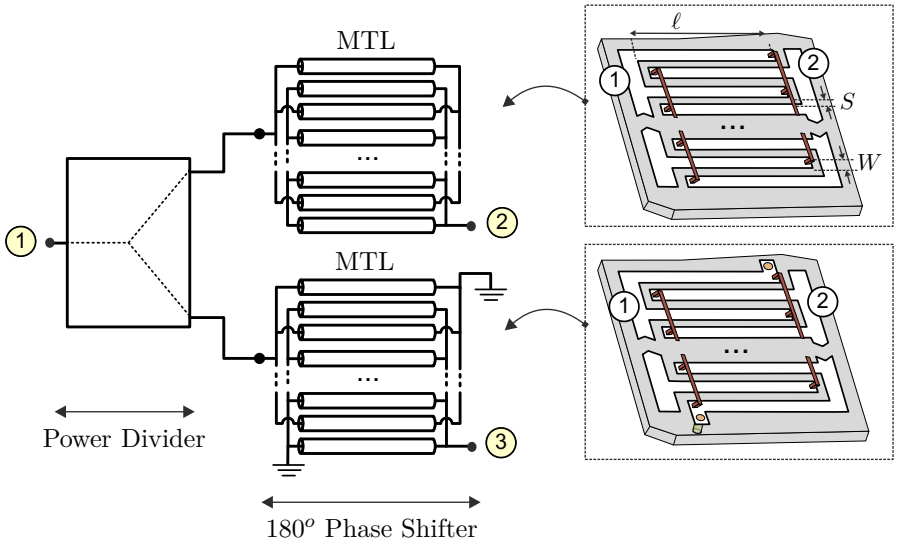

Figure 3.1.: Architecture of the balun consisting of an in-phase power divider and two wire-bonded multiconductor transmission lines. A snapshot of a wire-bonded MTL in microstrip technology is included.

the literature, but it is possible to establish two main groups. The first group comprises those baluns that consists of an equal in-phase power divider connected to a phase-shifting section to achieve the required 180-degree phase difference at the output ports. The second group consists of baluns that are designed from a symmetric four-port circuit with one of its ports open-circuited, short-circuited or loaded with an arbitrary impedance. Within the first group, some examples can be found in [1–3]. In [1], a noncoupled-line 180^o phase shifter was connected to the outputs of the divider and a composite right/left-handed transmission line was used in [2, 3]. However, the main drawback of these baluns is to achieve a good phase balance in a wide frequency band. Respect to the second group, we can include Marchand baluns [4–12], branch-line baluns [13, 14] and other circuits based on the same principle [15–18]. Among these baluns, Marchand baluns are probably the most popular. Marchand balun consists of two sections of quarter-wavelength coupled lines and in order to broaden the bandwidth a strong coupling level for the two coupled-line sections is required [19]. However, the main limitation is its poor balanced output ports matching and isolation. Therefore, based on the theory and new equivalent circuits developed in Chapter 2, it is proved that wire-bonded MTL-based baluns overcome most of the awkward limitations of recently published baluns.

In this work, a planar balun configuration consisting of two sections is considered (Fig. 3.1). The first section is a power divider which provides two well-balanced equal amplitude in-phase signals over a broad frequency range. The second section provides -90 degrees and +90 degrees phase shift over these two signals, so the balanced output signals have a 180 degree phase difference [1, 2, 20–22] . A Wilkinson in-phase power divider has been usually employed for the power splitter due to its broadband operation and good input/output match and

isolation. The last condition improves the main Marchand balun drawback, its poor balanced output ports matching and isolation [23]. For the phase shifter section, short-circuited and open-circuited coupled lines have been employed in [20] and [21] but, there is lack of both a design procedure and analysis for wire-bonded multiconductor transmission lines (MTL). The presented balun circumvents the limited output isolation and narrow operating bandwidth of most of the recently published baluns. Consequently, the use of wire-bonded MTLs is advisable in designing wideband baluns because both short- and open-circuited MTLs are dual components (see Fig. 2.6), and if they are properly designed a perfect theoretical output amplitude and phase balance can be achieved at all frequencies.

3.2. Analysis and Design Procedure

3.2.1. Balun Architecture

The circuit schematic of the proposed planar balun, consisting of a power divider connected to two wire-bonded multiconductor transmission lines, is sketched in Fig. 3.1. The power divider splits the input signal into two equal amplitude in-phase signals. Then, the two output signals pass through a pair of short-circuited and open-circuited MTLs configured to introduce +90 and -90 degrees phase shift respectively, over each signal. Therefore, output signals have equal amplitude and 180 degrees phase difference. According to the power divider, the Wilkinson divider seems to be a good choice because it provides equal power split, high output ports isolation and good match at all three ports. Besides, the Wilkinson can be designed with multiple stages in order to enlarge its bandwidth and fulfill the frequency band requirements.

3.2.2. Theoretical Study

A wire-bonded multiconductor transmission line is a four-port device and its input admittance matrix can be found in [24]. By placing open- or short-circuits at its diagonal ports, the two-port circuits drawn in the insets of Fig. 3.1 are obtained. These two circuits were previously analyzed in Section 2.3 and two equivalent circuit models were derived. Nevertheless, the study carried out in this section gives us some insights into the physical behaviour of both MTLs and provides the necessary analytical equations to properly design the proposed balun.

When losses are neglected and coupling between non adjacent strips is negligible, both devices are characterized by the following admittance matrices

$$[Y]_o = \frac{(M^2 - N^2)\sin\theta}{M^2\cos^2\theta - N^2}\begin{bmatrix} jM\cos\theta & jN \\ jN & jM\cos\theta \end{bmatrix} \tag{3.1}$$

$$[Y]_s = \frac{1}{\sin\theta}\begin{bmatrix} -jM\cos\theta & jN \\ jN & -jM\cos\theta \end{bmatrix}, \tag{3.2}$$

where the subscripts o and s stand for the open-circuit or short-circuit boundary conditions respectively. θ is the electrical length of the conductors (2.5), and M and N, defined in (2.2), can be written as

$$M = \frac{(k-1)(Z_{oe}^2 + Z_{oo}^2) + 2Z_{oe}Z_{oo}}{2(Z_{oe}+Z_{oo})Z_{oe}Z_{oo}}, \quad N = \frac{(k-1)(Z_{oo}-Z_{oe})}{2Z_{oe}Z_{oo}}, \tag{3.3}$$

where Z_{oe} and Z_{oo} are the odd and even modes impedances of a pair of adjacent lines and k relates to the number of strips. It is important to remark that in previous equations it has been considered that both wire-bonded MTLs are equal and only the boundary conditions, short-circuit or open-circuit, are changed. Besides, pure TEM and lossless propagation are assumed, being θ the average value of the even- and odd-mode electrical lengths (Section 2.2).

The propagation constant of the two-port structures obtained can be calculated from (3.1) and (3.2) as [25]

$$\cosh(\gamma\ell) = \frac{(Y_{11}Y_{22})^{1/2}}{Y_{21}}, \tag{3.4}$$

being ℓ the length of the MTL. When both wire-bonded MTLs are assumed lossless (3.4) is simply given by

$$\beta_o\ell = \cos^{-1}\left(-\frac{M}{N}\cos\theta\right), \quad \beta_s\ell = \cos^{-1}\left(\frac{M}{N}\cos\theta\right) \tag{3.5}$$

where clearly it is observed that $\beta_s = \beta_o + \pi$. Thus, the output signals of the open- and short-circuited MTLs are always 180 degree out-of-phase at all frequencies. Nevertheless, such equations are deduced considering that input and output ports are perfectly matched. The image impedances of both circuits can be calculated from (3.1) and (3.2) as

$$Z_{I_o} = \frac{(N^2 - M^2\cos^2\theta)^{1/2}}{(M^2-N^2)\sin\theta}, \quad Z_{I_s} = \frac{\sin\theta}{(N^2 - M^2\cos^2\theta)^{1/2}} \tag{3.6}$$

As seen, both image impedances are different and depend on the electrical length of the MTL. Consequently, it is necessary to find out some design rule in order to obtain 180 degrees differential phase and equal amplitude outputs. By means of simple transformations [25] and after some algebraic manipulations, the reflection S_{11} and transmission S_{21} coefficients of each wire-bonded MTL (see the insets in Fig. 3.1) are given by

$$S_{11_i} = \frac{K_i^2(N^2 - M^2\cos^2\theta) - Z_0^2}{\Delta_i} \tag{3.7a}$$

$$S_{21_i} = \frac{2G_iK_iZ_0N}{j\Delta_i}, \tag{3.7b}$$

where Z_0 is the reference impedance, the subindex i can be o or s depending on whether the S-parameters of the open-circuited MTL or short-circuited MTL are evaluated, and the

variables Δ_i, K_i and G_i are defined as

$$\Delta_i = K_i^2(N^2 - M^2\cos^2\theta) + Z_0^2 + j2K_iZ_0M\cos\theta \tag{3.8a}$$

$$K_o = \frac{1}{(N^2 - M^2)\sin\theta}; \qquad G_o = +1 \tag{3.8b}$$

$$K_s = \frac{\sin\theta}{M^2\cos^2\theta - N^2}; \qquad G_s = -1. \tag{3.8c}$$

These expressions are useful because valuable information as frequency response, operating bandwidth, phase balance, etc. can be easily calculated. If the condition

$$|S_{21_o}|e^{j\phi} = |S_{21_s}|e^{j(\phi+\pi)} \tag{3.9}$$

is imposed on (3.7b), the next equality is obtained

$$Y_0^2 = M^2 - N^2 = Y_{oe}Y_{oo}\frac{([(k-1)+u][(1+u(k-1)]}{(1+u)^2}, \tag{3.10}$$

which determines a specific relation between the even and odd mode impedances, being $u = Z_{oe}/Z_{oo}$. Therefore, whenever equation (3.10) is fulfilled, the output signals have equal amplitude and a phase difference of 180 degrees. Nevertheless, although output signals have equal amplitude, it does not imply to have a good impedance matching. Consequently, another condition related to port matching is necessary. Substituting (3.10) in (3.7a), it is found that

$$\cos^2\theta_d = 2 - \frac{M^2}{N^2} = 2 - \frac{1}{c^2} = 2 - \left(\frac{2u + (k-1)(1+u^2)}{(k-1)(1-u^2)}\right)^2, \tag{3.11}$$

where θ_d stands for the electrical length at which the MTL is match-terminated (S_{11}=0). Note that these equations (3.10) and (3.11), which have been calculated directly from the S-parameters of both structures, are equal to the given in previous chapter for the design of phase shifters. However, herein the study is extended to these two particular arrangements. Accordingly, there are two design equations: by using (3.10) a good amplitude and phase balance is guaranteed, and by means of (3.11) it is straightforward to control the point of perfect match of both short- and open-circuited MTLs. This implies that the image impedance of both structures is equal to the reference impedance Z_0 at θ_d. By evaluating (3.10), Fig. 3.2 represents the required coupling factors as a function of θ_d. As seen, only for θ_d=90^o the value of c is unique and equal to -3 dB, and for another higher value, the MTL will have two ideal input match frequencies within the operating frequency band.

Equation (3.11) can be expressed as

$$u = \frac{Z_{oe}}{Z_{oo}} = \frac{1 + \sqrt{(1 + (k-1)^2\sin^2\theta_d}}{(k-1)\left(\sqrt{1+\sin^2\theta_d} - 1\right)}, \tag{3.12}$$

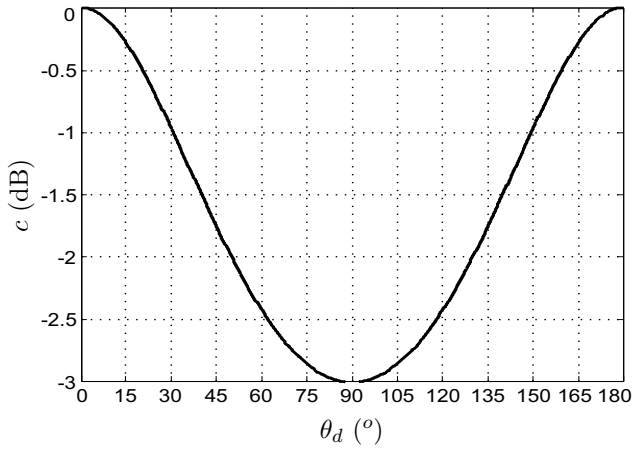

Figure 3.2.: Required coupling factor (c) to achieve a perfect match at θ_d (3.10).

that, given the number of strips k, allows the values of u to get a perfect input match at θ_d to be calculated. Consequently, once the $u = Z_{oe}/Z_{oo}$ ratio has been chosen taking into account (3.12), equation (3.10) can be split as

$$\frac{Z_{oe}}{Z_0} = \frac{\sqrt{u[(k-1)+u][1+u(k-1)]}}{(1+u)} \tag{3.13a}$$

$$\frac{Z_{oo}}{Z_0} = \frac{\sqrt{[(k-1)+u][1+u(k-1)]}}{\sqrt{u}(1+u)}, \tag{3.13b}$$

in order to compute the proper values of the even- and odd-mode impedances that guarantee an ideal output amplitude and phase balance at all frequencies, and a perfect input match at one (θ_d=90^o) or two single frequencies ($\theta_d \neq$90^o).

If the aforementioned design procedure is followed, some expressions can be simplified. Firstly, M and N can be rewritten as

$$\frac{M^2}{Y_0^2} = \frac{1+\sin^2\theta_d}{\sin^2\theta_d}, \qquad \frac{N^2}{Y_0^2} = \frac{1}{\sin^2\theta_d}, \tag{3.14}$$

where $Y_0 = 1/Z_0$. From (3.14), the most remarkable property is that neither M nor N no longer depend on the number of conductors and are determined by only a function of θ_d. Therefore, regardless of the number of conductors, if the even and odd mode impedances Z_{oe} and Z_{oo} are selected according to (3.12) and (3.13), all previous equations are drastically simplified. Hence, expressions for the image impedances (3.6) are reduced to

$$\frac{Z_{I_o}}{Z_0} = \left(1+\frac{\sin^2\theta-\sin^2\theta_d}{\sin^2\theta\ \sin^2\theta_d}\right)^{1/2} \qquad \frac{Z_{I_s}}{Z_0} = \left(1+\frac{\sin^2\theta-\sin^2\theta_d}{\sin^2\theta\ \sin^2\theta_d}\right)^{-1/2}. \tag{3.15}$$

Fig. 3.3 represents the real part of both normalized impedances as a function of θ for several values of θ_d. As seen, only for θ=θ_d curves are equal to unity and thus, the impedance matching is perfect. Besides, two singularities are observed, θ_1 and θ_2, which are the poles

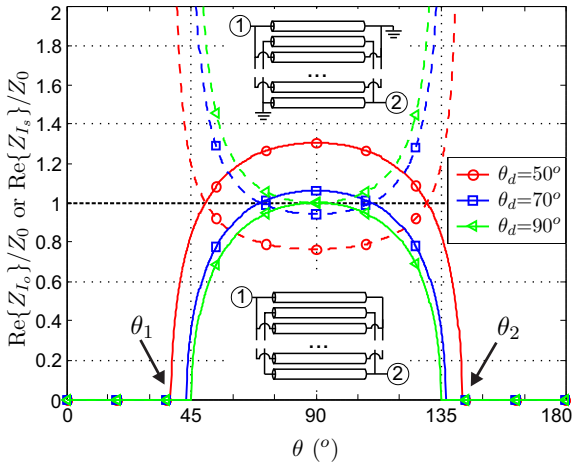

Figure 3.3.: Real part of normalized image impedances for two short- and open-circuited MTL designed by means of (3.12) and (3.13) as a function of θ for several number of θ_d (frequencies of ideal match).

of both functions in (3.15) and determine the frequency range where the image impedances pass from being purely real impedances to purely imaginary, capacitive and inductive reactances for the short-circuited and open-circuited elements, respectively. These singularities are calculated as

$$\theta_1 = \arccos\left(\frac{|N|}{M}\right) = \arccos\left(\frac{1}{\sqrt{1+\sin^2\theta_d}}\right), \quad \theta_2 = 180^o - \theta_1. \tag{3.16}$$

For the particular case θ_d=90^o, θ_1=45^o and thus, the frequency band of real impedances ranges from θ_1=45^o up to θ_2=135^o. From (3.14), equations for S-parameters, (3.7a) and (3.7b), can be also simplified as

$$S_{11_o} = \frac{\sin^2\theta - \sin^2\theta_d}{P - jQ} \qquad S_{11_s} = \frac{-\sin^2\theta + \sin^2\theta_d}{P - jQ} \tag{3.17a}$$

$$S_{21_o} = \frac{2\sin\theta\ \sin\theta_d}{Q + jP} \qquad S_{21_s} = \frac{-2\sin\theta\ \sin\theta_d}{Q + jP}, \tag{3.17b}$$

with

$$P = \sin^2\theta + \sin^2\theta_d(1-2\cos^2\theta) \tag{3.18a}$$

$$Q = \sin(2\theta)\sin\theta_d\sqrt{1+\sin^2\theta_d}. \tag{3.18b}$$

By analyzing (3.17a) and (3.17b) it is easy to observe that S_{11} and S_{21} parameters have equal magnitude but a phase difference of 180 degrees for the short- and open-circuited MTL. Moreover, a new simplification can be obtained to compute the magnitude of such parameters

Table 3.1.: Normalized Z_{oe} and Z_{oo} to get balanced equal amplitude out-of-phase output signals and perfect match at θ_d.

$\frac{Z_{oe}}{Z_0}$, $\frac{Z_{oo}}{Z_0}$	k=2	k=4	k=6	k=8	k=10
θ_d=50^o	2.95	4.02	5.40	6.84	8.30
	0.34	0.89	1.41	1.93	2.44
θ_d=60^o	2.68	3.78	5.14	6.55	7.98
	0.37	0.97	1.52	2.07	2.62
θ_d=70^o	2.52	3.63	4.98	6.37	7.78
	0.40	1.01	1.60	2.17	2.74
θ_d=80^o	2.44	3.55	4.89	6.27	7.67
	0.41	1.04	1.64	2.22	2.81
θ_d=90^o	2.41	3.52	4.86	6.24	7.64
	0.41	1.05	1.65	2.24	2.83

as

$$|S_{11_o}| = |S_{11_s}| = \frac{|\sin^2\theta - \sin^2\theta_d|}{\sin^2\theta + \sin^2\theta_d} \tag{3.19a}$$

$$|S_{21_o}| = |S_{21_s}| = 2\,\frac{|\sin\theta\ \sin\theta_d|}{\sin^2\theta + \sin^2\theta_d}, \tag{3.19b}$$

which, compared to (3.7a) and (3.7b), are valuable equations by their simplicity. These expressions will be used in next sections to evaluate the performance of both MTLs.

3.2.3. Bandwidth Considerations

In this point, the design procedure described in section 3.2.2 is evaluated. Firstly, the $u = Z_{oe}/Z_{oo}$ values to achieve perfect match at several θ_d are computed by means of (3.12). Then, using (3.13) the even and odd mode normalized impedances are obtained. Table 3.1 collects all these values for several number of strips, which can be directly translated to physical dimensions making previously a de-normalization operation by Z_0.

By using the values given in Table 3.1, Fig. 3.4(a) and Fig. 3.4(b) draws the S_{11} (3.19a) and S_{21} (3.19b) parameters. As expected, perfect match and thus, the minimum of S_{11}, is located at θ_d and, only for θ_d=90^o the S_{21} presents a maximally flat response. For any other value of θ_d a rippled response is obtained. In addition, to verify that both parameters are equal in magnitude but with 180 degrees out-of-phase for the short- and open-circuited wire-bonded MTL, Fig. 3.5 draws S_{11} and S_{21} on a Smith chart for two values of θ_d, 50^o and 90^o.

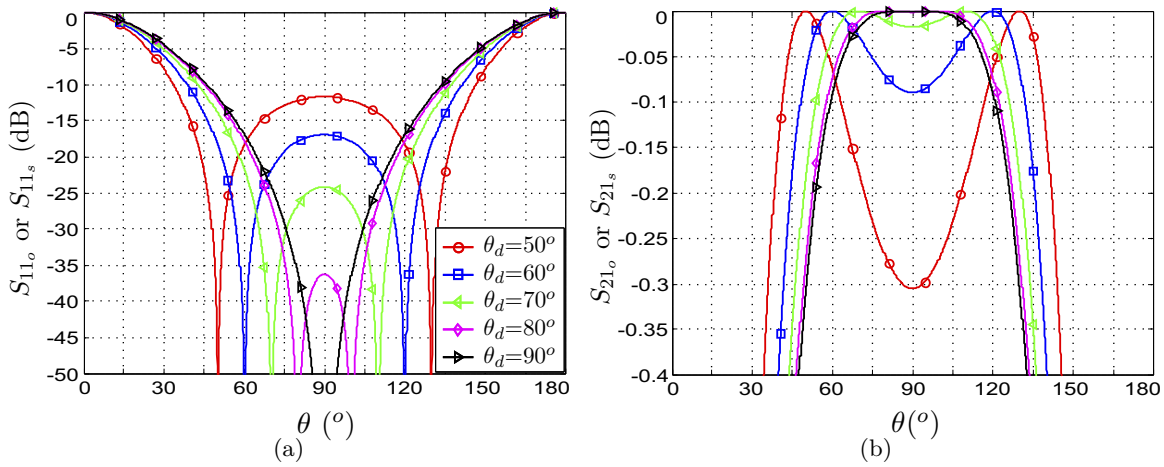

Figure 3.4.: S_{11} (a) and S_{21} (b) of two short- and open-circuited MTL designed using values of Table 3.1 as a function of θ for several θ_d.

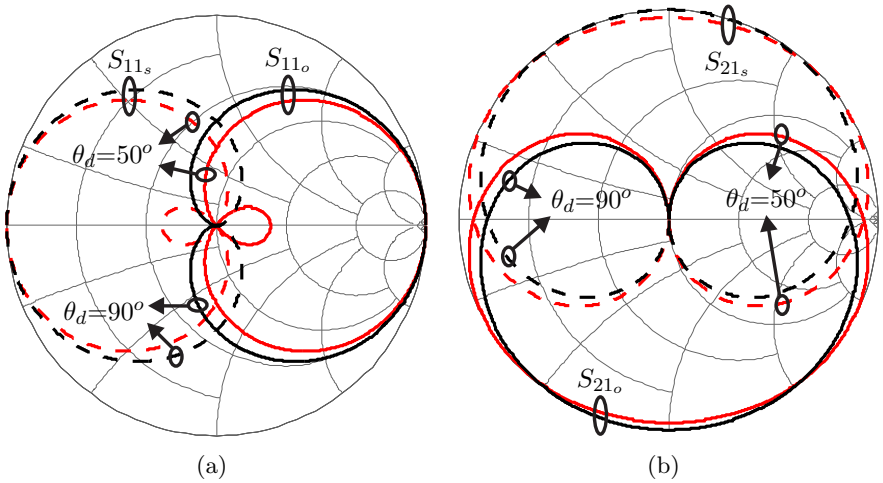

Figure 3.5.: S_{11} (a) and S_{21} (b) of two short- and open-circuited MTL designed using values of Table 3.1 as a function of θ for θ_d=[50^o, 90^o].

The magnitude of the ripple of S_{21} can be calculated at θ=90^o in (3.19b), or equivalently, from (3.19a) it is possible to determine the magnitude of S_{11} at θ=90^o and thus, to set a return loss limit. Considering $S_{21_{lim}}$=$\sqrt{0.9}$ ($S_{11_{lim}}$=-10 dB) as the conventional threshold limit value at the center frequency (θ=90^o), it is easy to obtain that $\theta_{d_{lim}}$=46.1^o is the limit value that could be used. This value can be computed as

$$\theta_{d_{lim}} = \arcsin\left(\frac{1-\sqrt{1-S_{21_{lim}}^2}}{S_{21_{lim}}}\right). \tag{3.20}$$

Fig. 3.6 depicts the operating fractional bandwidth as a function of θ_d, of a pair of short- and open-circuited wire-bonded MTLs that guarantees insertion loss lower than 0.9 dB, return

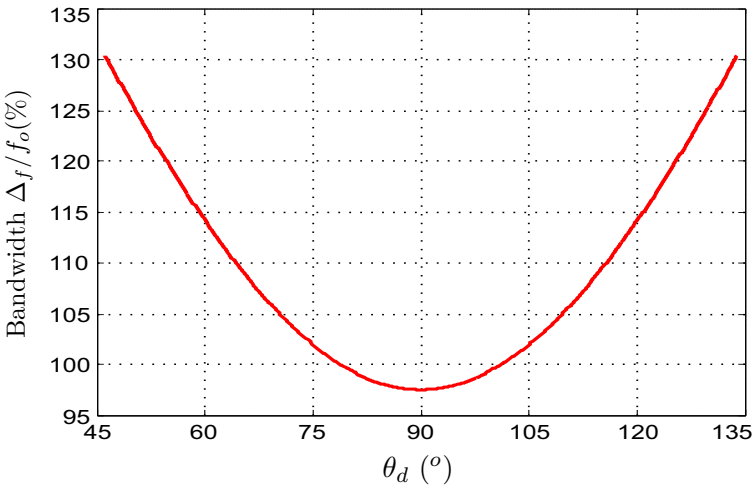

Figure 3.6.: Fractional bandwidth for two open- and short-circuited MTLs designed by means of (3.12) and (3.13) as a function of θ_d that guarantees S_{21} >-0.9 dB, S_{11} <-10 dB, and a phase difference of 180^o at their outputs.

loss higher than 10 dB and a perfect amplitude and phase balance at all frequencies. As seen in Fig. 3.6, the minimum bandwidth is achieved at θ_d=90^o and it broadens as θ_d separates from such value. Consequently, in order to broaden the operating bandwidth, both MTLs should be designed to have two ideal input match frequencies ($\theta_d \neq$90^o). However, as it was shown in Fig. 3.2, this involves increasing the coupling level. As a result, there is a trade-off between the operating frequency band of both MTLs and the required coupling level.

3.2.4. Experimental Validation

In this section, to demonstrate the proposed design methodology and show the goodness of using wire-bonded MTLs for designing baluns, a broadband balun is designed and manufactured. Firstly, the 180^o phase shifting section is analyzed, and after that, it is connected to a power divider to build the complete system. The divider is a three-section Wilkinson power divider designed to provide equal power split between the two outputs [26]. The use of a multi-stage Wilkinson power divider is necessary to guarantee a bandwidth larger than the one of the MTL structures, but thanks to this, it is possible to obtain an excellent output isolation. Consequently, depending on the application, this property may be more important than its size. Most of the balun configurations that can be found in the literature neglect this issue, but for some applications the output isolation is as important as the output amplitude and phase balance. Besides, for narrower bandwidths, the number of stages of the Wilkinson divider can be reduced. Thus, as it will be shown, this balun circumvents the limited output isolation and narrow operating bandwidth of most of the recently published baluns. The prototype is implemented in microstrip technology on a Rogers 4350B substrate with relative permittivity of 3.66 and thickness of 30 mil at a design frequency f_o=3.5 GHz.

The design of the pair of wire-bonded MTLs consists in finding out the number of strips k,

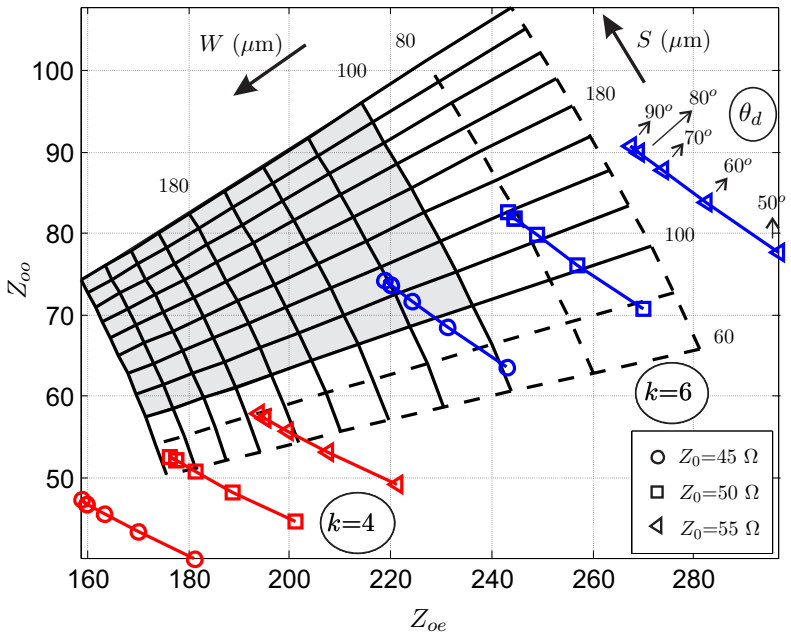

Figure 3.7.: Achieved even and odd mode impedances as functions of the width W and spacing S between a pair of adjacent parallel transmission lines on the substrate RO4350B with ϵ_r=3.66 and thickness of 30 mil. The design values of impedances for k=[4,6], θ_d=[90, 80, 70, 60, 50] degrees and Z_0=[45, 50, 55] Ω are also depicted. The design values are labeled with circle, square and triangle marks.

the line-width W and spacing S in order to satisfy (3.12) and (3.13), equations that depend on both θ_d and Z_0. Therefore, by using [27] and the considerations given in [28], the achieved even and odd mode impedances for different W, S and k=4,6 are represented in Fig. 3.7. The theoretical values obtained by means of (3.12) and (3.13), considered as the design parameters and identified by circle, square and triangle marks, are also depicted for three impedance characteristics Z_0 (45, 50, 55) and five θ_d (90^o, 80^o, 70^o, 60^o, 50^o). Hence, from this graph, once k, Z_0 and θ_d are chosen, the proper dimensions for the MTLs can be easily extracted. The shaded regions identify the allowed W and S values considering 100 μm as the limit dimension according to our fabrication capability. Design parameters for k=2 or k >6 are not represented because the required design impedances Z_{oe} and Z_{oo} for such number of conductors are very far from the obtained with the allowed W and S values (>100 μm). In addition, given Fig. 3.7, only if k=6 and Z_0=45 Ω, values inside the shaded region are found. Besides, the minimum achievable value of θ_d is 63^o, that is obtained with W=112 μm and S=100 μm. This value of θ_d determines a maximum attainable theoretical bandwidth of about 110%, as shown in Fig. 3.6.

Furthermore, it may be interesting to analyze the behaviour of the phase shifting section to changes in W or S, or equivalently, in Z_{oe} and Z_{oo}. By inspection of Fig. 3.7, if the design curve for k=6 and Z_0=45 Ω is considered, it is easy to note that the curve is fully contained inside the range W ∈[100,120] and S ∈[69, 137]. Therefore, changing W or S

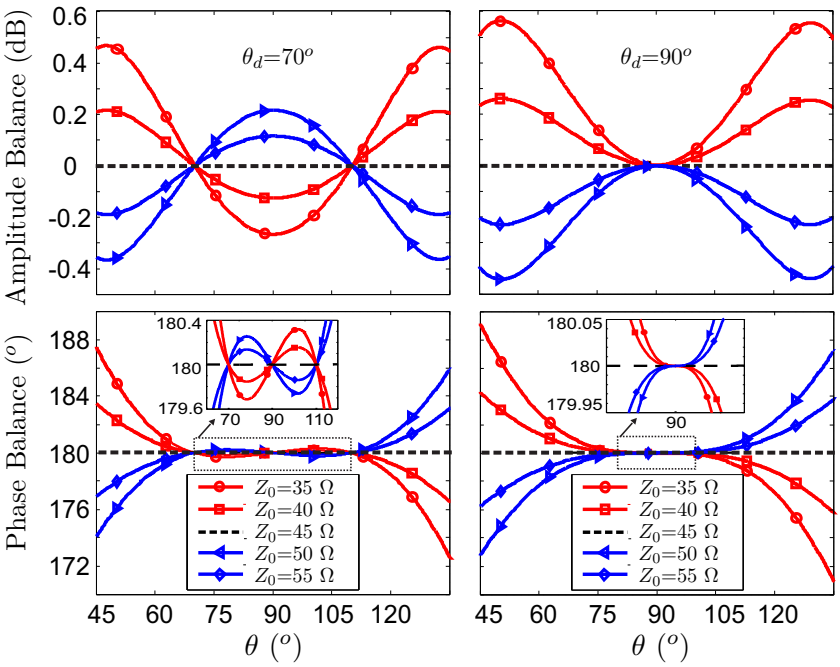

Figure 3.8.: Amplitude and phase imbalance when a reference impedance different to the design impedance (Z_0=45 Ω) is used for two values of θ_d, 70^o and 90^o.

Table 3.2.: Characteristics of the MTLs employed in the designed and fabricated balun at the center frequency f_o=3.5 GHz.

θ_d (^{o})	k	W (μm)	S (μm)	ℓ (mm)
63	6	112	100	13.6

respect to the computed nominal values for a particular design implies a modification on the characteristics of the shifting section, θ_d and Z_0. Besides, when a reference impedance that does not satisfy (3.13) is used, both amplitude and phase imbalance appear. The latter characteristic is exposed in Fig. 3.8 for two different designs, the first one with Z_0=45 Ω and θ_d=70^o, and the second one with Z_0=45 Ω but θ_d=90^o. In both cases, as shown, using a reference impedance different to the design one produce amplitude and phase imbalance. As a result, variations in W and S or Z_0, modify the frequency response of the two wire-bonded open-circuited and short-circuited MTLs. Nevertheless, taking into account the results of Fig. 3.8, small variations can be tolerated depending on the required final performance.

Hence, by means of equations derived in section 3.2.2 and Fig. 3.7, one prototype of the proposed balun using the MTLs summarized in Table 3.2 is fabricated and measured. A photograph of such a balun is shown in Fig. 3.9, where the Wilkinson divider and the wire-bonded short-circuited and open-circuited MTLs are clearly visible. The measured return and insertion losses, isolation, and both amplitude and phase balance are depicted in Fig. 3.10. It can be observed that good input matching and isolation are achieved. Return losses and

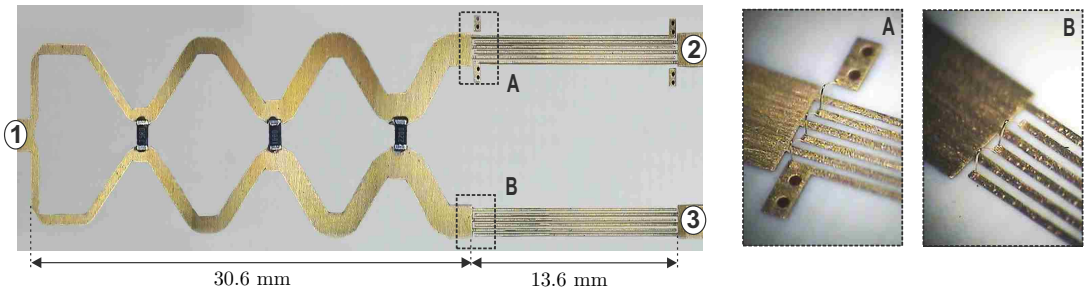

Figure 3.9.: Photograph of the fabricated balun.

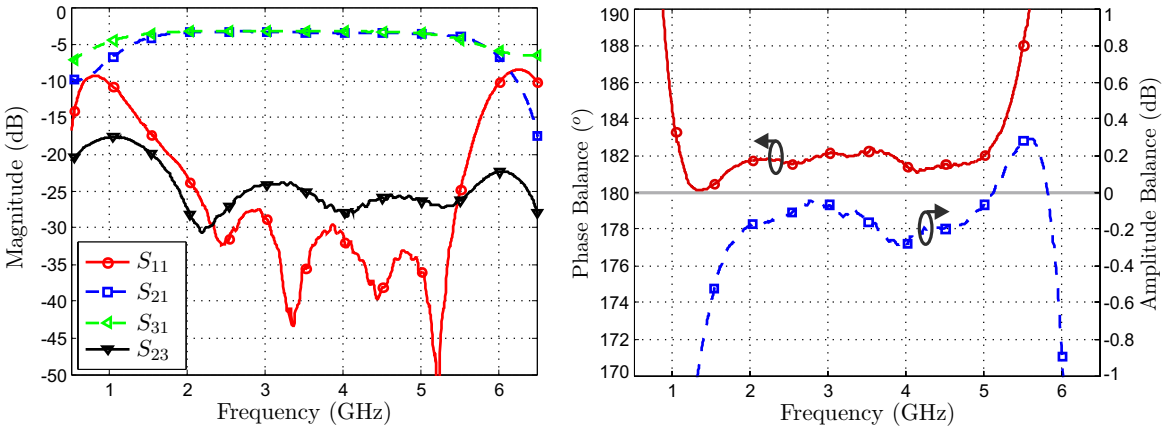

Figure 3.10.: Measured scattering matrix elements (a) and amplitude and phase balance (b) of the balun designed for θ_d=63^o (Table 3.2).

isolation are higher than 10 dB and 18 dB, respectively, in the range [1-6] GHz (142 %). Moreover, according to the amplitude and phase balance, values remain lower than 0.4 dB and 5 degrees approximately, from 1.64 GHz up to 5.36 GHz, or equivalently over a fractional bandwidth of 106 %. Therefore, by means of the general equations given in this work and considering values of θ_d different to the traditionally used 90 degrees, it is possible to design baluns with broader bandwidths.

As a way of integrating amplitude and phase offset into a single parameter, common-mode-rejection ratio (CMRR) is calculated. CMRR represents the splitter rejection of an undesired common-mode output signal resulting from a single-ended input signal. CMRR can be adapted as a measure of the imbalance in a 180 degrees splitter circuit, which can be determined from mixed-mode S-parameters or standard single-ended S-parameters as [29]

$$CMRR = \frac{S_{ds21}}{S_{cs21}} = \frac{S_{21} - S_{31}}{S_{21} + S_{31}}, \tag{3.21}$$

where S_{ds21} and S_{cs21} identify the differential-mode and common-mode responses for a single-ended stimulus.

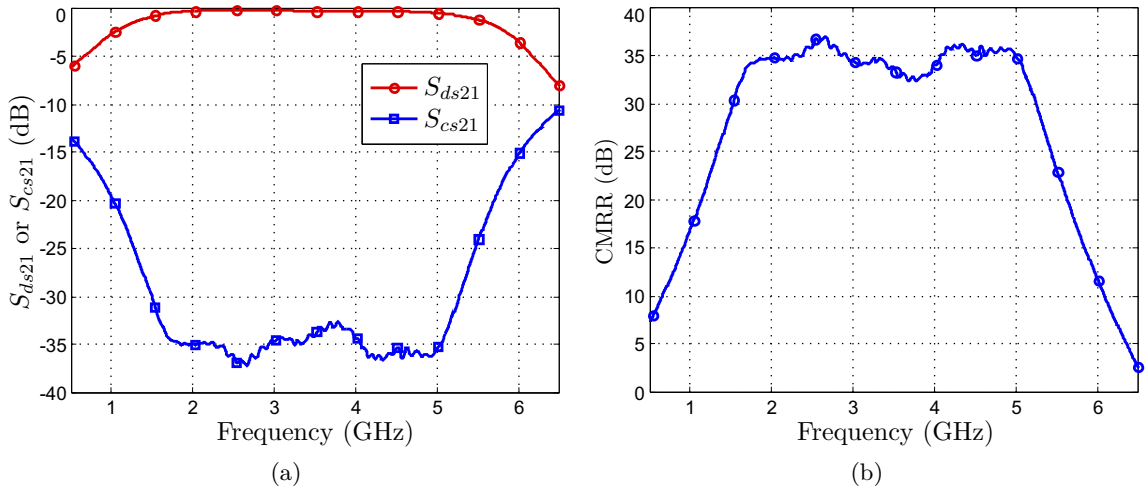

Figure 3.11.: Calculated S_{ds21}, S_{cs21} (a) and CMRR (b) values using the measured S-parameters of the balun designed for θ_d=63^o (Table 3.2).

CMRR values, along with the S_{ds21} and S_{cs21} parameters, are displayed in Fig. 3.11 for the fabricated balun. CMRR can be used as a direct figure of merit to describe the quality of the balun and so interpreting the impact of amplitude and phase imbalances on the system performance. As seen, the designed balun provides high CMRR, greater than 30 dB within the frequency band [1.52-5.25] GHz. Furthermore, maximum CMRR values are located around the design θ_d, 2.2 GHz (θ_d) and 4.8 GHz (180^o-θ_d), approximately. Curves are not perfectly symmetrical respect to the center frequency 3.5 GHz due to the unequal even and odd mode phase velocities in the MTL, which difference increases with the frequency.

Finally, Table 3.3 shows a comparative study among some published baluns attending to four parameters: operating fractional bandwidth, phase and amplitude balance, and output isolation is presented. The operating bandwidth is calculated as BW(%)=$2\Delta f/f_o$ where $2\Delta f$ stands for the symmetric bandwidth respect to the center design frequency f_o considering a threshold limit value of S_{11}=-10 dB. This allows the use of the same metric for all the considered baluns.

Taking into account the values given in Table 3.3, it is easy to deduce that the wire-bonded MTL-based balun is advisable to obtain wideband baluns (>100%) with excellent isolation (>20 dB) and input match (>15 dB). Besides, the good amplitude (<0.6 dB) and phase (<8^o) balance guarantees a good common-mode rejection ratio within the operating band [29]. Furthermore, it is appreciable that most of the published baluns with good output isolation are narrow-band baluns, with bandwidths lower than 64%, while those with broader operating bandwidths neglect this parameter. However, for some applications, such as measurement systems, the isolation between output ports is critical.

It should be highlighted that there has not been any optimization process during the electromagnetic simulations and all dimensions have been selected by following the design

Table 3.3.: Comparisons among some published baluns and the designed balun.

Ref	f_o (GHz)	BW (%)	I (dB)	PB (^{o})	AB (dB)
[1]	2.4	64	>15	±5	0.3
[2]	2	76		±10	0.7
[3]	0.915	49	>16	±6	0.5
[4]	13	77		±4	1
[5]	1.2	35	>15	±5	0.6
[6]	1	64		±2	0.2
[7]	0.9	44		±1	0.1
[8]	31	10		±5	1
[9]	2.45	6		±2	0.3
	5.55	14		±9	0.9
[10]	2	89		±1.4	0.69
[11]	2	130		±10	1
	2	148		±10	1
[12]	0.665	59		±6	0.7
[13]	1.53	38		±10	0.5
[14]	3	66		±10	1
[15]	2.6	77		±4	0.7
[16]	2.4	10	>20	±2	1
[17]	1	26		±3	0.2
[18]	1.5	67		±3.4	1
This Work	3.5	102	>22	±4	0.3
		106	>21	±5	0.4
		115	>20	±8	0.6

I=Isolation, PB=Phase Balance, AB=Amplitude Balance

equations (3.12) and (3.13). Besides, although results are good, it could be improved if the fabrication tolerances are overtaken because considerable variations of up to 10% have been measured.

3.3. Reconfigurable Measurement Test Set for Differential Circuit Characterization

3.3.1. Introduction

The use of differential circuits at RF and microwave frequencies are becoming more popular. Many communications systems, with a low power design, use differential signals to decrease the undesired effects of noise. Besides, differential circuits have interference-rejection capabilities and an increased linear dynamic range. Nevertheless, the measurement of differential devices can be a difficult and expensive task.

The S-parameter theory was extended to differential devices in [29, 30] and some measurement techniques, based on a four-port vector network analyzer (VNA) or a pure-mode VNA, have been presented in [31, 32]. However, the most widespread measuring instruments are two-port VNA intended for single-ended measurements. In this situation, a straightforward measurement technique can be performed with power dividers/combiners and baluns to obtain the common and differential parameters [33–35]. However, in order to get a full characterization several connections are required, and this could severely affect the repeatability. Therefore, a MEMS-based reconfigurable test set that allows the measurement of both, differential- and common-mode S-parameters using a commercial two-port VNA is developed (Fig. 3.12). Using the proposed test set, mixed-mode S-parameters can be directly measured. The main advantage of this architecture is the use of MEMS switches to provide re-configurability. Thus, a full characterization of common and differential S-parameters is possible without the need for multiple connections.

In Section 3.3.3 the test set is designed, fabricated and measured. These measurements are important to account for all the impairments that need to be compensated during the measurement procedure to place the calibration planes at the test set's ports with the right amplitude and phase. Finally, in Section 3.3.4, in order to evaluate the accuracy of the proposed test set, a known device-under-test (DUT) is characterized using a de-embedding technique.

3.3.2. Measurement Technique

The full characterization of a differential device in terms of normalized waves is given by

$$\begin{bmatrix} b_{d_1} \\ b_{d_2} \\ b_{c_1} \\ b_{c_2} \end{bmatrix} = \left[\begin{array}{cc|cc} & & & \\ & S_{dd}^{DUT} & & S_{dc}^{DUT} \\ & & & \\ \hline & & & \\ & S_{cd}^{DUT} & & S_{cc}^{DUT} \\ & & & \end{array}\right] \begin{bmatrix} a_{d_1} \\ a_{d_2} \\ a_{c_1} \\ a_{c_2} \end{bmatrix}, \tag{3.22}$$

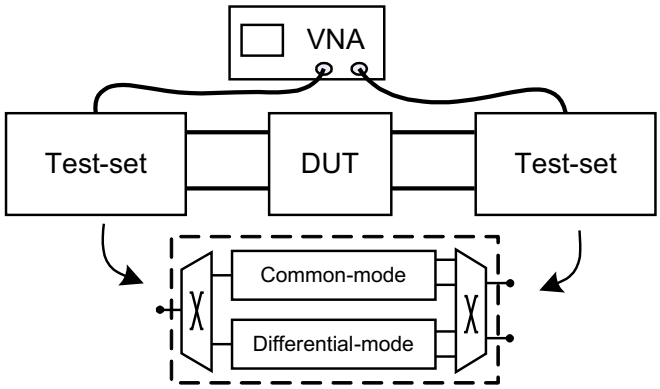

Figure 3.12.: Measurement scheme of a differential device under test.

where the sub-matrices S_{dd}^{DUT} and S_{cc}^{DUT} represent the differential- and common-mode S-parameters, respectively. S_{dc}^{DUT} and S_{cd}^{DUT} determine the conversion of common-mode into differential-mode waves and vice-versa [29]. The measurement scheme of a differential DUT using the proposed test set is shown in Fig. 3.12. The test set is introduced in a two-port measurement setup to provide differential/common excitations at one plane and to combine the signals at the other reference plane of the DUT (divider-combiner)[34]. Therefore, thanks to this configuration it is possible to directly measure the four sub-matrices S_{dd}^{DUT}, S_{cc}^{DUT}, S_{dc}^{DUT} and S_{cd}^{DUT}. Once the measurements are carried out, they are processed by means of a de-embedding technique in order to remove uncertainties and the effects of the test set.

3.3.3. Implementation and Characterization

Fig. 3.13 represents the block diagram of the proposed test set. As seen, there are two independent paths to generate the differential- and common-mode signals. For the generation of the common-mode excitation a Wilkinson divider is employed, while for the differential-mode excitation the wire-bonded MTL balun designed in Section 3.2.4 is used. This balun has a wideband bandpass response (>100%) centered at 3.5 GHz with an excellent output isolation. Besides, three switches based on MEMS technology [36] are connected to commute between the differential- and common-mode excitations. The RMSW221 from Radant MEMS is a high-end SPDT switch which provides the advantage of low losses, high bandwidth and low distortion. However, the main drawback of these switches is their vulnerability to hot-switching, greatly affecting their life-time. Therefore, as shown in Fig. 3.13, a detector block is incorporated at the input port in order to prevent switchings while the external RF signal is turned on. The detector, consisting of a 20 dB directional coupler with a HSCH5340 diode and a DC amplifier, has a sensitivity of -20 dBm. The coupled and rectified signal will be used to avoid hot-switching. The test set is manufactured on a Rogers RO4350B substrate with relative permittivity of 3.66 and thickness of 30 mil.

The proposed test set (see Fig. 3.13), depending on the configuration of switches, acts as

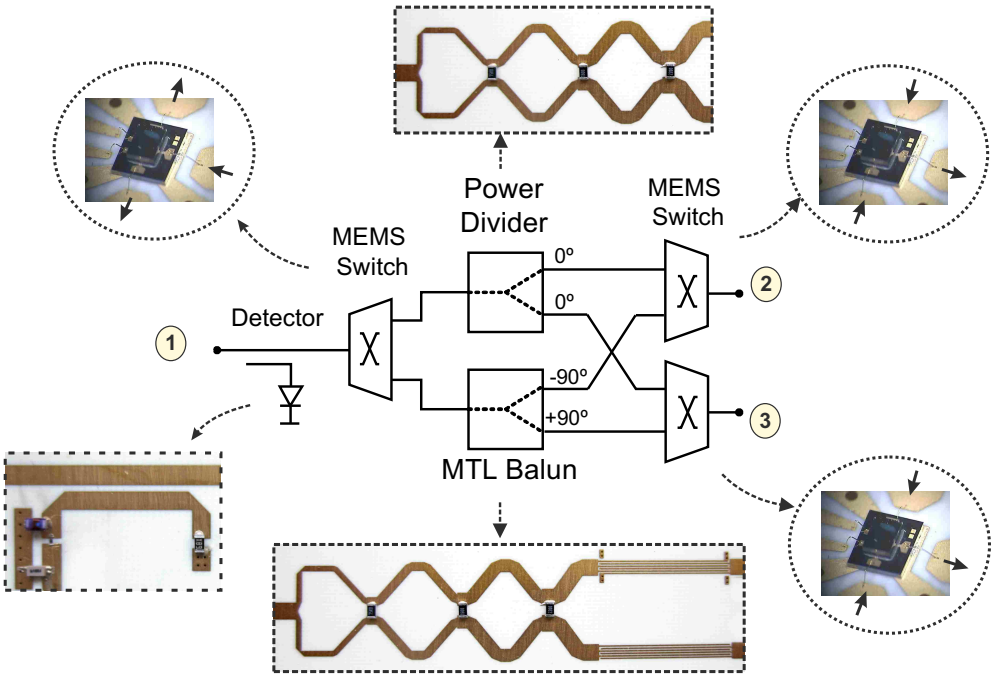

Figure 3.13.: Block diagram of the proposed test set.

a 0^o or 180^o splitter/combiner. The 0^o splitter/combiner provides common-mode to single-ended mixed-mode signal conversion. On the contrary, the 180^o splitter/combiner provides differential-mode to single-ended mixed-mode signal translation [29]. The performance of this type of circuits is mainly determined by its phase and magnitude balance. Thus, the use of mixed-mode S-parameters is appropriated because not only the single-ended to common- and differential-mode conversions are determined, but also because some unique figures of merit can be obtained. To calculate the 3x3 mixed-mode S-parameters a single-ended two-port VNA is used. The VNA is calibrated using the Thru-Reflect-Line (TRL) de-embedding technique [25] and the mixed-mode S-parameters (S^{tsi}) are obtained from the measured standard S-parameters as

$$[S^{sti}] = \left[\begin{array}{c|cc} S^{tsi}_{ss11} & S^{tsi}_{sd12} & S^{tsi}_{sc12} \\ \hline S^{tsi}_{ds21} & S^{tsi}_{dd22} & S^{tsi}_{dc22} \\ S^{tsi}_{cs21} & S^{tsi}_{cd22} & S^{tsi}_{cc22} \end{array}\right] = \frac{1}{2}\begin{bmatrix} 2S_{11} & \sqrt{2}(S_{12}-S_{13}) & \sqrt{2}(S_{12}+S_{13}) \\ \sqrt{2}(S_{21}-S_{31}) & S_{22}-S_{23}-S_{32}+S_{33} & S_{22}+S_{23}-S_{32}-S_{33} \\ \sqrt{2}(S_{21}+S_{31}) & S_{22}-S_{23}+S_{32}-S_{33} & S_{22}+S_{23}+S_{32}+S_{33} \end{bmatrix}, \tag{3.23}$$

where the superscript tsi can be tsc or tsd for the common-mode or differential-mode configuration of the test set, respectively.

Therefore, for the two possible configurations (Fig. 3.13), the test set is modeled as a mixed-mode two-port device (S^{tsc},S^{tsd}), with a pure single-ended S-parameter (S^{tsi}_{ss11}), two pure mixed-mode S-parameters (S^{tsi}_{dd22} and S^{tsi}_{cc22}) and six cross-mode S-parameters [29]. Besides, from (3.23), it is easy to deduce the importance of using a balun with good output matching and isolation (small values of S_{22}, S_{33} and S_{23}) to minimize the S^{tsi}_{cc22},S^{tsi}_{dd22}, S^{tsi}_{dc22} and S^{tsi}_{cd22}

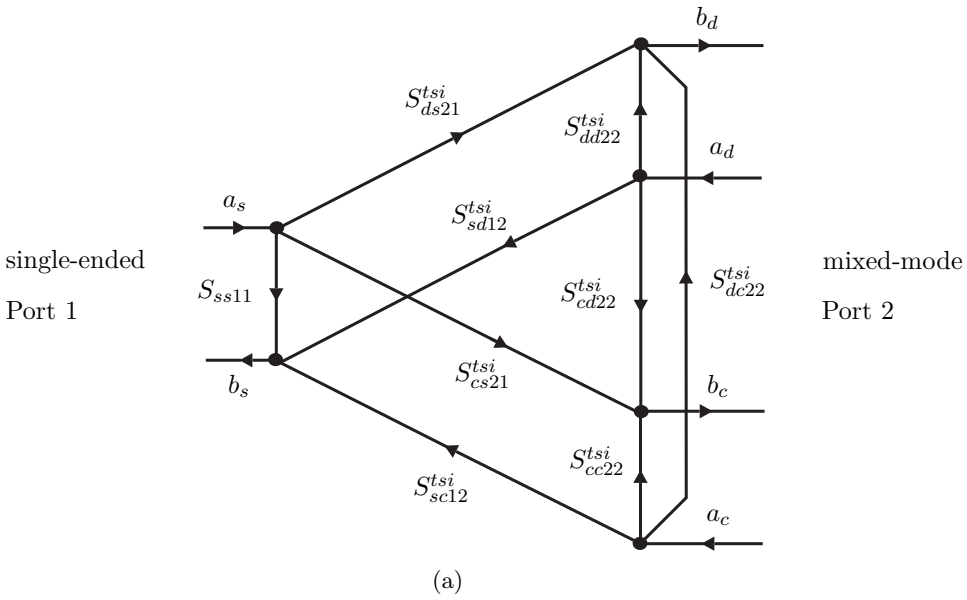

Figure 3.14.: Test set mixed-mode S-parameters flow diagram.

terms. The test set mixed-mode S-parameters flow diagram is shown in Fig. 3.14.

Once the mixed-mode matrices are known, the performance of the test set can be evaluated. Fig. 3.15(a) and Fig.3.15(b) show the measured amplitude and phase balance for the common- and differential-mode generation. As seen, the phase and amplitude imbalances are lower than 6^o and 0.2 dB for the common path, and lower than 6^o and 0.6 dB for the differential excitation, over the frequency band from 1.5 GHz to 5.5 GHz. These parameters can be integrated into two quantities that represent the rejection of an undesired mode component within the test set: the common-mode rejection ratio (CMRR), for the differential-mode generation, and the differential-mode rejection ratio (DMRR), for the common-mode excitation. Both parameters are calculated and represented in Fig. 3.15(c). Note that according to these results, a fractional bandwidth of about 100% at a center frequency of 3.5 GHz with values of CMRR and DMRR greater than 25 dB is achieved. The S-parameters transmission terms are depicted in Fig. 3.15(d), which are the single-ended signal-transfer parameters to common-mode or differential-mode signal at the mixed-mode port 2. Thus, from these curves it is straightforward to deduce that the proposed test set can be used as a high-performance measurement solution for characterization of differential devices.

CMRR and DMRR are intuitive figures of merit related to the test set transfer function. They are the most representative parameters in the scheme shown in Fig. 3.12, as any undesired mode generated by the test set will affect the measurement accuracy of the desired mode parameters. Nevertheless, the measurement can also be disturbed by reflections in any port, so these reflections must be avoided. Fig. 3.16 represents the return losses, S^{tsi}_{ss11}, S^{tsi}_{dd22} and S^{tsi}_{cc22}, for the two configurations of the test set. As seen, there is a good impedance matching with return losses higher than 15 dB within the operating band for both common

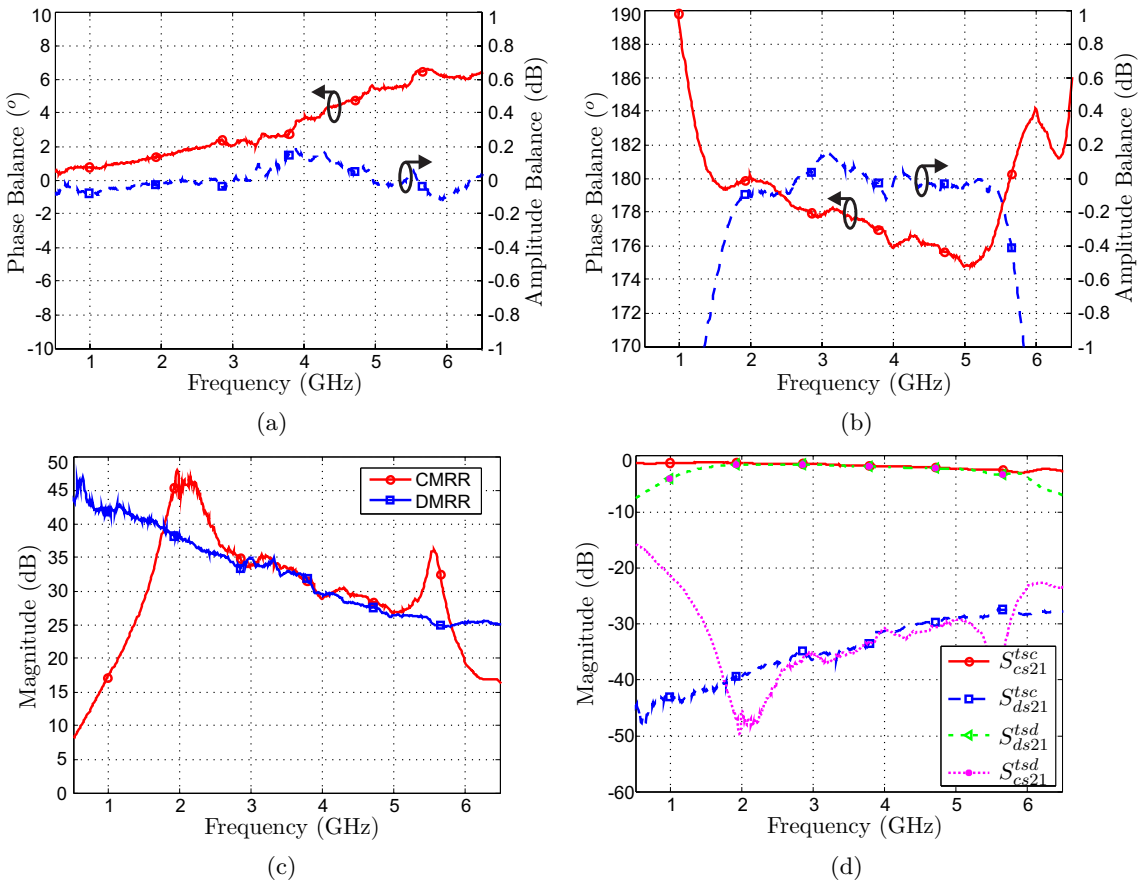

Figure 3.15.: Measured amplitude and phase balance for the (a) common- and (b) differential-mode excitations. (c) DMRR and CMRR parameters and (d) mixed-mode S-parameters transmission terms.

and differential states. Mixed-mode to mixed-mode S-parameter cross-mode terms, S_{cd22} and S_{dc22}, are drawn in Fig. 3.17(b). Clearly it can be noted that the differential path presents a worse behaviour, conditioned by the output matching of the wire-bonded MTL balun. Notwithstanding, these parameters maintain a value under -15 dB within the bandwidth of operation.

Finally, a photograph of the manufactured test-set is shown in Fig. 3.18. In this photo, all the elements previously described can be observed. On the left, the directional coupler, based on parallel coupled microstrip lines, is followed by an RF detector and a DC amplifier. The MEMS switch at the input allows the selection between the upper path, where the three-step Wilkinson power divider is used to generate a common-mode signal, and the lower path, where the MTL balun is used to generate a differential-mode excitation. The MEMS switches are connected to the circuit using bonding wires and a matching network based on capacitors is included to improve the return loss in the frequency band of interest. The output ports also use matched MEMS switches connected to both, the power divider and the balun. Besides, as can be seen on the right of Fig. 3.18, a cross of microstrip lines is unavoidable at the

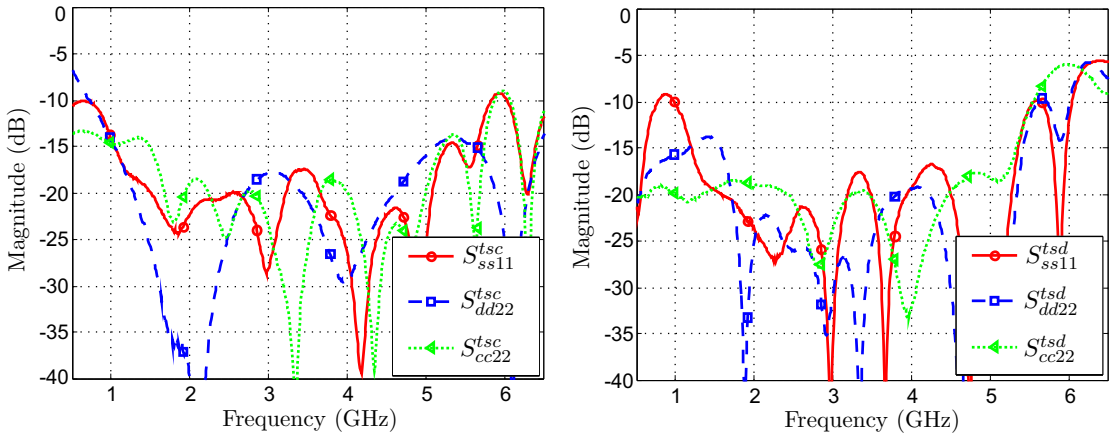

(a) (b)

Figure 3.16.: Measured return losses for (a) common- and (b) differential-mode configuration of the test set.

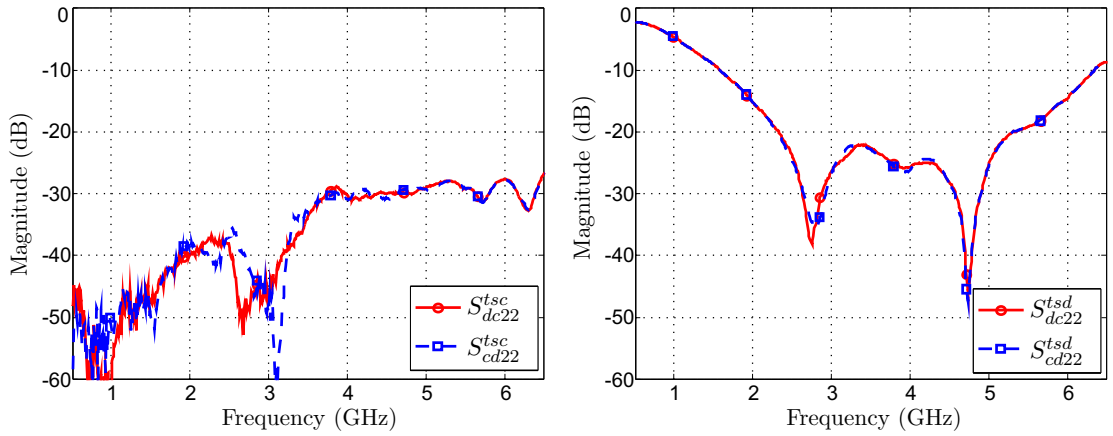

(a) (b)

Figure 3.17.: Measured cross-mode conversion at the mixed-mode port 2 for (a) common- and (b) differential-mode configuration of the test set.

output. This cross has been solved by designed a vertical microstrip transition to pass under the ground plane maintaining the phase balance. The control lines of the MEMS switches can be seen in the middle of the circuit.

3.3.4. Measurement Verification

In this section, the proposed test set is used to characterize a DUT by following the measurement setup shown in Fig. 3.12. Two asymmetrical coupled lines, which are used as a known DUT, are fabricated and measured. Besides, a de-embedding algorithm is developed to account for the impact of the test set and remove its undesired effect. However, because only one test set has been fabricated, this de-embedding algorithm is validated by simulation,

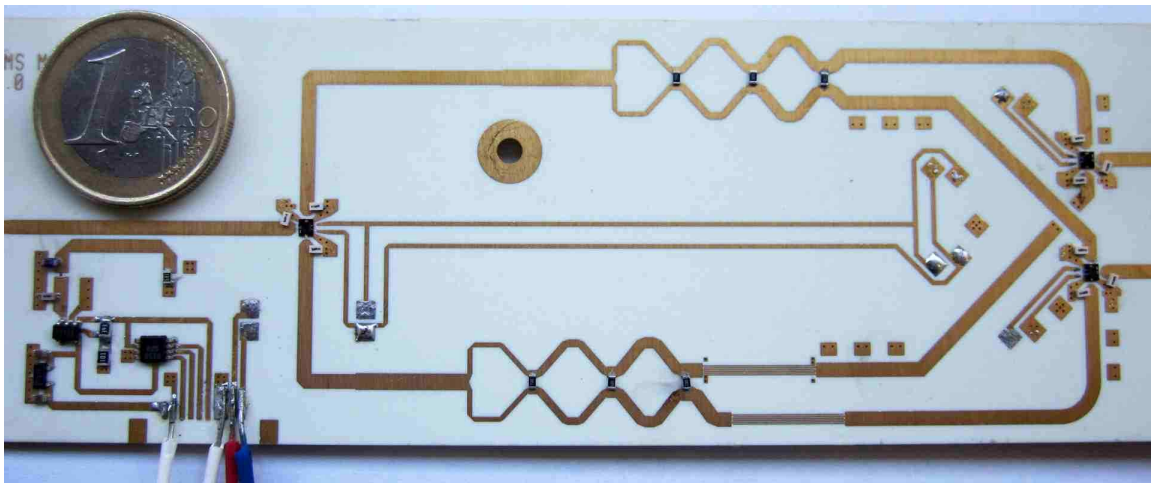

Figure 3.18.: Photograph of the fabricated reconfigurable test set.

considering that two equal test sets are placed at the input and output ports of the DUT (Fig. 3.12). Thus, some simulations are carried out by using the measured S-parameters of both, the test set and DUT, where the S-parameters of the test set are changed to generate the common- or differential-mode excitation. Once the four possible combinations of the signal path are evaluated (Fig. 3.19), the de-embedding algorithm employs the resulting four S-parameter matrices along with the measured S-parameters of the test set, to calculate the parameters of the DUT.

Theoretical, measured and de-embedded values of S_{dd11}^{DUT}, S_{cc11}^{DUT} and S_{dc21}^{DUT} are shown in Fig. 3.20. The theoretical terms are the known mixed-mode S-parameters of the DUT, while the measured terms are the calculated S-parameters taking into account the effect of both test sets. From these curves, it can be noted that the parameters obtained after the de-embedding process are very close to the theoretical values. Similar results are achieved for the rest of mixed-mode S-parameters of the DUT. Therefore, it is possible to conclude that the proposed test set provides the required performance to characterize differential circuits by using a two-port vector network analyzer.

3.4. Conclusion

A new theoretical study and design methodology of two open- and short-circuited wire-bonded MTLs has been presented when used for balance applications. Closed-form equations have been derived to properly design a 180^o phase section and thus, a systematic procedure for the design of wire-bonded MTL baluns has been given. The analytical equations allow to calculate easily the dimensions of both MTLs to get a theoretical perfect output phase and amplitude balance at all frequencies, and perfect input matching at one or two frequencies as a function of the number of conductors. To assess the design guidelines, a microstrip planar

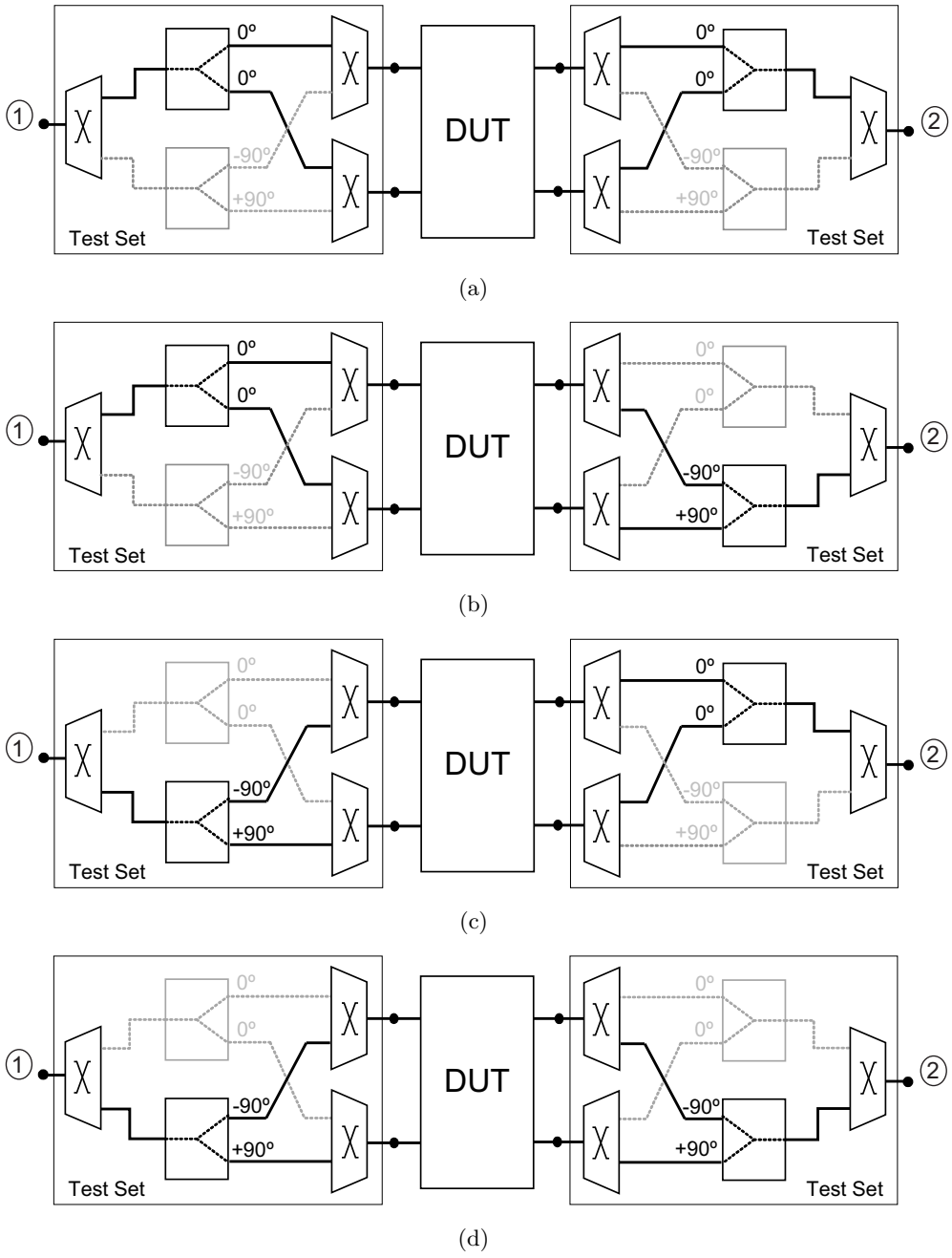

Figure 3.19.: Test set configurations for the characterization of differential circuits.

balun has been designed, fabricated and measured. The balun presents measured amplitude and phase balance lower than 0.4 dB and 5 degrees over a 106% bandwidth, very close to the theoretical one of 110 %. Furthermore, the presented balun has been proved to be an excellent alternative in order to obtain a perfect output isolation with values higher than 20 dB.

As one application of this MTL balun, a MEMS-based reconfigurable test set for the

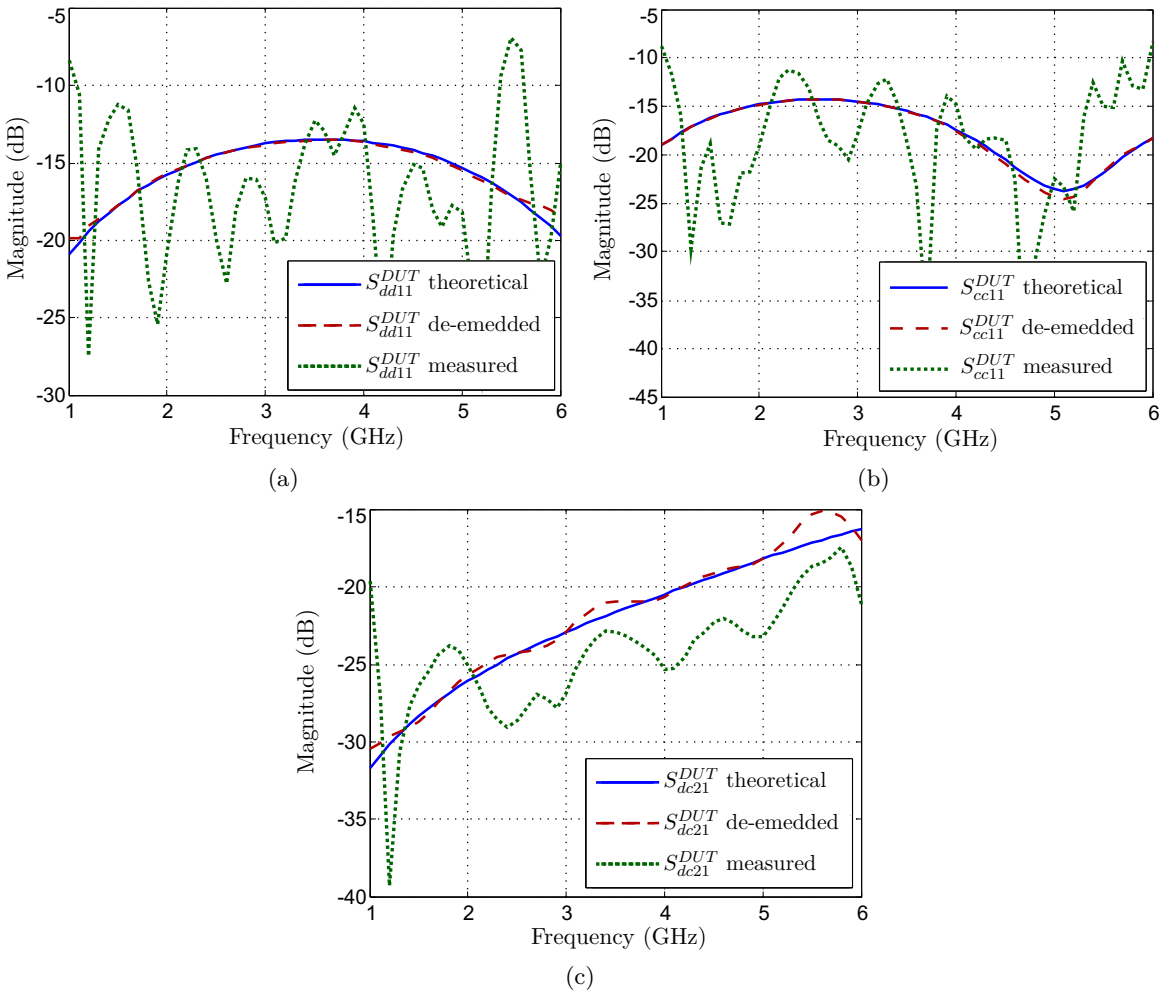

Figure 3.20.: Theoretical, measured and de-embedded S_{dd11}^{DUT} (a), S_{cc11}^{DUT} (b) and S_{cd21}^{DUT} (c) of a known DUT used to asses the performance of the proposed test set.

measurement of mixed-mode S-parameters by using a two-port VNA has been analyzed, designed and fabricated. The test set uses the MTL balun for the differential-mode excitation, which provides the required operating bandwidth with good amplitude/phase balance, port matching and output isolation. The measurement procedure, with a de-embedding technique, has been applied to calculate the mixed-mode S-parameters of a known DUT. Taking into account the good agreement between the theoretical and de-embedded results, the test set has been demonstrated to be a suitable solution for differential circuit measurement.

References

[1] Z.-Y. Zhang, Y.-X. Guo, L. C. Ong, and M. Chia, "A new wide-band planar balun on a single-layer pcb," *IEEE Microw. Wireless Compon. Lett.*, vol. 15, no. 6, pp. 416–418, Jun. 2005.

REFERENCES

[2] C.-H. Tseng and C.-L. Chang, "Wide-band balun using composite right/left-handed transmission line," *Electron. Lett.*, vol. 43, no. 21, pp. 1154–1155, Nov. 2007.

[3] F. Tan, W. Huang, Y. Chen, Y. Li, K. Huang, and C. Liu, "Design and implementation of compact microwave components with artificial transmission lines," *J. Electromagn. Waves Appl.*, vol. 27, no. 3, pp. 385–395, 2013.

[4] M. Tsai, "A new compact wideband balun," in *IEEE Microwave and Millimeter-Wave Monolithic Circuits Symposium*, 1993, pp. 123–125.

[5] K. S. Ang and I. Robertson, "Analysis and design of impedance-transforming planar marchand baluns," *IEEE Trans. Microw. Theory Tech.*, vol. 49, no. 2, pp. 402–406, Feb. 2001.

[6] W. Fathelbab and M. Steer, "New classes of miniaturized planar marchand baluns," *IEEE Trans. Microw. Theory Tech.*, vol. 53, no. 4, pp. 1211–1220, Apr. 2005.

[7] R. Phromloungsri, M. Chongcheawchamnan, and I. Robertson, "Inductively compensated parallel coupled microstrip lines and their applications," *IEEE Trans. Microw. Theory Tech.*, vol. 54, no. 9, pp. 3571–3582, Sep. 2006.

[8] C.-S. Lin, P.-S. Wu, M.-C. Yeh, J.-S. Fu, H.-Y. Chang, K.-Y. Lin, and H. Wang, "Analysis of multiconductor coupled-line marchand baluns for miniature mmic design," *IEEE Trans. Microw. Theory Tech.*, vol. 55, no. 6, pp. 1190–1199, Jun. 2007.

[9] L. Yeung, W.-C. Cheng, and Y. Wang, "A dual-band balun using broadside-coupled coplanar striplines," *IEEE Trans. Microw. Theory Tech.*, vol. 56, no. 8, pp. 1995–2000, Aug. 2008.

[10] C.-H. Tseng and Y.-C. Hsiao, "A new broadband marchand balun using slot-coupled microstrip lines," *IEEE Microw. Wireless Compon. Lett.*, vol. 20, no. 3, pp. 157–159, Mar. 2010.

[11] J.-C. Lu, C.-C. Lin, and C.-Y. Chang, "Exact synthesis and implementation of new high-order wideband marchand baluns," *IEEE Trans. Microw. Theory Tech.*, vol. 59, no. 1, pp. 80–86, Jan. 2011.

[12] E. Jafari, F. Hodjatkashani, and R. Rezaiesarlak, "A Wideband Compact Planar Balun for UHF DTV Applications," *J. Electromagn. Waves Appl.*, vol. 23, no. 14-15, pp. 2047–2053, 2009.

[13] J.-L. Li and S.-W. Qu, "Miniaturised branch-line balun with bandwidth enhancement," *Electron. Lett.*, vol. 43, no. 17, pp. 931–932, Aug. 2007.

[14] W. Shao and J.-L. Li, "A compact log-periodic branch-line balun with an octave bandwidth," *J. Electromagn. Waves Appl.*, vol. 25, no. 14-15, pp. 2033–2042, 2011.

[15] C. Liu and W. Menzel, "Broadband via-free microstrip balun using metamaterial transmission lines," *IEEE Microw. Wireless Compon. Lett.*, vol. 18, no. 7, pp. 437–439, Jul. 2008.

[16] C.-K. Lin and S.-J. Chung, "A Compact Filtering 180 Hybrid," *IEEE Trans. Microw. Theory Tech.*, vol. 59, no. 12, pp. 3030–3036, Dec. 2011.

[17] Z.-Y. Yeh and Y.-C. Chiang, "A miniature CPW balun constructed with length-reduced 3db couples and a short redundant transmission line," *Progr. Electromagn. Res.*, vol. 117, pp. 195–208, 2011.

[18] H.-X. Xu, G.-M. Wang, X. Chen, and T.-P. Li, "Broadband balun using fully artificial fractal-shaped composite right/left handed transmission line," *IEEE Microw. Wireless Compon. Lett.*, vol. 22, no. 1, pp. 16–18, Jan. 2012.

[19] R. Mongia, I. Bahl, and P. Bhartia, *RF and Microwave Coupled-Line Circuits*. Norwood, MA: Artech House, 1999.

[20] R. Jacques and D. Meignant, "Novel wide band microstrip balun," in *11th European Microwave Conference*, Sep. 1981, pp. 839–843.

[21] J. Rogers and R. Bhatia, "A 6 to 20 ghz planar balun using a wilkinson divider and lange couplers," in *IEEE MTT-S International Microwave Symposium Digest*, vol. 2, Jul. 1991, pp. 865 –868.

[22] M. Antoniades and G. Eleftheriades, "A broadband wilkinson balun using microstrip metamaterial lines," *IEEE Antennas Wireless Propag. Lett.*, vol. 4, pp. 209–212, Aug. 2005.

[23] M. Chongcheawchamnan, C. Y. Ng, K. Bandudej, A. Worapishet, and I. Robertson, "On miniaturization isolation network of an all-ports matched impedance-transforming marchand balun," *IEEE Microw. Wireless Compon. Lett.*, vol. 13, no. 7, pp. 281–283, Jul. 2003.

[24] W. Ou, "Design Equations for an Interdigitated Directional Coupler," *IEEE Trans. Microw. Theory Tech.*, vol. 23, no. 2, pp. 253–255, Feb. 1975.

[25] D. Pozar, *Microwave Engineering*, 2nd ed. New York: Wiley, 1998.

[26] S. Cohn, "A Class of Broadband Three-Port TEM-Mode Hybrids," *IEEE Trans. Microw. Theory Tech.*, vol. 19, no. 2, pp. 110–116, Feb. 1968.

[27] M. Kirschning and R. Jansen, "Accurate Wide-Range Design Equations for the Frequency-Dependent Characteristic of Parallel Coupled Microstrip Lines," *IEEE Trans. Microw. Theory Tech.*, vol. 32, no. 1, pp. 83–90, Jan. 1984.

[28] J. A. B. Faria, "Kirschning and Jansen computer-aided design formulae for the analysis of parallel coupled lines," *Microw. Opt. Techn. Let.*, vol. 51, no. 10, pp. 2466–2470, 2009.

[29] W. R. Eisenstadt, B. Stengel, and B. M. Thompson, *Microwave Differential Circuit Design Using Mixed-Mode S-Parameters*. Norwood, MA: Artech House, 2006.

[30] D. Bockelman and W. Eisenstadt, "Combined differential and common-mode scattering parameters: theory and simulation," *IEEE Trans. Microw. Theory Tech.*, vol. 43, no. 7, pp. 1530–1539, Jul. 1995.

[31] ——, "Pure-mode network analyzer for on-wafer measurements of mixed-mode S-parameters of differential circuits," *IEEE Trans. Microw. Theory Tech.*, vol. 45, no. 7, pp. 1071–1077, Jul. 1997.

[32] D. Bockelman, W. Eisenstadt, and R. Stengel, "Accuracy estimation of mixed-mode scattering parameter measurements," *IEEE Trans. Microw. Theory Tech.*, vol. 47, no. 1, pp. 102–105, Jan. 1999.

[33] S. Belkin, "Differential Circuit Characterization with Two-Port S-Parameters," *IEEE Microw. Mag.*, vol. 7, no. 6, pp. 86–99, Dec. 2006.

[34] V. Issakov, M. Wojnowski, A. Thiede, V. Winkler, M. Tiebout, and W. Simburger, "Considerations on the measurement of active differential devices using baluns," in *IEEE Int. Conf. on Microw. Commun., Antennas and Electron. Syst. (COMCAS)*, Nov. 2009, pp. 1–7.

[35] K. Jung, R. Campbell, L. Hayden, W. Eisenstadt, and R. Fox, "Evaluation of Measurement Uncertainties Caused by Common and Cross Modes in Differential Measurements Using Baluns," *IEEE Trans. Microw. Theory Tech.*, vol. 56, no. 6, pp. 1485–1492, Jun. 2008.

[36] S. Lucyszyn, *Advanced RF MEMS*, 1st ed. New York, NY, USA: Cambridge University Press, 2010.

Chapter 4

MTL-Based Stubs

WIRE-BONDED multiconductor transmission lines can be used as shunt stubs as a way of overcoming the limitations regarding impedance levels and frequency response of single transmission line stubs. The wire-bonded multiconductor transmission line is a particular case that provides greater bandwidth by eliminating high-frequency undesired resonances. In this chapter, a general analysis of the behaviour of this structure is presented. In Section 4.2, the performance of all eight possible configurations and an arbitrary number of strips is assessed and some physical insight into their frequency behaviour is provided. It will be demonstrated that six of them allow the implementation of shunt stubs with impedance levels that are complicated or unapproachable with a single stub, while the other two provide additional degrees of freedom that are of interest for the design of filtering structures.

The usefulness and validity of the proposed analytical design equations are illustrated by designing, manufacturing and measuring two artificial transmission lines with left-handed bandpass response and improved out-of-band rejection in Sections 4.3 and 4.4. In addition, the excellent agreement between the designed and experimental results suggests that the presented analytical equations are most convenient for a quick and reliable design of many passive and active microwave circuits.

4.1. Introduction

The use and development of coupled line components have been fostered for nearly half a century by their broad bandwidth, easy fabrication and low cost. There is an extensive bibliography that deals with planar coupled transmission lines from the mid-1950s up to now

[1–11] . There are many microwave components realized using coupled lines, such as directional couplers, resonators, interdigital capacitors, DC blocks, filters and baluns. The design of filters and couplers is possibly the most typical application, but in the last decade, and as a consequence of the synthesis of composite right-left handed transmission lines (CRLH-TLs), the design of capacitors has also been addressed [12–14].

In the last few years, coupled-line components have found new applications in the design of both filters and CRLH TLs. In many of these applications, shunt admittances are implemented by shunt stubs. To overcome the limitations of a single stub in terms of realizability and frequency response, alternative implementations based on coupled-line sections have recently been proposed [15–18].

Two- and three-strip coupled-line sections were used in [16] as shunt admittances in the design of wideband bandpass filters. However, the authors only provided design equations for the classic two-strip case. Two-strip coupled-line sections were also used in [17] to implement a high-impedance short-circuited stub. Nevertheless, in this chapter it is demonstrated that the structure proposed in [17] is most appropriate to implement low-impedance short-circuited stubs [19] and general design equations are provided. More recently, coupled two- and three-line have been proposed to design dual-wideband bandpass filters [18]. In this case, the authors have given the design equations for the three-line component, but for a specific set of loading conditions.

Wire-bonded multiconductor transmission line (MTL) sections, have been recently employed as series and shunt elements to design balanced CRLH-TLs [15]. In [15], some equations to calculate the required dimensions of both coupled-line sections to achieve a seamless transition between the left-handed (LH) frequency band and the right-handed (RH) one are presented. These equations are restricted to the particular case of implementing a CRLH unit-cell and, therefore, the performance of this element as single shunt admittance was not analyzed in depth.

The MTL component used in [15] is a specific case of MTL [9–11] in which bonding wires interconnect the ends of alternate conductors. In this chapter, a general analytical study of the performance of this so-called wire-bonded MTL component when used as a shunt stub is presented. The study considers all eight possible loading conditions of the structure (open- or short-circuiting the three remaining access ports). As a result, all the previously proposed configurations [15, 16, 18] emerge as particular cases and are, therefore, thoroughly analyzed. Moreover, it is proved that six out of the eight possible configurations are equivalent to a low-impedance short- or open-circuited single stub. By contrast, the other two configurations have a particular frequency response that is mainly governed by the coupling level of the MTL section. As an illustrative example of the usefulness of the developed equations, the design of artificial transmission lines with a LH pass-band and improved out-of-band rejection is presented.

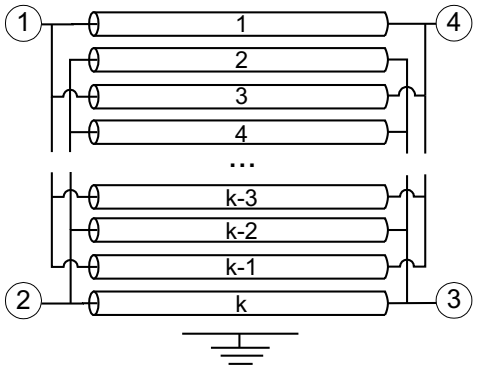

Figure 4.1.: Transmission line equivalent of a wire-bonded MTL.

4.2. Theoretical Analysis

The wire-bonded MTL, outlined in Fig. 4.1, was analyzed in [3] and [5] as a directional coupling scheme (Lange coupler). This element has been used in Chapters 2 and 3 by placing two purely reactive loads at the direct and coupled ports. The use of short circuits across the end of alternate strips improves the operating frequency band by eliminating undesired resonances at high frequencies [12]. When losses are neglected and the coupling between non-adjacent strips is negligible, the admittance matrix of the wire-bonded MTL can be expressed as [4]

$$[Y_L] = j \begin{bmatrix} -M\cot\theta_c & -N\cot\theta_c & N\csc\theta_c & M\csc\theta_c \\ -N\cot\theta_c & -M\cot\theta_c & M\csc\theta_c & N\csc\theta_c \\ N\csc\theta_c & M\csc\theta_c & -M\cot\theta_c & -N\cot\theta_c \\ M\csc\theta_c & N\csc\theta_c & -N\cot\theta_c & -M\cot\theta_c \end{bmatrix} \tag{4.1}$$

where θ_c is the electrical length of the fingers (2.5), and M and N were defined in (2.2) as a function of both, the number of conductors k (excluding the ground plane), and the even- (Z_{oe}) and odd-mode (Z_{oo}) impedances of a pair of adjacent lines. For a lossless medium happens that (2.4) [4]

$$M > 0, \quad N < 0, \quad M^2 > N^2. \tag{4.2}$$

It is important to note that pure TEM and lossless propagation are assumed. Besides, it can be considered all the assumptions commented in Section 2.2.

Now, by considering that port 1 is the input port and that the other three ports can be short- or open-circuited, it is straightforward to calculate the input admittance of the resultant one-port element. The different configurations analyzed in this work, labeled from m=0 up to m=7, are represented in Fig. 4.2. Table 4.1 contains the input admittances obtained by imposing the boundary conditions shown in Fig. 4.2, where variable vh_i is 1 when a via-hole is included in port i, and 0 when it is open-circuited.

Admittances shown in Table 4.1 clearly indicate, through an inspection of their dependence

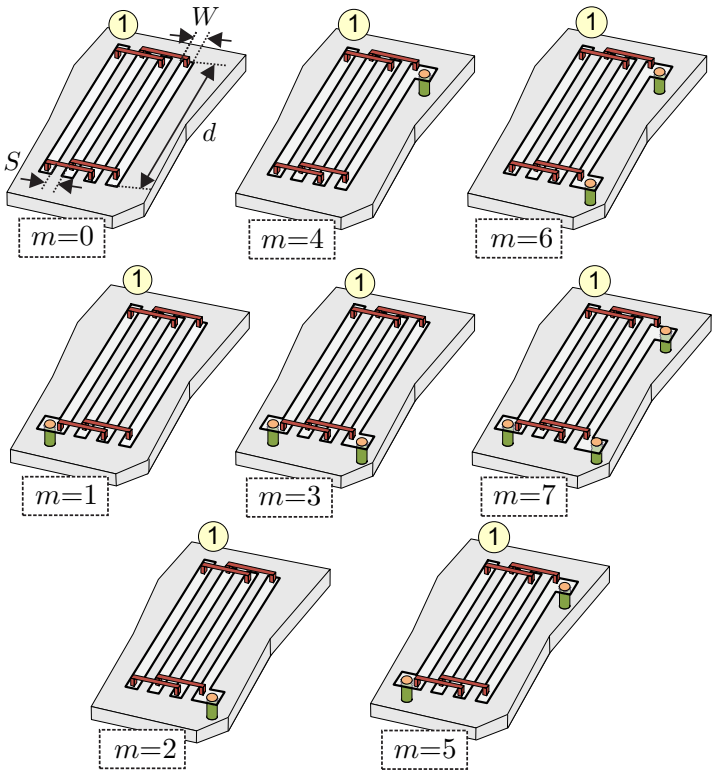

Figure 4.2.: Layout of the eight one-port wire-bonded MTL analyzed. Only four strips have been drawn as a particular case.

Table 4.1.: Input admittance for several configurations of a lossless one-port MTL

m	vh_2	vh_3	vh_4	$Y_{in,m}$
0	0	0	0	$j\dfrac{M^2-N^2}{M}\tan\theta_c$
1	0	0	1	$-j\dfrac{M^2-N^2}{M}\cot\theta_c$
2	0	1	0	$j\dfrac{M(M^2-N^2)\sin\theta_c\cos\theta_c}{M^2\cos^2\theta_c-N^2}$
3	0	1	1	$-j\dfrac{M^2-N^2}{M}\cot\theta_c$
4	1	0	0	$jM\tan\theta_c$
5	1	0	1	$-j\dfrac{M^2\cos^2\theta_c-N^2}{M\cos\theta_c\sin\theta_c}$
6	1	1	0	$jM\tan\theta_c$
7	1	1	1	$-jM\cot\theta_c$

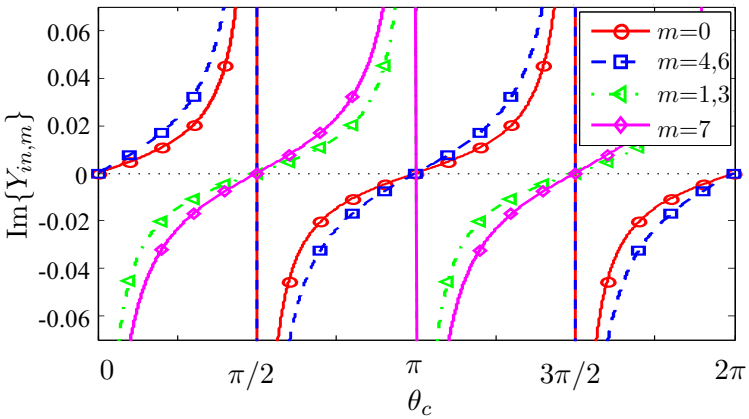

Figure 4.3.: Input susceptance for configurations m=0,4,6 and m=1,3,7 of a wire-bonded MTL.

on $\tan\theta_c$ and $\cot\theta_c$ and taking into account the inequalities (4.2), that configurations m=0,4,6 and m=1,3,7, are equivalent to a single open-circuited and short-circuited stub, respectively. However, configurations m=2 and m=5 have a more complex frequency response and require further analysis. The poles and zeros of the input admittances for m=2 and m=5 are not determined just by $\tan\theta_c$ or $\cot\theta_c$ functions and can be adjusted by designing the MTL properly. The study of all one-port circuits shown in Table 4.1 is carried out in the following sections.

4.2.1. One-Port Wire-Bonded MTL Equivalent to Open- or Short-Circuited Shunt Stubs (m=0, 4, 6 and m=1, 3, 7).

The input susceptance for configurations m=0,4,6 and m=1,3,7, given in Table 4.1, are represented in Fig. 4.3 for a particular wire-bonded MTL. These curves show the typical frequency response of such configurations, because the position of poles and zeros are preset by the $\tan\theta_c$ and $\cot\theta_c$ functions.

By taking into account the frequency response of these components, it is possible to realize single short- and open-circuited stubs by means of these arrangements. Furthermore, the following equivalent characteristic impedances Z_c for the equivalent single stubs can be established

$$Z_{c,m=0,1,3} = \frac{M}{M^2 - N^2} \tag{4.3a}$$

$$Z_{c,m=4,6,7} = \frac{1}{M}, \tag{4.3b}$$

where M and N were defined in (2.2). After some algebraic manipulations these expressions

can be written as

$$Z_{c,m=0,1,3} = Z_{oe}\,\frac{2(1+u)}{2u+(k-1)(1+u^2)}\,\frac{1}{1-c^2} \tag{4.4a}$$

$$Z_{c,m=4,6,7} = Z_{oe}\,\frac{2(1+u)}{2u+(k-1)(1+u^2)}, \tag{4.4b}$$

c being the coupling coefficient of a quarter-wavelength k-line coupler, given as [5]

$$c = \frac{-N}{M} = \frac{(k-1)(u^2-1)}{2u+(k-1)(u^2+1)}, \tag{4.5}$$

with $u{=}Z_{oe}/Z_{oo}$.

The above equations allow the advantages of using the wire-bonded MTL-based stub to be deduced with respect to a single short- or open-circuited stub. It is observed that (4.4a) and (4.4b) are only equal if the coupling coefficient c is zero ($u{=}1$). In this situation, the equivalent characteristic impedance of the MTL-based stub is $2Z_{oe}/k$ (the impedance of $k/2$ parallel single strips with a characteristic impedance of Z_{oe}). Nevertheless, for any other coupling level ($c>1$, $u>1$), the characteristic impedance for $m{=}4,6,7$ is always lower than that for $m{=}0,1,3$ and it is possible to modify its value by changing the coupling factor.

To illustrate graphically the aforementioned properties of arrangements m=0,4,6 (equivalent to single open-circuited stubs) and m=1,3,7 (equivalent to single short-circuited stubs), Fig. 4.4(a) and Fig. 4.4(b) show the values of Z_c as a function of the width W and spacing S (see Fig. 4.2), for a different number of conductors k. The curves are computed by using the Rogers 4350B substrate with a relative permittivity of 3.66 and thickness of 30 mil. This substrate will be used throughout this chapter.

From the inspection of Fig. 4.4(a) it is clear that the greater the coupling level, the more different are the values of Z_c for configurations 0,1,3 and 4,6,7, respectively. Furthermore, by considering the same number of strips and given a coupling factor value, Z_c is always lower for arrangements 4,6,7 than 0,1,3. This means that, for a particular MTL-based stub, it is important to place short- or open-circuits conveniently at the ports because it conditions not only the frequency behaviour, but also the value of the equivalent characteristic impedance. The same values of Z_c, but without considering the coupling factor, are drawn in Fig. 4.4(b). These curves allow a direct comparison to be established between these impedances and the corresponding characteristic impedances of a single strip with $S{=}0$. It is clear that by means of MTL-based stubs, it is feasible to obtain values of low impedances that would be complicated or unapproachable with a single strip. The advantage of using two strips is moderate or negligible for $m{=}0,1,3$ but, for configurations 4,6,7, the reduction in the equivalent Z_c is remarkable. As a result, configurations $m{=}4,6,7$ seem to be appropriate for the implementation of equivalent low-impedance short- or open- circuited stubs. Results for a greater number of conductors have not been depicted for the readability and clarity of

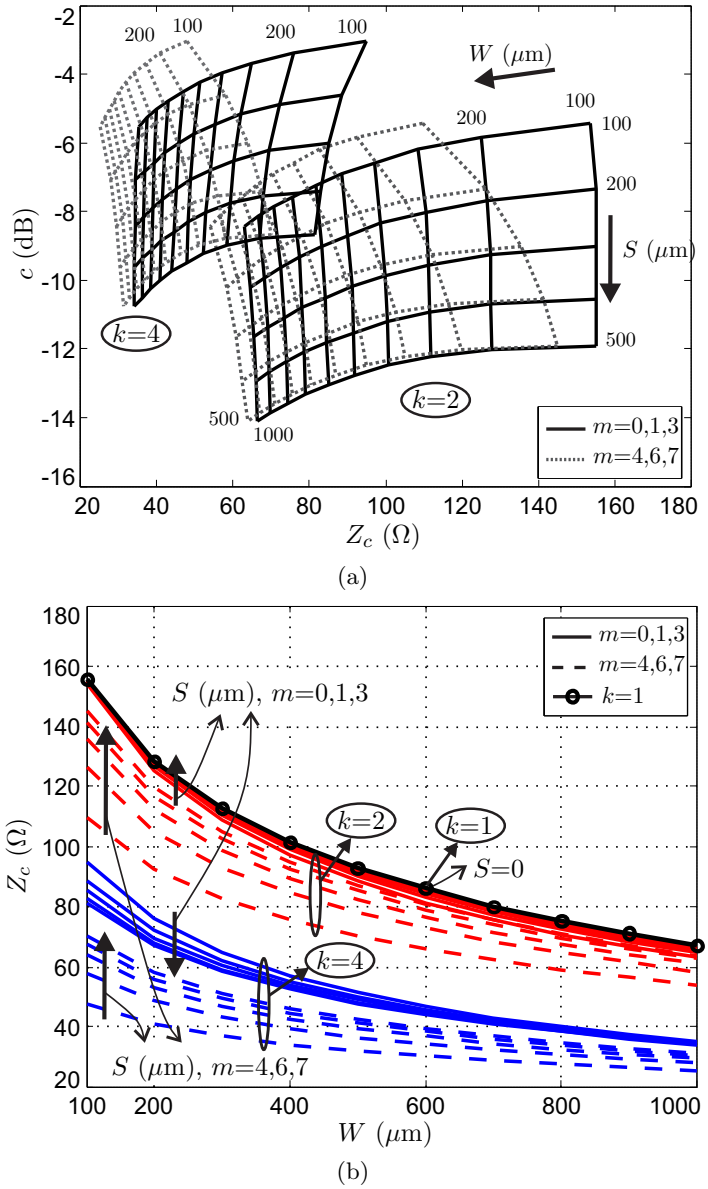

Figure 4.4.: Equivalent characteristic impedance Z_c of a one-port wire-bonded MTL for configurations m=0,4,6 and m=1,3,7, as a function of the number of conductors k and the width W and spacing S. (a) Z_c for k=2,4 including the coupling factor value (4.5) in dB. (b) Z_c for k=1,2,4. S=[100, 200, 300, 400, 500] μm.

Fig. 4.4(a) and Fig. 4.4(b). Nevertheless, it could be easily proven that the reduction of Z_c by increasing the number of strips can be useful for up to six conductors. Using more than six strips is counter-productive because the reduction of Z_c is very small compared to the manufacturing complexity that it involves.

Consequently, taking into account curves of Fig. 4.4, arrangements m=4,6 and m=7 are the most appropriate in implementing low-impedance open- and short-circuited stubs, respectively. Moreover, the lower the Z_c, the higher the value of the effective capacitance and

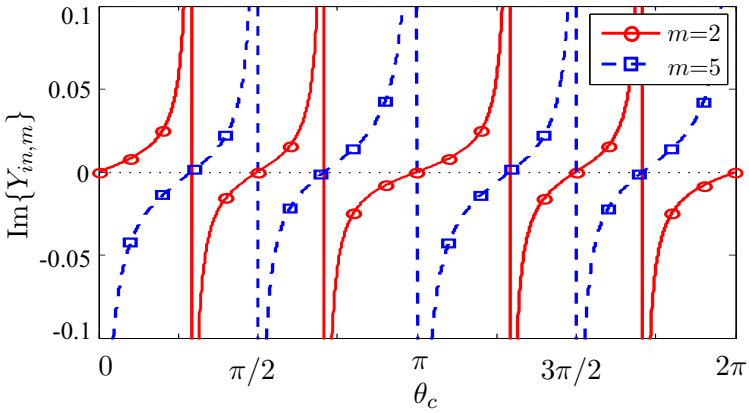

Figure 4.5.: Input susceptance for configurations m=2,5 of a wire-bonded MTL.

the lower the value of effective inductance that can be synthesized. It is worth mentioning that the two-strip (k=2) coupled line section proposed in [17] to implement a high-impedance corresponds to arrangement m=7. Nevertheless, the analysis carried out here indicates that this structure is most appropriate to realize low-impedance short-circuited stubs. It is also worth mentioning that (4.4b) corrects the equation given in [17] to calculate the equivalent characteristic impedance of the proposed structure when k=2.

4.2.2. One-Port Wire-Bonded MTL Equivalent to a Pair of Parallel or Series Short- and Open-Circuited Shunt Stubs (m=2, m=5).

Configurations m=2 and m=5 have a peculiar frequency response because the position of poles or zeros of the input admittances can be tuned by adjusting the coupling factor of the wire-bonded MTL. Fig. 4.5 shows the imaginary part of the input admittance of configurations m=2 and m=5, for a particular MTL. As shown, the poles and zeros of these admittances are not equally spaced in frequency and both admittances have a behaviour different to that achieved with a single short- or open-circuited stub.

The frequency response of both arrangements can be easily understood if their input admittances, given in Table 4.1, are expressed as

$$Z_{in,m=2} = -j\frac{1}{M}\cot\theta_c + j\frac{1}{M}\left(\frac{c^2}{1-c^2}\right)\tan\theta_c \tag{4.6a}$$

$$Y_{in,m=5} = -jM(1-c^2)\cot\theta_c + jMc^2\tan\theta_c, \tag{4.6b}$$

with $Z_{in,m=2}$=$1/Y_{in,m=2}$.

Therefore, from (4.6a) and (4.6b), it is easy to deduce that a MTL-based stub with configurations m=2 or m=5 is equivalent to two stubs, short- and open-circuited stubs connected in series for m=2, and in parallel for m=5. The equivalent circuits for such arrangements are

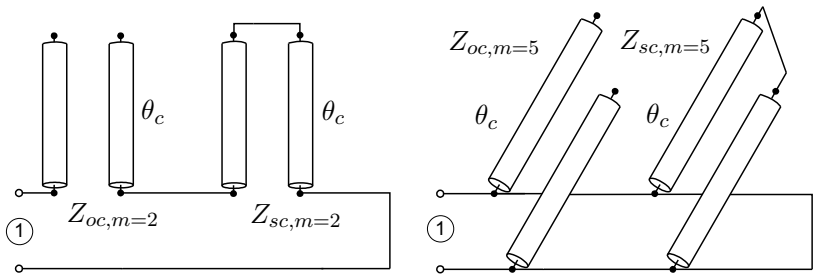

(a) (b)

Figure 4.6.: Equivalent circuits for a wire-bonded MTL using configurations m=2 (a) and m=5 (b).

shown in Fig. 4.6 and can be expressed as

$$Z_{in,m=2} = jZ_{sc,m=2}\tan\theta_c - jZ_{oc,m=2}\cot\theta_c \tag{4.7a}$$

$$Y_{in,m=5} = -j\frac{1}{Z_{sc,m=5}}\cot\theta_c + j\frac{1}{Z_{oc,m=5}}\tan\theta_c, \tag{4.7b}$$

where Z_{sc} and Z_{oc} stand for the equivalent characteristic impedance of the short- and open-circuited stubs, respectively, and are given by

$$Z_{sc,m=2} = Z_{oe}\frac{2(1+u)}{2u+(k-1)(1+u^2)}\frac{c^2}{1-c^2} \tag{4.8a}$$

$$Z_{oc,m=2} = Z_{oe}\frac{2(1+u)}{2u+(k-1)(1+u^2)} \tag{4.8b}$$

$$Z_{sc,m=5} = \frac{1}{c^2}Z_{sc,m=2} \tag{4.8c}$$

$$Z_{oc,m=5} = \frac{1}{c^2}Z_{oc,m=2}. \tag{4.8d}$$

Furthermore, as seen in Fig. 4.5, configurations m=2 and m=5 have a dual behaviour in frequency and poles and zeros for both configurations interchange their locations. Besides, the poles location for arrangement m=2 can be adjusted by selecting the coupling level properly. This property can be very useful when this structure is used as a shunt resonator to introduce transmission zeros at given frequencies, as was shown in [16] for k=2. By operating on $Y_{in,m=2}$ (Table 4.1) the location of poles are given by

$$\theta_{pn} = \pm\theta_{p0} + n\pi, \tag{4.9}$$

θ_{p0} being

$$\theta_{p0} = \arccos\left(\frac{|N|}{M}\right) = \arccos(c), \tag{4.10}$$

with n=0,1,2,3,... The first pole θ_{p0} depends only on c regardless of the number of conductors

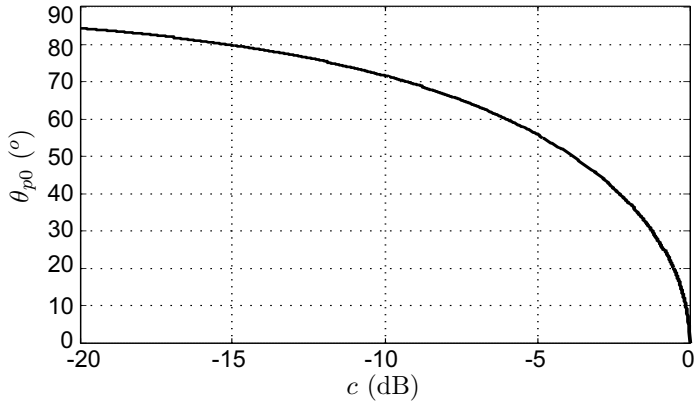

Figure 4.7.: θ_{p0} as a function of the coupling coefficient.

and, if the value of θ_{p0} (4.10) is known, the rest of singularities are perfectly identified. Fig. 4.7 represents θ_{p0} as a function of the coupling level. It is observed that the higher the coupling level, the lower the value of θ_{p0}, and consequently, the greater the bandwidth between the two first poles. This is important if such singularities are used to insert two transmission zeros on both sides of the pass-band of a bandpass filter, because the distance between them can determine the bandwidth of the filter. This characteristic will be used in the next chapters. Hence, the advantage of using more than two conductors is noticeable in order to achieve higher values of c and thus reducing the value of θ_{p0}. As known, to obtain tight coupling values such as 3 dB using only two strips, the spacing between the lines becomes too small to be implemented. Therefore, by means of (4.10) it is straightforward to determine the required coupling level to achieve a desired distance between transmission zeros.

As regards configuration m=5, it seems to be very appropriate to design dual bandpass filters where the bandwidth will be determined by the equivalent characteristic impedances $Z_{sc,m=5}$ and $Z_{oc,m=5}$. As known, when a short-circuited stub and a open-circuited stub are connected in parallel at the same point of a transmission line, a dual wide-band bandpass response is obtained [8, 20]. In this sense, as demonstrated in Subsection 4.2.1, it is possible to achieve values of characteristic impedance that are difficult to obtain or unapproachable with a single strip. Therefore, by using a wire-bonded MTL-based stub with this configuration and by means of (4.7b), it is easy to design filters with broader bandwidths than using two single short- and open-circuited stubs. This fact was proved in [18] for two conductors, but here, the generalized equation for wire-bonded MTLs is derived (4.7b), which allows both, the number of strips and the coupling coefficient to be controlled.

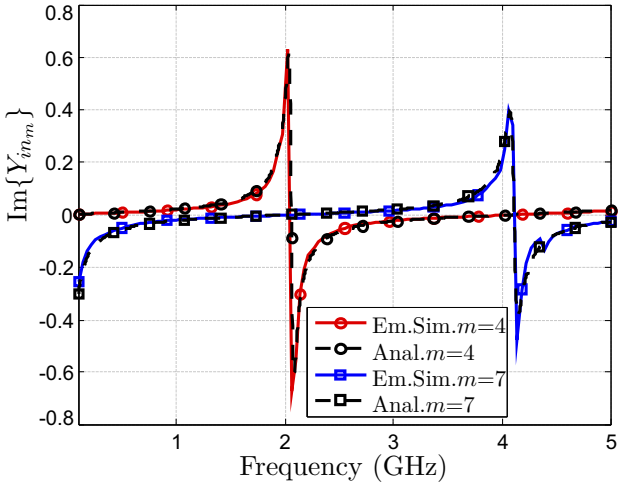

Figure 4.8.: Simulated and analytical imaginary part of the input admittance for configuration m=4 and m=7 of a wire-bonded MTL-based stub. k=4, W=250 μm, S=150 μm, d=22.07 mm.

4.3. Design of an Artificial TL with LH Pass-Band Behaviour and Improved Out-of-Band Rejection

An artificial left-handed TL [21–23] is synthesized by using a wire bonded MTL-based stub as a particular application of the theory described in Section 4.2. The transmission line approach of LH materials has opened up the possibility of designing new devices using simple concepts from transmission line theory [13][14]. The equivalent circuit model of a conventional RH transmission line consists of a series inductor and a shunt capacitor. If both elements interchange their positions, the circuit model of an artificial LH TL is formed. Therefore, the synthesis of LH structures involves using lumped or distributed elements to obtain a series-C/shunt-L behavior.

From here on, the goal is the design of a band-pass LH-TL but with a high selectivity. The proposed unit cell to synthesize the artificial TL consists of a broadband series capacitor (C_L) and a MTL-based stub. From the eight configurations analyzed in this work, arrangements m=4,6,7 are the most suitable for this purpose. Configurations m=0,1,3, although similar in frequency, only for k>4 allow obtaining values of characteristic impedances that are complicated or unapproachable with a single strip and configurations m=2 and m=5 have a narrower frequency band where the MTL acts as an inductance (see Fig. 4.5). Therefore, by using configurations m=4,6,7, it is possible to synthesize equivalent short- or open-circuited stubs and, as a result, low values of shunt inductances in the passband (series-C/shunt-L) and high values of shunt capacitances in the stopbands (series-C/shunt-C). Consequently, the use of a wire-bonded MTL-based stub seems to be appropriate in designing bandpass LH-TLs with sharpened roll-off skirts.

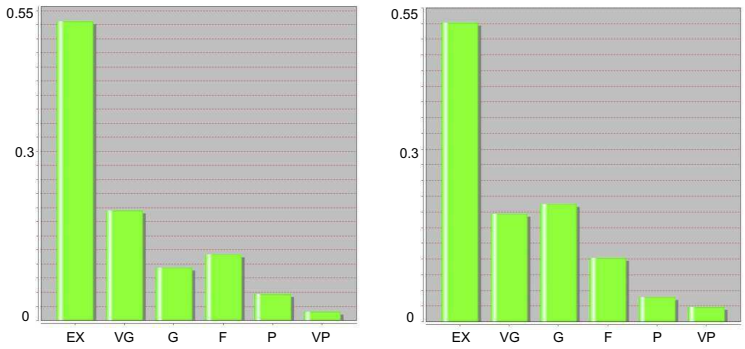

Figure 4.9.: Histogram of the GDM of the comparison between simulated and analytical input admittances represented in Fig. 4.8 for m=4 (a) and m=7 (b).

Nevertheless, prior to the design of the LH-TL and in order to demonstrate the validity of previous analytical equations a MoM-based electromagnetic simulator has been used. Fig. 4.8 draws the simulated and computed imaginary part of the admittances for m=4 and m=7 for a wire-bonded MTL-based stub with four strips 22.07-mm long and 250-μm wide, with gaps of 150 μm (same wire-bonded MTL that will be used in next sections). Only these two configurations have been considered because they are the most advisable structures to be used in designing circuits where a low-impedance open- or short-circuited stub is required. Structure m=6 has not been included in Fig. 4.8 because it has the same frequency response as configuration m=4 but its layout is more complex. From Fig. 4.8 it is easy to appreciate that there is a very good agreement between curves and consequently, that analytical equations derived in this chapter can be easily employed to model and design the equivalent wire-bonded MTL-based stubs. In addition, the Feature Selective Validation (FSV) technique [24, 25] has been employed to compare both simulated and theoretical results. Recently, this technique has been included in the IEEE Standard P1597 [26] (Standard for Validation of Computational Electromagnetics Computer Modeling and Simulation) as the procedure to quantify the agreement between simulation results and validation comparisons. The FSV technique includes three figures of merits, the Amplitude Difference Measure (ADM), the Feature Difference Measure (FDM) and the Global Difference Measure (GDM) that combines the ADM and FDM . Furthermore, two qualities factors for each figure of merit can be computed, the Grade and Spread values [24–26]. Fig. 4.9 represents the histogram of the GDM figure of merit [27] for configurations m=4 and m=7, where the values of Grade and Spread are 3 and 3, respectively, in both cases. From these values and taking into account Fig. 4.9, it is possible to confirm the excellent accuracy of the analytical equations.

The layout of the proposed unit cell is shown in Fig. 4.10, where configuration m=4 has been chosen. This configuration is the simplest one that starts as a capacitance at low frequencies, and as a result, the shunt branch is equivalent to a low-impedance, open-circuited stub. Besides, this unit cell is an option to solve the drawback exhibited by the standard unit

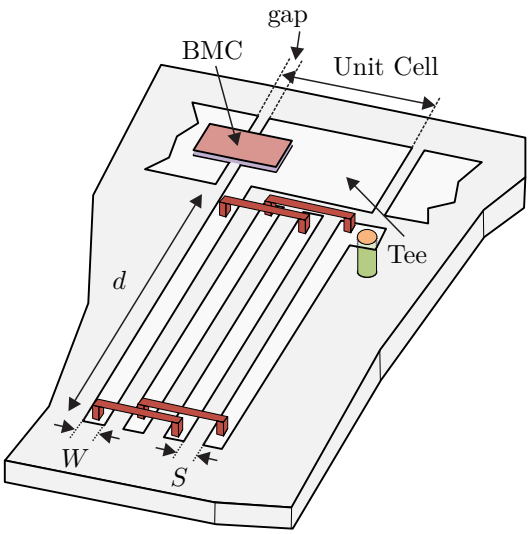

Figure 4.10.: Layout of a unit cell made up of a series surface mount capacitor and a shunt one-port MTL. A broadband multilayer capacitor (BMC) is used to connect adjacent unit cells.

cell that consists of an interdigital capacitor and short-circuited stub for biasing active devices [28]. Therefore, if the parasitic effects are neglected, stop-bands and LH-bands are expected when the wire-bonded MTL behaves as a capacitor or inductor, respectively [13] (see Fig. 4.3). This can be expressed as

$$\theta_c \in [0, \pi/2] + n\pi : \text{stop bands} \tag{4.11}$$

$$\theta_c \in [\pi/2, \pi] + n\pi : \text{LH bands.} \tag{4.12}$$

This frequency behaviour shows the advantages of using shunt wire-bonded MTL-based stubs instead of single strips in designing LH-TLs. By using equivalent low-impedance stubs, the value of the shunt inductance in the operating frequency band ($\theta_c \in [\pi/2,\pi]$) is lower and, as a consequence, the required series capacitance C_L to synthesize an artificial TL with a particular value of characteristic impedance Z_0 will also be lower. Besides, it is possible to obtain a greater sharp cutoff with larger rejection in the stop bands, because in these bands, the lower the equivalent characteristic impedance Z_c of the wire-bonded MTL, the greater the synthesized shunt capacitance.

By considering the impedance of a simple series capacitor $Z_s=(\mathrm{j}2\pi C_L)^{-1}$ and the admittance of the used MTL-based stub $Y_{in,m=4}$ (Table 4.1), the characteristic impedance Z_0 and the propagation constant γ of the synthesized TL by means of the proposed unit cell, can be

calculated as [13]

$$Z_0 = \sqrt{\frac{Z_s}{Y_{in,4}}} = -j\left(Z_{c,4}\cdot\frac{\sqrt{\epsilon_{reff}}\,d}{c\,C_L}\cdot\frac{\cot\theta_c}{\theta_c}\right)^{1/2} \tag{4.13a}$$

$$\gamma\Delta\ell = \sqrt{Z_s Y_{in,4}} = \left(\frac{1}{Z_{c,4}}\cdot\frac{\sqrt{\epsilon_{reff}}\,d}{c\,C_L}\cdot\frac{\tan\theta_c}{\theta_c}\right)^{1/2} \tag{4.13b}$$

where $Z_{c,m=4}$ is the equivalent characteristic impedance of the MTL-based stub (4.4b), c is the speed of light in vacuum, d is the length of the strips, $\Delta\ell$ is the length of a unit cell ($\gamma\Delta\ell \ll 1$ to satisfy the homogeneity condition) and the effective relative permittivity ϵ_{reff} is computed from the corresponding values of the even and odd modes of a pair of adjacent lines of the MTL as [9, 10]

$$\sqrt{\epsilon_{reff}} = \frac{\sqrt{\epsilon_{reffe}} + \sqrt{\epsilon_{reffo}}}{2}. \tag{4.14}$$

Therefore, by means of (4.13), the main parameters of the synthesized artificial TL can be computed. However, it would be interesting to determine the value of θ_c where the variation in the characteristic impedance Z_0 is minimum. If this value is used to design the MTL at the design center frequency, the widest LH operational frequency band is expected. This parameter can be easily obtained if we focus on Z_0 and calculate the derivative of $(\cot\theta_c/\theta_c)^{1/2}$ with respect to θ_c as

$$\theta_{cm} = arg\min_{\theta_c}\left\{\frac{\partial}{\partial\theta_d}\left(\frac{\cot\theta_c)}{\theta_c}\right)^{1/2}\right\}\ \frac{\pi}{2} < \theta_c < \pi. \tag{4.15}$$

By evaluating (4.15) θ_{cm}=0.7π is obtained approximately. Only the range $\pi/2 < \theta_c < \pi$ is considered because in this interval the MTL-based stub acts as inductance ((4.12), Fig. 4.3). Hence, by adopting this criterion and from (4.13a), the value of the series capacitance and the length of the strips d can be obtained as

$$C_L(\theta_c = \theta_{cm}) = -\frac{Z_{c,m=4}}{(Z_0)^2}\frac{1}{2\pi f_o}\cot(\theta_{cm}) \tag{4.16a}$$

$$d = \frac{c\cdot\theta_{cm}}{2\pi f_o\sqrt{\epsilon_{reff}}}, \tag{4.16b}$$

where f_o accounts for the design frequency, which should be the design center frequency.

Clearly, from (4.16a), the lower the characteristic impedance $Z_{c,m=4}$, the lower the value of C_L in order to achieve a particular Z_0. Table 4.2 shows an example of evaluating (4.16a) when the number of conductors is changed for several values of W and S. Z_0 is fixed to 50 Ω and the design frequency f_o is 3 GHz. The substrate used is the Rogers 4350B, the same used in section 4.2.1. As can be seen, by increasing the number of lines, both the equivalent characteristic impedance and the series capacitance reduce. This has a noticeable advantage, because reducing the required series capacitance allows the effects of the unavoidable parasitic

Table 4.2.: Design values for the unit cell of Fig. 4.10. Z_0=50 Ω, f_o=3 GHz.

	k=2	k=4	k=6
W=100, S=100 (μm)	$Z_{c,4}$=109.5 Ω	$Z_{c,4}$=47.9 Ω	$Z_{c,4}$=30.6 Ω
d=22.33 mm	c=-5.4 dB	c=-3.1 dB	c=-2.5 dB
	C_L=1.7 pF	C_L=0.74 pF	C_L=0.47 pF
W=250, S=100 (μm)	$Z_{c,4}$=87.1 Ω	$Z_{c,4}$=38.7 Ω	$Z_{c,4}$=24.9 Ω
d=22.1 mm	c=-6 dB	c=-3.5 dB	c=-2.9 dB
	C_L=1.3 pF	C_L=0.6 pF	C_L=0.4 pF
W=250, S=150 (μm)	$Z_{c,4}$=93.6 Ω	$Z_{c,4}$=42.5 Ω	$Z_{c,4}$=27.5 Ω
d=22.07 mm	c=-7 dB	c=-4.3 dB	c=-3.6 dB
	C_L=1.4 pF	C_L=0.7 pF	C_L=0.4 pF

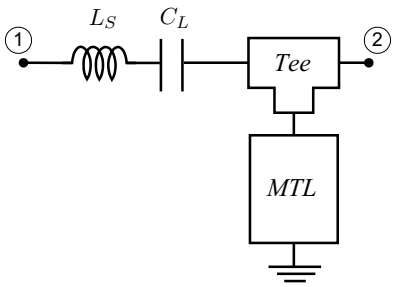

Figure 4.11.: Unit cell model considering a parasitic series inductance and the tee-junction where the series capacitor is placed.

series inductance to be moved to higher frequencies [13, 14].

4.4. Experimental Validation

Design equations of pass-band LH-TLs using shunt wire-bonded MTL-based stubs have been derived in Section 4.3 and some designs are detailed in Table 4.2. In this Section, to validate the analytical equations and design procedure, two prototypes for k=2 and k=4 are manufactured and measured. A line-width (W) of 250 μm and spacing (S) of 150 μm, as well as the capacitances shown in Table 4.2 for two and four conductors, are chosen. It is important to note that the widths and spacing between lines have been chosen large enough in order to avoid problems during the manufacturing process. The series lumped-element capacitors are implemented using the ATC 500S broadband microwave capacitors (BMC) which are suitable for surface mounting.

Furthermore, as is well known, any physical implementation includes parasitic effects that have not been considered so far; the model shown in Fig. 4.11 will be used to compute the S-parameters. This model includes a series parasitic inductance L_S and the microstrip tee-

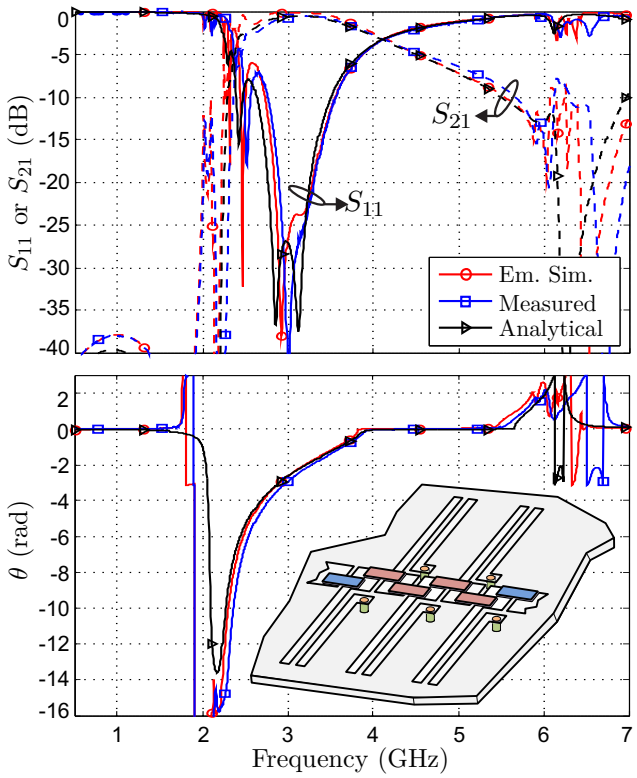

Figure 4.12.: Analytical, simulated and measured scattering matrix elements (S_{11}, S_{21}) and unwrapping electrical length θ for five unit cells in symmetric configuration. k=2, W=250 μm, S=150 μm, d=22.07 mm, C_L=1.5 pF, f_o=3 GHz.

junction [15] where the series capacitor is placed. The electrical length θ is computed by means of the expression [13]

$$\theta = \mathrm{Im}\left(\cosh^{-1}\left(\frac{1+S_{12}^2-S_{11}S_{22}}{2S_{12}}\right)\right), \tag{4.17}$$

where $\mathrm{Im}(x)$ denotes the imaginary part of x.

Measurements have been carried out by a vector network analyzer calibrated using the thru-reflect-line (TRL) method and all prototypes are made symmetrical by terminating them by two capacitances of value $2C_L$. In the next figures these capacitors of double value ($2C_L$) are colored blue in order to differentiate them from the intermediate ones (C_L) colored red.

Therefore, Fig. 4.12 and Fig. 4.13 represent the S_{11} and S_{21} parameters along with the unwrapped electrical length θ for two manufactured circuits, comparing the calculated parameters using a full-wave electromagnetic solver and an analytical model to measured results. A LH bandpass frequency response is achieved in both prototypes with return losses greater than 20 dB at the design frequency f_o=3 GHz. Insertion losses are lower than 1 dB and there is a very good agreement between analytical results and measurements. Furthermore, as expected, it is observed that by increasing the number of conductors of the MTL-based

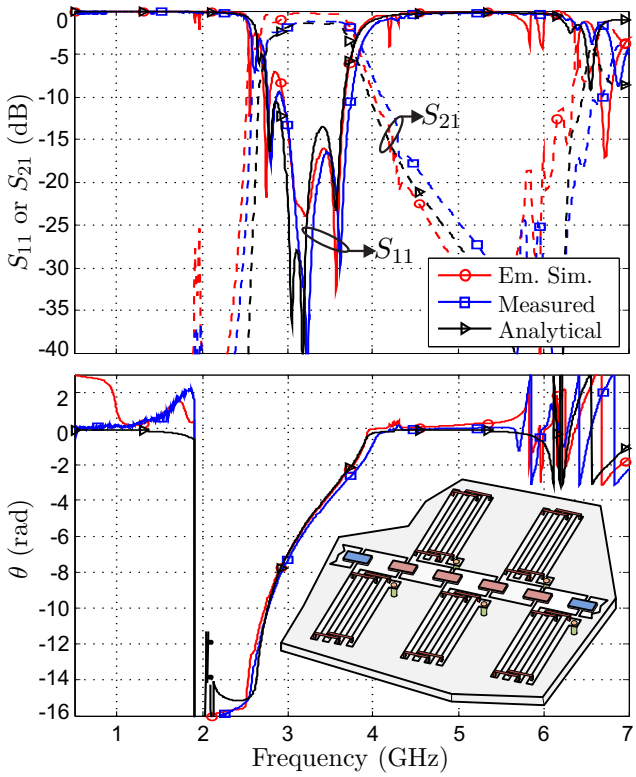

Figure 4.13.: Analytical, simulated and measured scattering matrix elements (S_{11}, S_{21}) and unwrapping electrical length θ for five unit cells in symmetric configuration. k=4, W=250 μm, S=150 μm, d=22.07 mm, C_L=0.6 pF, f_o=3 GHz.

stub the out-of-band rejection is improved. Therefore, bandpass LH-TLs with sharp rejection skirts can be achieved because the synthesized capacitance in the stop-bands is greater by using more fingers. However, using more strips implies a moderate increase in the insertion loss (0.5 dB approximately). This effect is reasonable because not only the number of conductors is higher but also the LH-TL is longer. However, attending to the concordance between analytical equations and measurements it is possible to notice the outgoing possibilities of this structure for applications where it is necessary to obtain a particular phase response. Some potential applications are the design of baluns, rat-race coupler, hybrid rings or phase-shifting sections. Besides, it is important to remark that the importance of LH-TLs mainly resides in its phase response. By contrary, if the goal is the design of a filter, configurations m=2 and m=5 are the expedient structures because of its peculiar behaviour in frequency. A photograph of the prototype with four strips is shown in Fig. 4.14.

In addition, it is important to emphasize that these prototypes have been designed using just the equations given in this work, with no optimization-based tuning of the manufactured circuits.

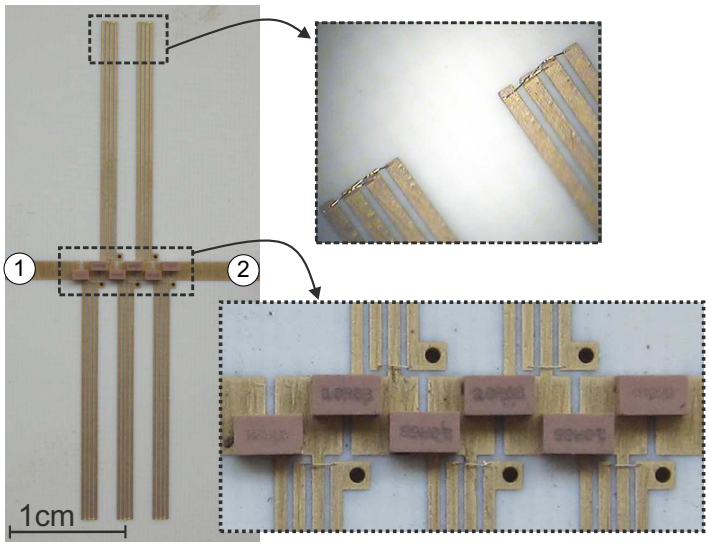

Figure 4.14.: Photograph of the prototype designed with five unit cells, k=4, W=250 μm, S=150 μm, d=22.07 mm, C_L=0.6 pF, f_o=3 GHz.

4.5. Conclusion

Wire-bonded multiconductor transmission lines with bonding wires between alternate strips (wire-bonded MTLs) have been proposed as an efficient way of implementing shunt stubs. A general analysis of the performance of all eight possible configurations and an arbitrary number of strips has been performed. This analysis has yielded compact equations that not only ease the design, but also provide a physical insight into the frequency behaviour of the different configurations. It has been demonstrated that six configurations are equivalent to low-impedance single short- or open-circuited stubs. The possibility of realizing values of equivalent characteristic impedances that would be complicated or unapproachable by means of a single strip has been proved. The other two configurations have particular frequency responses that can be very useful for the design of bandpass filters. For these two arrangements, analytical equations to calculate the pole and zero position of MTL-based stubs as a function of the coupling level have been given. It allows the position of the transmission zeros to be adjusted by designing the MTL-based stub properly. Moreover, two simple, but accurate, equivalent circuits have been developed that could easily be incorporated into the application design flow. In all the cases, the influence of the number of the strips on the MTL-based stub performance has also been assessed.

Finally, as an application of the theory developed here a LH-TL has been designed and manufactured. The experimental results have proven that by using MTL-based stubs it is possible to synthesize LH bandpass structures with a sharp cutoff. Furthermore, it has been demonstrated that skirt selectivity is augmented by increasing the number of strips.

In addition, an excellent agreement between analytical results and measurements has been

obtained without the need for any optimization process requiring a full-wave electromagnetic simulation. As a result, the use of the analytical equations presented in this work are advisable to obtain time-saving design procedures for many different devices such as filters, hybrid rings, baluns, rat-race couplers, and other microwave circuits.

References

[1] E. M. T. Jones and J. T. Bolljahn, "Coupled-Strip-Transmission-Line Filters and Directional Couplers," *IRE Trans. Microw. Theory Tech.*, vol. 4, no. 2, pp. 75–81, Apr. 1956.

[2] G. Zysman and A. Johnson, "Coupled transmission line networks in an inhomogeneous dielectric medium," *IEEE Trans. Microw. Theory Tech.*, vol. 17, no. 10, pp. 753–759, Oct. 1969.

[3] J. Lange, "Interdigitated Strip-Line Quadrature Hybrid," in *Microwave Symposium, 1969 G-MTT International*, May 1969, pp. 10–13.

[4] W. Ou, "Design Equations for an Interdigitated Directional Coupler," *IEEE Trans. Microw. Theory Tech.*, vol. 23, no. 2, pp. 253–255, Feb. 1975.

[5] A. Presser, "Interdigitated microstrip coupler design," *IEEE Trans. Microw. Theory Tech.*, vol. 26, no. 10, pp. 801–805, Oct. 1978.

[6] R. Levy and S. Cohn, "A History of Microwave Filter Research, Design, and Development," *IEEE Trans. Microw. Theory Tech.*, vol. 32, no. 9, pp. 1055–1067, Sep. 1984.

[7] S. Cohn and R. Levy, "History of Microwave Passive Components with Particular Attention to Directional Couplers," *IEEE Trans. Microw. Theory Tech.*, vol. 32, no. 9, pp. 1046–1054, Sep. 1984.

[8] G. L. Mattahei, L. Young, and E. M. T. Jones, *Microwave Filters, Impedance-Matching Networks, and Coupling Structures*, M. A. House, Ed. Norwood, 1985.

[9] J. A. B. Faria, *Multiconductor Transmission-line Structures: Modal Analysis Techniques.* New York: Wiley, 1993.

[10] C. R. Paul, *Analysis of Multiconductor Transmission Line.* New York: Wiley, 1994.

[11] R. Mongia, I. Bahl, and P. Bhartia, *RF and Microwave Coupled-Line Circuits.* Norwood, MA: Artech House, 1999.

[12] F. Casares-Miranda, P. Otero, E. Márquez-Segura, and C. Camacho-Peñalosa, "Wire Bonded Interdigital Capacitor," *IEEE Microw. Wireless Compon. Lett.*, vol. 15, no. 10, pp. 700–702, Oct. 2005.

[13] C. Caloz and I. Itoh, *Electromagnetic Metamaterials: Transmission Line Theory and Microwave Applications.* Wiley-Interscience, 2006.

[14] G. Eleftheriades and K. Balmain, *Negative-Refraction Metamaterials: Fundamental Principles and Applications.* Wiley-Interscience, 2006.

[15] J. J. Sánchez-Martínez, E. Márquez-Segura, P. Otero, and C. Camacho-Peñalosa, "Artificial Transmission Line with Left/Right-Handed Behavior Based on Wire Bonded Interdigital Capacitors," *Progr. Electromagn. Res. B*, vol. 11, pp. 245–264, 2009.

[16] Y. Omote, T. Yasuzumi, T. Uwano, and O. Hashimoto, "Design procedure of wideband band-pass filter consists of inter-digital finger resonator and parallel coupled lines," in *Proc. Asia-Pacific Microw. Conf.*, Dec. 2010, pp. 29–32.

[17] H.-R. Ahn and S. Nam, "Wideband coupled-line microstrip filters with high-impedance short-circuited stubs," *IEEE Microw. Wireless Compon. Lett.*, vol. 21, no. 11, pp. 586–588, Nov. 2011.

[18] J.-T. Kuo, C.-Y. Fan, and S.-C. Tang, "Dual-wideband bandpass filters with extended stopband based on coupled-line and coupled three-line resonators," *Progr. Electromagn. Res.*, vol. 124, pp. 1–15, 2012.

[19] J. J. Sánchez-Martínez and E. Márquez-Segura, "Comments on 'Wideband Coupled-Line Microstrip Filters With High-Impedance Short-Circuited Stubs'," *IEEE Microw. Wireless Compon. Lett.*, vol. 22, no. 9, p. 492, Sep. 2012.

[20] D. Pozar, *Microwave Engineering*, 2nd ed. New York: Wiley, 1998.

[21] G. Eleftheriades, A. Iyer, and P. Kremer, "Planar negative refractive index media using periodically L-C loaded transmission lines," *IEEE Trans. Microw. Theory Tech.*, vol. 50, no. 12, pp. 2702–2712, Dec. 2002.

[22] C. Caloz and T. Itoh, "Application of the Transmission Line Theory of Left-Handed (LH) Materials to the Realization of a Microstrip LH Line," in *IEEE Antennas and Propagation Society International Symposium*, vol. 2, 2002, pp. 412–415.

[23] A. Oliner, "A planar negative-refractive-index medium without resonant elements," in *IEEE MTT-S International Microwave Symposium Digest*, vol. 1, Jun. 2003, pp. 191–194.

[24] A. Duffy, A. Martin, A. Orlandi, G. Antonini, T. Benson, and M. Woolfson, "Feature selective validation (FSV) for validation of computational electromagnetics (CEM). part I-the FSV method," *IEEE Trans. Electromagn. Compat.*, vol. 48, no. 3, pp. 449–459, Aug. 2006.

[25] A. Orlandi, A. Duffy, B. Archambeault, G. Antonini, D. Coleby, and S. Connor, "Feature selective validation (FSV) for validation of computational electromagnetics (CEM). part II- assessment of FSV performance," *IEEE Trans. Electromagn. Compat.*, vol. 48, no. 3, pp. 460–467, Aug. 2006.

[26] "Draft standard for validation of computational electromagnetics computer modeling and simulations," *IEEE Unapproved Draft Std P1597.1/D4.3, Jun 2008*, 2008.

[27] [Online]. Available: http://uaqemc.ing.univaq.it/uaqemc/\FSV_Tool_2_0_0L

[28] J. Mata-Contreras, T. Martin-Guerrero, and C. Camacho-Peñalosa, "Assessment of a Composite Right/Left-Handed Transmission Line-based Distributed Amplifier implemented in microstrip technology," in *36th European Microwave Conference*, Sep. 2006, pp. 1586–1589.

Chapter 5

Ultra-Wideband Differential Bandpass Filters

A systematic design process of ultra-wideband differential bandpass filters based on wire-bonded multiconductor transmission lines is presented in this chapter. In Section 5.2 the proposed topology is thoroughly analyzed by means of analytical design equations that provide some insights into the physical behaviour of the structure. Single-section and double-section configurations are introduced and exact closed-form design equations are derived to design differential filters with either a Butterworth or Chebyhsev frequency response. To validate the design procedure, in Section 5.3 two differential filters are designed and fabricated with an equal-ripple fractional bandwidth (FBW) of 100% and 60%, respectively. In addition, the measurements demonstrate that this type of filter provide a high common-mode rejection levels, with values higher than 20 dB.

5.1. Introduction

Nowadays, the use of balanced circuits is increasingly widespread by their benefits over single-ended techniques. The signal processing in differential devices provides high-noise immunity, increased dynamic range, and reduced even-order distortion for differential low-noise amplifiers. In addition, the increase in the dynamic range compared to a similar single-ended circuit implementation is of great interest because it allows reducing the circuit supply voltage and, consequently, the circuit power consumption [1]. In that sense, differential filters with common-mode rejection capability have become essentials in the design of balanced circuits.

Different topologies have been proposed to differential filtering with common-mode suppression. A branch-line structure is proposed in [2], which is extended in [3] by increasing the selectivity. However, the circuit size is enlarged and the achieved differential-mode passband is only of 62%. Another branch-line structure, based on double-sided parallel-strip line, is introduced in [4], a three-layer broadside coupled microstrip-slot-microstrip structure is used in [5], and a differential wideband bandpass filter using a slot-line resonator is presented in [6]. Notwithstanding, these topologies increase the fabrication complexity and the introduction of slot-line can cause electromagnetic interference. Coupled-resonator configurations based on stepped-impedance resonators have been proposed in [7, 8] and recently, an S-shaped complementary split ring resonator has been employed in [9], but they have a limited bandwidth. Differential filters based on T-shaped structures [10] or with other different topologies have been also explored in [11, 12]. However, the design of compact ultra-wideband differential passband filters with common-mode suppression is still a challenge.

Coupled-line based differential filters are presented in [13] and [14]. Both works employ similar structures, but in [13], the design of an interdigital filter for the differential passband is proposed, while in [14] only two lines are employed. However, the differential-mode passband in [13] is degraded with return losses of about 5 dB, and filters in [14] are only suitable for narrowband applications. In addition, most of these designs either lack of a systematic design procedure in order to analytically compute the filter design parameters to met a prescribed frequency response, or are based on approximate techniques for narrow and moderate bandwidths employing ideal impedance or admittance inverters [15].

In this chapter, a compact differential bandpass filter based on wire-bonded multiconductor transmission lines is proposed and analyzed by means of analytical design equations. Under the odd-mode excitation the filter can be easily designed to have ultra-wideband differential-mode passband, while it provides a good common-mode rejection for common-mode signals. It can be demonstrated that the differential to differential S-parameters of the filter only depends on the design of the odd-mode equivalent circuit. The synthesis procedure, as in [16–18], is carried out by computing and equating the transfer functions of the proposed filters to Butterworth or Chebyshev filtering functions. Once the fractional bandwidth and required return losses are chosen, the circuit design parameters can be calculated. In Section 5.3 several prototypes are designed and fabricated to validate the predicted theoretical differential-mode frequency responses.

5.2. Analysis and Design Procedure

The proposed differential filter consists of cascaded two-port short-circuited wire-bonded MTLs. By increasing the number of MTLs the selectivity of the filter is enhanced, but the large overall size can be a cumbersome issue for practical applications. Taking into account

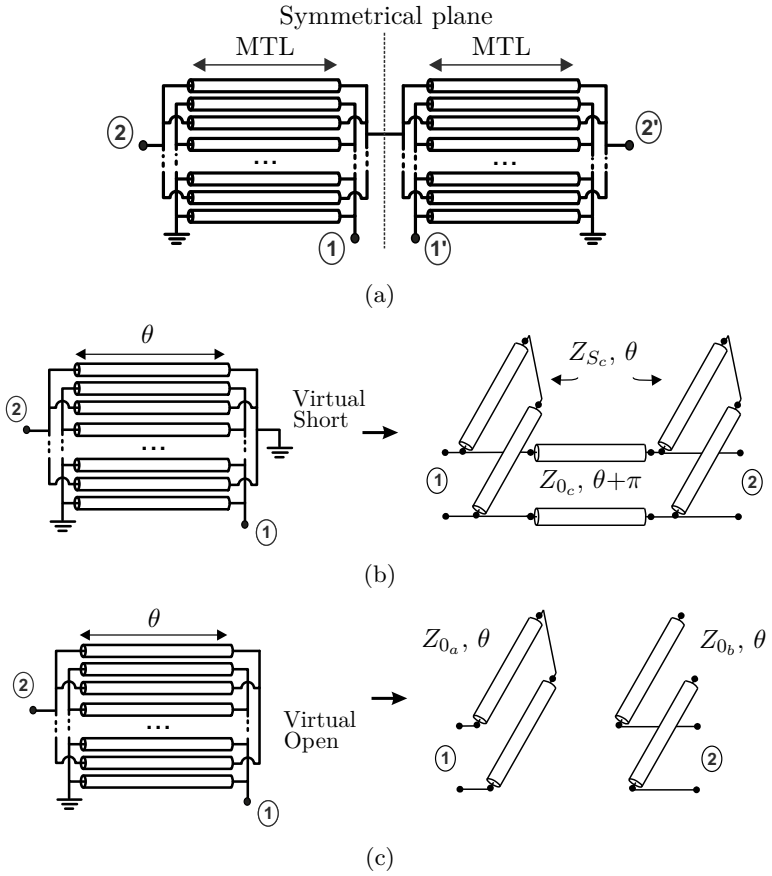

Figure 5.1.: (a) Transmission line equivalent model of the proposed wideband differential bandpass filter and corresponding equivalent circuit models under (b) odd- and (c) odd-mode excitations.

this consideration and pursuing the synthesis of wideband frequency responses, the following analytical study is carried out for single- and double-section filters.

5.2.1. Single-Section Differential Filter

For a single-section differential filter, two wire-bonded multiconductor transmission lines are connected as represented in Fig. 5.1(a). This topology is ideally symmetrical and thus, it can be readily analyzed under odd- and even-mode excitations. The equivalent half-circuits that result from differential and common mode are sketched in Fig. 5.1(b) and Fig. 5.1(c), respectively. The circuit under differential excitation was modeled in Chapter 2 and later used in Chapter 3 to synthesize wideband baluns and a test set for the characterization of differential devices. Thus, this circuit can be designed to have a bandpass frequency response. Nevertheless, to analyze the circuit under even excitation the admittance matrices of both equivalent circuits are calculated. By using the four-port admittance matrix given in [19] for

a Lange coupler, the next to admittance matrices are obtained

$$[Y]_o = \begin{bmatrix} Y_{11_o} & Y_{12_o} \\ Y_{21_o} & Y_{22_o} \end{bmatrix} = \begin{bmatrix} -jM\cot\theta & jN\csc\theta \\ jN\csc\theta & -jM\cot\theta \end{bmatrix} \tag{5.1a}$$

$$[Y]_e = \begin{bmatrix} Y_{11_e} & Y_{12_e} \\ Y_{21_e} & Y_{22_e} \end{bmatrix} = \begin{bmatrix} -j\frac{M^2-N^2}{M}\cot\theta & 0 \\ 0 & jM\tan\theta \end{bmatrix}, \tag{5.1b}$$

where subscripts o and e stand for the odd- and even-mode circuits, and θ is the electrical length of the conductors (2.5). M and N are related to the even- and odd-mode impedances of a pair of coupled lines and can be expressed as (2.2)

$$M = \frac{1}{Z_{oe}+Z_{oo}}\left(1+\frac{(k-1)}{2}\frac{Z_{oe}^2+Z_{oo}^2}{Z_{oe}Z_{oo}}\right) \tag{5.2a}$$

$$N = \frac{k-1}{2}\frac{Z_{oo}-Z_{oe}}{Z_{oe}Z_{oo}}, \tag{5.2b}$$

where k is the number of conductors. From (5.1), the two equivalent circuit models shown in Fig. 5.1 can be deduced. The equivalent circuit model under differential excitation was presented in Section 2.3, while the equivalent circuit model under odd-mode excitation can be easily derived from (5.1b) as two isolated short-circuited and open-circuited stubs (Y_{12_e}=Y_{21_e}=0). Therefore, the equivalent odd-mode circuit has a bandpass frequency response, whereas there is a theoretical perfect rejection of the common-mode. Similar equivalent circuit models were obtained in [20] for two parallel coupled lines (k=2). Now, the characteristic impedances of both equivalent circuits for multiconductor transmission lines, represented in Fig. 5.1(b) and Fig. 5.1(c), are given as

- Equivalent circuit model under odd-mode excitation (see Fig. 5.1(b)):

$$Z_{0_c} = \frac{-1}{N}, \qquad Z_{S_c} = \frac{1}{M+N} \tag{5.3}$$

- Equivalent circuit model under even-mode excitation (see Fig. 5.1(c)):

$$Z_{0_a} = \frac{M}{M^2-N^2}, \qquad Z_{0_b} = \frac{1}{M} \tag{5.4}$$

By simple transformations of (5.1), the mixed-mode S-parameters [1] of the balanced filter are determined as

$$[S]^{mm} = \begin{bmatrix} S_{dd_{11}} & S_{dd_{12}} & S_{dc_{11}} & S_{dc_{12}} \\ S_{dd_{21}} & S_{dd_{22}} & S_{dc_{21}} & S_{dc_{22}} \\ S_{cd_{11}} & S_{cd_{12}} & S_{cc_{11}} & S_{cc_{12}} \\ S_{cd_{21}} & S_{cd_{22}} & S_{cc_{21}} & S_{cc_{22}} \end{bmatrix} = \begin{bmatrix} S_{11_o} & S_{21_o} & 0 & 0 \\ S_{21_o} & S_{11_o} & 0 & 0 \\ 0 & 0 & S_{11_e} & 0 \\ 0 & 0 & 0 & S_{22_e} \end{bmatrix}, \tag{5.5}$$

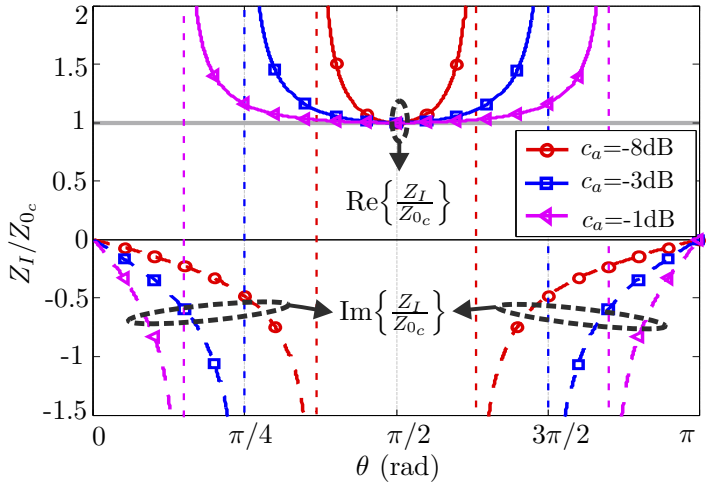

Figure 5.2.: Image impedance of a two-port short-circuited wire-bonded MTL normalized by its characteristic impedance Z_{0_c} for several coupling values (5.7).

where it can be seen, as expected, that the differential to differential terms only depend on the odd-mode equivalent circuit. Besides, because the proposed structure is reciprocal and symmetrical, the cross-mode S-parameters are zero [21]. In addition, it would be desirable to obtain a design procedure to synthesize the differential filter satisfying prescribed specifications (i.e., return losses and operating bandwidth).

The frequency response of the proposed filter can be inferred from the image impedance [22] of the odd-mode equivalent circuit. From (5.1), the image impedance of the two-port short-circuited wire-bonded MTL (Fig. 5.1(b)) is computed as

$$Z_I = Z_{0_c}\frac{c\sin\theta}{\sqrt{c^2-\cos^2\theta}}, \tag{5.6}$$

where Z_{0_c} was defined in (5.3) and c is related to the maximum coupling coefficient of a k-line quarter-wavelength four-port coupler as (2.11)

$$c = \frac{-N}{M}. \tag{5.7}$$

Considering (5.6), it is clear that the image impedance of the two-port circuit is equal to the characteristic impedance Z_{0_c} at $\theta{=}\pi/2$, that normally corresponds to the design center frequency. Besides, as it will be demonstrated later, the value of Z_{0_c} conditions the type of frequency response. Fig. 5.2 depicts the image impedance, normalized by Z_{0_c} for several values of c. As seen, there is a frequency range where the image impedance is purely real but, out of this band, it behaves as a capacitive reactance. In addition, from this figure, it is also possible to deduce two main properties of the structure. First, by increasing the coupling, the frequency range with purely real image impedance values is broaden. Thus, as it is well known in coupled-line filters [23], the greater the coupling factor, the wider the operating

bandwidth. Second, being Z_0 the characteristic impedance used to terminate the input and output ports, the filter can be designed to have either a Butterworth, or a Chebyshev type response with two transmission poles. If Z_{0_c}=Z_0, the wire-bonded MTL is matched at θ=$\pi/2$, regardless the coupling factor c, and for values of $Z_{0_c} < Z_0$ there are two frequencies with perfect matching. Therefore, if the MTL is a quarter-wavelength long at the center frequency, it can be readily designed to be matched at mid-band frequency for a maximally flat response, or to have an equal-ripple response with two transmission poles.

It is important to highlight that, although c is defined equal to the maximum coupling factor of a k-line quarter-wavelength coupler [19], the design equations deduced in this work are different to the given for a coupler. Consequently, the value of c may not be interpreted as the voltage coupling between the input and coupled ports of a four-port directional coupler. This property is useful for designers, because the fabrication complexity of the structure is not only conditioned by the value of c, but also by Z_c. Such behaviour is shown in Fig. 5.3, where the achievable values of c and Z_c are represented as a function of the line width W and spacing S, for several number of conductors k. The substrate chosen is Rogers 4350B with a relative permittivity of 3.66 and thickness of 30 mil. In particular, from Fig. 5.3 and taking into account the tendency of curves, it is remarkable that it is difficult to obtain low values of Z_{0_c} with high coupling factors with only two conductors. This is important because to design a two-pole wideband bandpass filter, it is necessary to achieve high values of c with values of Z_{0_c} lower than the load impedance Z_0. Therefore, it is demonstrated the importance of increasing the number of conductors in designing wideband differential filters using short-circuited wire-bonded MTLs.

The use of the image impedance enhances the physical insight into the frequency behaviour of the structure. However, as it was commented before, it should be worth to obtain a set of design expressions that allow synthesizing a desired response. In that case, the design procedure using the insertion loss method is more expedient [22] to find a direct relation between the filter performance (operating bandwidth and return loss) and the design variables Z_{0_c} and c.

From (5.1a), the differential S-parameters are computed by applying the following transformations

$$S_{dd_{11}} = S_{dd_{22}} = \frac{Y_0^2 - Y_{11_o}^2 + Y_{12_o}^2}{(Y_0 + Y_{11_o})^2 - Y_{12_o}^2} \tag{5.8a}$$

$$S_{dd_{12}} = S_{dd_{21}} = \frac{-2Y_{12_o}Y_0}{(Y_0 + Y_{11_o})^2 - Y_{12_o}^2} \tag{5.8b}$$

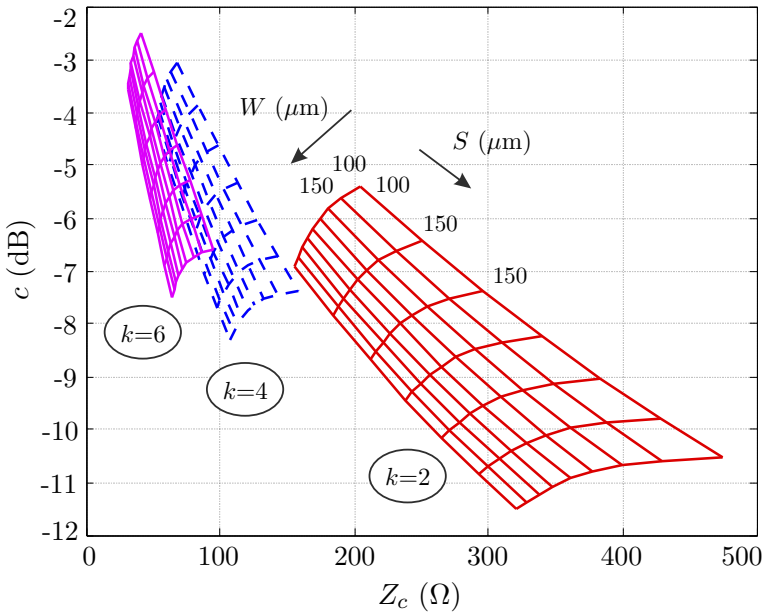

Figure 5.3.: Characteristic impedance Z_{0_c} (5.3) and coupling factor c (5.7) of a two-port short-circuited wire-bonded MTL as a function of the width W and spacing S for several number of conductors k.

with $Y_0 = 1/Z_0$. Using (5.8), the differential terms are expressed as

$$S_{dd_{11}} = \frac{c^2\left(\bar{Z}_{0_c}^2 \sin^2\theta\right) + \cos^2\theta}{c^2\left(\bar{Z}_{0_c}^2 \sin^2\theta + 1\right) - \cos^2\theta - j2c\bar{Z}_{0_c}\cos\theta\sin\theta} \tag{5.9a}$$

$$S_{dd_{21}} = \frac{j2c^2\bar{Z}_{0_c}\sin\theta}{c^2\left(\bar{Z}_{0_c}^2 \sin^2\theta + 1\right) - \cos^2\theta - j2c\bar{Z}_{0_c}\cos\theta\sin\theta}, \tag{5.9b}$$

where $\bar{Z}_{0_c} = Z_{0_c}/Z_0$. Thus, $\bar{Z}_{0_c}$ stands for the impedance Z_{0_c} (5.3) of the short-circuited MTL, normalized by the characteristic impedance Z_0 (reference impedance). In addition, the square of the modulus of these transmission and reflection terms, can be written as

$$|S_{dd_{21}}|^2 = \frac{1}{1+F_I^2}, \qquad |S_{dd_{11}}|^2 = \frac{F_I^2}{1+F_I^2}, \tag{5.10}$$

with

$$F_I = \frac{1-c^2\bar{Z}_{0_c}^2}{2c^2\bar{Z}_{0_c}}\left(\cos^2\theta + \frac{c^2(\bar{Z}_{0_c}^2-1)}{1-c^2\bar{Z}_{0_c}^2}\right)\frac{1}{\sin\theta} \tag{5.11}$$

and where a lossless system is considered. F_I is a second-order polynomial that determines the filtering properties of the structure. From filter theory, it is straightforward to calculate F_I in order to conform the transfer function as follows

$$\varepsilon F_n(x) = F_I, \tag{5.12}$$

where F_n is an nth-order Butterworth or Chebyshev polynomial, the pass band is determined for -1$\leq x \leq$1 and ε is the in-band ripple factor, related to the return losses as [24]

$$\varepsilon = \frac{1}{\sqrt{10^{L_R/10}-1}}. \tag{5.13}$$

Thus, the design of the filter consists in finding the values of c and Z_{0_c} to meet the requirements of bandwidth and return losses. The fractional bandwidth (FBW) of the filter is defined by

$$FBW = \frac{f_2 - f_1}{f_o}, \tag{5.14}$$

where f_1 and f_2 are the pass band limits of the filter, and f_o is the design frequency. Assuming a TEM propagation and that the wire-bonded MTL is a quarter-wavelength long at the design frequency, the electrical length of the circuit at f_1 is calculated as

$$\theta_{c1} = \frac{\pi}{2}\left(1 - \frac{FBW}{2}\right). \tag{5.15}$$

For Butterworth responses, f_1 and f_2 are the -3 dB points of the bandpass (L_R=3 dB), whereas for Chebyshev filters, both frequencies determine the bandwidth with equal-ripple level (5.13). Therefore, given a prescribed operating bandwidth and return loss, and by applying the mapping $x = \cos\theta/\cos\theta_{c1}$, the following two design equations can be found

$$\text{Butterworth response} = \begin{cases} \bar{Z}_{0_c} = 1 \\ c = \dfrac{1}{\sqrt{1 + 2\varepsilon \tan\theta_{c1} \sec\theta_{c1}}} \end{cases} \tag{5.16a}$$

$$\text{Chebyshev response} = \begin{cases} \bar{Z}_{0_c} = -\varepsilon + \sqrt{\varepsilon^2 + 1} \\ c = \dfrac{\cos\theta_{c1}}{\sqrt{2 + \bar{Z}_{0_c}^2\,(\cos\theta_{c1}^2 - 2)}} \end{cases}, \tag{5.16b}$$

where θ_{c1} is related to the FBW by means of (5.15). It is important to mention that, the design formula for the Butterworth response is exact, but for the Chebyshev type, it is an approximation because the polynomial F is not a standard second-order Chebyshev polynomial. The effect of this approximation is shown in Fig. 5.4, where the achieved bandwidths (FBW^*), calculated using (C.7b) and the relative error (Δ_{FBW}), are depicted as a function of the design fractional bandwidths (FBW). As seen, the error grows with the desired bandwidth, but considering its magnitude, lower that 12% for a fractional bandwidth of 120%, it can be deduced that the design equations (5.16b) provide a good result. Notwithstanding, the deviation from the design values, can be accurately estimated using the following formulas,

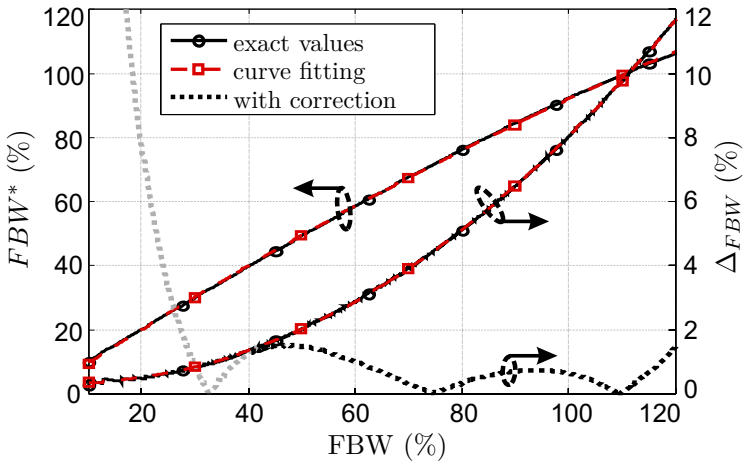

Figure 5.4.: Achieved fractional bandwidths (FBW^*) for a single-section differential filter, calculated using (C.7b), and relative error Δ_{FBW} with respect to the design fractional bandwidths (FBW) of Chebyshev filters, before and after the correction given by (5.17b).

which have been obtained by curve fitting

$$\Delta_{FBW}(\%) = 10^{-3}\left[0.872\,FBW^2 - 10.59\,FBW + 355.2\right] \tag{5.17a}$$

$$FBW = 10^{-3}\left[3.477(FBW^*)^2 + 710.9\,FBW^* + 6054\right] \tag{5.17b}$$

Therefore, to get a reliable synthesis process of wideband Chebyshev filters (5.16b) and, being FBW^* the final achieved bandwidths, the initial design fractional bandwidth (FBW) used to compute θ_{c1} (5.15) may be adjusted according to (5.17b). The error committed after that correction is depicted in Fig. 5.4. As seen, this correction has to be only applied for bandwidths greater than 40% in order to maintain the relative error lower than 2%.

5.2.2. Double-Section Differential Filter

The proposed configuration analyzed in previous section is straightforward to design ultra-wideband differential filters with good common-mode rejection. However, to increase the selectivity, double-section bandpass filters are introduced and investigated. The new topology, depicted in Fig. 5.5(a), can be bisected into two identical halves with respect to its symmetrical interface. Fig. 5.5(b) and Fig. 5.5(c) show the two bisections under differential- and common-mode operation, respectively. Considering these two half networks, it is seen that the odd mode circuit has a bandpass frequency response, whereas the even mode half circuit rejects the common-mode signals [20].

The design of the double-section differential filter is carried out analyzing the odd mode cir-

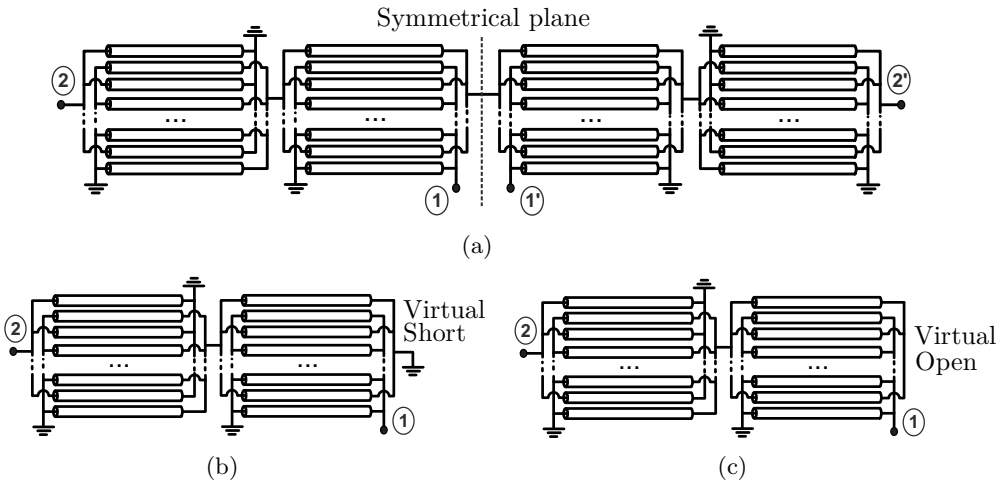

Figure 5.5.: (a) Transmission line equivalent model of the wideband differential bandpass filter and corresponding circuits in (b) odd- and (c) odd-mode excitations.

cuit. By using the admittance matrix (5.1b), the square of the magnitude of the S-parameters can be found as

$$|S_{dd_{21}}|^2 = \frac{1}{1+F_{II}^2}, \qquad |S_{dd_{11}}|^2 = \frac{F_{II}^2}{1-F_{II}^2}, \tag{5.18}$$

where

$$F_{II} = \frac{1-c^2\bar{Z}_{0_c}^2}{c^3\bar{Z}_{0_c}}\cos\theta\left(\cos^2\theta + \frac{c^2(\bar{Z}_{0_c}^2-1)}{1-c^2\overline{Z}_{0_c}^2}\right)\frac{1}{\sin\theta}. \tag{5.19}$$

F_{II} is a third-order polynomial that conditions the transfer function of the filter. In a similar way to the previous synthesis process, by properly designing F_{II} (5.12), the filtering transfer function can be synthesized as a Butterworth or a Chebyshev response. In addition, as the order of F_{II} is increased, the skirt selectivity of the filter is enhanced, and new design equations are required to find the values of c and Z_c that satisfy a particular frequency response. From (C.8b) and (5.19), the following closed-form expressions are deduced [25] (see Appendix B):

- Butterworth response, $\bar{Z}_{0_c} = 1$:

$$G = \varepsilon\tan\theta_{c1}\left(1+\tan^2\theta_{c1}\right), \tag{5.20a}$$

$$R = \frac{1}{2G} - \frac{1}{27G^3}, \quad Q = -\frac{1}{9G^2}, \tag{5.20b}$$

$$S_1 = \sqrt[3]{R+\sqrt{Q^3+R^2}}, \quad S_2 = \sqrt[3]{R-\sqrt{Q^3+R^2}} \tag{5.20c}$$

$$c = S_1 + S_2 - \frac{1}{3G} \tag{5.20d}$$

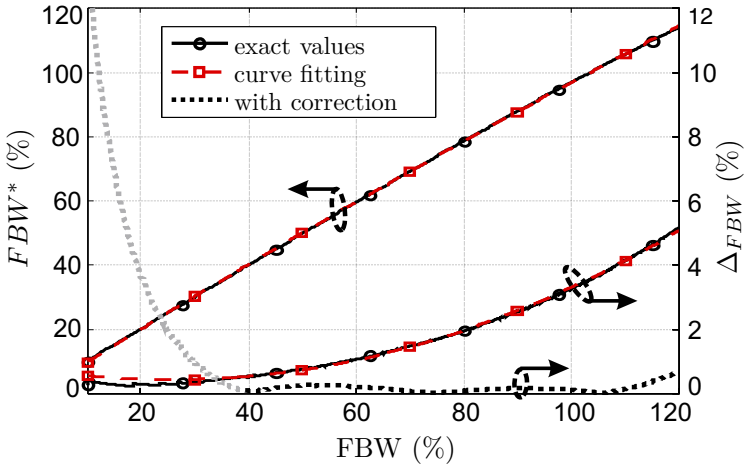

Figure 5.6.: Achieved fractional bandwidths (FBW^*) for a two-section differential filter, calculated using (C.8b), and relative error Δ_{FBW} with respect to the design fractional bandwidths (FBW) of Chebyshev filters, before and after the correction given by (5.23b).

- Chebyshev response:

$$\bar{Z}_{0_c} = \frac{1}{\sqrt{1+\frac{3}{4}(u^2-1)\cos^2\theta_{c1}}} \tag{5.21a}$$

$$c = \sqrt{\frac{\cos^3\theta_{c1}(u^2-1)}{4u\varepsilon}} \tag{5.21b}$$

with

$$u = S_1 + S_2 + \frac{\varepsilon}{\cos\theta_{c1}} \tag{5.22a}$$

$$r = \frac{\varepsilon\left(\varepsilon^2 - \cos^2\theta_{c1} + 2\right)}{\cos^3\theta_{c1}} \tag{5.22b}$$

$$g = \sqrt{\frac{3\varepsilon^2[6\cos^4\theta_{c1} - (27\varepsilon^2+36)\cos^2\theta_{c1} + 36(1+\varepsilon^2)] - \cos^6\theta_{c1}}{27\cos^6\theta_{c1}}} \tag{5.22c}$$

$$S_1 = \sqrt[3]{r+g}, \quad S_2 = \sqrt[3]{r-g}, \tag{5.22d}$$

where θ_{c1} is related to the desired fractional bandwidth by means of (5.15). For Butterworth response L_R is normally equal to 3 dB and thus, ε=1.

By using (5.20) and (5.21), a Butterworth type or a three-pole Chebyshev response with equal ripple can be readily designed. In addition, as in the previous discussion, the solution for Butterworth filters is exact, but the design equations (5.21b) and (5.21a) provide approximated solutions because F_b is not a standard third-order Chebyshev polynomial. Fig. 5.6 depicts the difference between the desired fractional bandwidths and the really obtained FBW^* by evaluating (C.8b). The relative error shows that the maximum error is always lower than 6% for bandwidths up to 120%. Thus, the design equations for Chebyshev fil-

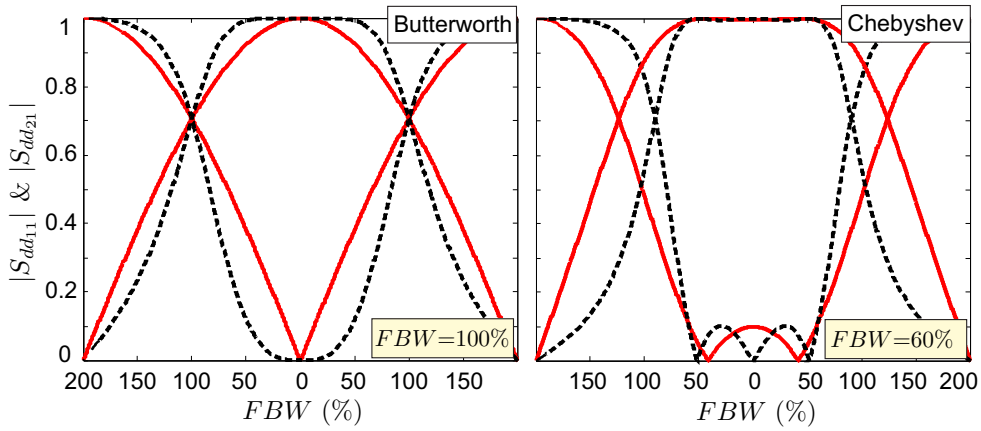

Figure 5.7.: Magnitude of the theoretical $S_{dd_{11}}$ and $S_{dd_{21}}$ for a single-section (solid line) and double-section filter (dashed line) designed with a Buterworth or Chebyshev function response (L_R=20 dB).

Table 5.1.: Design parameters of filters depicted in Fig.5.7

	Butterworth			Chebyshev (LR=-20dB)		
	FBW	c	Z_c	FBW	c	Z_c
single-section	100	-4.78	50	60	-4.12	45.23
two-section	100	-3.65	50	60	-4.45	41.03

ters provide very good results. Nevertheless, as in previous section, both the deviation from the expected FBW and the relative error committed, can be computed using the following formulas obtained by curve fitting

$$\Delta_{FBW}(\%) = 10^{-3}\left[0.522\,FBW^2 - 26.81\,FBW + 751.7\right] \tag{5.23a}$$

$$FBW = 10^{-3}\left[1.11(FBW^*)^2 + 904.5\,FBW^* + 2256\right] \tag{5.23b}$$

Therefore, to improve the precision, the design FBW may be modified according to (5.23b). As depicted in Fig. 5.6, by making this correction for operating bandwidths greater than 40%, the relative error is always below 1%.

To compare the performance of both single- and double-section differential filters, Fig. 5.7 represents the magnitude of the calculated $S_{dd_{11}}$ and $S_{dd_{21}}$ for two Butterworth and Chebyshev filters. For the Butterworth response, a 3-dB FBW of 100% is used, while for the Chebyshev type, an equal-ripple FBW of 60% is selected. The design of these filters is carried out by means of (5.16a) and (5.20), for the Buttherworth response, and (5.16b) and (5.21) with L_R=20 dB for the Chebyshev function. From these curves, it can be deduced that the Chebyshev response, with two or three transmission poles, is more suitable to achieve wideband bandpass filters with a good selectivity. The design parameters obtained for each filter are listed in Table 5.1.

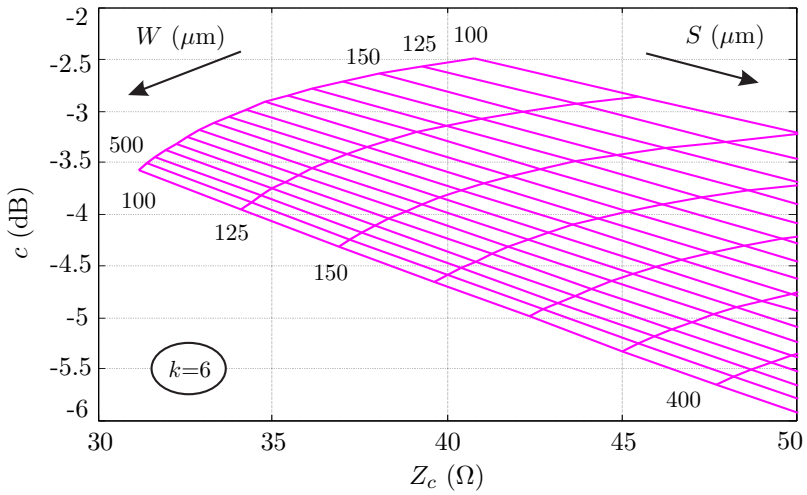

Figure 5.8.: Line-width W and spacing S of a two-port short-circuited wire-bonded in order to achieve values of characteristic impedance $Z_c \leq 50\Omega$.

The theory presented in Sections 5.2.1 and 5.2.2 allows the values of c and Z_{0_c} to be computed in order to obtain a desired frequency response taking into account both, the fractional bandwidth and the return losses. Once these values are known by means of either design formula (5.16a), (5.16b), (5.20) or (5.21), the required even- and odd-mode impedances can be calculated from (5.3) and (5.2b) as

$$Z_{oe} = \frac{k-1}{2} Z_c (R-1), \quad Z_{oo} = \frac{Z_{oe}}{R} \tag{5.24a}$$

$$R = \frac{c + \sqrt{(k-1)^2(1-c^2)+c^2}}{(k-1)(1-c)}. \tag{5.24b}$$

5.3. Experimental Validation

In this section, several prototypes of the proposed differential filter are designed and manufactured in order to validate the presented analytical design process. The dielectric substrate used is Rogers 4350B with a permittivity of 3.66 and thickness of 30 mil (the same substrate employed in section 5.2). From theory, it was demonstrated that a value of $Z_{0_c} \leq 50\ \Omega$ is required to synthesize wideband Butterworth or Chebyshev type responses. In that sense, Fig. 5.8 depicts the allowed physical dimensions of a wire-bonded MTL to obtain useful values of Z_{0_c} (5.3). As seen, for the selected substrate, only if k=6 the value of Z_c is less than 50 Ω. Therefore, from Fig. 5.8 it is possible to highlight the importance of using more than two conductors in designing wideband differential filters (see Fig. 5.3). The minimum line-width and spacing is limited to 100 μm according to our fabrication capability.

Taking into account the above considerations, one two-pole (single-section) and one three-

Table 5.2.: Design parameters and physical dimensions of the fabricated Chebyshev differential filters

	FBW (%)	L_R (dB)	c (dB)	Z_c (Ω)	k	W (μm)	S (μm)	d (mm)
single-section	100	-15	-3.47	44	6	110	110	13.6
double-section	60	-25	-2.67	42	6	190	150	13.8

pole (double-section) Chebyshev differential filters are designed for a mid-band frequency f_o=3.5 GHz. The theoretical operating bandwidth, return losses and the physical dimensions of both filters are collected in Table 5.2. The design values c and Z_{0_c} are easily computed by means of (5.16b) and (5.21), for the two- and three-pole filters, respectively. Once these values are known, the required even- and odd-mode impedances as a function of the number of conductors k are calculated (5.24) and then, translated into physical dimensions [26, 27].

Fig.5.9 depicts the wideband differential- and common-mode theoretical, simulated and measured responses of the fabricated filters. Ansys HFSS v15 is used to simulate both prototypes, while the measured responses are obtained by using a dual-source 4-port vector network analyzer (Agilent N5247A PNA-X) in order to apply true-differential or true-common-mode stimulus in both forward and reverse direction. The photographs of these two- and three-pole filters, are shown in Fig. 5.9(a) and Fig. 5.9(b), respectively.

From Fig.5.9, it is noted that there is a good agreement between the measurements and the predicted results by using the analytical formulas derived in Section 5.2. There is an excellent concordance between the theoretical and measured differential insertion losses ($S_{dd_{21}}$), but there are some discrepancies in the differential-mode return losses ($S_{dd_{11}}$). It is important to remark that both filters have been fabricated by directly using the computed theoretical values without any optimization during the electromagnetic simulations. This fact is important because the goal of this work is not only to prove the feasibility of designing wideband differential filters, but also the validity of the presented theory. In that sense, the new design equations are valuable to design differential bandpass filters with a desired operating bandwidth with great exactitude. The measured insertion losses are lower than 1 dB within the designed differential passband, and the 3-dB fractional bandwidths extends up to 145% and 97%, for the single- and double-section filters, respectively. In addition, the common-mode rejection level ($S_{cc_{21}}$) is better than 20 dB in both prototypes and the measured group delay (see Fig. 5.9) is below 0.4 ns, indicating a good phase linearity.

It is important to mention that the reduction on the common-mode rejection capability (in both, simulated and measured responses) and the discrepancies in the return loss are mainly due to the difference between the even- and odd-mode phase velocities in the wire-bonded MTL. This effect is well known, and it can be mitigated by equalizing both phase velocities [28]. Notwithstanding, even without this compensation, the closed-form design equations derived in this work are useful to synthesize wideband differential filters with a prescribed

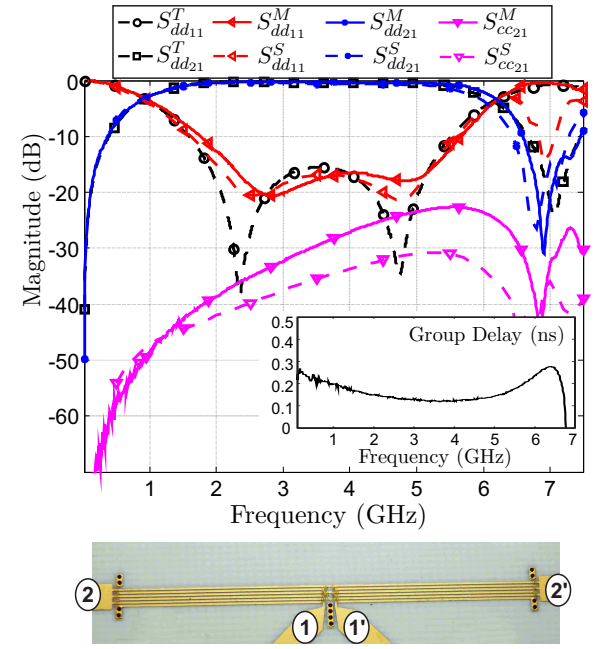

(a)

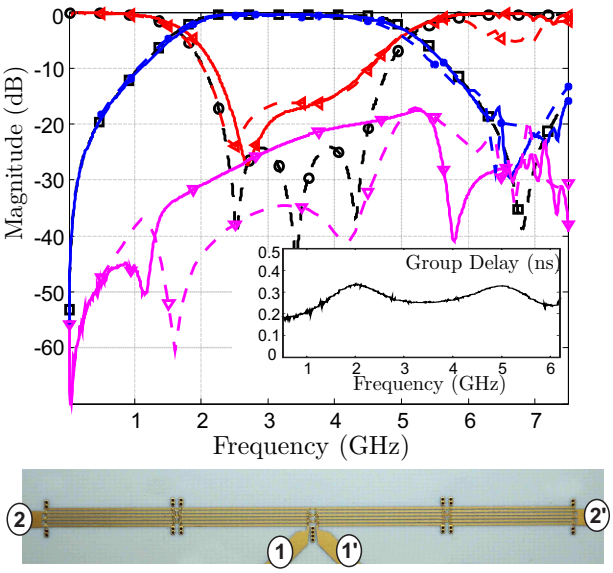

(b)

Figure 5.9.: Wideband differential- and common-mode theoretical (T), simulated (S) and measured (M) responses of the fabricated filters.

operating bandwidth.

5.4. Conclusion

In this chapter, a structure consists of short-circuited wire-bonded multiconductor transmission lines has been analyzed to design ultra-wideband differential filters with a good common-

mode rejection. A set of new design equations has been presented to synthesize filters with a Butterworth or Chebyshev type response by means of a quick and reliable procedure. These analytical equations allow designers to compute the required even- and odd-mode impedances of the wire-bonded MTLs in order to obtain a desired frequency response. Expressions for two configurations, single- and double-section filters, have been deduced and validated by means of experimental results.

References

[1] W. R. Eisenstadt, B. Stengel, and B. M. Thompson, *Microwave Differential Circuit Design Using Mixed-Mode S-Parameters*. Norwood, MA: Artech House, 2006.

[2] T. B. Lim and L. Zhu, "A Differential-Mode Wideband Bandpass Filter on Microstrip Line for UWB Application," *IEEE Microw. Wireless Compon. Lett.*, vol. 19, no. 10, pp. 632–634, Oct 2009.

[3] T. Lim and L. Zhu, "Differential-mode ultra-wideband bandpass filter on microstrip line," *Electron. Lett.*, vol. 45, no. 22, pp. 1124–1125, October 2009.

[4] X.-H. Wang, Q. Xue, and W.-W. Choi, "A Novel Ultra-Wideband Differential Filter Based on Double-Sided Parallel-Strip Line," *IEEE Microw. Wireless Compon. Lett.*, vol. 20, no. 8, pp. 471–473, Aug 2010.

[5] A. Abbosh, "Ultrawideband Balanced Bandpass Filter," *IEEE Microw. Wireless Compon. Lett.*, vol. 21, no. 9, pp. 480–482, Sept 2011.

[6] Y.-J. Lu, S.-Y. Chen, and P. Hsu, "A Differential-Mode Wideband Bandpass Filter With Enhanced Common-Mode Suppression Using Slotline Resonator," *IEEE Microw. Wireless Compon. Lett.*, vol. 22, no. 10, pp. 503–505, Oct 2012.

[7] C.-H. Wu, C.-H. Wang, and C. H. Chen, "Balanced Coupled-Resonator Bandpass Filters Using Multisection Resonators for Common-Mode Suppression and Stopband Extension," *IEEE Trans. Microw. Theory Tech.*, vol. 55, no. 8, pp. 1756–1763, Aug 2007.

[8] J. Shi and Q. Xue, "Novel Balanced Dual-Band Bandpass Filter Using Coupled Stepped-Impedance Resonators," *IEEE Microw. Wireless Compon. Lett.*, vol. 20, no. 1, pp. 19–21, Jan 2010.

[9] A. Horestani, M. Duran-Sindreu, J. Naqui, C. Fumeaux, and F. Martin, "S-Shaped Complementary Split Ring Resonators and Their Application to Compact Differential Bandpass Filters With Common-Mode Suppression," *IEEE Microw. Wireless Compon. Lett.*, vol. PP, no. 99, pp. 150–152, 2014.

[10] W. Feng and W. Che, "Novel Wideband Differential Bandpass Filters Based on T-Shaped Structure," *IEEE Trans. Microw. Theory Tech.*, vol. 60, no. 6, pp. 1560–1568, June 2012.

[11] X.-H. Wu and Q.-X. Chu, "Compact Differential Ultra-Wideband Bandpass Filter With Common-Mode Suppression," *IEEE Microw. Wireless Compon. Lett.*, vol. 22, no. 9, pp. 456–458, Sept 2012.

[12] W. J. Feng, W. Q. Che, Y. M. Chang, S. Y. Shi, and Q. Xue, "High Selectivity Fifth-Order Wideband Bandpass Filters With Multiple Transmission Zeros Based on Transversal Signal-Interaction Concepts," *IEEE Trans. Microw. Theory Tech.*, vol. 61, no. 1, pp. 89–97, Jan 2013.

[13] W. Fathelbab and M. Steer, "Four-Port Microwave Networks With Intrinsic Broad-Band Suppression of Common-Mode Signals," *IEEE Trans. Microw. Theory Tech.*, vol. 53, no. 5, pp. 1569–1575, May 2005.

[14] C.-H. Wu, C.-H. Wang, and C. H. Chen, "Novel Balanced Coupled-Line Bandpass Filters With Common-Mode Noise Suppression," *IEEE Trans. Microw. Theory Tech.*, vol. 55, no. 2, pp. 287–295, Feb 2007.

REFERENCES

[15] G. L. Mattahei, L. Young, and E. M. T. Jones, *Microwave Filters, Impedance-Matching Networks, and Coupling Structures*, M. A. House, Ed. Norwood, 1985.

[16] R. Li, S. Sun, and L. Zhu, "Synthesis Design of Ultra-Wideband Bandpass Filters With Composite Series and Shunt Stubs," *IEEE Microw. Wireless Compon. Lett.*, vol. 57, no. 3, pp. 684–692, March 2009.

[17] J.-Y. Li, C.-H. Chi, and C.-Y. Chang, "Synthesis and Design of Generalized Chebyshev Wideband Hybrid Ring Based Bandpass Filters With a Controllable Transmission Zero Pair," *IEEE Trans. Microw. Theory Tech.*, vol. 58, no. 12, pp. 3720–3731, Dec 2010.

[18] R. Zhang and L. Zhu, "Synthesis Design of a Wideband Bandpass Filter With Inductively Coupled Short-Circuited Multi-Mode Resonator," *IEEE Trans. Microw. Theory Tech.*, vol. 22, no. 10, pp. 509–511, Oct 2012.

[19] W. Ou, "Design Equations for an Interdigitated Directional Coupler," *IEEE Trans. Microw. Theory Tech.*, vol. 23, no. 2, pp. 253–255, Feb. 1975.

[20] E. M. T. Jones and J. T. Bolljahn, "Coupled-Strip-Transmission-Line Filters and Directional Couplers," *IRE Trans. Microw. Theory Tech.*, vol. 4, no. 2, pp. 75–81, Apr. 1956.

[21] D. Bockelman and W. Eisenstadt, "Combined differential and common-mode scattering parameters: theory and simulation," *IEEE Trans. Microw. Theory Tech.*, vol. 43, no. 7, pp. 1530–1539, Jul. 1995.

[22] D. Pozar, *Microwave Engineering*, 2nd ed. New York: Wiley, 1998.

[23] J.-S. Hong, *Microstrip Filters for RF/Microwave Applications*, K. Chang, Ed. Wiley-Interscience, 2011.

[24] J.-S. Hong and M. J. Lancaster, *Microstrip Filters for RF/Microwave Applications*, K. Chang, Ed. Wiley-Interscience, 2001.

[25] M. Abramowitz and I. Stegun, *"Handbook of Mathematical Functions with Formulas, Graphs, and Mathematical Tables"*. US Government Printing Office, Washington, December 1972.

[26] M. Kirschning and R. Jansen, "Accurate Wide-Range Design Equations for the Frequency-Dependent Characteristic of Parallel Coupled Microstrip Lines," *IEEE Trans. Microw. Theory Tech.*, vol. 32, no. 1, pp. 83–90, Jan. 1984.

[27] J. A. B. Faria, "Kirschning and Jansen computer-aided design formulae for the analysis of parallel coupled lines," *Microw. Opt. Techn. Let.*, vol. 51, no. 10, pp. 2466–2470, 2009.

[28] R. Mongia, I. Bahl, and P. Bhartia, *RF and Microwave Coupled-Line Circuits*. Norwood, MA: Artech House, 1999.

Chapter 6

Selective Wideband Quasi-Elliptic Bandpass Filters

A comprehensive study of high-selectivity filters that employ series and a shunt MTLs is presented in this chapter. Two asymmetric and symmetric configurations are analyzed, demonstrating that these configurations are suitable for implementing three- and/or five-pole bandpass filters with a quasi-elliptic frequency response. Besides, an exact synthesis procedure with analytical design equations for achieving equal-ripple pass band response as a function of the operating bandwidth is described. To validate the theory, several bandpass filters are designed, fabricated and measured. The excellent agreement between the measurements and the predicted results validates the proposed procedure as a reliable and quick technique for designing wideband quasi-elliptic bandpass filters.

6.1. Introduction

Increasing consumer demands for higher data rates and the release of the unlicensed use of the ultra-wide band (UWB) from 3.1 to 10.6 GHz is driving research into new UWB techniques; especially with those having monolithic and hybrid integrated circuit solutions. UWB bandpass filters [1, 2] are key for new applications (in ultra-high speed wireless communications and radar systems), where it is necessary to reject undesired signals and to confine transmitted power spectral densities. Several imperfections and impairments occur in the RF components that, if not corrected for, can cause spectrum regrowth, interference and noise; degrading the performance of the system. Thus, it is important to realise filters with sharp

cut-off regions, low insertion losses, low in-band group delay variation and flat amplitude responses.

Consequently, in recent years there has been growing interest in the design of bandpass filters with large fractional bandwidths and high selectivity. Conventional microwave filter theory is based on narrowband fractional bandwidths [3, 4], which has prompted the development of new types of broadband filters [1, 2, 5]. A variety of filters have been reported, with different forms of multiple-mode-resonator (MMR) having stepped-impedance or stub-loaded configurations, in order to position the first resonant frequencies into the desired wide pass band [6–23]. Most of these MMR-based filters combine parallel-coupled lines with different types of MMR structures.

The conventional high-pass prototype with short-circuited stubs for designing wideband bandpass filters have been explored in [24, 25]. Bandpass filters with single and multiple stages using composite series and shunt stubs are proposed in [11] and ring-based wideband bandpass filters are described in [26, 27]. Wideband filters based on transversal signal-interaction concepts have been realized in [28] and a stepped-impedance parallel-coupled microstrip structure is employed in [29]. Nevertheless, although a great amount of wideband bandpass filters have been reported, in most of these works, there lacks a systematic design methodology, based purely on filter synthesis (i.e. without the need for additional tuning or optimization to reach the final specifications). Only few works, as in [10–12, 23, 27], face this issue in order to calculate the circuit design parameters for achieving a specific frequency response.

A shunt-coupled $\lambda/4$ short-circuited line section was used in [14] to design bandpass filters with two transmission zeros. According to the study presented in [14], only a three-pole bandpass filter can be designed by using $\lambda/4$ open input/output coupled lines. Therefore, the two $\lambda/4$ open-circuited lines are replaced by two $\lambda/2$ short-circuited lines to generate two additional transmission poles within the pass band. However, here it is demonstrated that, with two input and output $\lambda/4$ coupled-line sections it is possible to design both three- and five-pole filters. Moreover, closed-form design equations are provided for both conditions.

The use of two- and three- shunt-coupled lines to design wideband bandpass filters was previously addressed in [16], but only equations for the special two-strip case were given and without design guidelines. More recently, a shunt broad-side-coupled microstrip/CPW stub was used in [17] to generate two transmission zeros; improving the upper passband selectivity. However, although some equations were given to calculate the resonance frequencies of the structure, there was no design procedure neither for the input/output coupled lines or for the shunt structure, to obtain a desired frequency response.

In this chapter, wideband planar bandpass filters consist of one or two series MTL and a shunt short-circuited MTL are analyzed in rigorous detail and a comprehensive study of the filters is presented. By using the proposed topologies and design techniques, three- or five-pole wideband bandpass filters having two transmission zeros on both sides of the passband

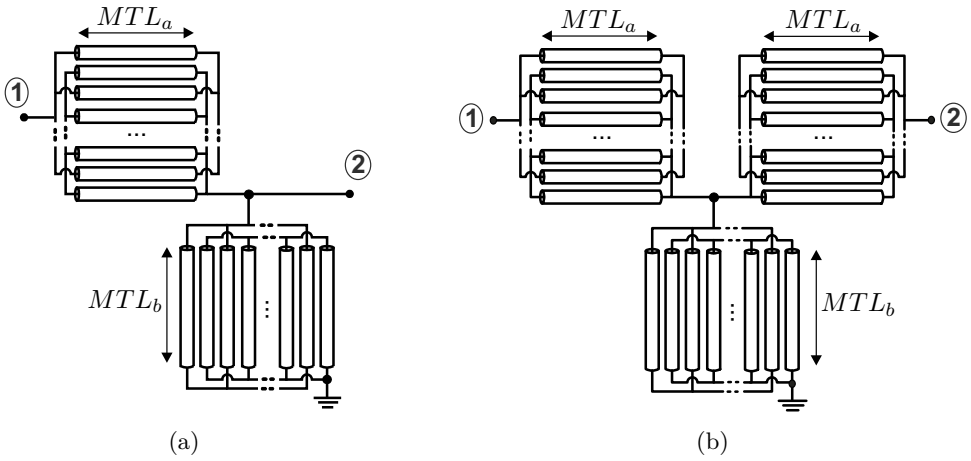

Figure 6.1.: Transmission line equivalent circuit model for the proposed wideband bandpass filters consisting of one or two series MTL and a shunt short-circuited MTL.

can be easily designed. A set of accurate analytical design equations are derived from first principles, which allows the designer to optimize the in-band flatness and enhance the roll-off slopes at the cut-off frequencies.

First, to provide some insights into the physical behavior of the filter, both series and shunt wire-bonded MTLs are analyzed separately in Sections 6.2.1 and 6.2.2, respectively. Some preliminary design equations are obtained to clarify the effects and benefits of introducing the shunt MTL. Based on this theory, the complete structure of both filters is rigorously analyzed in Sections 6.2.3 and 6.2.4. Finally, in Section 6.3, several prototypes are designed, fabricated and measured to validate the new theory and techniques.

6.2. Analysis and Design Procedure

The transmission line equivalent circuit models for the proposed wideband bandpass filters are given in Fig. 6.1. Two configurations are considered, a compact asymmetric circuit composed of a series MTL and a short-circuited MTL, and a symmetric T-shaped structure with two series input-output MTLs and a shunt short-circuited MTL. As it was explained in Chapter 2, assuming ideal short circuits across alternate conductors (i.e. the bonding wires are very short compared to wavelength and have insignificant series inductor or resistance), the connections can be neglected and the equivalent circuit model for a wire-bonded MTL can be reduced to just a pair of coupled lines [30]. As a result, with this simplified configuration, there are now only two independent conductors and the operating bandwidth is increased, since undesired resonances are suppressed. This scenario allows the use of a simplified model, in order to obtain analytical design equations [31]. In addition, the use of wire-bonded MTLs is recommended for achieving tight coupling, which would not be possible with only two strips without any backside aperture [30].

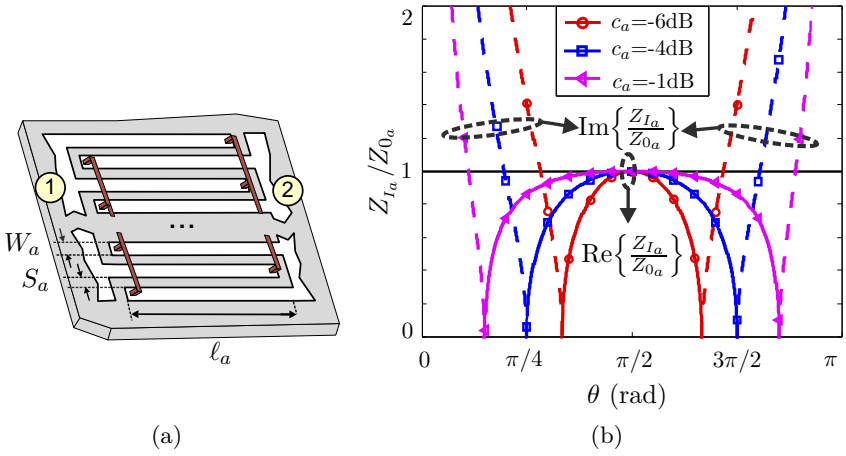

(a) (b)

Figure 6.2.: (a) Layout and (b) image impedance of a two-port wire-bonded MTL.

In the following equations, subscripts a and b represent the series and shunt wire-bonded MTLs, respectively (as also seen in Fig. 6.1). However, for common expressions, the variable i is also used; this, can represent either a or b.

6.2.1. Single- and Double-Section Open-Circuited Wire-Bonded MTLs

The layout of a two-port wire-bonded MTL in microstrip technology is shown in Fig. 6.2(a). A transmission line equivalent circuit model as a function of the number of strips was obtained in Chapter 2 and in Chapter 3 this element was used to design broadband baluns. Assuming a lossless medium, its admittance matrix can be given as (3.1)

$$[Y]_a = \begin{bmatrix} Y_{11_a} & Y_{12_a} \\ Y_{21_a} & Y_{22_a} \end{bmatrix} = \frac{(M_a^2 - N_a^2)\sin\theta_a}{M_a^2\cos^2\theta_a - N_a^2} \begin{bmatrix} jM_a\cos\theta_a & jN_a \\ jN_a & jM_a\cos\theta_a \end{bmatrix}, \tag{6.1}$$

where M_a and N_a are related to the even- and odd-mode impedances of a pair of coupled lines [32]

$$M_i = \frac{1}{Z_{oe_i} + Z_{oo_i}} \left(1 + \frac{(k_i - 1)}{2} \frac{Z_{oe_i}^2 + Z_{oo_i}^2}{Z_{oe_i} Z_{oo_i}}\right) \tag{6.2a}$$

$$N_i = \frac{k_i - 1}{2} \frac{Z_{oo_i} - Z_{oe_i}}{Z_{oe_i} Z_{oo_i}}. \tag{6.2b}$$

k_i represents the number of conductors and θ_a is the electrical length of the conductors, which is calculated as the average value for the even- and odd-mode electrical lengths (2.5) (an approximation for inhomogeneous substrates) [30, 31, 33]. From (6.1), the image impedance of the series wire-bonded MTL can be expressed as (3.6)

$$Z_{I_a} = Z_{0_a} \sqrt{1 + \left(1 - \frac{1}{c_a^2}\right) \cot^2\theta_a}, \tag{6.3}$$

with

$$Z_{0_a} = \frac{-N_a}{M_a^2 - N_a^2} \tag{6.4}$$

and c_a (2.11) is equal to the maximum coupling coefficient of a k-line quarter-wavelength four-port coupler, given by [32]

$$c_i = \frac{-N}{M}. \tag{6.5}$$

The image impedance can be used to design the input-output coupled-line structures [3] and it is of great importance for understanding the behavior of the two-port wire-bonded MTL (see Section 3.2.2). Fig. 6.2(b) represents the image impedance (6.3) normalized by Z_{0_a} for several coupling factors c_a. As seen, Z_{0_a} is the image impedance value of the structure at θ_a=$\pi/2$, that normally corresponds to the design center frequency. There is a frequency range where the image impedance is purely real, which can be broadened by increasing the coupling factor. However, outside of this frequency range, the image impedance is purely imaginary and the MTL behaves as an inductive reactance. From these curves it is straightforward to deduce that if the MTL is a quarter-wavelength long at the design center frequency, and with Z_0 being the reference impedance at both ports, the wire-bonded MTL can be designed to be perfectly matched at one (with Z_{0_a}=Z_0) or two frequencies (with $Z_{0_a} > Z_0$). Therefore, a single-section wire-bonded MTL can be easily designed to have either a Butterworth or a Chebyshev response, having two transmission poles [34].

However, the design procedure using the insertion loss method is preferred over the use of the image impedance, in order to synthesize the desired frequency response. The insertion loss method allows a higher degree of control over the passband and stopband characteristics. By using the admittance matrix in (6.1), the square of the magnitude of S-parameters for single- and double-section wire-bonded MTLs reduce to

- Single-section

$$|S_{11_s}|^2 = \frac{F_s^2}{1+F_s^2}, \quad |S_{21_s}|^2 = \frac{1}{1+F_s^2}, \tag{6.6a}$$

$$F_s = \frac{c_a^2 - \bar{Z}_{0_a}^2}{2\bar{Z}_{0_a}^2 c_a^2}\left(\cos^2\theta + \frac{c_a^2\left(\bar{Z}_{0_a}^2 - 1\right)}{c_a^2 - \bar{Z}_{0_a}^2}\right)\frac{1}{\sin\theta}, \tag{6.6b}$$

- Double-section

$$|S_{11_{ss}}|^2 = \frac{F_{ss}^2}{1+F_{ss}^2}, \quad |S_{21_{ss}}|^2 = \frac{1}{1+F_{ss}^2}, \tag{6.7a}$$

$$F_{ss} = \frac{c_a^2 - \bar{Z}_{0_a}^2}{\bar{Z}_{0_a} c_a^3}\cos\theta\left(\cos^2\theta + \frac{c_a^2\left(\bar{Z}_{0_a}^2 - 1\right)}{c_a^2 - \bar{Z}_{0_a}^2}\right)\frac{1}{\sin\theta}, \tag{6.7b}$$

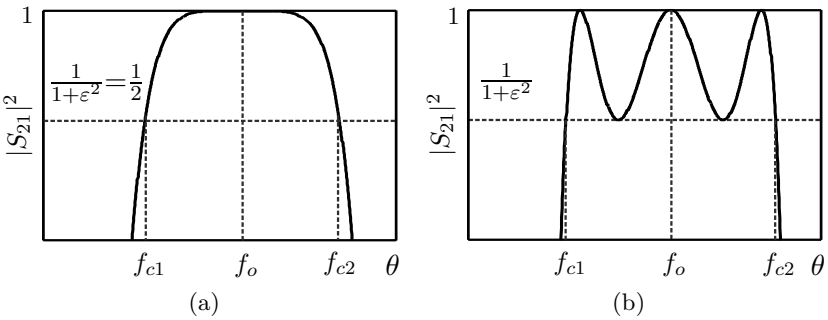

Figure 6.3.: (a) Butterworth and (b) Chebyshev pass band responses using (6.10).

where subscripts s and ss are used to denote both configurations with one or two series MTL, respectively, and $\bar{Z}_{0_a}$ is the normalized impedance of the MTL (with Z_{0_a}/Z_0). From these transfer functions it is straightforward to derive analytical design equations to obtain either a Butterworth or Chebyshev type response. The design equations can be calculated by setting Z_{0_a}=Z_0, if a Butterworth response is desired, or by equating F_s and F_{ss} with a standard second or third order Chebyshev polynomial for a Chebyshev response. For a bandpass filter, the fractional bandwidth (FBW) is defined as

$$FBW = \frac{f_{c2} - f_{c1}}{f_o}, \tag{6.8}$$

where f_o is the design frequency and f_{c1} and f_{c2} are the pass band limits of the filter (Fig. 6.3). Besides, by considering that the MTLs are one-quarter wavelength at the design frequency and assuming a TEM propagation, it is possible to obtain the electrical length of the structure at the lower cut-off frequency f_{c1} as

$$\theta_{c1} = \theta_o \left(1 - \frac{FBW}{2}\right) = \frac{\pi}{2}\left(1 - \frac{FBW}{2}\right). \tag{6.9}$$

Fig. 6.3 shows typical maximally flat and equal-ripple responses. With the latter, for the Chebyshev filter, the pass band limits are established for the equal ripple-level. Here, ε is a ripple constant related to a given return loss L_R in decibels within the pass band, given by the common textbook expression [1]

$$\varepsilon = \frac{1}{\sqrt{10^{L_R/10} - 1}}. \tag{6.10}$$

In contrast, for Butterworth filters, f_{c1} and f_{c2} are the -3 dB points of the frequency response; thus, the return loss L_R=3 dB and consequently, ε=1. Taking into account the above-mentioned considerations, from (C.10) and (C.11), the design equations are calculated by equating the transfer functions (F_s, F_{ss}) to the theoretical filtering functions $F_n(x)$ as

$$\epsilon F_n(x) = F_{s,ss}, \tag{6.11}$$

where the bandpass is determined for -1≤x≤1, and $F_n(x)$ is a Butterworth or a Chebyshev polynomial (second and third-order polynomial) [3]. In addition, the transformation $x = \cos\theta/\cos\theta_{c1}$ is used to map x=1 to θ_{c1} (cutoff frequency).

Therefore, with this methodology, from (C.10a), (C.11a) and (6.11), the following closed-form design equations for single and double sections are found:

1. **Single-section bandpass filter**

   - Second-order Butterworth response

$$\bar{Z}_{0_a} = 1 \tag{6.12a}$$

$$c_a = \frac{1}{\sqrt{1 + 2\varepsilon \tan\theta_{c1} \sec\theta_{c1}}} \tag{6.12b}$$

   - Second-order Chebyshev response

$$\bar{Z}_{0_a} = \frac{1}{-\varepsilon + \sqrt{1+\varepsilon^2}} \tag{6.13a}$$

$$c_a = \frac{\bar{Z}_{0_a} \cos\theta_{c1}}{\sqrt{2 + \bar{Z}_{0_a}^2(\cos^2\theta_{c1} - 2)}} \tag{6.13b}$$

2. **Double-section bandpass filter**

   - Third-order Butterworth response

$$\bar{Z}_{0_a} = 1 \tag{6.14a}$$

$$c_a = S_1 + S_2 - \frac{1}{3G}, \tag{6.14b}$$

   where

$$G = \varepsilon \tan\theta_{c1} \left(1 + \tan^2\theta_{c1}\right), \tag{6.15a}$$

$$R = \frac{1}{2G} - \frac{1}{27G^3}, \quad Q = -\frac{1}{9G^2}, \tag{6.15b}$$

$$S_1 = \sqrt[3]{R + \sqrt{Q^3 + R^2}},\ S_2 = \sqrt[3]{R - \sqrt{Q^3 + R^2}}. \tag{6.15c}$$

   - Third-order Chebyshev response

     For this filter, by comparing F_{ss} (C.11b) with a third-order Chebyshev polynomial [3], it is possible to obtain a simple expression that relates the coupling value c_a with the characteristic impedance of the MTL Z_{c_a} and the fractional bandwidth,

as

$$c_a = \sqrt{\frac{3\bar{Z}_{0_a}^2 \cos^2\theta_{c1}}{4(\bar{Z}_{0_a}^2 - 1) + 3\cos^2\theta_{c1}}}. \tag{6.16}$$

Given the values of Z_{0_a} and FBW (θ_{c1}) (6.9), the required value of c_a can be computed by means of (6.16). Once these values are known, the ripple level within the passband can be obtained with (C.11a). However, a closed-form design equation that directly relates the desired fractional bandwidth and ripple level with the values of c_a and Z_{0_a}, can be derived. By comparing F_{ss} (C.11b) with $F_3 = 4x^3 - 3x$ (third-order Chebyshev polynomial), a cubic equation is found. Thus, solving this equation [35], the next design formulas are calculated

$$c_a = \sqrt{\frac{\cos^3\theta_{c1}(u^2-1)}{4u\varepsilon}} \tag{6.17a}$$

$$\bar{Z}_{0_a} = \sqrt{1 + \frac{3}{4}(u^2-1)\cos^2\theta_{c1}}, \tag{6.17b}$$

where u is given by

$$u = S_1 + S_2 + \frac{\varepsilon}{\cos\theta_{c1}}, \tag{6.18}$$

with

$$S_1 = \sqrt[3]{r+g}, \quad S_2 = \sqrt[3]{r-g} \tag{6.19a}$$

$$r = \frac{\varepsilon\left(\varepsilon^2 - \cos^2\theta_{c1} + 2\right)}{\cos^3\theta_{c1}} \tag{6.19b}$$

$$g = \sqrt{\frac{3\varepsilon^2(6\cos^4\theta_{c1} - (27\varepsilon^2+36)\cos^2\theta_{c1} + 36(1+\varepsilon^2)) - \cos^6\theta_{c1}}{27\cos^6\theta_{c1}}}. \tag{6.19c}$$

It is important to note that the obtained design equations are equivalent to the calculated in Chapter 5 for the design of differential filters, but considering the inverse of the normalized characteristic impedance for the MTLs ($\bar{Z}_{0_{diff}} = 1/\bar{Z}_{0_{c_a}}$). This result is easily deduced because both structures, wire-bonded MTLs with open- or short-circuited diagonal ports, are dual circuits. Besides,it must be emphasized that for a Butterworth response the solutions (6.12) and (6.14) are exact. The value of c_a is calculated as a function of the fractional bandwidth (6.9). If the FBW is defined for a return losses of L_R=3 dB, then ε=1 (6.10). However, for a Chebyshev response, because of the $\sin\theta$ term in the denominator of F_s and F_{ss}, these expressions are not standard Chebyshev polynomials, and thus, the obtained equations (6.13) and (6.17) will provide an approximated synthesis procedure. Nevertheless, the accuracy of these equations was analyzed in Chapter 5. It was found that without any correction, the error committed in the predicted FBW is always lower than 12% for bandwidths up to 120%. To reduce this error (<2%), several formulas were derived in (5.17b) and (5.23b). Therefore,

Table 6.1.: Design parameters of two single- and double-section Butterworth and Chebyshev filters

		Butterworth		Chebyshev (LR=20dB)		
	FBW_{3dB}	c_a	Z_{0_a}	c_a	Z_{0_a}	FBW^*
Single Section	60	-9.85	50	-9.82	55.28	26.1
	100	-5.84	50	-5.77	55.28	45.6
Double Section	60	-7.15	50	-7.48	61.6	39.25
	100	-3.65	50	-3.78	60.7	66.7

FBW^*: Fractional bandwidth with equal-ripple response

attending to this performance, these formulas provide a very good solution in designing either narrow or broadband filters.

Using these design equations, two first- and second-order Butterworth and Chebyshev filters are designed for 3-dB fractional bandwidths (FBW) of 60% and 100%. The Chebyshev filters are designed for a return loss L_R of 20 dB and the equal-ripple bandpass is adjusted to meet the 3 dB FBW. The computed design values of these filters are shown in Table 6.1, and the magnitudes of their calculated S-parameters are given in Fig. 6.4. As expected, by using the Chebyshev type, both the selectivity of the filter and in-band flatness are improved. Therefore, the above closed-form expressions provide a quick design procedure for Butterworth and Chebyshev filters, having a specific bandwidth and in-band flatness. To achieve sharpened roll-off skirts, in the next subsection, a shunt wire-bonded MTL will be used to place two transmission zeros at the lower and upper cut-off frequencies.

6.2.2. Shunt Short-Circuited Wire-Bonded MTL

The shunt section used in the proposed filter is created by short-circuiting the output port of a two-port wire-bonded MTL (i.e. port 2 in Fig. 6.2(a)). The layout and equivalent circuit model for this one-port circuit are given in Fig. 6.5. This element, which was previously analyzed in Section 4.2.2, is equivalent to a pair of series short-circuited and open-circuited shunt stubs, having equivalent characteristic impedances Z_{oc_b} and Z_{sc_b} given by

$$Z_{oc_b} = Z_{0_b}\frac{1-c_b^2}{c_b}, \quad Z_{sc_b} = Z_{0_b}\, c_b \tag{6.20}$$

with (6.4)

$$Z_{0_b} = \frac{-N_b}{M_b^2 - N_b^2}. \tag{6.21}$$

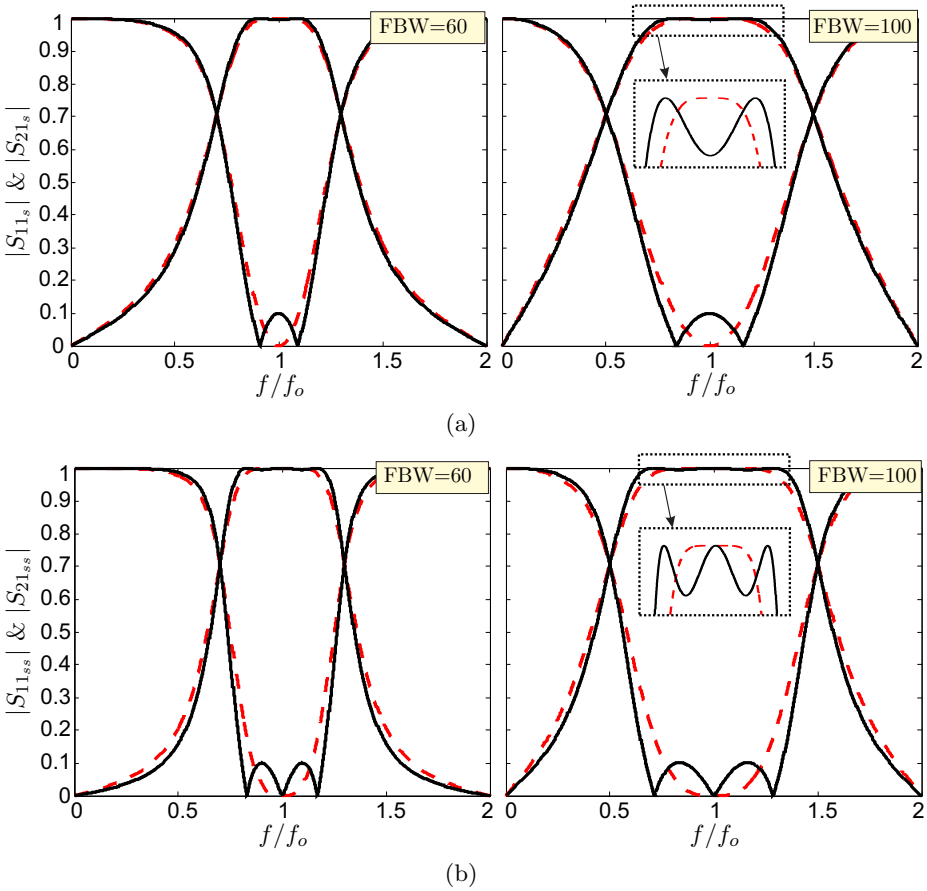

Figure 6.4.: Calculated magnitudes of S_{11} and S_{21} for two (a) single- and (b) double-section wire-bonded MTL filters designed with Butterworth (dashed line) and Chebyshev (solid line) responses for two 3 dB fractional bandwidths of 60% and 100%.

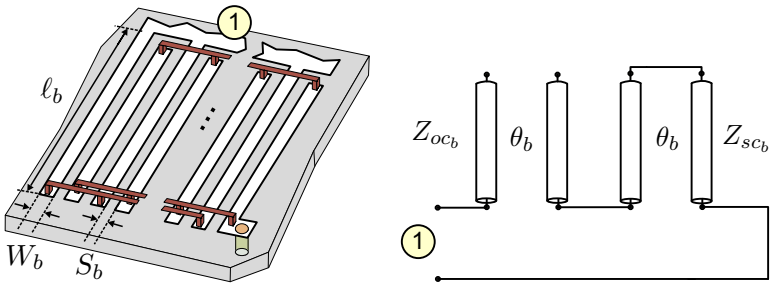

Figure 6.5.: (a) Layout and (b) equivalent circuit model for the shunt short-circuited wire-bonded MTL.

M and N were defined in (6.2) and c_b is the coupling coefficient (6.5). The input admittance Y of the shunt section can be easily calculated from

$$Y = \frac{1}{Z_{in_b}} = j\frac{1}{Z_{0_b}}\left(\frac{1-c_b^2}{c_b}\cot\theta_b - c_b\tan\theta_b\right)^{-1}. \tag{6.22}$$

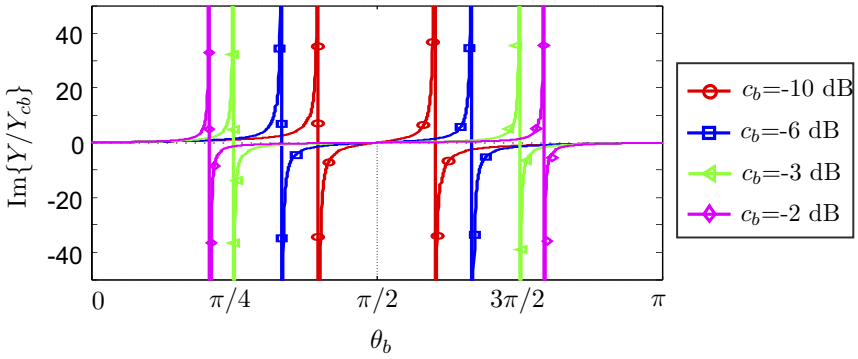

Figure 6.6.: Input susceptance of the shunt short-circuited MTL for several coupling (c_b) values.

The imaginary part of Y, normalized by $Y_{0_b} = 1/Z_{0_b}$, is represented in Fig. 6.6 for several coupling levels. It can be seen that the structure has two poles and three zeros. The zeros always appear at θ_b=0, $\pi/2$ and π, regardless of the value of c_b, but the position of the poles can be controlled by simply adjusting the value of c_b. Taking into account this frequency response, the shunt MTL will be used as a shunt resonator to create transmission zeros at different electrical lengths. These electrical lengths can be calculated as (4.9)

$$\theta_{pn} = \pm\theta_{p0} + n\pi \tag{6.23}$$

where

$$\theta_{p0} = \arccos\left(\frac{|N_b|}{M_b}\right) = \arccos\left(c_b\right) \tag{6.24}$$

and n=0,1,2,3,... Consequently, from Fig. 6.6 it can be deduced that, the shunt structure is appropriate for inserting two transmission zeros at the cut-off frequencies (θ_{p0} and $\pi - \theta_{p0}$) of the bandpass filter. As it will be shown in the next section, the shunt short-circuited wire-bonded MTL will be designed not only to generate two transmission zeros but also to include one or two new transmission poles within the pass band.

6.2.3. Asymmetrical Topology

The scheme of the proposed filter is depicted in Fig. 6.1, consisting of one series wire-bonded MTL and a shunt short-circuited wire-bonded MTL. Assuming a lossless medium, the admittance matrix of the series wire-bonded MTL can be computed as given in (6.1). Thus, considering (6.1) and (6.22), the admittance matrix for the complete filter can be calculated as

$$[Y]_a = \begin{bmatrix} Y_{11_a} & Y_{12_a} \\ Y_{21_a} & Y_{22_a} + Y \end{bmatrix} = \frac{-jc_a \sin\theta_a \cos\theta_a}{Z_{0_a}(c_a^2 - \cos^2\theta_a)} \begin{bmatrix} 1 & \frac{-c_a}{\cos\theta_a} \\ \frac{-c_a}{\cos\theta_a} & 1 + Y \end{bmatrix} \tag{6.25}$$

The S-parameters of the filter can be obtained by simple transformations of (6.25), but these equations are quite involved. Nevertheless, as both, series and shunt MTLs, will be

designed to be a quarter-wavelength long at the design center frequency (f_o) to obtain the maximum operating bandwidth, it can be considered that θ_a and θ_b are similar and equal to $\theta = (\pi/2)(f/f_o)$. Hence, after some algebraic manipulations, the following relations can be deduced to calculate the magnitude of the S-parameters as

$$|S_{21}|^2 = \frac{1}{1+F_a^2}, \qquad |S_{11}|^2 = \frac{F_a^2}{1+F_a^2}, \tag{6.26}$$

with

$$F_a^2 = \frac{(g_6\cos^6\theta + g_4\cos^4\theta + g_2\cos^2\theta + g_0)\cos^2\theta}{4c_a^4\left(c_b^2-\cos^2\theta\right)^2\sin^2\theta} \tag{6.27a}$$

$$g_6 = (c_a^2-1)\left[(c_a+\bar{Z}c_b)^2-1\right] \tag{6.27b}$$

$$g_4 = \bar{Z}^2c_b^2 - 2c_b(c_a^2-1)\left[\bar{Z}c_a(1+c_b^2)+c_b(c_a^2-1)\right] \tag{6.27c}$$

$$g_2 = -\bar{Z}^2c_a^2c_b^2(1+c_a^2) + c_b^2(c_a^2-1)\left[2\bar{Z}c_ac_b + c_b^2(c_a^2-1)\right] \tag{6.27d}$$

$$g_0 = \bar{Z}^2c_a^4c_b^2 \tag{6.27e}$$

and $\bar{Z} = Z_{0_a}/Z_{0_b}$. In (6.27) it was considered that $Z_{0_a} = Z_0$, being Z_0 the reference impedance, to achieve a wideband impedance-matched filter. As seen, the S-parameters depend on the values of c_a and c_b but also on the impedance ratio $\bar{Z}$. Taking into account the function F_a^2, it is clear that the filter can be designed to have a quasi-elliptic frequency response with three transmission poles. Besides, the transmission zeros of the circuit can be obtained from (6.26) as

$$\theta_{z_1}=0, \quad \theta_{z_2}=\pi, \quad \theta_{z_3}=\arccos(c_b), \quad \theta_{z_4}=\pi-\theta_{z3}. \tag{6.28}$$

The symmetrical transmission zeros z_3 and z_4, that exclusively depend on the coupling factor c_b of the shunt MTL, can be placed at the edges of the passband to increase the roll-off rejection. However, the design condition to achieve a equiripple response is not straightforward and it requires determining the relation among c_a, c_b and $\bar{Z}$. From (6.27), and after some rigorous transformations, the following simplified design equation is found

$$c_a = -\frac{c_b}{2}\left(\bar{Z}-\sqrt{\bar{Z}^2+4}\right), \tag{6.29}$$

that specifies the relationships between the series and shunt wire-bonded MTLs to obtain a quasi-elliptic function response.

Fig. 6.7 depicts the magnitude of the S-parameters of the proposed filter designed by means of (6.29) for $\bar{Z}$=1. As expected, the filter has three poles and two transmission zeros at the lower and upper cut-off frequencies and it is easy to note that, the greater the coupling factors, the broader the passband. Besides, Fig. 6.8 depicts the required coupling values c_a and c_b as well as the expected return loss and stopband minimum rejection level as a

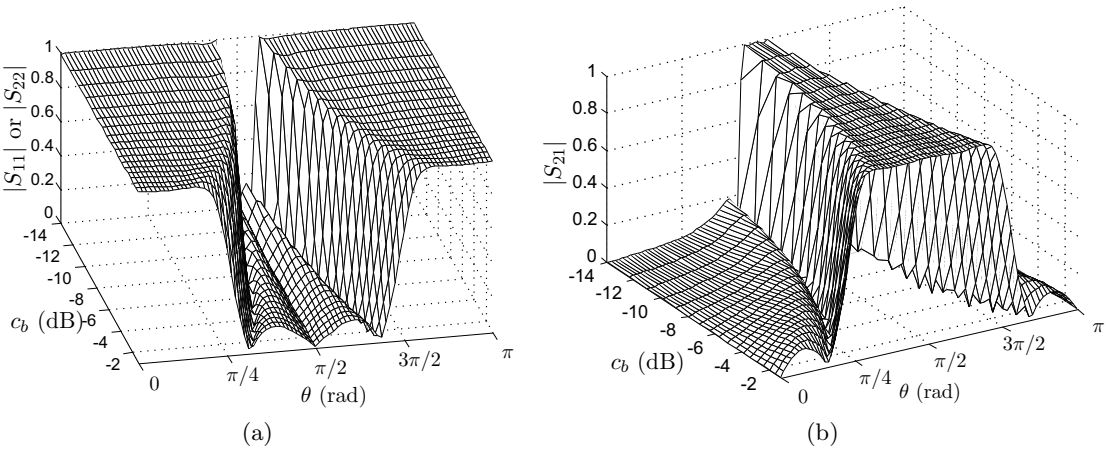

Figure 6.7.: Magnitude of S-parameters of the proposed filter designed by means of (6.29) for $\bar{Z}$=1 (c_a(dB)=c_b(dB)-4.18).

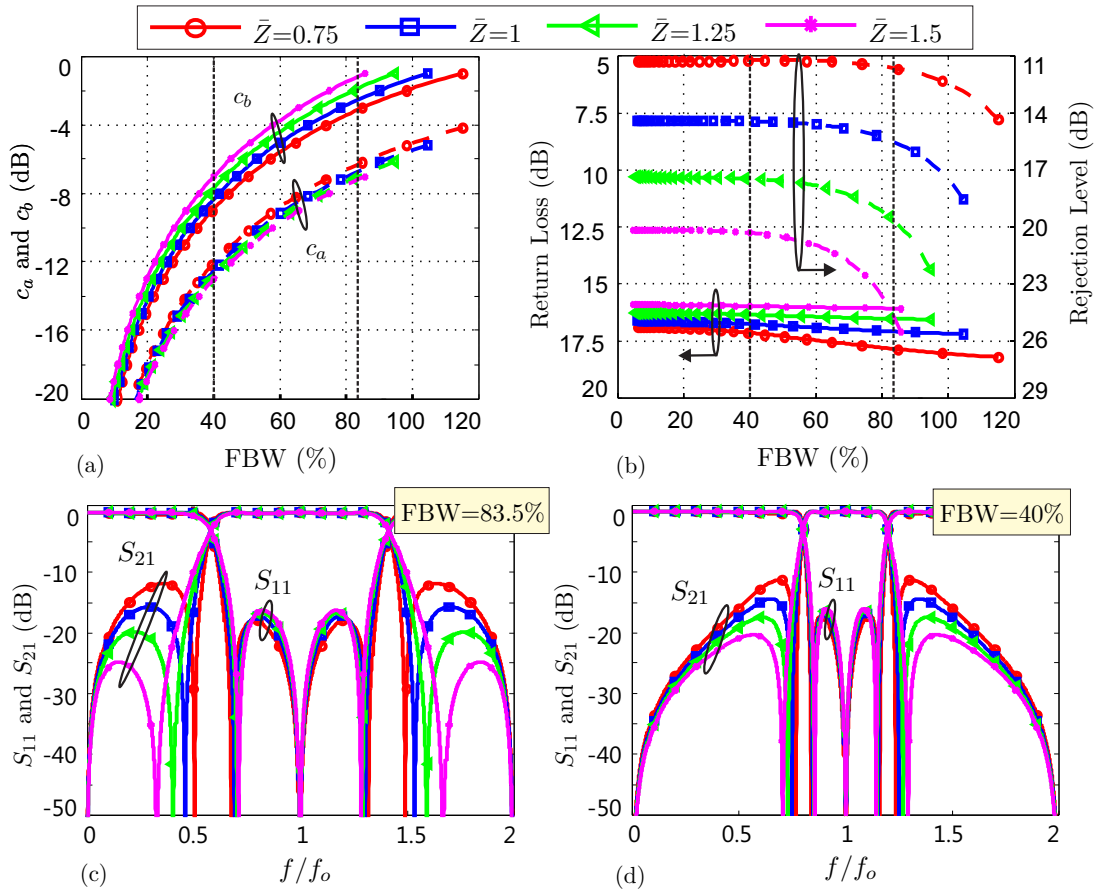

Figure 6.8.: (a) Coupling values c_a and c_b, (b) return loss and stopband minimum rejection level as a function of the 3 dB fractional bandwidth (FBW) for different impedance ratios $\bar{Z}$. (c)-(d) Magnitude of S-parameters for two particular FBW, 83.5% and 40%.

function of the 3 dB fractional bandwidth (FBW). These curves are obtained from (6.26) by imposing the design condition (6.29). To visualize the filtering characteristics of the proposed

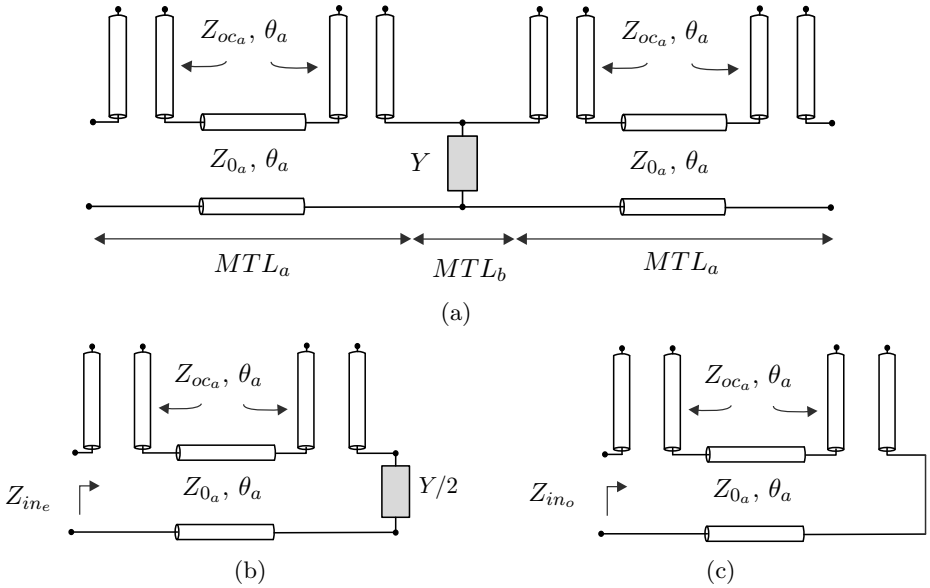

Figure 6.9.: (a) Equivalent circuit model for the proposed filter and corresponding circuits under (b) even- and (c) odd-mode excitations.

filter, the magnitude of S-parameters are depicted for two particular FBW, 83.5% and 40%, respectively. As seen, the higher the impedance ratio, the greater the rejection level. However, it is important to remark that the possible values of c_a, c_b and $\bar{Z}$ are directly related with the manufacturing capabilities.

6.2.4. Symmetrical Topology

The equivalent circuit transmission-line model for this proposed filter, comprising of two series wire-bonded MTLs and a shunt short-circuited wire-bonded MTL, is depicted in Fig. 6.9(a). The shunt MTL is modeled as a shunt admittance Y(6.22), while the open-circuited MTL is represented by its equivalent circuit consisting of a transmission-line section with two series open circuit stubs. Z_{0_a} was defined in (6.4) and Z_{oc_a} is given by

$$Z_{oc_a} = Z_{0_a}\frac{1-c_a}{c_a}. \tag{6.30}$$

From Fig. 6.9(a), it can be seen that the configuration of the proposed filter is a symmetrical structure and thus, the analytical study of this arrangement can be easily decomposed into even- and odd-mode excitations, as shown in Fig. 6.9(b) and Fig. 6.9(c), respectively. To achieve the maximum operating bandwidth, both series and shunt wire-bonded MTLs are designed with a length of $\lambda/4$ at the design center frequency f_o. Therefore, as in the asymmetrical filter, it can be considered that their electrical lengths θ_a and θ_b are similar and equal to $\theta = (\pi/2)(f/f_o)$, and the even- and odd-mode input impedances can be expressed

as

$$Z_{in_e}=jZ_{0_a}\frac{(Z_{0_a}c_a+2Z_{0_b}c_b)\tan^2\theta-\left(\frac{1-c_a^2}{c_a}Z_{0_a}+2Z_{0_b}\frac{1-c_b^2}{c_b}\right)}{c_a\left(\left(\frac{Z_{0_a}}{c_a}-2Z_{0_b}\frac{1-c_b^2}{c_b}\right)\tan\theta-2Z_{0_b}c_b\tan^3\theta\right)} \tag{6.31a}$$

$$Z_{in_o}=-jZ_{0_a}\left(\frac{1-c_a^2}{c_a}\cot\theta-c_a\tan\theta\right). \tag{6.31b}$$

Using the definitions (6.31a) and (6.31b), the S-parameters of the proposed structure are easily determined in terms of Z_{in_e} and Z_{in_o} as

$$S_{11}=\frac{Z_{in_e}Z_{in_o}-Z_0^2}{\Delta},\quad S_{21}=\frac{Z_0\left(Z_{in_e}-Z_{in_o}\right)}{\Delta} \tag{6.32a}$$

$$\Delta=Z_0^2+Z_0\left(Z_{in_e}+Z_{in_o}\right)+Z_{in_e}Z_{in_o}, \tag{6.32b}$$

Z_0 being the characteristic impedance used to terminate the input and output ports. By evaluating (6.32) and after several algebraic manipulations and rigorous transformations, the squared magnitude of S_{11} and S_{21}, are

$$|S_{11}|^2=\frac{F^2}{1+F^2},\quad |S_{21}|^2=\frac{1}{1+F^2} \tag{6.33}$$

with

$$F=\left(\frac{c_b}{2c_a^4\bar{Z}_{0_b}}\right)\frac{\cos\theta\left(g_4\cos^4\theta+g_2\cos^2\theta+g0\right)}{\left(c_b^2-\cos^2\theta\right)\sin\theta} \tag{6.34a}$$

$$g_4=\left(\bar{Z}_{0_a}^2-c_a^2\right)\left(\frac{2c_a\bar{Z}_{0_b}}{c_b\bar{Z}_{0_a}}+1\right) \tag{6.34b}$$

$$g_2=\frac{2c_a\bar{Z}_{0_b}}{c_b\bar{Z}_{0_a}}\left(c_a^2\left(1+c_b^2\right)-\bar{Z}_{0_a}^2\left(c_a^2+c_b^2\right)\right)+c_a^2\left(1-2\bar{Z}_{0_a}^2\right) \tag{6.34c}$$

$$g_0=c_a^3\left(\bar{Z}_{0_a}^2c_a+2\frac{\bar{Z}_{0_b}}{\bar{Z}_{0_a}}c_b\left(\bar{Z}_{0_a}^2-1\right)\right) \tag{6.34d}$$

and

$$\bar{Z}_{0_a}=Z_{0_a}/Z_0,\quad \bar{Z}_{0_b}=Z_{0_b}/Z_0. \tag{6.35}$$

The form of F (6.34a) shows that the proposed topology is straightforward for the design of selective bandpass filters having a quasi-elliptic response. The rational function F has simple poles at $\cos\theta=c_b$ and its numerator is a fifth-order polynomial. This topology is also suitable for the design of a five-pole pass band filter with two transmission zeros [1, 36]. This result highlights the main difference between the proposed symmetric topology and the asymmetric configuration (Fig. 6.1(a)) analyzed in previous section. The asymmetric configuration can be used to obtain a three-pole bandpass filter. However, by including the output series MTL, two new poles can be created, that improves both, the flatness and the selectivity of the

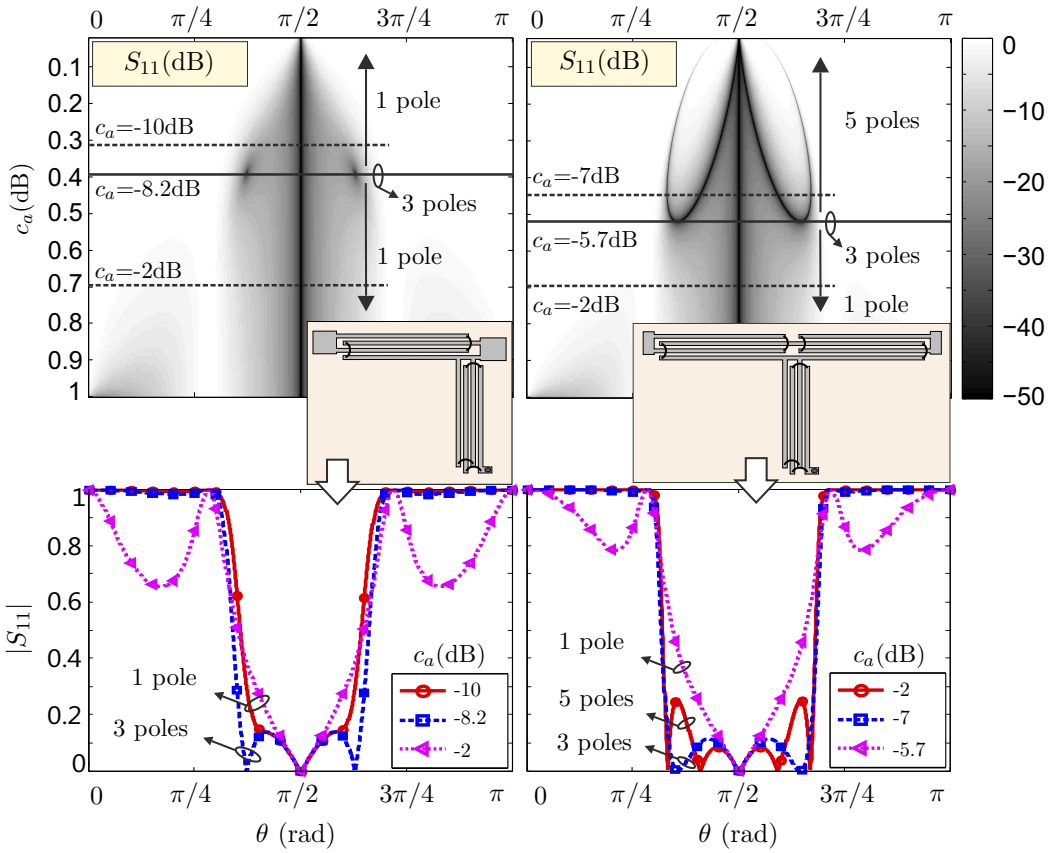

Figure 6.10.: Magnitude of S_{11} as a function of c_a considering an asymmetric or symmetric filtering topology. $\bar{Z}_{0_a}$=$\bar{Z}_{0_b}$=1, c_b=-4 dB.

passband. Fig. 6.10 shows the contour plots for the magnitude of S_{11} for the asymmetric and symmetric topologies, as a function of c_a, for a particular value of $\bar{Z}_{0_a}$=$\bar{Z}_{0_b}$=1 and c_b=-4 dB. From these curves, it can now be seen that the asymmetric scheme can only be designed to have three transmission poles, while the symmetric filter can be configured to have three or five poles. Moreover, where the asymmetric filter has three poles the range of values for c_a is very small. In contrast, for the symmetric configuration, there is a coupling level c_a where the filter presents three transmission poles and, for lower values the filter always has five poles. This frequency behavior demonstrates that the new topology not only provides a better frequency response but is also less sensitive to small deviations from the theoretical design parameters.

The design of the proposed filter for an equal-ripple pass band can be directly accomplished by evaluating (6.33). However, its frequency response depends on c_a, Z_{0_a}, c_b and Z_{0_b} and this involves a laborious process, in order to achieve the desired bandwidth with particular insertion losses or rejection level and with an equal-ripple pass band. Therefore, analytical equations are desirable for a quick design process. This procedure is carried out by comparison

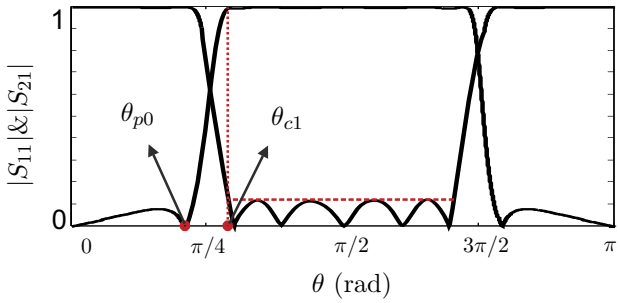

Figure 6.11.: Magnitude of S-parameters for a quasi-elliptic filter having five transmission poles and two transmission zeros.

of F with the rational function $f(x)$ [36]

$$f(x) = \frac{\alpha^2 x T_{n-1}(x) + \beta^2 x T_{n-3}(x) - 2a^2 T_{n-2}(x)}{2\,(a^2 - x^2)} \tag{6.36a}$$

$$\alpha = a + \sqrt{a^2 - 1}, \quad \beta = a - \sqrt{a^2 - 1}, \tag{6.36b}$$

where $f(x)$ is expressed in terms of Chebyshev polynomials of order n. This has simple poles at $x = \pm a$ and the equal-ripple passband is determined for -1≤ x ≤ 1. This region is mapped to the passband of the filter by replacing $\cos\theta$ with $\cos\theta/\cos\theta_{c1}$ to map x=1 to θ_{c1}. After this substitution, a can be written as (6.24)

$$a = \frac{\cos\theta_{p0}}{\cos\theta_{c1}} = \frac{c_b}{\cos\theta_{c1}}, \tag{6.37}$$

which defines the ratio between the transmission zero θ_{p0} and the cut-off frequency θ_{c1}, being $a > 1$, as illustrated in Fig. 6.11. The lower the value of a, the closer the transmission zeros are to the cut-off frequencies. From (6.37), it is seen that for a particular FBW, c_b is determined for each value of a.

In addition, from (6.33) and (6.36), the following relationships between the design parameters are found to design a five-pole quasi-elliptic filter:

$$\bar{Z}_{0_a} = \left(\frac{-C_2 - \sqrt{C_2^2 - 4C_4C_0}}{2C_4} \right)^{1/2}, \tag{6.38a}$$

$$\bar{Z}_{0_b} = \frac{c_a c_b \bar{Z}_{0_a} [\bar{Z}_{0_a}^2 (Ac_a^2 + 2B) - B]}{2[c_a^2(B + c_b^2(A + B)) - \bar{Z}_{0_a}^2 (c_a^2(B + Ac_b^2) + Bc_b^2)]} \tag{6.38b}$$

with

$$A=\frac{2(\beta^2-4\alpha^2-4a^2)\cos\theta_{c1}^2}{8\alpha^2},\ B=\frac{(6a^2+\alpha^2-\beta^2)\cos\theta_{c1}^4}{8\alpha^2} \tag{6.39a}$$

$$C_0=c_a^4c_b^2\,(1+A+B) \tag{6.39b}$$

$$C_2=c_a^6(A+1+c_b^2)+c_a^4(B-c_b^2(3+A))-c_a^2c_b^2(A+2B) \tag{6.39c}$$

$$C_4=Bc_b^2-c_a^6+c_a^4(c_b^2-A)+c_a^2(Ac_b^2-B). \tag{6.39d}$$

Equation (6.38) can be easily solved and allows the characteristic impedances of the series and shunt MTL ($\bar{Z}_{0_a}$ and $\bar{Z}_{0_b}$) to be calculated as a function of c_a and c_b in order to obtain a particular equal-ripple operating bandwidth. The solutions of the above equations guarantee that the designed filter will have a quasi-elliptic response with five transmission poles and two transmission zeros. The design procedure can be summarized as follows:

1. Calculate θ_{c1} according to the desired operating bandwidth with equiripple response (6.9) (see Fig. 6.11).
2. Specify a particular value of a, taking into account the required selectivity. The lower the value of a the closer the attenuation poles to the cutoff frequency and, consequently, the greater the skirt selectivity of the filter. Once the value of a is determined, c_b is computed as $c_b=a\cos\theta_{c1}$ (6.37).
3. Obtain values for $\bar{Z}_{0_a}$ and $\bar{Z}_{0_b}$, as a function of c_a, using (6.38).
4. Evaluate (6.34a) with the computed values c_b, c_a, $\bar{Z}_{0_a}$ and $\bar{Z}_{0_b}$, to obtain the desired minimum return losses (or ripple level) and the minimum stopband rejection level.
5. Select the values of c_a, $\bar{Z}_{0_a}$ and $\bar{Z}_{0_a}$ to obtain a particular rejection level and ripple value. If a higher rejection level is needed, increase the value of a and go back to Step 2. By increasing a, the skirt selectivity is reduced but the minimum rejection level is improved.

Using the above design procedure, Fig. 6.12 shows the contour plots for the design parameters obtained as a function of the fractional bandwidth, for a particular value of a=1.2. It can be seen that, depending on the final selected values, it is possible to change both the return losses and the minimum rejection level. Furthermore, for a particular FBW, the lower the return losses (higher ripple level) the higher the rejection level. Therefore, to improve the out-band rejection without reducing the return losses, it is necessary to use a higher value of a (decreasing the skirt selectivity). However, it is important to mention that the allowed values of Z_{0_a}, c_a, Z_{0_b} and c_b will be dictated by the fabrication process.

To highlight the enhancement of the filtering performances by including the shunt MTL, Fig. 6.13 shows the S-parameters for Butterworth and Chebyshev filters, with only two series MTLs, and of the proposed quasi-elliptic filter for two 3-dB fractional operating bandwidths

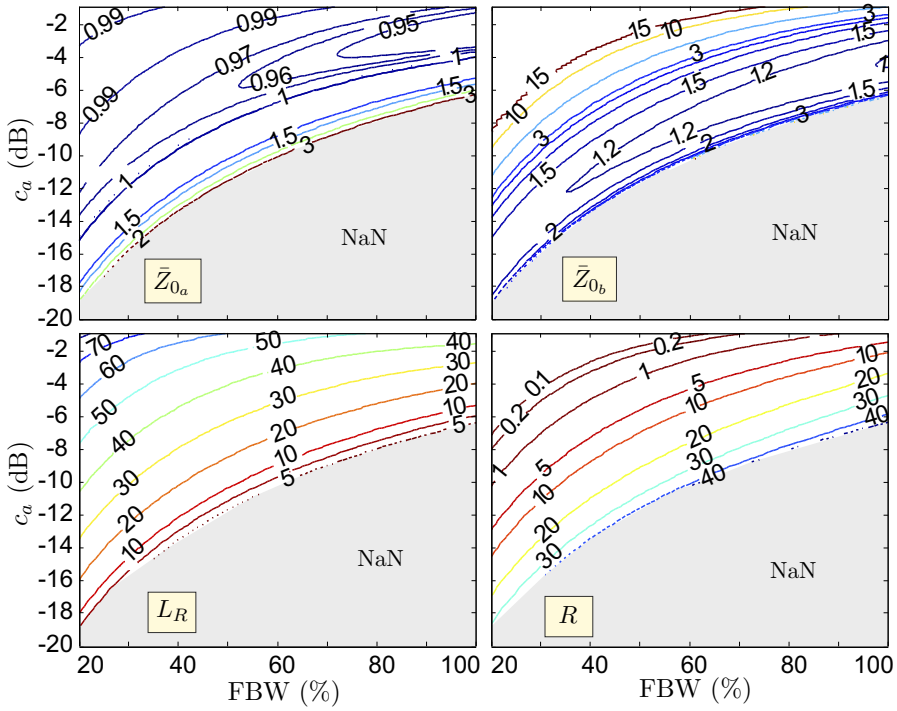

Figure 6.12.: Design parameters $\bar{Z}_{0_a}$ and $\bar{Z}_{0_b}$, return loss L_R (dB) and minimum out-of-band rejection level R (dB) as a function of both, the coupling factor c_a of the series MTL and the fractional equal-ripple bandwidth FBW.

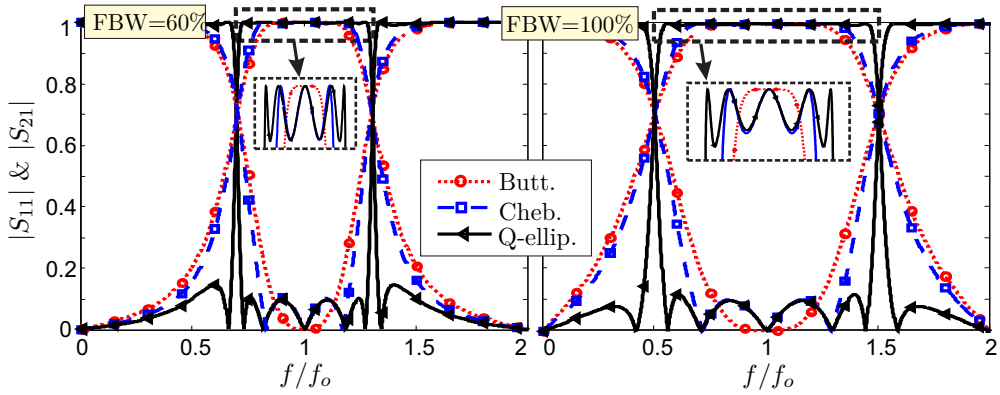

Figure 6.13.: Magnitude of S_{11} and S_{21} for a two-stage wire-bonded MTL filter designed with a Butterworth and Chebyshev response, and the proposed quasi-elliptic filter for two 3 dB fractional bandwidths of 60% and 100%.

of 60% and 100% (L_R=20 dB for Chebyshev and quasi-elliptic responses). The improvements in the skirt selectivity and flatness of the pass band are exceptionally good. The design parameters are given in Table 6.2 and, compared with Table 6.1, it is seen that for both 3-dB operating bandwidths, the fractional bandwidth with the equal-ripple response is increased by approximately 100%, for a single-section MTL filter, and by about 40% for double-section filters.

Table 6.2.: Design parameters for a five-pole quasi-elliptic filter

	Quasi-elliptic (LR=20dB, a=1.2)				
FBW_{3dB}	c_a	Z_{0_a}	c_b	Z_{0_b}	FBW^*
60	-7.5	51	-5.8	61.2	56
100	-4.4	50	-2	52.4	92

FBW^*: Fractional bandwidth with equal-ripple response

The general design equations in (6.38) can be greatly simplified if $\bar{Z}_{0_a}$=1 (i.e. $Z_{0_a} = Z_0$). Under this specific condition, the following two closed-form design equations are found

$$c_a = \left(\frac{-B(1+c_b^2) + \sqrt{B^2(1+c_b^2)^2 + 4Bc_b^2(A+c_b^2)}}{2(A+c_b^2)} \right)^{1/2} \tag{6.40a}$$

$$\bar{Z}_{0_b} = \frac{c_a(Ac_a^2+B)}{2Bc_b(c_a^2-1)}, \tag{6.40b}$$

where A and B are defined in (6.39a). Now, by setting a (with $c_b = a\cos\theta_{c1}$), parameters c_a and Z_{0_b} are defined precisely using (6.40). This means that, for a particular operating bandwidth, both the ripple value and the minimum rejection level are fixed. The computational complexity of (6.40) compared to (6.38) is similar. However, given a desired FBW by means of the general equations, it is possible to synthesize the filter with different ripple and rejection levels (see Fig. 6.12). Fig. 6.14 shows the S-parameters for the proposed filter having two bandwidths and several values of a, by using the general equations (6.38) with L_R=[20,30] dB, and by means of the simplified expressions in (6.40) with $\bar{Z}_{0_a}$=1. As can be seen, general design equations allow the value of L_R to be adjusted, but when $\bar{Z}_{0_a}$=1 the frequency response is automatically fixed for each value of a. Nevertheless, from these curves, it is noted that for values of L_R between 15 and 20 dB, the use of Z_{0_a}=Z_0 provides excellent results.

Furthermore, as shown in Fig. 6.10, the proposed topology can also be used to synthesize a three-pole quasi-elliptic filter. By imposing this condition on (6.33), the following equation has been derived

$$\begin{aligned} \bar{Z}_{0_b}^2 + \frac{4\bar{Z}_{0_a}c_ac_b\left[\bar{Z}_{0_a}^2\left(c_a^2(2c_a^2-3)+c_b^2\right)+c_a^2(1-c_b^2)\right]}{4\left[\bar{Z}_{0_a}^2(c_b^2-c_a^2)+c_a^2(1-c_b^2)\right]^2}\bar{Z}_{0_b} + \\ + \frac{\bar{Z}_{0_a}^2c_a^2c_b^2\left(4\bar{Z}_{0_a}^2(c_a^2-1)+1\right)}{4\left[\bar{Z}_{0_a}^2(c_b^2-c_a^2)+c_a^2(1-c_b^2)\right]^2} = 0, \end{aligned} \tag{6.41}$$

where $\bar{Z}_{0_b}$ can be calculated by solving the quadratic equation as a function of c_a, c_b and $\bar{Z}_{0_a}$. Similar to the simplification for the general design expressions, if $\bar{Z}_{0_a}$=1 then, (6.41) reduces

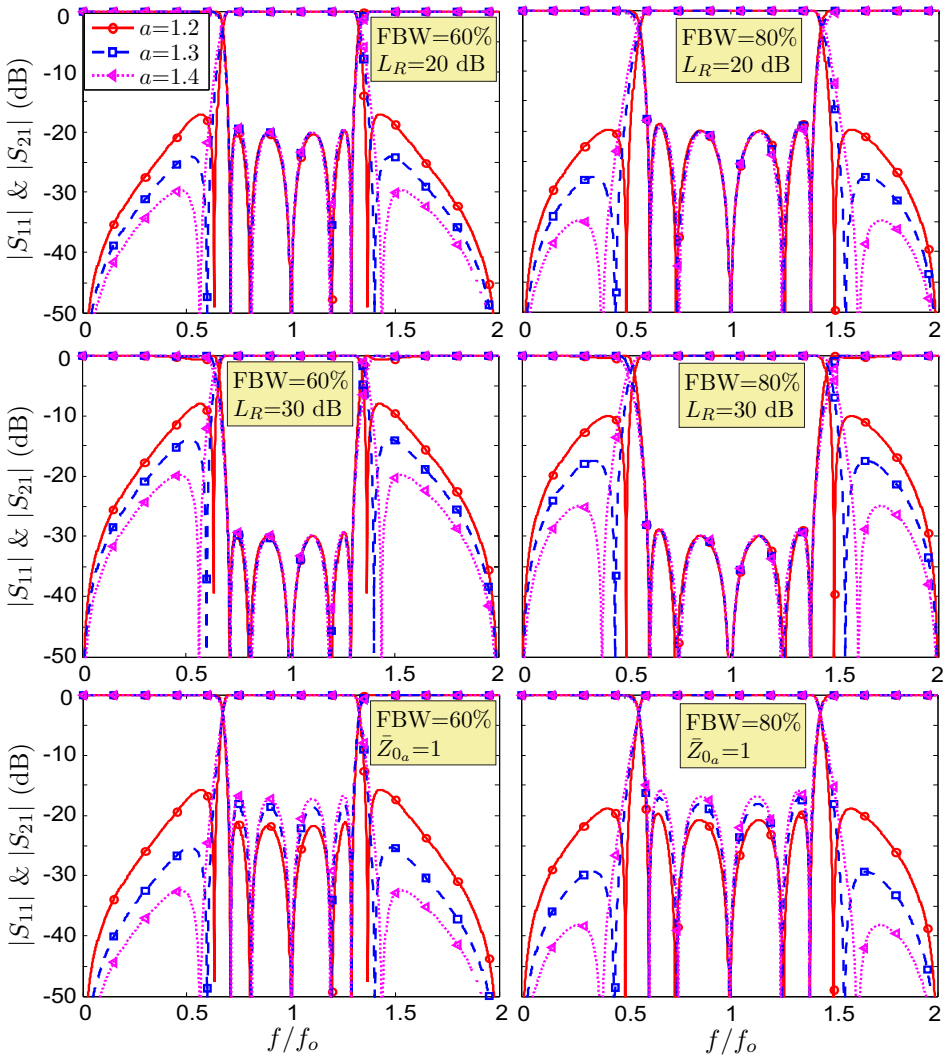

Figure 6.14.: Magnitude of S_{11} and S_{21} calculated using (6.38) with L_R=[20,30]dB and by using (6.40) with $\bar{Z}_{0_a}$=1, for two operating fractional bandwidths FBW=[60,80]% and several values of a=[1.2,1.3,1.4].

to

$$\bar{Z}_{0_b} = \frac{c_a\left(2c_a^2 - c_b^2 + 2\sqrt{c_a^4 - c_b^2c_a^2(1+c_b^2) + c_b^4}\right)}{2c_b^3\left(1-c_a^2\right)}. \tag{6.42}$$

It is important to note that (6.41) and (6.42) establish a unique relationship between the series and shunt MTL, to obtain three poles within the pass band, but unlike the general expressions for five poles, (6.38) or (6.40)($\bar{Z}_{0_a}$=1), there is no control on the required operating bandwidth. Therefore, some iteration is necessary before the desired performance can be achieved.

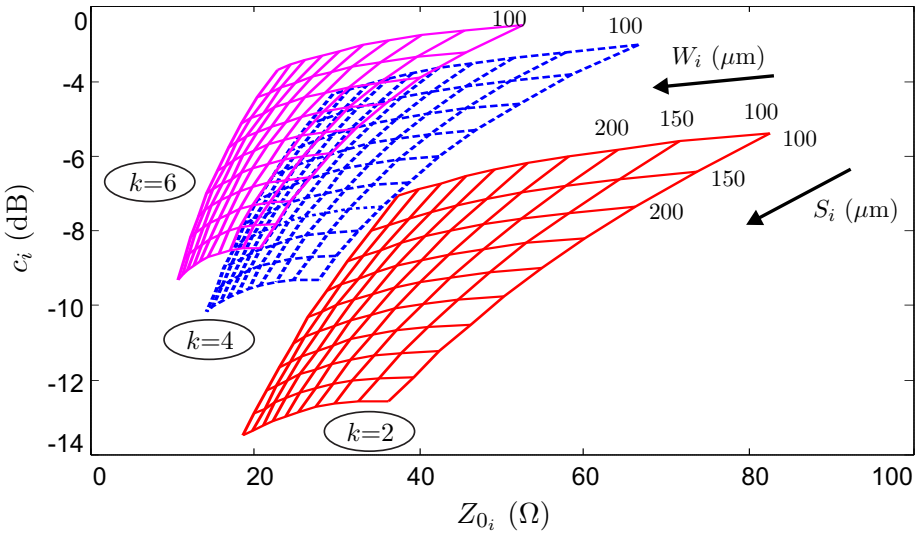

Figure 6.15.: Characteristic impedance Z_{0_i} (6.4) and coupling factor c_i (6.5) for the series and shunt wire-bonded MTL as a function of the number of conductors k, the line-width W and spacing S (grid spacing=50μm).

6.2.5. Calculation of Even- and Odd-Mode Impedances

Once the design parameters (c_a, Z_{0_a}, c_b, Z_{0_b}) for three- or five-pole quasi-elliptic bandpass filters have been calculated, for either an asymmetric or symmetric topology, the even and odd-mode impedances for the series and shunt MTLs are determined using the following expressions

$$Z_{oe_i} = \frac{k_i - 1}{2} Z_{0_i} (R-1) \frac{1-c_i^2}{c_i^2}, \qquad Z_{oo_i} = \frac{Z_{oe_i}}{R} \tag{6.43a}$$

$$R = \frac{c_i + \sqrt{(k_i-1)^2(1-c_i^2)+c_i^2}}{(k_i-1)(1-c_i)} \tag{6.43b}$$

The above expression for (6.43) is derived from (6.4),(6.5) and (6.21), and provides the values for the even and odd-mode impedances of both MTLs, as a function of the number of conductors k. It is important to note that the equations in (6.43) are different to the design equations for a k-line coupler [32]. In a four-port directional coupler, a condition for perfect match and perfect isolation ($Z_0^2 = 1/(M^2 - N^2)$) is imposed [32], but in this work the characteristic impedances of both MTLs (Z_{0_i}), c_a and c_b are calculated to achieve the desired frequency response. Here, c_a and c_b are design variables and may not be interpreted as the coupling factor of a directional coupler. In that sense, for example, the fabrication of a MTL with c_i=-10 dB can be more complicated than another with c_i=-4 dB, depending on its characteristic impedance Z_{0_i}. This behavior is illustrated in Fig. 6.15, where Z_{0_i} and c_i are represented as a function of the width W_i and spacing S_i for several numbers of conductors k.

Table 6.3.: Physical dimensions of the asymmetric three-pole fabricated filters for a design center frequency f_o=3.5 GHz.

	FBW (%)	$\bar{Z}$	Z_{0_a} (Ω)	Z_{0_b} (Ω)	c_a (dB)	c_b (dB)	Z_{oe_a} (Ω)	Z_{oo_a} (Ω)	Z_{oe_b} (Ω)	Z_{oo_b} (Ω)	k_a	W_a (μm)	S_a (μm)	k_b	W_b (μm)	S_b (μm)
Fig. 6.16(a)	84	1	50	50	-6.7	-2.54	158	58	230	70	2	307	124	6	112	100
Fig. 6.16(b)	64	1.5	50	33.3	-9.22	-3.2	195	95	167	59	2	130	309	6	274	115

FBW: Fractional bandwidth with equal-ripple response, ℓ_a=ℓ_b=13.5 mm

These curves have been calculated by using the Rogers 4350B substrate (having a dielectric constant of 3.66 and thickness of 30 mil). This substrate will be used throughout the rest of this chapter.

6.3. Experimental Validation

To validate our theory and techniques, several asymmetric and symmetric filters have been designed, fabricated and measured. For the asymmetric topology, two three-pole prototypes are designed (6.29), while for the symmetric configuration four five-pole and two three-pole quasi-elliptic filters are designed (6.38a),(6.38b),(6.41).

- Asymmetric prototypes.

Two filters with a 3 dB fractional bandwidth of about 84% and 64% are designed at a center frequency f_o=3.5 GHz. The value of c_b is firstly computed to allocate the two transmission zeros at the edges of the passband (6.28), and then, the coupling factor c_a is obtained by means of (6.29). Once the values of c_a, c_b and $\bar{Z}$ are obtained (6.29), the required even- and odd-mode impedances are easily computed as a function of the number of conductors (6.43) and translated into physical dimensions [37]. The design parameters and physical dimensions of the MTLs are shown in Table 6.3. It is important to mention that these theoretical dimensions have not been optimized with any EM simulator and that two values of $\bar{Z}$, $\bar{Z}$=1 and $\bar{Z}$=1.5, have been selected to observe the impact on the rejection level. The minimum allowed width and spacing dimensions are limited to 100 μm, according to our in-house fabrication capability, which determines the range of achievable values of Z_{0_i} and c_i (see Fig. 6.15).

Fig. 6.16 shows the measured and analytical (6.26) S-parameters and the group delay of the designed and fabricated bandpass filters. It can be observed that a very good agreement is seen between measurements and theory, with insertion and return losses less than 0.6 dB and greater than 13 dB in the passband, respectively. The group delay is less than 0.7 ns and the two symmetrical transmission zeros provide sharp cut-off slopes and a wide upper stopband is achieved with a rejection level greater than 15 dB, for $\bar{Z}$=1, and 22 dB for $\bar{Z}$=1.5. A photograph of both prototypes is also included in Fig. 6.16. In addition, Table 6.4 shows a

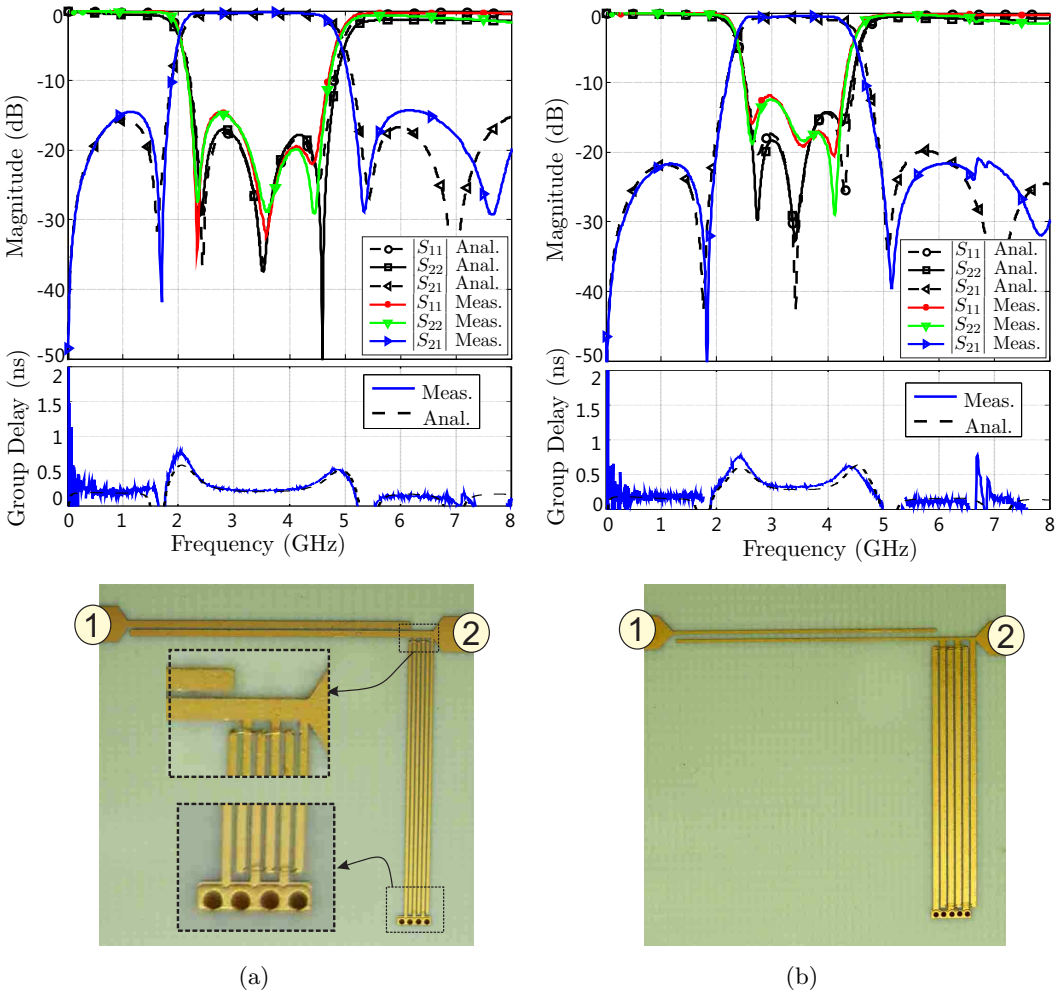

Figure 6.16.: Measured and analytical (6.26) S-parameters and group delay of the fabricated filters.

comparison between our proposed filter and others reported topologies. It can be seen a very good performance according to the insertion loss, return losses and attenuation slopes.

- Symmetric Prototypes.

Fig. 6.17 and Fig. 6.18 give the predicted (6.33) and measured S-parameter results for the manufactured five- and three-pole symmetric prototypes, respectively. The measured group delay responses and photographs of these filters are also shown in Fig. 6.17 and Fig. 6.18. The design center frequency is chosen to be f_o=3.5 GHz. The physical dimensions and design parameters are given in Table 6.5, where the minimum allowed width and spacing dimensions are limited to 100 μm.

Fig. 6.17 and Fig. 6.18 show agreement between the predicted and measured S-parameter results; it should be emphasized that there was no post-manufacture tuning. Three out of the four five-pole filters have been designed with an operating fractional bandwidth of 80% and

Table 6.4.: Comparison of fabricated asymmetric filters with other topologies

Ref.	f_o (GHz)	FBW (%)	IL (dB)	RL (dB)	Roll-off slope lower & upper (dB/GHz)	Size ($\lambda_o \times \lambda_o$)
[14]	5.95	80	0.9	14	52 & 40	0.17×0.17
	6.85	105	0.8	17	50 & 35	0.18×0.17
[38]	5.3	45	1.2	15	13 & 18	0.5 ×0.18
[19]	6.85	110	1.5	11	56 & 35	0.51×0.31
[20]	3	63	1	11	36 & 41	0.24×0.07
[5]	6.85	110	1	11	14 & 11	0.07×0.12
[22]	6.85	120	1.5	10	35 & 24	0.51×0.33
⋆	3.5	84	0.4	14.6	93 & 59	0.17×0.16
⋆	3.5	64	0.6	12	62 & 48	0.17×0.16

f_o: design center frequency; IL & RL: insertion and return loss;
roll-off slope: defined between 3 and 30 dB rejection frequency points;
λ_o: free-space wavelength at design center frequency; ⋆:This work.

Table 6.5.: Physical dimensions of the symmetric three- and five-pole fabricated filters for a design center frequency f_o=3.5 GHz.

	FBW (%)	a	Z_{0_a} (Ω)	Z_{0_b} (Ω)	c_a (dB)	c_b (dB)	Z_{oe_a} (Ω)	Z_{oo_a} (Ω)	Z_{oe_b} (Ω)	Z_{oo_b} (Ω)	k_a	W_a (μm)	S_a (μm)	k_b	W_b (μm)	S_b (μm)
Fig. 6.17(a)	80	1.22	50	48	-5.1	-2.9	217	92	223	74	4	100	230	6	114	125
Fig. 6.17(b)	80	1.17	50	65	-4.8	-3.1	219	90	235	72	4	100	215	4	100	105
Fig. 6.17(c)	80	1.17	60	65	-6.1	-3.1	180	59	235	72	2	230	100	4	100	105
Fig. 6.17(d)	50	1.4	52	30	-9.1	-5.4	203	96	140	62	2	115	290	4	375	200
Fig. 6.18(a)	84	1.21	50	52	-4	-2.5	198	72	236	71	4	160	150	6	100	100
Fig. 6.18(b)	34	1.3	40	32	-10.5	-10	174	93	128	66	2	170	390	2	430	300

FBW: Fractional bandwidth with equal-ripple response, ℓ_a=ℓ_b=13.5 mm

the last one is designed with a bandwidth of 50%. For the three-pole filters, two operating bandwidths of 84% and 34% have been selected. It is important to highlight the excellent in-band flatness of the filters, with insertion losses below 1 dB in all the prototypes, and steep roll-off skirts. From these figures, it can be seen that, given a desired FBW and a particular value of a, the rejection levels can be improved by increasing the value of Z_a but at the expense of worsening the return losses. In addition, all the filters exhibit sharp cutoff slopes ($a \leq$1.4) and, as expected from theory, by increasing the value of a it is possible to obtain higher rejection levels with good return losses (Fig. 6.17(d)). Therefore, there is a trade-off between selectivity, return losses and out of band rejection. Nevertheless, given an operating bandwidth, the attainable performance of the filter will be ultimately limited by the capability of the fabrication process.

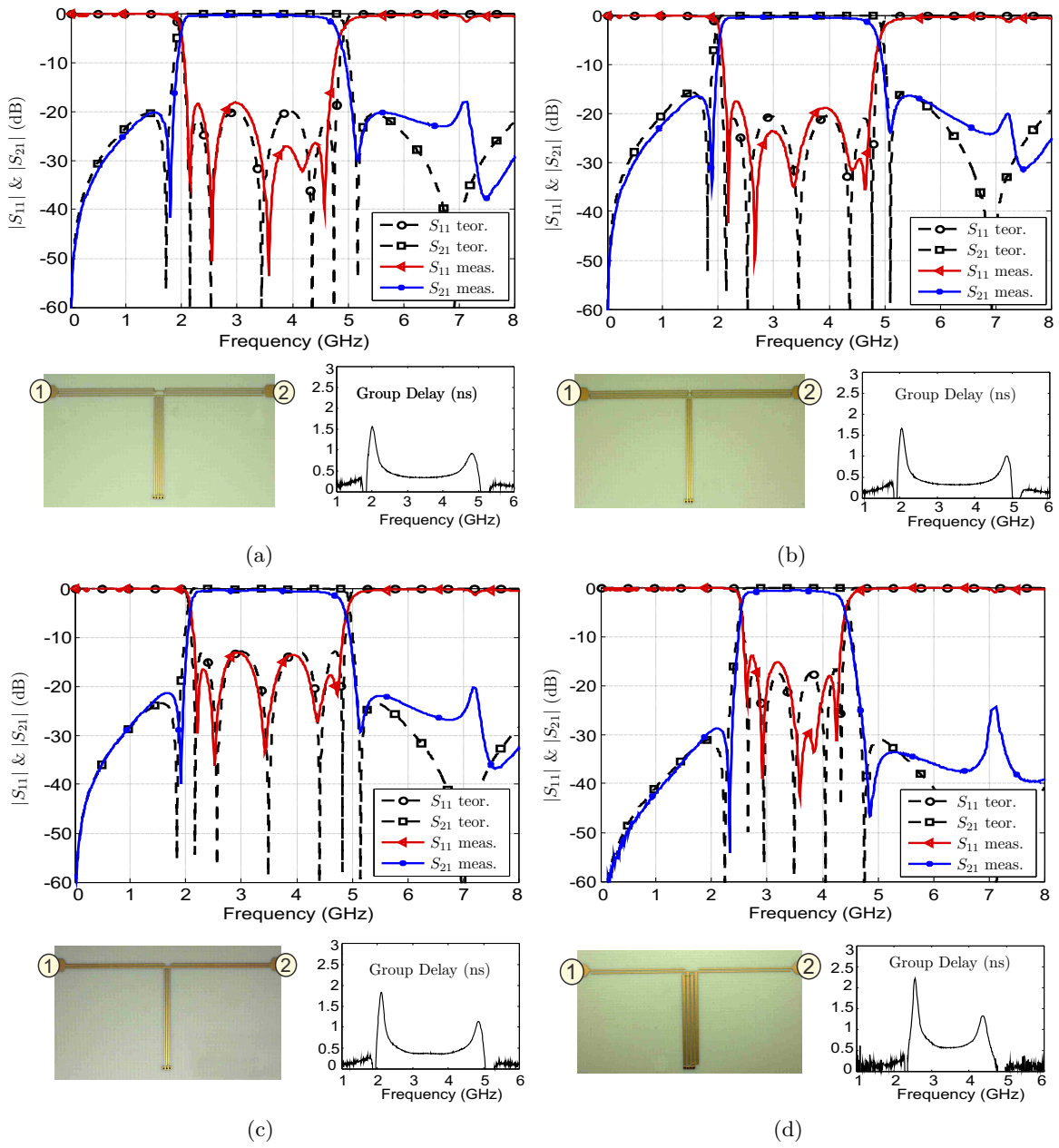

Figure 6.17.: Theoretical prediction (6.33) and measured S_{11} and S_{21} parameter performances for the manufactured five-pole quasi-elliptic filters.

Finally, it should be mentioned that the dimensions of the series and shunt MTL have been calculated theoretically [37, 39] and have not been optimized by any EM simulator. Discrepancies between the theory and measurements can be mainly attributed to material and fabrication tolerances (variations of up to 10% have been measured), as well as unequal even- and odd-mode phase velocities in the MTLs. Because of this inequality, a spurious response can be seen at approximately twice the mid-band frequency ($2f_o$=7 GHz). Fortunately, there are a number of different techniques (distributed and lumped-element compensation approaches),

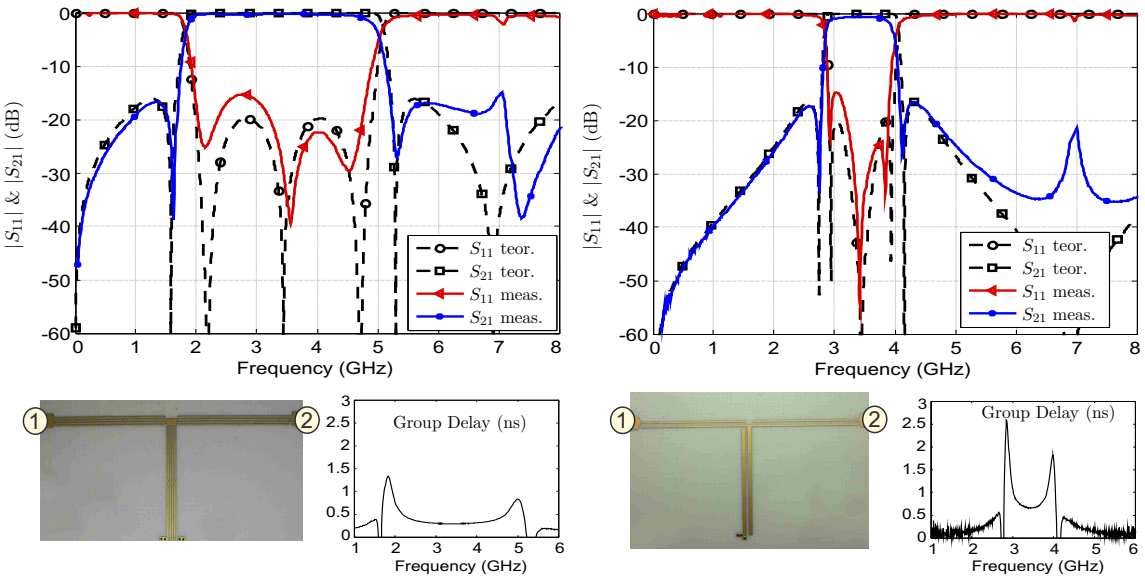

Figure 6.18.: Theoretical prediction (6.33) and measured S_{11} and S_{21} parameter performances for the manufactured three- quasi-elliptic filters.

to equalize the phase velocity of both modes; beyond the scope of this work. Nevertheless, even without any optimization, the minimum rejection level is always better than 15 dB.

6.4. Conclusion

In this chapter, a rigorous and comprehensive study of bandpass filters consisting of series wire-bonded MTL with a shunt MTL has been presented. First, closed-form design equations have been derived for the design of second- and third-order Butterworth and Chebyshev responses by using one or two series MTLs. From this, a new design procedure has been derived for the design of quasi-elliptic function filters, by introducing an additional shunt MTL. It has been shown that the two new topologies, asymmetric and symmetric configurations, are suitable for synthesizing three- and five-pole quasi-elliptic filters with sharp cut-off slopes. To demonstrate the validity and accuracy of the proposed analytical design equations, several prototypes have been designed, fabricated and measured. All the prototypes exhibited low insertion losses (<1dB) with enhanced roll-off characteristic at both the lower and upper cut-off frequencies. In addition, the excellent agreement between the theoretical predictions and measured results, allows the use of the theory given in this work for a fast and accurate synthesis of bandpass filters for a desired frequency response.

References

[1] J.-S. Hong, *Microstrip Filters for RF/Microwave Applications*, K. Chang, Ed. Wiley-Interscience, 2011.

[2] Z.-C. Hao and J.-S. Hong, "Ultrawideband Filter Technologies," *IEEE Microw. Mag.*, vol. 11, no. 4, pp. 56–68, Jun. 2010.

[3] G. L. Mattahei, L. Young, and E. M. T. Jones, *Microwave Filters, Impedance-Matching Networks, and Coupling Structures*, M. A. House, Ed. Norwood, 1985.

[4] I. C. Hunter, *Theory and Design of Microwave Filters*, Stevenage, Ed. U.K.: IEE Press, 2001.

[5] X. Huang and S. Lucyszyn, "Silicon RFIC UWB bandpass filter using bulk-micromachined trench couplers," in *IEEE International Wireless Symposium (IWS2013)*, Beijing, China, Apr. 2013.

[6] S. Sun and L. Zhu, "Multiple-resonator-based bandpass filters," *IEEE Microw. Mag.*, vol. 10, no. 2, pp. 88–98, Apr. 2009.

[7] W. Menzel, L. Zhu, K. Wu, and F. Bogelsack, "On the design of novel compact broad-band planar filters," *IEEE Trans. Microw. Theory Tech.*, vol. 51, no. 2, pp. 364 – 370, Feb. 2003.

[8] L. Zhu, S. Sun, and W. Menzel, "Ultra-wideband (UWB) bandpass filters using multiple-mode resonator," *IEEE Microw. Wireless Compon. Lett.*, vol. 15, no. 11, pp. 796 – 798, Nov. 2005.

[9] Y.-C. Chiou, J.-T. Kuo, and E. Cheng, "Broadband quasi-Chebyshev bandpass filters with multimode stepped-impedance resonators (SIRs)," *IEEE Trans. Microw. Theory Tech.*, vol. 54, no. 8, pp. 3352 –3358, Aug. 2006.

[10] C.-P. Chen, Z. Ma, and T. Anada, "Synthesis of ultra-wideband bandpass filter employing parallel-coupled stepped-impedance resonators," *IET Microw. Antennas Propag.*, vol. 2, no. 8, pp. 766–772, December 2008.

[11] R. Li, S. Sun, and L. Zhu, "Synthesis Design of Ultra-Wideband Bandpass Filters With Composite Series and Shunt Stubs," *IEEE Microw. Wireless Compon. Lett.*, vol. 57, no. 3, pp. 684–692, March 2009.

[12] S. Sun, R. Li, L. Zhu, and W. Menzel, "Studies on synthesis design of ultra-wideband parallel-coupled line bandpass filters with Chebyshev responses," in *Proc. Asia-Pacific Microw. Conf.*, Dec 2009, pp. 155–158.

[13] S. W. Wong and L. Zhu, "Quadruple-Mode UWB Bandpass Filter With Improved Out-of-Band Rejection," *IEEE Microw. Wireless Compon. Lett.*, vol. 19, no. 3, pp. 152–154, Mar. 2009.

[14] T. H. Duong and I. S. Kim, "New Elliptic Function Type UWB BPF Based on Capacitively Coupled $\lambda/4$ Open T Resonator," *IEEE Trans. Microw. Theory Tech.*, vol. 57, no. 12, pp. 3089–3098, 2009.

[15] L. Han, K. Wu, and X. Zhang, "Development of Packaged Ultra-Wideband Bandpass Filters," *IEEE Trans. Microw. Theory Tech.*, vol. 58, no. 1, pp. 220–228, Jan. 2010.

[16] Y. Omote, T. Yasuzumi, T. Uwano, and O. Hashimoto, "Design procedure of wideband band-pass filter consists of inter-digital finger resonator and parallel coupled lines," in *Proc. Asia-Pacific Microw. Conf.*, Dec. 2010, pp. 29–32.

[17] X. Luo, J.-G. Ma, and E.-P. Li, "Wideband Bandpass Filter With Wide Stopband Using Loaded BCMC Stub and Short-Stub," *IEEE Microw. Wireless Compon. Lett.*, vol. 21, no. 7, pp. 353–355, Jul. 2011.

[18] S. Khalid, P. W. Wong, and L. Y. Cheong, "A novel synthesis procedure for ultra wideband (UWB) bandpass filters," *Progr. Electromagn. Res.*, vol. 141, pp. 249–266, 2013.

[19] Q.-X. Chu, X.-H. Wu, and X.-K. Tian, "Novel UWB Bandpass Filter Using Stub-Loaded Multiple-Mode Resonator," *IEEE Microw. Wireless Compon. Lett.*, vol. 21, no. 8, pp. 403–405, Aug. 2011.

[20] H. Shaman, "New S-Band Bandpass Filter (BPF) With Wideband Passband for Wireless Communication Systems," *IEEE Microw. Wireless Compon. Lett.*, vol. 22, no. 5, pp. 242–244, May 2012.

[21] C.-P. Chen, J. Oda, T. Anada, Z. Ma, and S. Takeda, "Theoretical design of wideband filters with attenuation poles using improved parallel-coupled three-line units," in *IEEE MTT-S International Microwave Symposium Digest (MTT)*, Jun. 2012, pp. 1–3.

[22] H. Zhu and Q.-X. Chu, "Compact Ultra-Wideband (UWB) Bandpass Filter Using Dual-Stub-Loaded Resonator (DSLR)," *IEEE Microw. Wireless Compon. Lett.*, vol. 23, no. 10, pp. 527–529, 2013.

[23] R. Zhang and L. Zhu, "Synthesis Design of a Wideband Bandpass Filter With Inductively Coupled Short-Circuited Multi-Mode Resonator," *IEEE Trans. Microw. Theory Tech.*, vol. 22, no. 10, pp. 509–511, Oct 2012.

[24] W.-T. Wong, Y.-S. Lin, C.-H. Wang, and C. H. Chen, "Highly selective microstrip bandpass filters for ultra-wideband (UWB) applications," in *Proc. Asia-Pacific Microw. Conf.*, vol. 5, Dec 2005, pp. 4 pp.–.

[25] H. Shaman and J.-S. Hong, "Input and output cross-coupled wideband bandpass filter," *IEEE Trans. Microw. Theory Tech.*, vol. 55, no. 12, pp. 2562–2568, Dec. 2007.

[26] S. Sun and L. Zhu, "Wideband Microstrip Ring Resonator Bandpass Filters Under Multiple Resonances," *IEEE Trans. Microw. Theory Tech.*, vol. 55, no. 10, pp. 2176–2182, Oct 2007.

[27] J.-Y. Li, C.-H. Chi, and C.-Y. Chang, "Synthesis and Design of Generalized Chebyshev Wideband Hybrid Ring Based Bandpass Filters With a Controllable Transmission Zero Pair," *IEEE Trans. Microw. Theory Tech.*, vol. 58, no. 12, pp. 3720–3731, Dec 2010.

[28] W. J. Feng, W. Q. Che, Y. M. Chang, S. Y. Shi, and Q. Xue, "High Selectivity Fifth-Order Wideband Bandpass Filters With Multiple Transmission Zeros Based on Transversal Signal-Interaction Concepts," *IEEE Trans. Microw. Theory Tech.*, vol. 61, no. 1, pp. 89–97, Jan 2013.

[29] A. Abbosh, "Design Method for Ultra-Wideband Bandpass Filter With Wide Stopband Using Parallel-Coupled Microstrip Lines," *IEEE Trans. Microw. Theory Tech.*, vol. 60, no. 1, pp. 31–38, Jan 2012.

[30] R. Mongia, I. Bahl, and P. Bhartia, *RF and Microwave Coupled-Line Circuits.* Norwood, MA: Artech House, 1999.

[31] E. Márquez-Segura, F. Casares-Miranda, P. Otero, C. Camacho-Peñalosa, and J. Page, "Analytical Model of the Wire-Bonded Interdigital Capacitor," *IEEE Trans. Microw. Theory Tech.*, vol. 54, no. 2, pp. 748–754, Feb. 2006.

[32] W. Ou, "Design Equations for an Interdigitated Directional Coupler," *IEEE Trans. Microw. Theory Tech.*, vol. 23, no. 2, pp. 253–255, Feb. 1975.

[33] J. J. Sánchez-Martínez, E. Márquez-Segura, and C. Camacho-Peñalosa, "Synthesis of CRLH-TLs Based on a Shunt Coupled-line Section," in *42nd European Microwave Conference (EuMC)*, Oct. 2012, pp. 675–678.

[34] H.-R. Ahn and T. Itoh, "Impedance-Transforming Symmetric and Asymmetric DC Blocks," *IEEE Trans. Microw. Theory Tech.*, vol. 58, no. 9, pp. 2463–2474, Sep. 2010.

[35] M. Abramowitz and I. Stegun, *"Handbook of Mathematical Functions with Formulas, Graphs, and Mathematical Tables"*. US Government Printing Office, Washington, December 1972.

[36] R. Levy, "Filters with single transmission zeros at real or imaginary frequencies," *IEEE Trans. Microw. Theory Tech.*, vol. 24, no. 4, pp. 172–181, Apr. 1976.

[37] M. Kirschning and R. Jansen, "Accurate Wide-Range Design Equations for the Frequency-Dependent Characteristic of Parallel Coupled Microstrip Lines," *IEEE Trans. Microw. Theory Tech.*, vol. 32, no. 1, pp. 83–90, Jan. 1984.

[38] K. Ma, K. Liang, R. Jayasuriya, and K.-S. Yeo, "A Wideband and High Rejection Multimode Bandpass Filter Using Stub Perturbation," *IEEE Microw. Wireless Compon. Lett.*, vol. 19, no. 1, pp. 24–26, 2009.

[39] J. A. B. Faria, "Kirschning and Jansen computer-aided design formulae for the analysis of parallel coupled lines," *Microw. Opt. Techn. Let.*, vol. 51, no. 10, pp. 2466–2470, 2009.

Chapter 7

Conclusions

NOVEL capabilities offered by MTL structures have been analyzed in this work. This final Chapter summarizes the research work developed in this dissertation and highlights the main original contributions.

7.1. Summary and Thesis Achievements

The synthesis and main contributions of this thesis are listed next.

Phase Shifters

The analysis of wire-bonded MTL-based reflection-type phase shifters has been derived to obtain time-saving design procedures and wide frequency band of operation. In this context, the main contributions are:

- A comprehensive study of reflection-type phase shifters has been carried out.
- New simplified and generalized analytical design equations of wire-bonded MTL-based phase shifting sections, by using reactive loads at the coupled and direct ports, have been calculated. These new analytical equations are suited for designing compact and miniature reflection phase shifters without the need for a parametric study.
- Two new general equivalent circuits for open- and short-circuited wire-bonded MTLs are presented. The new equivalent circuits are of interest and advisable in designing filtering structures.

Baluns

A new theoretical study and design methodology of two open- and short-circuited wire-bonded MTLs has been presented when used for balance applications. To validate the design procedure a microstrip planar balun has been designed, fabricated and measured. According to the good measured results, the use of the presented analytical equations are advisable to obtain time-saving design procedures of other devices as filters, ring hybrids, rat-race couplers, DC blocks, coupled-line impedance transformer, and so on. By using this type of balun, a novel reconfigurable test set for the characterization of differential devices has been proposed, designed and fabricated. The measurement procedure, with a de-embedding technique, has been validated through simulations. The test set has been demonstrated to be a suitable solution for differential circuit measurement. Thus, the main contributions about this topic are:

- Closed-form design equations to synthesize wire-bonded MTL baluns have been deduced. By means of these new formulas it is possible to obtain a theoretical perfect output phase and amplitude balance at all frequencies, and perfect input matching at one or two frequencies as a function of the number of conductors.
- The proposed MTL-based balun overcome most of the limitations of recently published baluns, the poor balanced output ports matching and isolation.
- A novel MEMS-based reconfigurable test set for the measurement of mixed-mode S-parameters by using a two-port VNA has been analyzed, designed and fabricated.

MTL-based Stubs

Multiconductor transmission lines have been proposed as an efficient way of implementing shunt stubs. As an application of the theory developed, a LH-TL has been designed and manufactured. The experimental results have proven that by using MTL-based stubs it is possible to synthesize LH bandpass structures with a sharp cutoff. Furthermore, it has been demonstrated that skirt selectivity is augmented by increasing the number of strips. The main contributions are:

- A general analysis of the performance of all eight possible configurations with an arbitrary number of strips has been performed.
- It has been demonstrated the possibility of realizing values of equivalent characteristic impedances that would be complicated or unapproachable by means of a single strip.
- It has been demonstrated that six configurations are equivalent to low-impedance single short- or open-circuited stubs.

- Two configurations have particular frequency responses that can be very useful for the design of bandpass filters by adjusting the positions of zeros and poles. For these configurations two simple equivalent circuit models have been calculated.

Ultra-wideband Differential Bandpass Filters

The analysis and design of ultra-wideband differential filters based on MTLs has been presented. The analytical equations allow designers to compute the required even- and odd-mode impedances of the wire-bonded MTLs in order to obtain a desired frequency response. The theoretical results have been validated by means of experimental results. Two differential filters have been designed and fabricated with an equal-ripple fractional bandwidth (FBW) of 100% and 60%, respectively. The main contributions on this topic are:

- A novel structure consists of short-circuited wire-bonded MTL have been proposed to design differential filters with a good common-mode rejection.
- A set of new design equations has been presented to synthesize single- or double-section filters with a Butterworth or Chebyshev type response.

Wideband Quasi-Elliptic Bandpass Filters

The use of series and shunt MTLs have been studied to design bandpass filters with a quasi-elliptic response. To demonstrate the validity and accuracy of the proposed analytical design equations, several prototypes have been designed, fabricated and measured. In addition, the excellent agreement between the theoretical predictions and measured results should give designers the confidence to use the theory given in this work for a fast and accurate synthesis of bandpass filters for a desired frequency response. The main contributions are:

- Closed-form design equations have been derived for the design of second- and third-order Butterworth and Chebyshev responses by using one or two series MTLs.
- A rigorous and comprehensive study of bandpass filters consisting of series wire-bonded MTL with a shunt MTL has been presented.
- Closed-form design equations for the two new proposed topologies, asymmetric and symmetric configurations, have been calculated for synthesizing three- and five-pole quasi-elliptic filters with sharp cut-off slopes.

7.2. Future Work

In this thesis, it has been proved the suitability of wire-bonded multiconductor transmission lines to synthesize phase shifters, baluns or bandpass filters. Every proposed circuit has

been analytically studied and a design methodology has been derived and assessed by means of measurements. However, there are some points which should be dealt with. In the first instance, in order to improve the performance of the fabricated prototypes, some research work about the suppression of the undesired spurious at twice the design central frequency could be carried out. In the second place, the topology proposed for the design of differential bandpass filters needs to be optimized in order to reduce the discrepancies between the theoretical and measured results. In this case, it is necessary not only to address the problem of unequal phase velocities, but also to reduce the discontinuities at the input ports to minimize the reflections.

Finally, given the excellent results of the fabricated prototypes it could be thought the possibilities of design new applications, e.g. dual-band bandpass filters.

Appendix A

Characterization of a MTL as a Pair of Coupled Lines

Coupled transmission lines consists usually of three conductors in close proximity, where the coupling between lines can be expressed in terms of self- and mutual capacitances. Fig. A.1 shows a cross section of two coupled lines, where C_a and C_b represent the capacitance between one strip and ground, while C_m represents the capacitance between the two strips [1, 2]. If both coupled lines are equal, then C_a=C_b. Note that the electrical characteristics of the coupled lines are completely determined from these capacitances and the velocity of propagation on the lines.

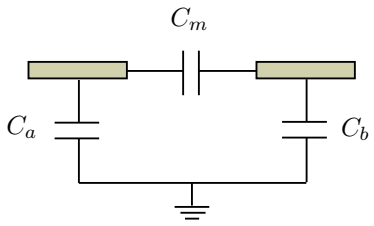

Figure A.1.: Equivalent capacitance network for two coupled lines.

Because there are three independent conductors, this structure supports the propagation of two modes. The study of these two modes can be easily carried out if the structure is analyzed under even- and odd-mode excitation. In this case, the two coupled lines will be expressed in terms of even- and odd-mode capacitances. As seen in Fig. A.2, there is a symmetrical plane between both lines. This plane acts as a magnetic wall (open circuit) under even-mode excitation and as an electric wall (short circuit) under odd-mode excitation. Therefore, the

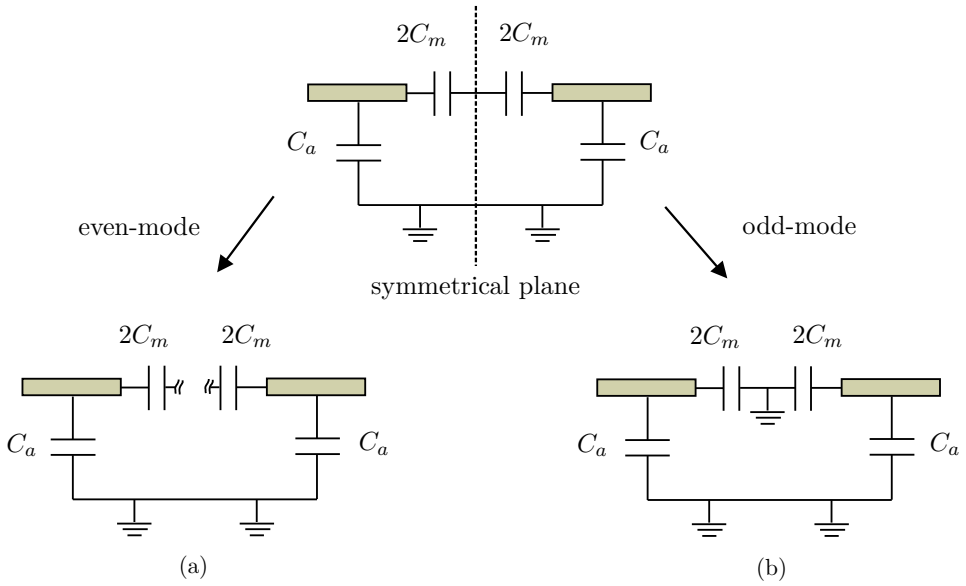

Figure A.2.: (a) Even- and (b) odd-mode excitation of symmetrical coupled lines.

circuits that result from even- and odd-mode are sketched in Fig. A.2, and the resulting capacitances for each mode are given by

$$\text{Even-mode}: \quad C_e = C_a \tag{A.1a}$$

$$\text{Odd-mode}: \quad C_o = C_a + 2C_m. \tag{A.1b}$$

Consequently, once these capacitances are known, the even- and odd-mode characteristic impedances are calculated as

$$Z_{oe} = \frac{1}{v_{pe} C_e} = \frac{1}{v_{pe} C_a} \tag{A.2a}$$

$$Z_{oo} = \frac{1}{v_{po} C_o} = \frac{1}{v_{po}\left(C_a + 2C_m\right)}, \tag{A.2b}$$

where v_{pe} and v_{po} are the phase velocities of both modes. In inhomogeneous mediums (e.g., coupled microstrip lines) v_{pe} and v_{po} are different and are determined as

$$v_{pe} = \frac{c}{\sqrt{\epsilon_{reffe}}} \tag{A.3a}$$

$$v_{po} = \frac{c}{\sqrt{\epsilon_{reffo}}}. \tag{A.3b}$$

Nevertheless, to simplify the following equations, pure TEM propagation is assumed, where the effective relative permittivity is computed from the values of the even- and odd-modes as

$$\sqrt{\epsilon_{reff}} = \frac{\sqrt{\epsilon_{reffe}} + \sqrt{\epsilon_{reffo}}}{2}. \tag{A.4}$$

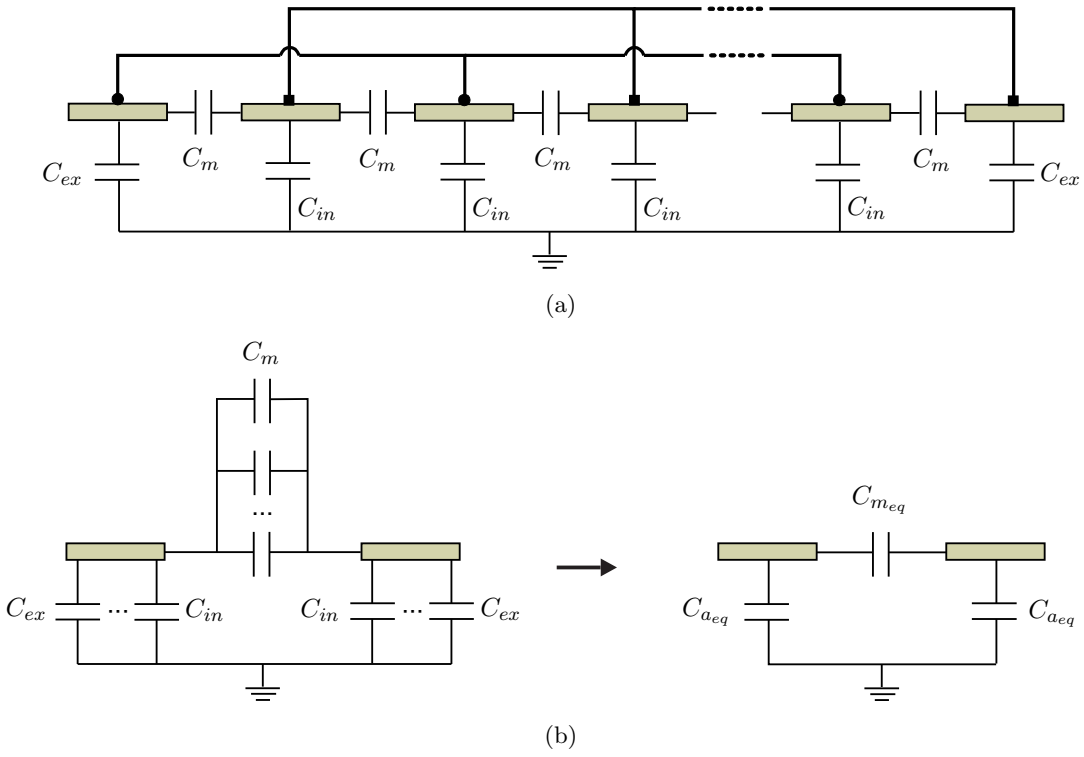

Figure A.3.: (a) Equivalent capacitance network for a wire-bonded multiconductor transmission lines and (b) simplification as a two-line structure.

Thus, from (A.4), equations (A.2) and (A.3) can be written as

$$v_{pe} = v_{po} = v_p = \frac{c}{\sqrt{\epsilon_{reff}}} \tag{A.5a}$$

$$Z_{oe} = \frac{1}{v_p C_a} \tag{A.5b}$$

$$Z_{oo} = \frac{1}{v_p \left(C_a + 2C_m\right)}, \tag{A.5c}$$

and the maximum coupling coefficient c is [1, 2]

$$c = \frac{Z_{oe} - Z_{oo}}{Z_{oe} + Z_{oo}} = \frac{Y_{oo} - Y_{oe}}{Y_{oe} + Y_{oo}}, \tag{A.6}$$

with Y_{oe}=1/Z_{oe} and Y_{oo}=1/Z_{oo}.

Once the study has been accomplished for two coupled lines, the same process can be carried out for multiconductor transmission lines. Fig. A.3(a) represents the cross section of such as circuit with the effective capacitances between the conductors, where alternate strips are connected togethers. It has been considered that the spacing between lines is the same, all the lines have the same width and the coupling between non-adjacent strips is negligible. It can be seen that there are two types of capacitances to ground depending on whether the

line is on the outside (C_{ex}) or on the inside (C_{in}). C_{in} is approximately related to C_{ex} and C_m as [1, 3]

$$C_{in} = C_{ex} - \frac{C_{ex}C_m}{C_{ex}+C_m} = \frac{C_{ex}^2}{C_{ex}+C_m}. \tag{A.7}$$

Furthermore, if the bonding wires across alternate strips are considered ideal short circuits (bonding wires very short compared to the wavelength), the complete circuit can be simplified as a two-line structure. If the number of lines (k) is even, the equivalent capacitance network can be determined as depicted in Fig. A.3(b), where $C_{m_{eq}}$ and $C_{a_{eq}}$ are given by

$$C_{m_{eq}} = (k-1)C_m \tag{A.8a}$$

$$C_{a_{eq}} = \left(\frac{k}{2}-1\right)C_{in} + C_{ex}. \tag{A.8b}$$

Thus, the multiconductor transmission lines is equivalent to two lines, and the structure can be analyzed under even- and odd-mode excitation. From (A.7) and Fig. A.3(b), the equivalent capacitances for both modes are calculated as

$$\text{Even-mode}: \quad C_{ek} = C_{a_{eq}} = \left(\frac{k}{2}-1\right)\frac{C_{ex}^2}{C_{ex}+C_{in}} + C_{ex} \tag{A.9a}$$

$$\text{Odd-mode}: \quad C_{ok} = C_{a_{eq}} + 2C_{m_{eq}} = \left(\frac{k}{2}-1\right)\frac{C_{ex}^2}{C_{ex}+C_{in}} + C_{ex} + 2C_{m_{eq}}, \tag{A.9b}$$

and the corresponding characteristic impedances are

$$v_{pe} = v_{po} = v_p = \frac{c}{\sqrt{\epsilon_{reff}}} \tag{A.10a}$$

$$Z_{oek} = \frac{1}{v_p C_{a_{eq}}} \tag{A.10b}$$

$$Z_{ook} = \frac{1}{v_p\left(C_{a_{eq}} + 2C_{m_{eq}}\right)}. \tag{A.10c}$$

Now, it is straightforward to find a relation between A.5 and A.10, with C_{ex}=C_a. From A.5 and A.7, it is obtained that

$$C_a = C_{ex} = \frac{Y_{oe}}{v_p} \tag{A.11a}$$

$$C_m = \frac{Y_{oo}-Y_{oe}}{2v_p} \tag{A.11b}$$

$$C_{in} = \frac{2Y_{oe}^2}{v_p\left(Y_{oe}+Y_{oo}\right)}, \tag{A.11c}$$

Finally, substituting (A.11) into (A.10), the following two useful equations can be calcu-

lated

$$Y_{oek} = Y_{oe}\left(\frac{(k-1)Y_{oe} + Y_{oo}}{Y_{oe} + Y_{oo}}\right) \tag{A.12a}$$

$$Y_{ook} = Y_{oo}\left(\frac{(k-1)Y_{oo} + Y_{oe}}{Y_{oe} + Y_{oo}}\right), \tag{A.12b}$$

which give the equivalent even/odd mode characteristic admittances of a k-line multiconductor transmission lines (k is even) in terms of the characteristic admittances of a two-line coupled-line structure. Using (A.12), the coupling coefficient of a k-line wire-bonded MTL is expressed as

$$c_k = \frac{Y_{ook} - Y_{oek}}{Y_{oek} + Y_{ook}} = \frac{(k-1)(Y_{oo}^2 - Y_{oe}^2)}{(k-1)(Y_{oe}^2 + Y_{oo}^2) + 2Y_{oe}Y_{oo}} = \frac{(k-1)(Z_{oe}^2 - Z_{oo}^2)}{(k-1)(Z_{oe}^2 + Z_{oo}^2) + 2Z_{oe}Z_{oo}}, \tag{A.13}$$

which is equal to the given by Ou (2.11) [3].

References

[1] D. Pozar, *Microwave Engineering*, 2nd ed. New York: Wiley, 1998.

[2] R. Mongia, I. Bahl, and P. Bhartia, *RF and Microwave Coupled-Line Circuits*. Norwood, MA: Artech House, 1999.

[3] W. Ou, "Design Equations for an Interdigitated Directional Coupler," *IEEE Trans. Microw. Theory Tech.*, vol. 23, no. 2, pp. 253–255, Feb. 1975.

Appendix B

Solution of Cubic Equations

Given the equation [1]

$$z^3 + a_2 z^2 + a_1 z + a_0 = 0, \tag{B.1}$$

let

$$q = \frac{1}{3}a_1 - \frac{1}{9}a_2^2, \quad r = \frac{1}{6}\left(a_1 a_2 - 3a_0\right) - \frac{1}{27}a_2^3. \tag{B.2}$$

If

- $q^3 + r^2 > 0$, one real root and a pair of of complex conjugate roots,
- $q^3 + r^2 = 0$, all roots real and at least two are equal,
- $q^3 + r^2 < 0$, all roots real (irreducible case).

Let

$$s_1 = \left[r + \left(q^3 + r^2\right)^{\frac{1}{2}}\right]^{\frac{1}{3}}, \quad s_2 = \left[r - \left(q^3 + r^2\right)^{\frac{1}{2}}\right]^{\frac{1}{3}}, \tag{B.3}$$

then

$$z_1 = (s_1 + s_2) - \frac{a_2}{3} \tag{B.4a}$$

$$z_2 = -\frac{1}{2}(s_1 + s_2) - \frac{a_2}{3} + j\frac{\sqrt{3}}{2}(s_1 - s_2) \tag{B.4b}$$

$$z_3 = -\frac{1}{2}(s_1 + s_2) - \frac{a_2}{3} - j\frac{\sqrt{3}}{2}(s_1 - s_2). \tag{B.4c}$$

If z_1, z_2 y z_3 are the roots of the cubic equation

$$z_1 + z_2 + z_3 = -a_2 \tag{B.5a}$$

$$z_1 z_2 + z_1 z_3 + z_2 z_3 = a_1 \tag{B.5b}$$

$$z_1 z_2 z_3 = -a_0. \tag{B.5c}$$

References

[1] M. Abramowitz and I. Stegun, *"Handbook of Mathematical Functions with Formulas, Graphs, and Mathematical Tables"*. US Government Printing Office, Washington, December 1972.

Appendix C

Summary in Spanish

C.1. Introducción

C.1.1. Marco Contextual

Las estructuras basadas en líneas acopladas tienen un papel muy importante en numerosos circuitos de RF y de microondas [1–7]. Como elementos de circuito han sido ampliamente utilizadas en baluns, acopladores direccionales, desfasadores, transformadores de impedancias, para el rechazo de continua (DC blocks), como condensadores interdigitales, filtros e inductores en espiral. En tecnología microstrip suele utilizarse el acoplamiento entre líneas paralelas situadas en un mismo plano, lo que se conoce como acoplamiento lateral (*edge-coupled lines*). Sin embargo, esta configuración no es adecuada para conseguir valores altos de acoplamiento, pues implica utilizar un espaciado entre líneas muy pequeño, de forma que puede ser no realizable físicamente. Así pues, estas estructuras están pensadas para conseguir valores de acoplamiento por debajo de 8 o 10 dB. Por el contrario, para niveles de acoplamiento superiores, de hasta 2 y 3 dB, existen otras alternativas como configuraciones multicapa, acopladores Lange o acopladores conectados en tándem [2].

El uso de líneas acopladas para el diseño tanto de acopladores direccionales como de filtros es posiblemente una de las aplicaciones más populares [8, 9]. El primer acoplador direccional, utilizando dos líneas de longitud $\lambda/4$, suele atribuirse a H. A. Affel de la compañía A.T.T., quien depositó la patente en el año 1922 [8]. Durante los años 1940 y 1950 el trabajo presentado por Affel fue mejorado [10, 11], y ya en los los años 1960 y 1970 [12–18], son numerosos las artículos que describen la teoría de diseño así como las múltiples aplicaciones de las líneas acopladas. Respecto al diseño de filtros con líneas acopladas, los más extendidos

son los basados en secciones de líneas paralelas acopladas entre sí [11], los filtros interdigitales [12, 15], los filtros *combline* [19] y los filtros tipo *hairpin* [20, 21].

La configuración utilizando líneas paralelas acopladas resulta interesante para diseñar filtros paso banda de gran ancho de banda con una selectividad moderada, donde tanto la selectividad como el ancho de banda pueden incrementarse aumentando el número de secciones. El diseño de este tipo de filtros ha sido ampliamente documentado y existen fórmulas aproximadas de diseño en función de las prestaciones a conseguir [1, 11]. Estas expresiones permiten el diseño de un filtro donde el número de polos en la banda es proporcional al número de etapas (n polos para n+1 etapas). Sin embargo, para deducir estas ecuaciones, cada etapa se modela por dos tramos de líneas de transmisión unidas por un inversor de impedancia [1]. El problema de esta aproximación es que se asume que el inversor no varía con la frecuencia, por lo que la aproximación es sólo exacta a la frecuencia central de diseño. Por este motivo, la teoría clásica de diseño de filtros está pensada para anchos de banda pequeños o moderados, donde la precisión conseguida está directamente relacionada con el ancho de banda deseado.

En los útlimos años, dado que la teoría clásica de diseño de filtros se fundamenta en el uso de inversores de impedancia/admitancia y por lo tanto, en una hipótesis de banda estrecha, diferentes técnicas para el diseño de filtros de banda muy ancha (*ultra-wideband*) han sido propuestas. Una de estas propuestas hace uso de resonadores multi-modo (*multiple-mode resonator* MMR), que se caracterizan por su reducido tamaño y buenas prestaciones. En general, ya sea mediante el uso de resonadores basados en saltos de impedancia (*stepped-impedance resonator*, SIR) o configuraciones con líneas de transmisión $\lambda/4$ o $\lambda/2$ en paralelo (*stub-loaded resonator*, SLR), el objetivo de estas estructuras consiste en generar múltiples modos resonantes (polos de transmisión o ceros de reflexión) dentro de la banda de paso para conseguir que la respuesta en frecuencia sea lo más plana posible. Muchas de las arquitecturas basadas en MMR combinan el uso de estructuras de líneas acopladas a la entrada y salida, con diferentes arquitecturas resonantes [22]. Sin embargo, el principal problema que plantea esta solución es la falta de una metodología de diseño y normalmente sus diseños están regidos por procedimientos de optimización llevados a cabo en simuladores electromagnéticos. Además, en estas topologías el ancho de banda conseguido está directamente relacionado con el valor de acoplamiento de las estructuras acopladas de entrada y salida.

Desfasadores de tipo reflexivo basadas en líneas acopladas hacen uso de un acoplador direccional de 3 dB y dos cargas, teóricamente iguales, que son puramente reactivas. Cuando la potencia se divide por igual entre los puertos directo y acoplado, es posible conseguir una adaptación perfecta, tanto a la entrada como a la salida, con pérdidas de inserción nulas. En este sistema, el desfase relativo de la señal de salida se controla directamente con el coeficiente de reflexión de las cargas conectadas a los puertos directo y acoplado, mientras el ancho de banda depende del acoplador y de las cargas usadas [5]. Así pues, para esta aplicación es necesario usar acopladores que permitan alcanzar un valor de acoplamiento de 3 dB.

Las líneas acopladas son también utilizadas para diseñar baluns. Un balun es un dispositivo utilizado para convertir una señal de entrada no balanceada en una señal de salida balanceada diferencial. Diferentes configuraciones han sido propuestas, pero entre los baluns usando líneas acopladas, el balun de Marchand es el más popular [2, 23]. El balun de Marchand está formado por dos secciones de líneas acopladas de longitd $\lambda/4$, y para conseguir aumentar el ancho de banda se requiere de un valor de acoplamiento alto. Sin embargo, las principales limitaciones de este balun son su pobre adaptación de salida y el mal aislamiento entre los dos puertos de salida [24].

En general, todos los circuitos que se han comentado requiren de un alto factor de acoplamiento para aumentar el ancho de banda de funcionamiento. Conseguir esos valores usando líneas paralelas con acoplamiento lateral es posible si se conectan múltiples líneas con una configuración interdigitada. Una implementación de esta idea es el acoplador Lange [25], que consiste en un acoplador con tres o más líneas done las líneas alternas se conectan entre sí. Otras alternativas para conseguir niveles altos de acoplamiento son el uso de estructuras multicapa, pero son complicadas de realizar en sustratos cerámicos o monolíticos, así como estructuras en tandem o acopladores *branch-line*, los cuales tienen un ancho de banda estrecho.

El acoplador Lange es un acoplador direccional con múltiples conductores que permite incrementar la capacidad mutua entre líneas sin la necesidad de utilizar un espacio entre las mismas demasiado pequeño. Lógicamente, al incrementar dicha capacidad se aumenta de forma directa el factor de acoplamiento [2]. Las ecuaciones de diseño para un acoplador de k líneas, en función de las impedancias del modo par e impar de un par de líneas acopladas, fueron dadas por Ou in [26].

Recientemente, estructuras multiconductoras con líneas alternas conectadas entre sí han sido también utilizadas para mejorar el comportamiento en frecuencia de capacidades interdigitales. El elemento resultante es conocido como *wire-bonded interdigital capacitor* La conexión entre líneas alternas permite eliminar resonancias no deseadas a altas frecuencias, por lo que de forma sencilla se incrementa el margen de frecuencia de funcionamiento [27]. En un acoplador interdigital la longitud eléctrica de las líneas de transmisión es de 90^o a la frecuencia de diseño. Por el contrario, las líneas en una capacidad interdigital son simpre menores para tener un comportamiento capacitivo. Un modelo analítico de este nuevo circuito, válido para un número par de líneas, fue publicado en [28], mientras que un análisis exacto, válido para cualquier número de líneas, fue presentado en [29].

En definitiva, el ámbito de aplicación de las líneas acopladas es grande y en la actualidad siguen apareciendo nuevos circuitos con nuevas funcionalidades que hacen uso de ellas. Así pues, el usar líneas multiconductoras, las cuales permiten conseguir un valor alto de acoplamiento y para las cuales se disponen de expresiones analíticas, va a permitir diseñar nuevos circuitos y posiblemente mejorar las prestaciones de algunos ya existentes.

C.1.2. Motivación y Objetivos

Como se ha descrito en la sección anterior, las estucturas basadas en un par de líneas acopladas han sido ampliamente utilizadas para múltiples aplicaciones. Sin embargo, puesto que existe una relación directa entre el ancho de banda y el nivel de acoplamiento conseguido, el utilizar líneas de transmisión multiconductoras (MTL) parece una solución adecuada para el diseño de dispositivos de gran ancho de banda. Además, gracias al modelado y la caracterización de múltiples líneas acopladas, será posible obtener ecuaciones analíticas de diseño [26, 28, 29].

Así pues, en este trabajo se pretende estudiar las ventajas del uso de líneas multiconductoras en aplicaciones existentes así como diseñar nuevas configuraciones. Además, el principal objetivo será proporcionar una metodología de diseño para cada uno de los circuitos propuestos. Toda la teoría desarrollada durante este proceso será validada de forma experimental.

C.1.3. Estructura de la Tesis

Este trabajo se ha dividido en seis capítulos, en los cuales se ha realizado un estudio de diferentes componentes como desfasadores, baluns para la conversión del modo común al diferencial y filtros paso banda. Todos estos dispositivos están diseñados usando líneas de transmisión multiconductoras.

En el **Capítulo 2**, las líneas de transmisión multiconductoras son investigadas para la síntesis de desfasadores de tipo reflexivo de banda ancha. El análisis llevado a cabo extiende la teoría tradicional donde suele utilizarse un acoplador direccional de 3 dB, demonstrando que con un valor superior de acoplamiento existe la posibilidad de miniaturizar el acoplador. Además, se han obtenido dos circuitos equivalentes considerando que los puertos directo y acoplado de un MTL están en abierto o cortocircuitados a tierra. Toda la teoría desarrollada y presentada en este capítulo será utilizada en los restantes capítulos.

En el **Capítulo 3**, se presenta un nuevo procedimiento de diseño de baluns de banda ancha en tecnología planar usando dos MTLs. Estos baluns son utilizados para convertir una señal de entrada no balanceada en una señal de salida diferencial. Ecuaciones de diseño para tener un balance perfecto tanto de amplitud como de fase a la salida son obtenidas en función del número de conductores y de los modos par e impar de un par de líneas de transmisión acopladas. Además, haciendo uso de este balun, se ha diseñado y fabricado un nuevo sistema reconfigurable, basado en conmutadores MEMS, para la caracterización de dispositvos diferenciales. Este nuevo sistema permite caracterizar dispositivos de cuatro puertos mediande un analizador vectorial de redes de dos puertos.

En el **Capítulo 4**, las estructuras multiconductoras son analizadas como elementos de un solo puerto para su utilización como stubs. Se ha realizado un estudio genérico para las diferentes configuraciones, cortocircuitando a tierra o dejando en abierto tres de los cuatro puertos de un MTL. Este estudio ha permitido determinar las características de cada una de

las ocho configuraciones y por lo tanto su potencial aplicación atendiendo a su respuesta en frecuencia. Para validar las ecuaciones deducidas, se han diseñado, fabricado y medido dos líneas de transmisión artificial con un comportamiento zurdo en la banda de paso.

Una vez que las líneas multiconductoras han sido analizadas tanto como elementos de dos puertos, en los capítulos 2 y 3, como estructuras de un solo puerto en el capítulo 4, los restantes dos capítulos hacen uso de esta teoría para el diseño de filtros paso banda. En el **Capítulo 5** se presenta un procedimiento sistemático de diseño de filtros diferenciales paso banda, de banda muy ancha (*ultra-wideband*). Se han obtenido ecuaciones para el diseño de estos filtros, formados por una o dos secciones de MTLs, para tener una respuesta en frecuencia de tipo Butterworth o Chebyshev. La teoría ha sido verificada diseñando y fabricando varios prototipos.

El **Capítulo 6** se centra en el estudio de filtros paso banda con alta selectividad y con un comportamiento cuasi-elíptico. Se han propuesto y analizado dos configuraciones, una asimétrica y otra simétrica. Ambas topologías permiten implementar filtros paso banda con tres o cinco polos y dos ceros de transmisión. Los resultados experimentales han validado las ecuaciones de diseño obtenidas y han demostrado que las topologías propuestas son adecuadas para sintetizar filtros con pendientes abruptas de rechazo.

Finalmente, el **Capítulo 7** resume los principales resultados y las contribuciones originales derivadas de esta tesis.

C.1.4. Publicaciones

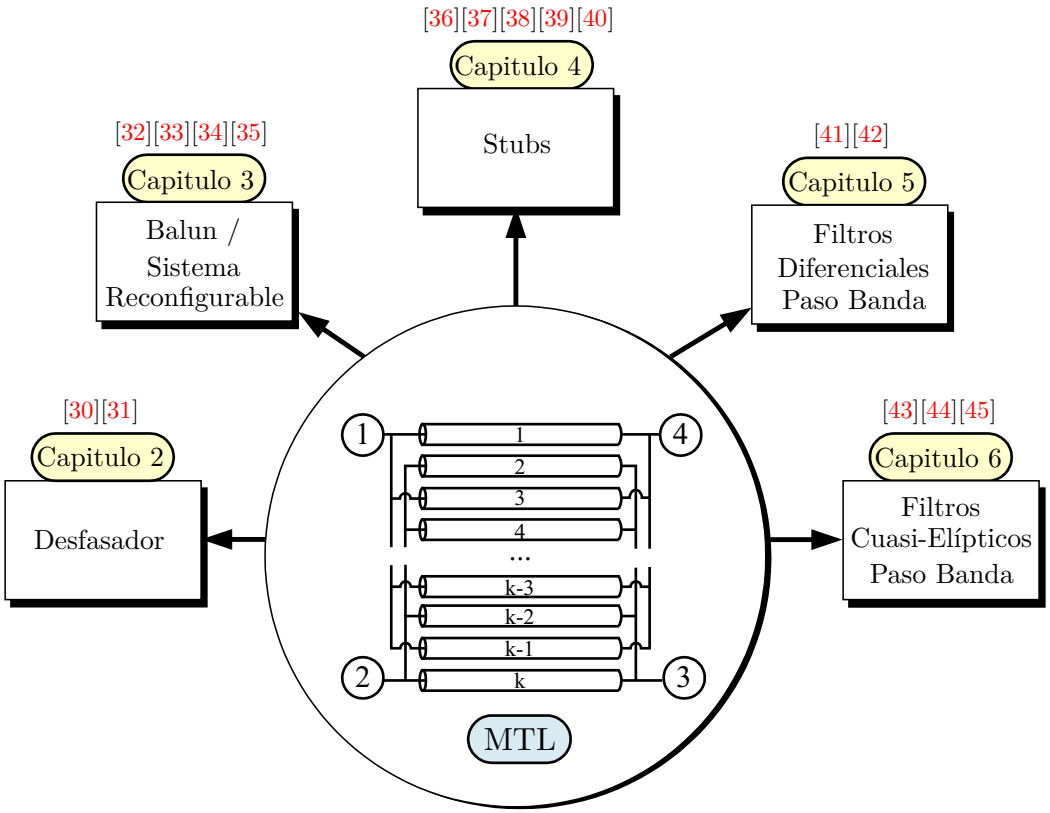

Figure C.1.: Estructura de la tesis y contribuciones derivadas.

Las siguientes publicaciones han sido derivadas de este trabajo de investigación (ver Fig. C.1).

Artículos

- [36] J. J. Sánchez-Martínez, E. Márquez-Segura, P. Otero, and C. Camacho-Peñalosa "Artificial Transmission Line with Left/Right-Handed Behavior Based on Wire Bonded Interdigital Capacitors," *Progr. Electromagn. Res. B*, vol. 11, pp. 245-264, 2009.
- [30] J. J. Sánchez-Martínez and E. Márquez-Segura, "Analytical Study of Wide-band Bandpass Filters Based on Wire-Bonded Multiconductor Transmission Lines With LH Behaviour,"*Progr. Electromagn. Res. Lett.*, vol. 31, pp. 1-13, 2012.
- [37] J. J. Sánchez-Martínez and E. Márquez-Segura, "Comments on 'Wideband Coupled-Line Microstrip Filters With High-Impedance Short-Circuited Stubs'," *IEEE Microw. Wireless Compon. Lett.*, vol. 22, no. 9, p. 492, Sep. 2012.
- [32] J. J. Sánchez-Martínez and E. Márquez-Segura, "Generalized analytical design of broadband planar baluns based on wire-bonded multiconductor transmission lines," *Progr. Electromagn. Res.*, vol. 134, pp. 169-187, 2013.

- [38] J. J. Sánchez-Martínez, E. Márquez-Segura, and C. Camacho-Peñalosa, "Analysis of wire-bonded multiconductor transmission-line-based stubs," *IEEE Trans. Microw. Theory Tech.*, vol. 61, no. 4, pp. 1467-1476, Apr. 2013.
- [31] J. J. Sánchez-Martínez and E. Márquez-Segura, "Analysis of wire-bonded multiconductor transmission line-based phase-shifting sections," *J. Electromagn. Waves Appl.*, vol. 27, no. 16, pp. 1997-2009, Sep. 2013.
- [43] J. J. Sánchez-Martínez, E. Márquez-Segura and S. Lucyszyn, "Design of Compact Wideband Bandpass Filters Based on Multiconductor Transmission Lines With Interconnected Alternate Lines," *IEEE Microw. Wireless Compon. Lett.*, vol. 24, no. 7, pp. 454-456, Jul. 2014.
- [41] J. J. Sánchez-Martínez and E. Márquez-Segura, "Analytical Design of Wire-Bonded Multiconductor Transmission Line-Based Ultra-Wideband Differential Bandpass Filters," Accepted to be published in *IEEE Trans. Microw. Theory Tech.*, Jun. 2014.
- [44] J. J. Sánchez-Martínez, E. Márquez-Segura and S. Lucyszyn, "Synthesis and Design of High-Selectivity Wideband Quasi-elliptic Bandpass Filters Using Multiconductor Transmission Lines," Submitted to *IEEE Trans. Microw. Theory Tech.*, Apr. 2014.

Conferencias Internacionales

- [39] J. J. Sánchez-Martínez, E. Márquez-Segura, and C. Camacho-Peñalosa, "Analysis of Composite Left/Right-Handed Transmission Line Using Shunt Wire Bonded Interdigital Capacitors," in *4th Young Scientist Meeting on Metamaterials (YSMM)*, Feb. 2011, ISBN: 978-84-693-9971-2.
- [40] J. J. Sánchez-Martínez, E. Márquez-Segura, and C. Camacho-Peñalosa,"Synthesis of CRLH-TLs Based on a Shunt Coupled-line Section," in *42nd European Microwave Conference (EuMC)*, Oct. 2012, pp. 675-678.
- [33] S. Cobos-Bandera, J. J. Sánchez-Martínez, and E. Márquez-Segura, "Mems-based reconfigurable test-set for differential and common mode measurement using a two-port network analyzer," in *42nd European Microwave Conference (EuMC)*, Oct. 2012.

Conferencias Nacionales

- [34] S. Cobos-Bandera, J. J. Sánchez-Martínez, and E. Márquez-Segura, "Sistema de Medida Reconfigurable para la Caracterización de Dispositivos Diferenciales de Microondas," in *XXVII Simposium Nacional de la Unión Científica Internacional de Radio (URSI)*, Sep. 2012, ISBN: 978-84-695-4326-9.

- [35] J. J. Sánchez-Martínez and E. Márquez-Segura, "Análisis de un Balun Basado en Líneas de Transmisión Multiconductoras," in *XXVII Simposium Nacional de la Unión Científica Internacional de Radio (URSI)*, Sep. 2012, ISBN: 978-84-695-4326-9.
- [45] J. J. Sánchez-Martínez and E. Márquez-Segura, "Análisis y Diseño de Filtros Paso Banda con Alta Selectividad Espectral Basados en Líneas de Transmisión Multiconductoras," in *XXVIII Simposium Nacional de la Unión Científica Internacional de Radio (URSI)*, Sep. 2013, ISBN: 978-84-941537-1-6.
- [42] J. J. Sánchez-Martínez and E. Márquez-Segura, "Análisis y Diseño de Filtros Diferenciales Basados en Líneas Acopladas," Accepted in *XXIX Simposium Nacional de la Unión Científica Internacional de Radio (URSI)*, Sep. 2014.

C.2. Desfasadores de Tipo Reflexivo

Las estructuras desfasadoras son dispositivos clave en numerosos circuitos de microondas, como moduladores, baluns, conversores de frecuencia, matrices de elementos desfasadores para conformación de haz (*beamforming*), así como para sistemas de medida. Existen diferentes tipos de desfasadores, de entre los cuales el tipo reflexivo [5, 46] es uno de los más comunes. Un desfasador de tipo reflexivo utiliza un acoplador de longitud $\lambda/4$ con un factor de acoplamiento de 3 dB, colocando en los puertos directo y acoplado dos cargas puramente reactivas. Obviamente, los elementos desfasadores juegan un papel crucial para el diseño de baluns, de dispositivos que permitan convertir una señal de entrada no balanceada en una señal de salida balanceada diferencial. Esta aplicación tiene gran importancia para nuevos sistemas de comunicaciones donde el uso de señales diferenciales cada vez es más común. El usar señales diferenciales proporciona una mayor inmunidad al ruido externo, un mayor rango dinámico y permite minimizar la distorsión de los armónicos pares. Consecuentemente, cada vez es más habitual encontrar un balun a la entrada de los receptores para convertir una entrada *single-ended* en una señal diferencial. Por este motivo, el análisis teórico sobre los desfasadores será particularizado en el siguiente capítulo para la síntesis de baluns de banda ancha.

C.2.1. Analisis y Principio de Funcionamiento

Una línea de transmisión multiconductora (MTL) es un dispositivo de cuatro puertos, donde debido al acoplo entre los distintos modos que se propagan pueden aparecer frecuencias de resonancias no deseadas [3]. Para eliminar estas resonancias, en este trabajo los extremos finales de las líneas alternas se conectan entre sí, como se representa en la Fig. 2.1(a) [27]. Este dispositivo se denomina *wire-bonded* MTL. Sin embargo, para evitar tener que repetir de forma continuada el término *wire-bonded*, siempre que hablemos de MTL o línea multiconductora hay que tener presente que los conductores alternos están conectados entre sí.

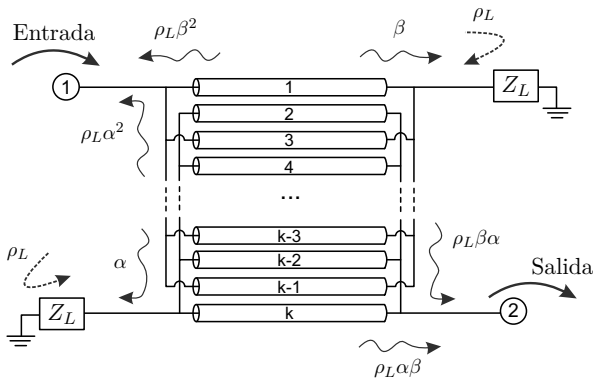

Figure C.2.: Señales transmitidas y reflejadas dentro de un MTL, diseñado según (C.1), cuando los puertos acoplado y directo son terminados con dos cargas puramente reactivas.

Esta configuración de línea multiconductora permite incrementar el ancho de banda de operación, al eliminar las resonancias no deseadas, pero además permite obtener modelos analíticos simplificados. Si la longitud eléctrica de las conexiones entre líneas alternas es despreciable (mucho menor que la longitud de onda), el modelo de un MTL puede simplificarse a un par de líneas acopladas [2, 47].

Asumiendo un sistema sin pérdidas, que el acoplamiento entre líneas no adyacentes es despreciable y que existe una propagación TEM, la matriz de parámetros admitancia de un MTL fue derivada en [26]. Esta matriz de parámetros admitancia depende del número de conductores (k) así como de las admitancias del modo par e impar de un par de líneas acopladas (2.1). Considerando que los cuatro puertos de un MTL son cargados con una impedancia característica Z_0 [26, 48] de valor

$$Z_0 = \frac{1}{\sqrt{M^2 - N^2}}, \tag{C.1}$$

los parámetros S de la estructura (Figure 2.1(a)) pueden expresarse como

$$[S] = \begin{bmatrix} 0 & 0 & \alpha & \beta \\ 0 & 0 & \beta & \alpha \\ \alpha & \beta & 0 & 0 \\ \beta & \alpha & 0 & 0 \end{bmatrix}, \tag{C.2}$$

donde M y N se definen en (2.2). α y β se calculan fácilmente en función de la longitud eléctrica del MTL (θ) y del factor de acoplamiento c (2.11) en base a las ecuaciones (2.9) y (2.10). De esta forma, el MTL se comporta como un acoplador direccional con sus cuatro puertos perfectamente adaptados y con un aislamiento ideal entre los puertos 1-3 y 2-4. c representa el acoplamiento máximo de la estructura, que sucede para una longitud eléctrica θ=90^o.

Para construir un desfasador, los puertos acoplado y directo se cargan con dos elementos

puramente reactivos (Z_L), como se muestra en la Fig. C.2. Tradicionalmente, siempre se ha utilizado un factor de acoplamiento c=-3 dB [49, 50]. Sin embargo, de forma sencilla puede deducirse que esta condición es únicamente una solución particular. Haciendo uso de (C.2), los parámetros S_{11} y S_{21} de la estructura resultante quedan determinados como

$$S_{11} = |\rho_L| \frac{1 - c^2(1 + \sin^2\theta)}{1 - c^2\cos^2\theta} e^{j(\angle\rho_L + 2\phi)} \tag{C.3a}$$

$$S_{21} = |\rho_L| \frac{2c\sqrt{1-c^2}\sin\theta}{1 - c^2\cos^2\theta} e^{j(\angle\rho_L + 2\phi + \pi/2)} \tag{C.3b}$$

$$\phi = \arctan\left(\frac{-\sin\theta}{\sqrt{1-c^2}\cos\theta}\right), \tag{C.3c}$$

donde ρ_L indica el coeficiente de reflexión en los puertos acoplado y directo (2.12). De estas relaciones se deduce fácilmente que el valor de acoplamiento usado condiciona la adaptación, las pérdidas de inserción y la pendiente de la respuesta en fase. Sin embargo, una vez fijado el valor de c, la fase del parámetro S_{21} (C.3b) depende únicamente de la carga reactiva. Así pues, independientemente del valor de acoplamiento c, si el MTL se diseña teniendo en cuenta la condición (C.1), el desfase relativo entre la entrada y la salida puede controlarse variando las impedancias de carga (Z_L). No obstante, es necesario notar que la adaptación sí está directamente condicionada por el acoplamiento.

Haciendo uso de (C.3a) y (C.3b), puede calcularse la longitud eléctrica de adaptación θ_d en función de c (2.15). Únicamente cuando $c \geq$-3 dB, la estructura desfasadora estará perfectamente adaptada, en una única frecuencia (θ_d=90^o) para c=-3 dB, o en dos frecuencias (θ_d <90^o y $\pi - \theta_d$) cuando c>-3 dB (ver Fig. 2.3(a)). Además, con (2.15), es posible reducir el tamaño del desfasador si en lugar de diseñarse para una longitud eléctrica de 90^o a la frecuencia central de diseño, se diseña con una longitud igual a θ_d con un valor de c superior a -3 dB. Claramente se aprecia la ventaja de usar estructuras multiconductoras, pues el valor mínimo de acoplamiento necesario es -3 dB, algo que resulta complicado de conseguir con dos líneas acopladas.

Usando (2.7), (2.11) y (2.15), las impedancias de los modos par e impar quedan perfectamente determinadas en función del número de conductores y de la frecuencia de adaptación de la estructura (θ_d), sin necesidad de hacer ningún estudio paramétrico como el llevado a cabo en [51]. No obstante, si lo que se busca es maximizar el ancho de banda, debido a la simetría de la respuesta en frecuencia, la longitud eléctrica de diseño debe ser 90^o a la frecuencia central de trabajo (ver Fig. 2.4(a)). Además, operando sobre (C.3a) y (C.3b), se pueden obtener ecuaciones de diseño para determinar en función del ancho de banda, los niveles de acoplamiento que pueden utilizarse (2.18)

C.2.2. Modelos Equivalentes para MTL en Abierto o en Cortocircuito

Una vez caracterizado el MTL con cargas reactivas en los puertos acoplado y directo, resulta sencillo analizar la estructura para dos situaciones particulares, dejando ambos puertos en abierto (Z_L=∞) o cortocircuitados a tierra (Z_L=0). Estas dos configuraciones resultan de gran interés tanto para el diseño de filtros, baluns, transformadores de impedancia, capacidades interdigitales, etc. [1, 2, 47]. Haciendo uso de la matriz de parámetros admitancia (2.1) se pueden calcular dos modelos equivalentes basados en líneas de transmisión para ambas configuraciones (Fig. 2.5). Estos modelos extienden a los ya existentes para dos líneas de transmisión (k=2) [1, 2], y por su simplicidad han sido utilizados para el diseño de filtros paso banda.

C.2.3. Validación Experimental

Para verificar tanto la teoría desarrollada como los dos modelos equivalentes obtenidos, se han diseñado y fabricado dos MTLs con sus puertos diagonales en abierto y en cortocircuito, para tener una adaptación a dos longitudes eléctricas diferentes, para θ_d=90^o y θ_d=65^o. Haciendo uso de las ecuaciones (2.15), (2.7),(2.2) y (2.11), se han calculado de forma sencilla tanto el número de conductores k como las impedancias de los modos par e impar.

La Fig. 2.6 muestra los parámetros S de las estructuras fabricadas. Tanto el ancho de banda coseguido como la respuesta en fase de ambas estructuras valida las ecuaciones de diseño obtenidas.

C.3. Baluns: Conversión del Modo Común al Modo Diferencial

C.3.1. Análisis y Caracterización

Un balun es un dispositivo de tres puertos cuya función reside en convertir una señal de entrada no balanceada en una señal de salida balanceada diferencial. Se han propuesto diferentes topologías en la literatura, pudiendo establecer dos grupos. El primer grupo utiliza un divisor de potencia seguido de una sección desfasadora para conseguir un desfase de 180^o entre los puertos de salida [52–54]. El segundo grupo de baluns se diseñan a partir de estructuras simétricas de cuatro puertos, donde uno de los puertos se deja en abierto, se cortocircuita a tierra o bien se termina con una impedancia concreta [23, 55–68]. Dentro del segundo grupo destaca el balun de Marchand, formado por dos secciones de líneas acopladas de longitud $\lambda/4$. Sin embargo, la mayoría de los baluns publicados o bien son de banda estrecha o bien presentan una mala adaptación de salida con un pésimo aislamiento entre los puertos de salida. Así pues, teniendo en cuenta la teoría descrita en (C.2), se ha propuesto un nuevo balun usando líneas multiconductras para solucionar estos problemas.

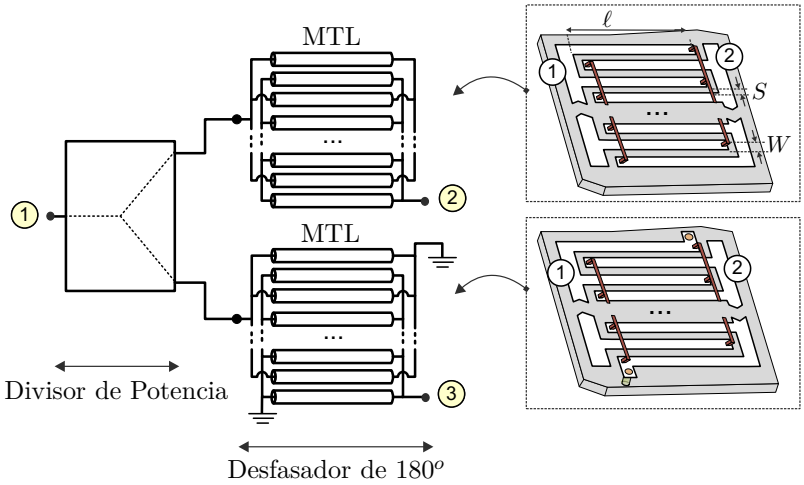

Figure C.3.: Arquitectura del balun propuesto formado por un divisor de potencia y dos líneas multiconductoras.

La Fig. C.3 muestra la arquitectura del balun propuesto, formada por un divisor de potencia y dos líneas multiconductoras con los puertos diagonales en abierto o cortocircuitados a tierra. La primera sección divide la entrada en dos señales de salida de igual fase, mientras que la segunda sección introduce un desfase de -90^o y +90^o para conseguir un desfase entre ambas señales a la salida de 180^o. Como divisor de potencia se emplea un divisor Wilkinson, el cual proporciona una buena adaptación en los tres puertos con un gran aislamiento a la salida. Además, otra de las ventajas de usar un Wilkinson es la posibilidad de aumentar el ancho de banda incrementando el número de secciones.

El diseño de cada una de las estructuras multiconductoras se lleva a cabo a partir de sus parámetros admitancia (3.1), (3.2), calculando dos ecuaciones sencillas de diseño (3.10) y (3.11). La primera ecuación (3.10) especifica la condición necesaria para que ambos MTL se comporten de forma dual, es decir, con parámetros de transmisión de igual magnitud pero desfasados 180^o. La segunda ecuación (3.11) determina el valor de acoplamiento en función de la adaptación dentro de la banda de operación. Combinando (3.10) y (3.11), las ecuaciones para calcular las impedancias de los modos par e impar, en función del número de conductores k y de la condición de adaptación (θ_d) pueden expresarse como

$$\frac{Z_{oe}}{Z_0} = \frac{\sqrt{u[(k-1)+u][1+u(k-1)]}}{(1+u)} \tag{C.4a}$$

$$\frac{Z_{oo}}{Z_0} = \frac{\sqrt{[(k-1)+u][1+u(k-1)]}}{\sqrt{u}(1+u)} \tag{C.4b}$$

$$u = \frac{1+\sqrt{(1+(k-1)^2\sin^2\theta_d}}{(k-1)\left(\sqrt{1+\sin^2\theta_d}-1\right)}. \tag{C.4c}$$

La Fig. 3.4 muestra el módulo de los parámetros S_{11} y S_{21} de dos estructuras MTL con los puertos diagonales en abierto o en cortocircuito diseñadas mediante (C.4). Se observa que las estructuras presentan la misma respuesta en magnitud y que pueden diseñarse para tener uno o dos máximos de adaptación. Sin embargo, para observar el comportamiento dual, la Fig. 3.5 representa los parámetros S_{11} y S_{21} sobre una carta de Smith. En este caso, la diferencia de fase de 180^o se hace claramente visible.

Para validar la teoría desarrollada se ha diseñado y fabricado un balun de banda ancha. Para este cometido se utiliza un divisor Wilkinson de tres etapas [69], de forma que el ancho de banda de las líneas multiconductoras no sea limitado por el ancho de banda del propio divisor. Los MTL se han diseñado para conseguir una adaptación θ_d=63^o (Table 3.2). Una fotografía del balun fabricado se muestra en la Fig. 3.9, donde tanto el divisor Wilkinson como las estructuras multiconductoras son claramente visibles. La Fig. 3.10 representa las pérdidas de inserción y de retorno, el aislamiento y el balance tanto de amplitud como de fase de las señales de salida. Las pérdidas de retorno y el aislamiento son superiores a 10 dB y 18 dB, respectivamente, en el rango [1-6] GHz (142 %). Además, se consigue un balance de amplitud y de fase de 0.4 dB y 5 grados, aproximadamente, entre 1.64 GHz y 5.36 GHz (106 %). Así pues, se demuestra que haciendo uso de las ecuaciones de diseño se puede obtener de forma sencilla un balun de banda ancha con unas muy buenas prestaciones.

Como una forma de integrar el desbalance de amplitud y de fase en un único parámetro, se determina el rechazo al modo común (*common-mode-rejection ratio*, CMRR), el cual se calcula como

$$CMRR = \frac{S_{ds21}}{S_{cs21}} = \frac{S_{21} - S_{31}}{S_{21} + S_{31}}, \tag{C.5}$$

donde S_{ds21} y S_{cs21} identifican la respuesta del modo diferencial y del modo común para una señal de entrada (*single-ended*). Los valores medidos de CMRR, S_{ds21} y S_{cs21} se muestran en la Fig. 3.11. Se ha conseguido un valor de CMRR superior a 30 dB dentro de la banda [1.52-5.25] GHz. Además, el CMRR alcanza sus valores máximos en torno a las frecuencias de diseño de adaptación, 2.2 GHz (θ_d) and 4.8 GHz (180^o-θ_d), aproximadamente.

Finalmente, la Tabla 3.3 muestra una comparativa entre el balun fabricado y otros baluns encontrados en la literatura. Atendiendo a los resultados, resulta sencillo intuir que el balun propuesto con líneas multiconductoras es una muy buena solución para diseñar baluns de banda ancha (>100%), con excelente aislamiento (>20 dB) y adaptación (>15 dB). Además, el buen balance de amplitud (<0.6 dB) y de fase (<5^o) garantiza un gran rechazo al modo común [70]. Notar que los baluns publicados con buen aislamiento son de banda estrecha o moderada (<64%), mientras que aquellos con un mayor ancho de banda no consideran este parámetro. Sin embargo, para determinadas aplicaciones, como sistemas de medida, el aislamiento entre los puertos de salida es tan importante como el desbalance de fase o de amplitud.

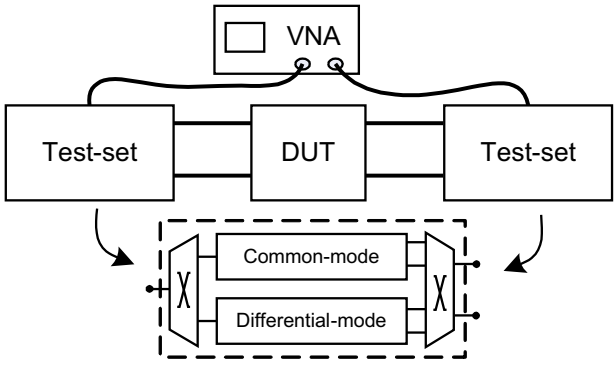

Figure C.4.: Esquema de medida de un dispositivo diferencial bajo prueba (DUT).

C.3.2. Sistema de Medida Reconfigurable Para Dispositivos Diferenciales

El uso de dispositivos diferenciales de microondas es cada día más popular. Muchos sistemas de comunicaciones, con diseños de baja potencia, utilizan señales diferenciales para reducir los efectos indeseados del ruido externo. Además, los circuitos diferenciales incrementan el rechazo a la interferencia electromagnética y el margen dinámico lineal. Por contra, tienen mayor complejidad circuital y su medida puede resultar especialmente difícil y cara.

La teoría de parámetros S se extendió a dispositivos diferenciales en [70, 71] y existen técnicas de medida basadas en analizadores de redes vectoriales (VNA) de cuatro puertos [72], que realizan una conversión de los parámetros S estándares, o el conocido como *pure-mode* VNA [73] que permite realizar una medida directa. Sin embargo, el instrumento de medida más extendido en la actualidad es el VNA de dos puertos, destinado a la medida de dispositivos estándares de dos puertos. En esta situación puede aplicarse una técnica de medida basada en divisores/combinadores de potencia y baluns para obtener, respectivamente, el modo común y diferencial [74–76]. No obstante, se necesitan múltiples conexiones para conseguir una caracterización completa, lo cual afecta gravemente a la repetibilidad de las medidas.

Así pues, en este trabajo se presenta una nueva matriz de conmutación basada en conmutadores MEMS que permite realizar la medida de los parámetros S diferenciales, tanto en modo común como en modo diferencial, utilizando para ello un VNA comercial de dos puertos (Fig. 3.12). Utilizando la matriz de conmutación propuesta como *test set* se pueden medir los parámetros S diferenciales de manera directa, en la banda de interés, sin la necesidad de un VNA de alta gama como un *pure-mode* VNA. La principal ventaja de este sistema es el uso de conmutadores MEMS para conseguir reconfigurabilidad, permitiendo la obtención de los parámetros S para los modos común y diferencial sin realizar más de una conexión.

El esquema de medida de un dispositivo diferencial bajo prueba (DUT) usando el sistema propuesto se muestra en la Fig. C.4. La matriz de conmutación o *test set* se utiliza junto con un VNA de dos puertos para generar los modos común y diferencial en un extremo del

DUT y para combinarlos en el otro plano de referencia. Así pues, el *test set* actúa como un divisor/combinador [75]. Gracias a esta configuración se pueden medir las cuatro submatrices necesarias para calcular los parámetros S del modo mixto [70]. No obstante, es necesario aplicar a cada una de las medidas un algoritmo de *de-embedding* para corregir y eliminar todos los errores introducidos por el sistema de medida.

La Fig. 3.13 representa el diagrama de bloques de la matriz de conmutación propuesta. Se aprecian dos caminos independientes para generar el modo común y el modo diferencial. Para la generación del modo común se utiliza un divisor Wilkinson, mientras para el modo diferencial se utiliza el balun diseñado en la Sección C.3.1. Además, se incluyen tres conmutadores basados en tecnología MEMS [77], que serán los encargados de conmutar entre los caminos del modo común y del modo diferencial.

La matriz de conmutación se caracteriza utilizando los parámetros S del modo mixto, medidos en sus dos posibles configuraciones: cuando se activa el camino del divisor Wilkinson (modo común) o cuando se activa el camino del balun (modo diferencial). Esto da lugar a dos matrices de parámetros S, que serán utilizadas en el proceso de *de-embedding*. La Fig. 3.15(a) y la Fig. 3.15(b) representan el balance de amplitud y de fase para la generación de los modos común y diferencial. Los valores medidos son inferiores a 6^o y 0.2 dB para el modo común, y 6^o y 0.6 dB para el camino diferencial, en la banda comprendida entre 1.5 GHz y 5.5 GHz. Estos desbalances dan lugar a valores de rechazo del modo diferencial (DMRR) y del modo común (CMRR) (ver Fig. 3.15(c)) superiores a 25 dB en un ancho de banda relativo del 100% aproximadamente. Estos valores, unidos a los parámetros de adaptación (>15 dB) (Fig. 3.16), indican que la matriz de conmutación propuesta constituye una solución adecuada para la medida de dispositivos diferenciales. Una fotografía del *test set* fabricado se muestra en la Fig. 3.18.

Finalmente, el *test set* se ha utilizado para medir un dispositivo diferencial conocido, aplicando para ello una técnica de *de-embedding*. Los parámetros teóricos (conocidos a priori), los medidos (con el efecto del *test set*) y los calculados tras aplicar el *de-embedding* se muestran en la Fig. 3.20. Se observa que los parámetros obtenidos tras aplicar el algoritmo de *de-embedding* son muy parecidos a los teóricos, lo que permite verificar que el *test set* fabricado proporciona la calidad necesaria para caracterizar circuitos diferencias usando un VNA de dos puertos.

C.4. Dispositivos de un Puerto

C.4.1. Análisis y Caracterización

Las estructuras multiconductoras pueden también utilizarse como elementos de un sólo puerto (stubs) para mejorar las limitaciones en cuanto a niveles de impedancia y de respuesta en

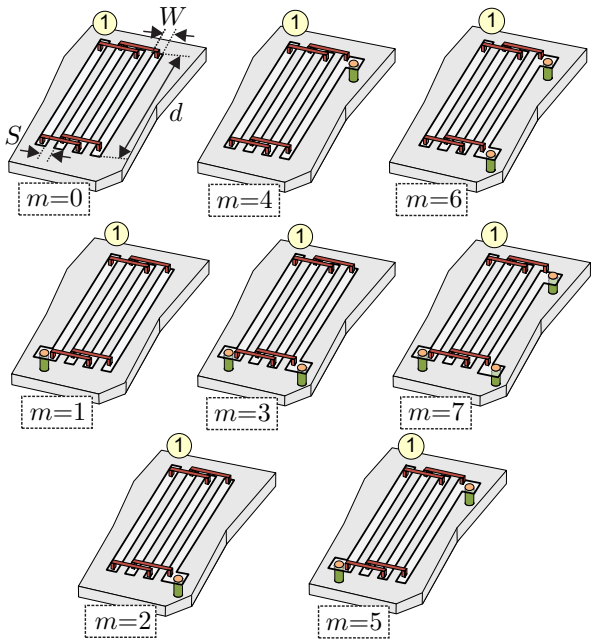

Figure C.5.: Dispositivos de un puerto obtenidos tras colocar un cortocircuito o un circuito abierto en tres de los cuatro puertos de un MTL.

frecuencia de simples líneas de transmisión. En muchas aplicaciones, como filtros, las admitancias en paralelo se implementan mediante stubs. Recientemente, en [78–80] se han propuesto algunas implementaciones alternativas basadas en líneas acopladas. En [78] y [80], estructuras con dos y tres líneas acopladas son usadas como stubs paralelos para diseñar filtros paso banda y de doble banda, mientras en [79] se propone el uso de líneas acopladas para implementar stubs en cortocircuito de alta impedancia. En esta tésis, no sólo se analizan las ocho posibles configuraciones de stub, generalizando el estudio para cualquier número de conductores, sino que además se demuestra que la estructura propuesta en [79] no es apropiada para sintetizar stubs de alta impedancia.

Una línea de transmisión multiconductora tiene cuatro puertos, por lo que considerando uno de ellos como puerto de entrada, las ocho configuraciones posibles de stubs se obtienen cortocircuitando o dejando en circuito abierto los restantes tres puertos. Estas configuraciones, etiquetadas desde m=0 hasta m=7, se representan en la Fig. C.5. La Tabla 4.1 contiene las admitancias de entrada para cada una de las configuraciones, pudiendo deducir que las configuraciones m=0,4,6 y m=1,3,7, son equivalentes a un simple stub, en cierto abierto o en cortocircuito, respectivamente. Por el contrario, las configuraciones m=2 y m=5 presentan un comportamiento en frecuencia particular que no puede asociarse con un simple stub.

Para las configuraciones m=0,4,6 y m=1,3,7, la impedancia equivalente de un simple stub

puede calcularse como

$$Z_{c,m=0,1,3} = Z_{oe}\,\frac{2(1+u)}{2u+(k-1)(1+u^2)}\,\frac{1}{1-c^2} \tag{C.6a}$$

$$Z_{c,m=4,6,7} = Z_{oe}\,\frac{2(1+u)}{2u+(k-1)(1+u^2)}, \tag{C.6b}$$

siendo c el coeficiente de acoplamiento (4.5) y $u{=}Z_{oe}/Z_{oo}$. La Fig. 4.4(a) representa la variación de la impedancia equivalente en función de las dimensiones y del número de conductores de un MTL. Se observa que todas las configuraciones tienen una impedancia caracterísica inferior a la presentada por una simple línea, pudiendo además reducirse incrementando el valor de acoplamiento. En particular, las configuraciones m=4,6,7 son las que menor valor de impedancia equivalente poseen. Así pues, variando el factor de acoplamiento y el número de conductores es posible sintetizar valores bajos de impedancia que serían complicados de conseguir con una simple línea. La configuración de líneas acopladas propuesta en [79] para implementar stubs de alta impedancia coresponde a la configuración m=7. Así pues, con el estudio llevado a cabo se demuestra que la teoría presentada en [79] es incorrecta.

El comportamiento en frecuencia para m=2 y m=5 es diferente porque para estas configuraciones la posición de los zeros de la admitancia de entrada puede ajustarse con el factor de acoplamiento (Fig. 4.5). Operando sobre la impedancia/admitancia de entrada (4.6), se demuestra que ambas estructuras son equivalentes a dos stubs en circuito abierto y en cortocircuito, conectados en serie para m=2 y en paralelo para m=5 (Fig. 4.6). Atendiento a la distribución de los polos, la configuración m=2 puede utilizarse como elemento resonante para introducir dos ceros de transmisión y aumentar la selectividad de un filtro paso banda. La separación de estos ceros es proporcional al valor de acoplamiento. Por el contrario, la configuración m=5 es más apropiada para diseñar filtros de doble banda, donde el ancho de banda dependerá del valor de la impedancia equivalente [1, 47]. En este sentido, al poder sintetizar valores de impedancia menores a los conseguidas con un simple stub, podrán diseñarse filtros con un mayor ancho de banda. Este hecho fue comprobado en [80] utilizando únicamente dos conductores.

Como ejemplo experimental de las configuraciones analizadas, se ha diseñado, fabricado y medido una línea de transmisión artificial con un comportamiento zurdo [81–83]. Para este cometido se ha utilizado la configuración m=4, la cual es equivalente a un stub de baja impedancia terminado en circuitado abierto. La Fig. 4.12 y la Fig. 4.13 representan los parámetros medidos, simulados y teóricos para los dos prototipos fabricados con k=2 y k=4. En ambos casos existe un gran parecido entre los resultados teóricos y medidos, con unas pérdidas de retorno superiores a 20 dB a la frecuencia de diseño. Además, al incrementar el número de conductores y reducir la impedancia equivalente, se mejora el rechazo fuera de banda. De esta forma, se ha verificado el comportamiento teórico y se ha diseñado una línea de transmisión con únicamente una banda zurda.

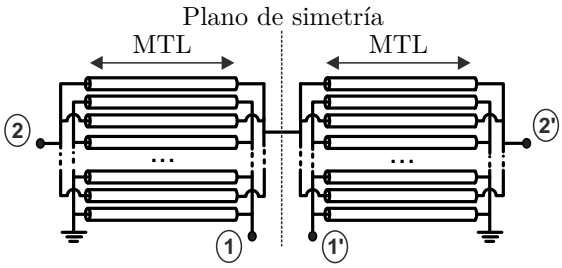

Figure C.6.: Circuito equivalente mediante líneas de transmisión del filtro diferencial propuesto de una sola etapa.

C.5. Filtros Diferenciales Paso Banda de Banda Ancha

C.5.1. Análisis y Caracterización

El uso de filtros diferenciales es crucial en circuitos balanceados donde se requiere de un gran rechazo al modo común. Diferentes arquitecturas se han propuesto [84–91], pero la mayoría son de banda estrecha/moderada (<50%) y carecen de un procedimiento de diseño para obtener una respuesta en frecuencia deseada. Así pues, en este trabajo se propone un filtro diferencial de banda ancha basado en líneas de transmisión multiconductoras. La topología del filtro propuesto se muestra en la Fig. C.6 para un filtro de una sola etapa. Conectando más MTLs en serie se incremenenta el número de etapas y por lo tanto puede mejorarse la selectividad. Sin embargo, esto supone aumentar el tamaño de la estructura. Por este motivo únicamente se han considerado el diseño de filtros diferenciales de una y de dos etapas.

La estructura presenta una configuración simétrica y por lo tanto, el análisis de la misma puede llevarse a cabo mediante una excitación par e impar. De esta forma, el estudio completo del filtro se simplifica al análisis de la mitad del circuito estableciendo un cortocircuito (Fig. 5.1(b)) o un circuito abierto (Fig. 5.1(c)) en el plano de simetría. Este procedimiento de análisis permite además obtener de forma directa la respuesta del filtro a una entrada diferencial (excitación impar) o común (excitación par). Las estructuras que resultan tras aplicar una excitación par e impar, junto con sus circuitos equivalentes mediante líneas de transmisión, se representan en la Fig. 5.1. Estos circuitos equivalentes permiten de una forma sencilla predecir el comportamiento del filtro. De forma teórica, la topología propuesta presenta un rechazo infinito al modo común para todas las frecuencias, pues los puertos de entrada y salida están aislados, mientras posee un comportamiento paso banda para el modo diferencial.

Por consiguiente, para el diseño del filtro basta con analizar la estructura que resulta de la excitación impar. Haciendo uso de su matriz de parámetros admitancia (5.1a), los parámetros S diferenciales para una y dos etapas pueden expresarse como

- Una etapa:

$$|S_{dd_{21}}|^2 = \frac{1}{1+F_I^2}, \qquad |S_{dd_{11}}|^2 = \frac{F_I^2}{1+F_I^2} \tag{C.7a}$$

$$F_I = \frac{1-c^2\bar{Z}_{0_c}^2}{2c^2\bar{Z}_{0_c}}\left(\cos^2\theta + \frac{c^2(\bar{Z}_{0_c}^2-1)}{1-c^2\bar{Z}_{0_c}^2}\right)\frac{1}{\sin\theta} \tag{C.7b}$$

- Dos etapas:

$$|S_{dd_{21}}|^2 = \frac{1}{1+F_{II}^2}, \qquad |S_{dd_{11}}|^2 = \frac{F_{II}^2}{1-F_{II}^2} \tag{C.8a}$$

$$F_{II} = \frac{1-c^2\bar{Z}_{0_c}^2}{c^3\bar{Z}_{0_c}}\cos\theta\left(\cos^2\theta + \frac{c^2(\bar{Z}_{0_c}^2-1)}{1-c^2\overline{Z}_{0_c}^2}\right)\frac{1}{\sin\theta}. \tag{C.8b}$$

$\bar{Z}_{0_c}$ representa la impedancia Z_{0_c} (5.3) de una estructura MTL con sus puertos diagonales cortocircuitaos a tierra, normalizada por la impedancia de referencia Z_0. F_I y F_{II} son polinomios de segundo y de tercer orden que determinan las propiedades de filtrado de la estructura. Comparando F_I y F_{II} con polinomos de Chebyshev o Butterworth, se han obtenido ecuaciones de diseño (5.16a), (5.16b), (5.20), (5.21), que permiten calcular el valor de $\bar{Z}_{0_c}$ y c para tener una respuesta en frecuencia concreta de tipo Butterworth o Chebyshev. Una vez que estos valores son conocidos, las impedancias de los modos par e impar se calculan como

$$Z_{oe} = \frac{k-1}{2}Z_c(R-1), \quad Z_{oo} = \frac{Z_{oe}}{R} \tag{C.9a}$$

$$R = \frac{c+\sqrt{(k-1)^2(1-c^2)+c^2}}{(k-1)(1-c)}. \tag{C.9b}$$

Finalmente, dos prototipos de filtro diferencial, de una y dos secciones, son diseñados y fabricados. Ambos se diseñan para tener un comportamiento Chebyshev, por lo que se require un valor de Z_{0_c} <50 Ω. Esta condición obliga, segun los resultados mostrados en la Fig. 5.8, a utilizar k=6. De esta forma se pone de manifiesto la importancia de usar estructuras multiconductoras. Las fotografías de estos filtros se muestran en la Fig. 5.9(a) y Fig. 5.9(b).

Los parámetros S diferenciales ($S_{dd_{11}}$,$S_{dd_{21}}$) así como la respuesta al modo común ($S_{cc_{21}}$) medidos y analíticos de los filtros fabricados se muestran en la Fig. 5.9. Como se observa, existe una buena concordancia entre la teoría presentada y los resultados finalmente conseguidos. Los filtros fabricados poseen pérdidas de inserción inferiores a 1 dB, presentan un buen rechazo al modo común con un nivel superior a 20 dB en toda la banda y un retardo de grupo inferior a 0.4 ns. Los anchos de banda relativos a 3 dB son de 145% y 97%, para una y dos secciones, respectivamente.

Cabe destacar que los filtros se han diseñado acorde a las dimensiones teóricas calculadas

y no han sido optimizados en ningún simulador electromagnético. Sin embargo, puede apreciarse que aunque existe un excelente parecido entre los parámetros de transmisión medidos y teóricos, ciertas discrepancias aparecen en los parámetros de reflexión. Este comportamiento indica que las ecuaciones obtenidas permiten calcular las dimensiones de los MTL a utilizar, pero atendiendo a la implementación física de estos filtros, sería necesario optimizar las transiciones usadas en los puertos de entrada.

C.6. Filtros Paso Banda Cuasi-Elípticos

C.6.1. Análisis y Caracterización

El diseño de filtros con una alta selectividad espectral es un tema de especial relevancia para sistemas de comunicaciones donde es necesario tanto conformar la densidad espectral de potencia en el transmisor, como atenuar/eliminar las señales no deseadas y el ruido fuera de la banda de interés. Para conseguir la selectividad en frecuencia diferentes técnicas han sido propuestas para la generación de ceros de transmisión en frecuencias próximas a las frecuencias de corte inferior y superior del filtro. Estas técnicas están basadas fundamentalmente en el uso de acoplo cruzado entre resonadores no adyacentes [1, 92], en el empleo de un acoplamiento directo entre los puertos de entrada y de salida [93] o bien empleando la técnica de extracción de polos [94, 95].

La teoría clásica de diseño de filtros [1, 92], basada en ciertas aproximaciones alrededor de la frecuencia central de diseño, es una herramienta potente para el diseño de filtros de banda estrecha o moderada (<60%). Sin embargo, en los últimos años se ha experimentado un interés creciente en el desarrollo tanto de aplicaciones como de técnicas de transmisión de banda muy ancha, lo que ha supuesto la concepción y el diseño de nuevas arquitecturas de filtros paso banda [92, 96]. De entre estas arquitecturas, las basadas en resonadores multi-modo (*multiple-mode resonator* MMR) han sido ampliamente utilizadas [22] por su reducido tamaño y buenas prestaciones. En general, ya sea mediante el uso de resonadores basados en saltos de impedancia (*stepped-impedance resonator*, SIR) o configuraciones con líneas de transmisión $\lambda/4$ o $\lambda/2$ en paralelo (*stub-loaded resonator*, SLR), el objetivo de estas estructuras consiste en generar múltiples modos resonantes (polos de transmisión o ceros de reflexión) dentro de la banda de paso para conseguir que la respuesta en frecuencia sea lo más plana posible. Muchas de las arquitecturas basadas en MMR combinan el uso de líneas acopladas con diferentes estructuras resonantes [22]. Sin embargo, el principal problema que plantea esta solución es la falta de una metodología de diseño y normalmente sus diseños están regidos por procedimientos de optimización llevados a cabo en simuladores electromagnéticos.

En este trabajo se proponen y analizan dos nuevas topologías, una asimétrica y otra simétrica, formadas exclusivamente por líneas de transmisión multiconductoras para el diseño analítico de filtros paso banda con alta selectividad espectral y gran ancho de banda.

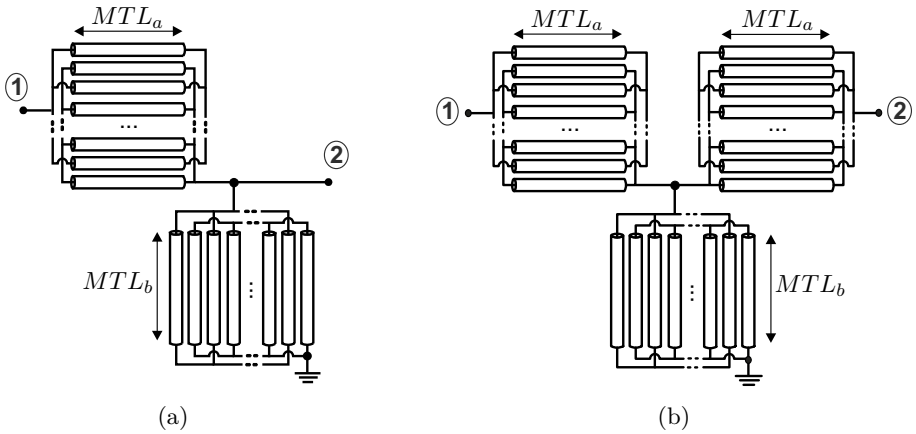

Figure C.7.: Circuitos equivalentes mediante líneas de transmisión de los filtros paso banda propuestos.

La topología asimétrica, más compacta, está formada por un MTL serie y otro paralelo cortocircuitado a tierra, mientras que en la topología simétrica se añade otro MTL serie a la salida. El MTL paralelo corresponde a la configuración m=2 analizada en el capítulo 4. La Fig. C.7 representa ambas topologías utilizando sus circuitos equivalentes mediante líneas de transmisión.

En primer lugar las estructuras multiconductoras serie y paralela han sido analizadas por separado (Secciones 6.2.1 y 6.2.2), obteniéndose ecuaciones analíticas que son de especial interés para caracterizar la topología completa. De esta forma, puede determinarse el efecto de cada uno de los elementos sobre la respuesta final del filtro.

Para los elementos serie, se han estudiado y obtenido ecuaciones de diseño para dos estructuras paso banda formadas por una o dos secciones de MTL en serie 6.2.1. Haciendo uso de la matriz de parámetros admitancia de un MTL con sus puertos diagonales en abierto, los parámetros S de estas dos estructuras pueden expresarse como

- Una etapa:

$$|S_{11_s}|^2 = \frac{F_s^2}{1+F_s^2}, \quad |S_{21_s}|^2 = \frac{1}{1+F_s^2}, \tag{C.10a}$$

$$F_s = \frac{c_a^2 - \bar{Z}_{0_a}^2}{2\bar{Z}_{0_a}^2 c_a^2}\left(\cos^2\theta + \frac{c_a^2\left(\bar{Z}_{0_a}^2 - 1\right)}{c_a^2 - \bar{Z}_{0_a}^2}\right)\frac{1}{\sin\theta}, \tag{C.10b}$$

- Dos etapas:

$$|S_{11_{ss}}|^2 = \frac{F_{ss}^2}{1+F_{ss}^2}, \quad |S_{21_{ss}}|^2 = \frac{1}{1+F_{ss}^2}, \tag{C.11a}$$

$$F_{ss} = \frac{c_a^2 - \bar{Z}_{0_a}^2}{\bar{Z}_{0_a} c_a^3} \cos\theta \left(\cos^2\theta + \frac{c_a^2\left(\bar{Z}_{0_a}^2 - 1\right)}{c_a^2 - \bar{Z}_{0_a}^2} \right) \frac{1}{\sin\theta}, \tag{C.11b}$$

donde los subíndices s y ss se utilizan para denotar la configuración con uno o dos MTLs en serie, respectivamente, y $\bar{Z}_{0_a}$ representa la impedancia característica del MTL normalizada (Z_{0_a}/Z_0). De forma similar al estudio llevado a cabo para los filtros diferenciales, los polinomos F_s y F_{ss} condicionan el tipo de filtrado. Comparando y ajustando los coeficientes de estos polinomios con polinomios de Butterworth y Chebyshev, se han calculado expresiones de diseño para sintetizar filtros paso banda de segundo o tercer orden (6.12), (6.13), (6.14), (6.17). Así pues, el número máximo de polos en la banda de paso será tres. Es importante notar que las ecuaciones de diseño obtenidas son equivalentes a las deducidas para el filtro diferencial. Esto se debe a que las líneas multiconductoras con sus puertos diagonales en abierto y en cortocircuito son estructuras duales. Además, para incrementar la selectividad del filtro, se ha incluido un MTL paralelo, el cual introduce dos ceros de transmisión cercanos a las frecuencias de corte (Seción 6.2.2).

Una vez que se han analizado los elementos serie y paralelo, se ha caracterizado la estructura completa. Tanto para la configuración asimétrica como para la simétrica se ha calculado la magnitud de los parámetros S de la forma

$$|S_{21}|^2 = \frac{1}{1+F^2}, \qquad |S_{11}|^2 = \frac{F^2}{1+F^2}, \tag{C.12}$$

donde el polinomio F condiciona la respuesta del filtro. Nuevamente, el diseño del filtro consiste en ajustar los coeficientes del polinomio F para conseguir un determinado ancho de banda con unas pérdidas de retorno concretas. Para la estructura asímetrica dichos coeficientes se ajustan para tener tres polos en la banda de paso, mientras que en la situación simétrica se demuestra que el filtro puede sintetizarse para generar tres o cinco polos. Por consiguiente, el tener dos MTL series, además de incrementar la selectividad, permite tener dos polos adicionales en la banda de paso. La Fig. 6.10 representa este comportamiento en frecuencia. Una vez calculadas las características de los MTL serie y paralelo (c_a, Z_{0_a}, c_b, Z_{0_b}) en base a la respuesta en frecuencia deseada, las impedancias de los modos par e impar

se obtienen fácilmente en función del número de conductores como

$$Z_{oe_i} = \frac{k_i - 1}{2} Z_{0_i} (R - 1) \frac{1 - c_i^2}{c_i^2}, \qquad Z_{oo_i} = \frac{Z_{oe_i}}{R} \tag{C.13a}$$

$$R = \frac{c_i + \sqrt{(k_i - 1)^2 (1 - c_i^2) + c_i^2}}{(k_i - 1)(1 - c_i)}. \tag{C.13b}$$

Finalmente, tras obtener Z_{oe} y Z_{oo} las dimensiones físicas de las estructuras multiconductoras se calculan usando expresiones analíticas conocidas [97, 98].

Para validar toda la teoría desarrollada así como las ecuaciones de diseño (6.29), (6.39) y (6.41), varios prototipos de estos filtros han sido diseñados, fabricados y medidos en tecnología microstrip. Las Tablas 6.3 y 6.5 recogen los valores de diseño y las dimensiones físicas de los filtros asimétricos y simétricos fabricados. En todos los prototipos se observa una excelente concordancia entre los parámetros S medidos y los calculados teóricamente, con pérdidas de inserción siempre inferiores a 1 dB. Así pues, los resultados no sólo permiten validar las ecuaciones de diseño sino que también muestran el grado de precisión de las mismas, puesto que las dimensiones teóricas no han sido optimizadas con ningún simulador electromagnético.

C.7. Conclusiones

En este trabajo de investigación se han desarrollado y mejorado aplicaciones usando líneas de transmisión multiconductoras. Los resultados derivados de este trabajo pueden resumirse en los siguientes puntos:

Desfasadores de tipo reflexivo

Se ha llevado a cabo un estudio genérico de desfasadores usando líneas de transmisión multiconductoras donde los puertos directo y acoplado se terminan con cargas puramente reactivas. En este contexto, las principales contribuciones son:

- Estudio exhaustivo de desfasadores de tipo reflexivo usando MTLs.
- Nuevas y simplificadas ecuaciones de diseño útiles para reducir el tamaño de los MTL sin necesidad de ningún estudio paramétrico.
- Se han obtenido dos nuevos circuitos equivalentes basados en líneas de transmisión para dos configuraciones particulares: con los puertos acoplado y directo en abierto o cortocircuitados a tierra. Estos circuitos son de gran interés para el diseño de filtros paso banda.

Baluns: Conversión del Modo Común al Modo Diferencial

Se ha realizado un estudio teórico usando líneas de transmisión multiconductoras para sintetizar baluns de banda ancha para la conversión del modo común al modo diferencial. Además haciendo uso del balun propusto se ha fabricado un sistema reconfigurable para la caracterización de dispositivos diferenciales. Todas las expresiones analíticas han sido validadas de forma experimental mediante la fabricación de sendos prototipos. Las principales contribuciones han sido:

- Conjunto de ecuaciones analíticas de diseño de baluns que garantizan un buen balance de fase y de amplitud, una buena adaptación y un excelente aislamiento entre los puertos de salida.
- El balun propuesto mejora las prestaciones de la mayoría de los baluns existentes en la literatura, que o bien son de banda estrecha o bien tienen un mal aislamiento a la salida.
- Se ha diseñado y fabricado un nuevo sistema reconfigurable basado en conmutadores MEMS para medir los parámetros S del modo mixto de dispositivos diferenciales haciendo uso de un analizador de redes vectorial de dos puertos.

Dispositivos de un Puerto

Las líneas de transmisión multiconductoras se han analizado como dispositivos de un puerto para obtener valores de impedancia o respuestas en frecuencia que son complicados o imposibles de conseguir mediante una simple línea de transmisión. Nuevamente, para validar los comportamientos en frecuencia obtenidos de forma teórica, se han fabricado dos líneas de transmisión artificial con comportamiento zurdo usando una de las configuraciones analizadas. Las principales contribuciones sobre esta temática son:

- Análisis teórico de las ocho posibles configuraciones de dispositivos de un puerto. De este estudio se han deducido las características particulares de cada una de las configuraciones.
- Se ha demostrado que seis de las ocho configuraciones son adecuadas para sintetizar stubs de baja impedancia equivalente, terminados en cortocircuito o en circuito abierto.
- Dos configuraciones poseen una respuesta en frecuencia particular, donde las posiciones de los polos o ceros pueden ajustarse variando el factor de acoplamiento. Esto permite que una de las estructuras sea adecuada para diseñar filtros paso banda, generando dos ceros de transmisión en los extremos de la banda de paso para aumentar la selectividad, mientras la otra es de utilidad para el diseño de filtros de doble banda.

Filtros Diferenciales Paso Banda de Banda Ancha

Se ha propuesto y analizado una nueva topología basada en líneas de transmisión multiconductoras para la síntesis de filtros diferenciales de banda muy ancha. Para el diseño de estos filtros se han derivado ecuaciones analíticas que permiten determinar en función del ancho de banda y la adaptación las impedancias de los modos par e impar de los MTL en función del número de conductores. Usando estas expresiones analíticas se han diseñado y fabricado dos filtros diferenciales de una y dos etapas con anchos de banda relativos a -3 dB de 145% y 97%. En este ámbito, las principales contribuciones han sido:

- Nueva estructura basada en líneas multiconductoras con los puertos diagonales en cortocircuito para la síntesis de filtros diferenciales de banda muy ancha con un buen rechazo al modo común (>20dB).
- Conjunto de ecuaciones analíticas para el diseño de filtros diferenciales de una y dos etapas con un comportamiento en frecuencia tipo Butterworth o Chebyshev.

Filtros Paso Banda Cuasi-Elípticos

Las líneas multiconductoras se han utilizado para sintetizar filtros paso banda con una respuesta en frecuencia cuasi-elíptica. Se ha desarrollado la teoría necesaria para el diseño de los filtros teniendo en cuenta el ancho de banda, la adaptación y el nivel de rechazo fuera de banda. Todas las ecuaciones se han validado mediante el diseño, la fabricación y la medida de hasta ocho prototipos. En todos los diseños se ha demostrado una excelente concordancia entre los resultados medidos y los teóricos, lo que garantiza que las ecuaciones de diseño constituyen una herramienta útil para el diseño de filtros de forma precisa. Las principales contribuciones en esta temáticas son:

- Ecuaciones analíticas para el diseño de fitros paso banda con un comportamiento Butterworth o Chebyshev usando una o dos secciones de MTL en serie.
- Ecuaciones analíticas para el diseño de filtros paso banda cuasi-elípticos incorporando un MTL en paralelo para introducir dos ceros de transmisión.
- Analísis de dos nuevas topologías, una asimétrica y otra simétrica, para el diseño de filtros con tres o cinco polos/zeros de reflexión en la banda de paso. En ambas configuraciones se demuestra que los filtros presentan una alta selectividad y un buen rechazo fuera de banda.

References

[1] G. L. Mattahei, L. Young, and E. M. T. Jones, *Microwave Filters, Impedance-Matching Networks, and Coupling Structures*, M. A. House, Ed. Norwood, 1985.

[2] R. Mongia, I. Bahl, and P. Bhartia, *RF and Microwave Coupled-Line Circuits*. Norwood, MA: Artech House, 1999.

[3] J. A. B. Faria, *Multiconductor Transmission-line Structures: Modal Analysis Techniques*. New York: Wiley, 1993.

[4] I. C. Hunter, *Theory and Design of Microwave Filters*, Stevenage, Ed. U.K.: IEE Press, 2001.

[5] I. D. Robertson and S. Lucyszyn, *RFIC and MMIC Design and Technology*. London, UK: IEE Press, 2001.

[6] J.-S. Hong and M. J. Lancaster, *Microstrip Filters for RF/Microwave Applications*, K. Chang, Ed. Wiley-Interscience, 2001.

[7] C. Caloz and I. Itoh, *Electromagnetic Metamaterials: Transmission Line Theory and Microwave Applications*. Wiley-Interscience, 2006.

[8] S. Cohn and R. Levy, "History of Microwave Passive Components with Particular Attention to Directional Couplers," *IEEE Trans. Microw. Theory Tech.*, vol. 32, no. 9, pp. 1046–1054, Sep. 1984.

[9] R. Levy and S. Cohn, "A History of Microwave Filter Research, Design, and Development," *IEEE Trans. Microw. Theory Tech.*, vol. 32, no. 9, pp. 1055–1067, Sep. 1984.

[10] E. M. T. Jones and J. T. Bolljahn, "Coupled-Strip-Transmission-Line Filters and Directional Couplers," *IRE Trans. Microw. Theory Tech.*, vol. 4, no. 2, pp. 75–81, Apr. 1956.

[11] S. B. Cohn, "Parallel-Coupled Transmission-Line-Resonator Filters," *IRE Trans. Microw. Theory Tech.*, vol. 6, no. 2, pp. 223–231, Apr. 1958.

[12] G. Matthaei, "Interdigital Band-Pass Filters," *IRE Trans. Microw. Theory Tech.*, vol. 10, no. 6, pp. 479–491, Nov. 1962.

[13] R. Levy, "General Synthesis of Asymmetric Multi-Element Coupled-Transmission-Line Directional Couplers," *IEEE Trans. Microw. Theory Tech.*, vol. 11, no. 4, pp. 226–237, Jul. 1963.

[14] H. Carlin and W. Kohler, "Direct Synthesis of Band-Pass Transmission Line Structures," *IEEE Trans. Microw. Theory Tech.*, vol. 13, no. 3, pp. 283–297, May 1965.

[15] R. Wenzel, "Exact Theory of Interdigital Band-Pass Filters and Related Coupled Band-Pass Structures," *IEEE Trans. Microw. Theory Tech.*, vol. 13, no. 5, pp. 559–575, Sep. 1965.

[16] E. Cristal, "Coupled-Transmission-Line Directional Couplers with Coupled Lines of Unequal Characteristic Impedances," *IEEE Trans. Microw. Theory Tech.*, vol. 14, no. 7, pp. 337–346, Jul. 1966.

[17] G. Zysman and A. Johnson, "Coupled transmission line networks in an inhomogeneous dielectric medium," *IEEE Trans. Microw. Theory Tech.*, vol. 17, no. 10, pp. 753–759, Oct. 1969.

[18] V. Tripathi, "Asymmetric Coupled Transmission Lines in an Inhomogeneous Medium," *IEEE Trans. Microw. Theory Tech.*, vol. 23, no. 9, pp. 734–739, Sep. 1975.

[19] R. Wenzel, "Synthesis of Combline and Capacitively Loaded Interdigital Bandpass Filters of Arbitrary Bandwidth," *IEEE Transactions on Microwave Theory and Techniques*, vol. 19, no. 8, pp. 678–686, Aug. 1971.

[20] E. Cristal and S. Frankel, "Hairpin-Line and Hybrid Hairpin-Line/Half-Wave Parallel-Coupled-Line Filters," *IEEE Trans. Microw. Theory Tech.*, vol. 20, no. 11, pp. 719–728, Nov. 1972.

[21] U. H. Gysel, "New Theory and Design for Hairpin-Line Filters," *IEEE Trans. Microw. Theory Tech.*, vol. 22, no. 5, pp. 523–531, May 1974.

[22] S. Sun and L. Zhu, "Multiple-resonator-based bandpass filters," *IEEE Microw. Mag.*, vol. 10, no. 2, pp. 88–98, Apr. 2009.

REFERENCES

[23] M. Tsai, "A new compact wideband balun," in *IEEE Microwave and Millimeter-Wave Monolithic Circuits Symposium*, 1993, pp. 123–125.

[24] M. Chongcheawchamnan, C. Y. Ng, K. Bandudej, A. Worapishet, and I. Robertson, "On miniaturization isolation network of an all-ports matched impedance-transforming marchand balun," *IEEE Microw. Wireless Compon. Lett.*, vol. 13, no. 7, pp. 281–283, Jul. 2003.

[25] J. Lange, "Interdigitated Strip-Line Quadrature Hybrid," in *Microwave Symposium, 1969 G-MTT International*, May 1969, pp. 10–13.

[26] W. Ou, "Design Equations for an Interdigitated Directional Coupler," *IEEE Trans. Microw. Theory Tech.*, vol. 23, no. 2, pp. 253–255, Feb. 1975.

[27] F. Casares-Miranda, P. Otero, E. Márquez-Segura, and C. Camacho-Peñalosa, "Wire Bonded Interdigital Capacitor," *IEEE Microw. Wireless Compon. Lett.*, vol. 15, no. 10, pp. 700–702, Oct. 2005.

[28] E. Márquez-Segura, F. Casares-Miranda, P. Otero, C. Camacho-Peñalosa, and J. Page, "Analytical Model of the Wire-Bonded Interdigital Capacitor," *IEEE Trans. Microw. Theory Tech.*, vol. 54, no. 2, pp. 748–754, Feb. 2006.

[29] J. Page, E. Márquez-Segura, F. Casares-Miranda, J. Esteban, P. Otero, and C. Camacho-Peñalosa, "Exact Analysis of the Wire-Bonded Multiconductor Transmission Line," *IEEE Trans. Microw. Theory Tech.*, vol. 55, no. 8, pp. 1585–1592, Aug. 2007.

[30] J. J. Sánchez-Martínez and E. Márquez-Segura, "Analytical Study of Wide-band Bandpass Filters Based on Wire-Bonded Multiconductor Transmission Lines With LH Behaviour," *Progr. Electromagn. Res. Lett.*, vol. 31, pp. 1–13, 2012.

[31] ——, "Analysis of wire-bonded multiconductor transmission line-based phase-shifting sections," *J. Electromagn. Waves Appl.*, vol. 27, no. 16, pp. 1997–2009, Sep. 2013.

[32] ——, "Generalized analytical design of broadband planar baluns based on wire-bonded multiconductor transmission lines," *Progr. Electromagn. Res.*, vol. 134, pp. 169–187, 2013.

[33] S. Cobos-Bandera, J. J. Sánchez-Martínez, and E. Márquez-Segura, "Mems-based reconfigurable test-set for differential and common mode measurement using a two-port network analyzer," in *42nd European Microwave Conference (EuMC)*, Oct. 2012, pp. 601–604.

[34] ——, "Sistema de Medida Reconfigurable para la Caracterización de Dispositivos Diferenciales de Microondas," in *XXVII Simposium Nacional de la Unión Científica Internacional de Radio (URSI)*, Sep. 2012, ISBN: 978-84-695-4326-9.

[35] J. J. Sánchez-Martínez and E. Márquez-Segura, "Análisis de un Balun Basado en Líneas de Transmisión Multiconductoras," in *XXVII Simposium Nacional de la Unión Científica Internacional de Radio (URSI)*, Sep. 2012, ISBN: 978-84-695-4326-9.

[36] J. J. Sánchez-Martínez, E. Márquez-Segura, P. Otero, and C. Camacho-Peñalosa, "Artificial Transmission Line with Left/Right-Handed Behavior Based on Wire Bonded Interdigital Capacitors," *Progr. Electromagn. Res. B*, vol. 11, pp. 245–264, 2009.

[37] J. J. Sánchez-Martínez and E. Márquez-Segura, "Comments on 'Wideband Coupled-Line Microstrip Filters With High-Impedance Short-Circuited Stubs'," *IEEE Microw. Wireless Compon. Lett.*, vol. 22, no. 9, p. 492, Sep. 2012.

[38] J. J. Sánchez-Martínez, E. Márquez-Segura, and C. Camacho-Peñalosa, "Analysis of wire-bonded multiconductor transmission-line-based stubs," *IEEE Trans. Microw. Theory Tech.*, vol. 61, no. 4, pp. 1467–1476, Apr. 2013.

[39] ——, "Analysis of Composite Left/Right-Handed Transmission Line Using Shunt Wire Bonded Interdigital Capacitors," in *4th Young Scientist Meeting on Metamaterials (YSMM)*, Feb. 2011, ISBN: 978-84-693-9971-2.

[40] ——, "Synthesis of CRLH-TLs Based on a Shunt Coupled-line Section," in *42nd European Microwave Conference (EuMC)*, Oct. 2012, pp. 675–678.

[41] J. J. Sánchez-Martínez and Márquez-Segura, "Analytical Design of Wire-Bonded Multiconductor Transmission Line-Based Ultra-Wideband Differential Bandpass Filters," *Submitted to IEEE Trans. Microw. Theory Tech.*, Mar. 2014.

[42] J. J. Sánchez-Martínez and E. Márquez-Segura, "Análisis y Diseño de Filtros Diferenciales Basados en Líneas Acopladas," in *enviado a XXIX Simposium Nacional de la Unión Científica Internacional de Radio (URSI)*, Sep. 2014.

[43] J. J. Sánchez-Martínez, E. Márquez-Segura, and S. Lucyszyn, "Design of Compact Wideband Bandpass Filters Based on Multiconductor Transmission Lines With Interconnected Alternate Lines," *IEEE Microw. Wireless Compon. Lett.*, vol. 24, no. 7, pp. 454–456, Jul. 2014.

[44] J. J. Sánchez-Martínez, Márquez-Segura, and S. Lucyszyn, "Synthesis and Design of High-Selectivity Wideband Quasi-elliptic Bandpass Filters Using Multiconductor Transmission Lines," *Submitted to Trans. Microw. Theory Tech.*, Apr. 2014.

[45] J. J. Sánchez-Martínez and E. Márquez-Segura, "Análisis y Diseño de Filtros Paso Banda con Alta Selectividad Espectral Basados en Líneas de Transmisión Multiconductoras," in *XXVIII Simposium Nacional de la Unión Científica Internacional de Radio (URSI)*, Sep. 2013, ISBN: 978-84-941537-1-6.

[46] R. Garver, "Broad-band diode phase shifters," *IEEE Trans. Microw. Theory Tech.*, vol. 20, no. 5, pp. 314 – 323, May 1972.

[47] D. Pozar, *Microwave Engineering*, 2nd ed. New York: Wiley, 1998.

[48] A. Presser, "Interdigitated microstrip coupler design," *IEEE Trans. Microw. Theory Tech.*, vol. 26, no. 10, pp. 801–805, Oct. 1978.

[49] S. Lucyszyn and I. Robertson, "Synthesis techniques for high performance octave bandwidth 180 deg; analog phase shifters," *IEEE Trans. Microw. Theory Tech.*, vol. 40, no. 4, pp. 731 –740, Apr. 1992.

[50] ——, "Analog reflection topology building blocks for adaptive microwave signal processing applications," *IEEE Trans. Microw. Theory Tech.*, vol. 43, no. 3, pp. 601 –611, Mar. 1995.

[51] A. Abbosh, "Compact tunable reflection phase shifters using short section of coupled lines," *IEEE Trans. Microw. Theory Tech.*, vol. 60, no. 8, pp. 2465–2472, Aug. 2012.

[52] Z.-Y. Zhang, Y.-X. Guo, L. C. Ong, and M. Chia, "A new wide-band planar balun on a single-layer pcb," *IEEE Microw. Wireless Compon. Lett.*, vol. 15, no. 6, pp. 416–418, Jun. 2005.

[53] C.-H. Tseng and C.-L. Chang, "Wide-band balun using composite right/left-handed transmission line," *Electron. Lett.*, vol. 43, no. 21, pp. 1154–1155, Nov. 2007.

[54] F. Tan, W. Huang, Y. Chen, Y. Li, K. Huang, and C. Liu, "Design and implementation of compact microwave components with artificial transmission lines," *J. Electromagn. Waves Appl.*, vol. 27, no. 3, pp. 385–395, 2013.

[55] K. S. Ang and I. Robertson, "Analysis and design of impedance-transforming planar marchand baluns," *IEEE Trans. Microw. Theory Tech.*, vol. 49, no. 2, pp. 402–406, Feb. 2001.

[56] W. Fathelbab and M. Steer, "New classes of miniaturized planar marchand baluns," *IEEE Trans. Microw. Theory Tech.*, vol. 53, no. 4, pp. 1211–1220, Apr. 2005.

[57] R. Phromloungsri, M. Chongcheawchamnan, and I. Robertson, "Inductively compensated parallel coupled microstrip lines and their applications," *IEEE Trans. Microw. Theory Tech.*, vol. 54, no. 9, pp. 3571–3582, Sep. 2006.

[58] C.-S. Lin, P.-S. Wu, M.-C. Yeh, J.-S. Fu, H.-Y. Chang, K.-Y. Lin, and H. Wang, "Analysis of multiconductor coupled-line marchand baluns for miniature mmic design," *IEEE Trans. Microw. Theory Tech.*, vol. 55, no. 6, pp. 1190–1199, Jun. 2007.

[59] L. Yeung, W.-C. Cheng, and Y. Wang, "A dual-band balun using broadside-coupled coplanar striplines," *IEEE Trans. Microw. Theory Tech.*, vol. 56, no. 8, pp. 1995–2000, Aug. 2008.

[60] C.-H. Tseng and Y.-C. Hsiao, "A new broadband marchand balun using slot-coupled microstrip lines," *IEEE Microw. Wireless Compon. Lett.*, vol. 20, no. 3, pp. 157–159, Mar. 2010.

[61] J.-C. Lu, C.-C. Lin, and C.-Y. Chang, "Exact synthesis and implementation of new high-order wideband marchand baluns," *IEEE Trans. Microw. Theory Tech.*, vol. 59, no. 1, pp. 80–86, Jan. 2011.

[62] E. Jafari, F. Hodjatkashani, and R. Rezaiesarlak, "A Wideband Compact Planar Balun for UHF DTV Applications," *J. Electromagn. Waves Appl.*, vol. 23, no. 14-15, pp. 2047–2053, 2009.

[63] J.-L. Li and S.-W. Qu, "Miniaturised branch-line balun with bandwidth enhancement," *Electron. Lett.*, vol. 43, no. 17, pp. 931–932, Aug. 2007.

[64] W. Shao and J.-L. Li, "A compact log-periodic branch-line balun with an octave bandwidth," *J. Electromagn. Waves Appl.*, vol. 25, no. 14-15, pp. 2033–2042, 2011.

[65] C. Liu and W. Menzel, "Broadband via-free microstrip balun using metamaterial transmission lines," *IEEE Microw. Wireless Compon. Lett.*, vol. 18, no. 7, pp. 437–439, Jul. 2008.

[66] C.-K. Lin and S.-J. Chung, "A Compact Filtering 180 Hybrid," *IEEE Trans. Microw. Theory Tech.*, vol. 59, no. 12, pp. 3030–3036, Dec. 2011.

[67] Z.-Y. Yeh and Y.-C. Chiang, "A miniature CPW balun constructed with length-reduced 3db couples and a short redundant transmission line," *Progr. Electromagn. Res.*, vol. 117, pp. 195–208, 2011.

[68] H.-X. Xu, G.-M. Wang, X. Chen, and T.-P. Li, "Broadband balun using fully artificial fractal-shaped composite right/left handed transmission line," *IEEE Microw. Wireless Compon. Lett.*, vol. 22, no. 1, pp. 16–18, Jan. 2012.

[69] S. Cohn, "A Class of Broadband Three-Port TEM-Mode Hybrids," *IEEE Trans. Microw. Theory Tech.*, vol. 19, no. 2, pp. 110–116, Feb. 1968.

[70] W. R. Eisenstadt, B. Stengel, and B. M. Thompson, *Microwave Differential Circuit Design Using Mixed-Mode S-Parameters.* Norwood, MA: Artech House, 2006.

[71] D. Bockelman and W. Eisenstadt, "Combined differential and common-mode scattering parameters: theory and simulation," *IEEE Trans. Microw. Theory Tech.*, vol. 43, no. 7, pp. 1530–1539, Jul. 1995.

[72] ——, "Pure-mode network analyzer for on-wafer measurements of mixed-mode S-parameters of differential circuits," *IEEE Trans. Microw. Theory Tech.*, vol. 45, no. 7, pp. 1071–1077, Jul. 1997.

[73] D. Bockelman, W. Eisenstadt, and R. Stengel, "Accuracy estimation of mixed-mode scattering parameter measurements," *IEEE Trans. Microw. Theory Tech.*, vol. 47, no. 1, pp. 102–105, Jan. 1999.

[74] S. Belkin, "Differential Circuit Characterization with Two-Port S-Parameters," *IEEE Microw. Mag.*, vol. 7, no. 6, pp. 86–99, Dec. 2006.

[75] V. Issakov, M. Wojnowski, A. Thiede, V. Winkler, M. Tiebout, and W. Simburger, "Considerations on the measurement of active differential devices using baluns," in *IEEE Int. Conf. on Microw. Commun., Antennas and Electron. Syst. (COMCAS)*, Nov. 2009, pp. 1–7.

[76] K. Jung, R. Campbell, L. Hayden, W. Eisenstadt, and R. Fox, "Evaluation of Measurement Uncertainties Caused by Common and Cross Modes in Differential Measurements Using Baluns," *IEEE Trans. Microw. Theory Tech.*, vol. 56, no. 6, pp. 1485–1492, Jun. 2008.

[77] S. Lucyszyn, *Advanced RF MEMS*, 1st ed. New York, NY, USA: Cambridge University Press, 2010.

[78] Y. Omote, T. Yasuzumi, T. Uwano, and O. Hashimoto, "Design procedure of wideband band-pass filter consists of inter-digital finger resonator and parallel coupled lines," in *Proc. Asia-Pacific Microw. Conf.*, Dec. 2010, pp. 29–32.

[79] H.-R. Ahn and S. Nam, "Wideband coupled-line microstrip filters with high-impedance short-circuited stubs," *IEEE Microw. Wireless Compon. Lett.*, vol. 21, no. 11, pp. 586–588, Nov. 2011.

[80] J.-T. Kuo, C.-Y. Fan, and S.-C. Tang, "Dual-wideband bandpass filters with extended stopband based on coupled-line and coupled three-line resonators," *Progr. Electromagn. Res.*, vol. 124, pp. 1–15, 2012.

[81] G. Eleftheriades, A. Iyer, and P. Kremer, "Planar negative refractive index media using periodically L-C loaded transmission lines," *IEEE Trans. Microw. Theory Tech.*, vol. 50, no. 12, pp. 2702–2712, Dec. 2002.

[82] C. Caloz and T. Itoh, "Application of the Transmission Line Theory of Left-Handed (LH) Materials to the Realization of a Microstrip LH Line," in *IEEE Antennas and Propagation Society International Symposium*, vol. 2, 2002, pp. 412–415.

[83] A. Oliner, "A planar negative-refractive-index medium without resonant elements," in *IEEE MTT-S International Microwave Symposium Digest*, vol. 1, Jun. 2003, pp. 191–194.

[84] T. B. Lim and L. Zhu, "A Differential-Mode Wideband Bandpass Filter on Microstrip Line for UWB Application," *IEEE Microw. Wireless Compon. Lett.*, vol. 19, no. 10, pp. 632–634, Oct 2009.

[85] X.-H. Wang, Q. Xue, and W.-W. Choi, "A Novel Ultra-Wideband Differential Filter Based on Double-Sided Parallel-Strip Line," *IEEE Microw. Wireless Compon. Lett.*, vol. 20, no. 8, pp. 471–473, Aug 2010.

[86] A. Abbosh, "Ultrawideband Balanced Bandpass Filter," *IEEE Microw. Wireless Compon. Lett.*, vol. 21, no. 9, pp. 480–482, Sept 2011.

[87] Y.-J. Lu, S.-Y. Chen, and P. Hsu, "A Differential-Mode Wideband Bandpass Filter With Enhanced Common-Mode Suppression Using Slotline Resonator," *IEEE Microw. Wireless Compon. Lett.*, vol. 22, no. 10, pp. 503–505, Oct 2012.

[88] C.-H. Wu, C.-H. Wang, and C. H. Chen, "Balanced Coupled-Resonator Bandpass Filters Using Multisection Resonators for Common-Mode Suppression and Stopband Extension," *IEEE Trans. Microw. Theory Tech.*, vol. 55, no. 8, pp. 1756–1763, Aug 2007.

[89] J. Shi and Q. Xue, "Novel Balanced Dual-Band Bandpass Filter Using Coupled Stepped-Impedance Resonators," *IEEE Microw. Wireless Compon. Lett.*, vol. 20, no. 1, pp. 19–21, Jan 2010.

[90] A. Horestani, M. Duran-Sindreu, J. Naqui, C. Fumeaux, and F. Martin, "S-Shaped Complementary Split Ring Resonators and Their Application to Compact Differential Bandpass Filters With Common-Mode Suppression," *IEEE Microw. Wireless Compon. Lett.*, vol. PP, no. 99, pp. 150–152, 2014.

[91] W. Feng and W. Che, "Novel Wideband Differential Bandpass Filters Based on T-Shaped Structure," *IEEE Trans. Microw. Theory Tech.*, vol. 60, no. 6, pp. 1560–1568, June 2012.

[92] J.-S. Hong, *Microstrip Filters for RF/Microwave Applications*, K. Chang, Ed. Wiley-Interscience, 2011.

[93] H. Shaman and J.-S. Hong, "Input and output cross-coupled wideband bandpass filter," *IEEE Trans. Microw. Theory Tech.*, vol. 55, no. 12, pp. 2562–2568, Dec. 2007.

[94] J. Rhodes and R. J. Cameron, "General Extracted Pole Synthesis Technique with Applications to Low-Loss TE011 Mode Filters," *IEEE Trans. Microw. Theory Tech.*, vol. 28, no. 9, pp. 1018–1028, Sep 1980.

[95] J. Montejo-Garai, J. Ruiz-Cruz, J. Rebollar, M. Padilla-Cruz, A. Onoro-Navarro, and I. Hidalgo-Carpintero, "Synthesis and design of in-line N-order filters with N real transmission zeros by means of extracted poles implemented in low-cost rectangular H-plane waveguide," *IEEE Trans. Microw. Theory Tech.*, vol. 53, no. 5, pp. 1636–1642, May 2005.

[96] Z.-C. Hao and J.-S. Hong, "Ultrawideband Filter Technologies," *IEEE Microw. Mag.*, vol. 11, no. 4, pp. 56–68, Jun. 2010.

[97] M. Kirschning and R. Jansen, "Accurate Wide-Range Design Equations for the Frequency-Dependent Characteristic of Parallel Coupled Microstrip Lines," *IEEE Trans. Microw. Theory Tech.*, vol. 32, no. 1, pp. 83–90, Jan. 1984.

[98] J. A. B. Faria, "Kirschning and Jansen computer-aided design formulae for the analysis of parallel coupled lines," *Microw. Opt. Techn. Let.*, vol. 51, no. 10, pp. 2466–2470, 2009.